UCSF
UC San Francisco Electronic Theses and Dissertations

Title
Experimental and computional analysis of left ventricular aneurysm mechanics

Permalink
https://escholarship.org/uc/item/4c01v7t5

Author
Moonly, Scott Michael

Publication Date
2003

Peer reviewed|Thesis/dissertation

eScholarship.org
Powered by the California Digital Library
University of California

Experimental and Computational Analysis of Left Ventricular Aneurysm Mechanics

by

Scott Michael Moonly

DISSERTATION

Submitted in partial satisfaction of the requirements for the degree of

DOCTOR OF PHILOSOPHY

in

Bioengineering

in the

GRADUATE DIVISIONS

of the

UNIVERSITY OF CALIFORNIA SAN FRANCISCO

and

UNIVERSITY OF CALIFORNIA BERKELEY

[redacted]

Date .... University Librarian

Degree Conferred: ....

Copyright 2003
by
Scott Michael Moonly

ACKNOWLEDGEMENTS

This thesis is the culmination of four years of research under the guidance of Dr. Julius Guccione. I am extremely grateful to Dr. Guccione for his support and guidance throughout my entire time as a graduate student. He has been a knowledgeable teacher, advisor and friend. Chapters 4,5, and 6 are currently being prepared to be submitted as a two part manuscript to be submitted to a biomedical engineering journal in the near future.

I would also like to thank Dr. Mark Ratcliffe for his support and guidance over the past years. His support and critiquing of all of the work I have completed while a graduate student has certainly improved the quality of the research I have produced. Dr. Ratcliffe was also great at finding diversionary projects to break up the monotony of continuously programming all day. Dr. Arthur Wallace has also provided much insight and guidance to me while a graduate student. His extensive comments on the final draft of this thesis certainly helped to create a clear and concise document. Additionally, Dr. Wallace also helped to create an air of levity to all members of the laboratory through his quick wit and sharp mind. Dr. Kevin Healy has also provided constructive comments on the progress of my thesis throughout the writing process.

I would also like to thank Dr. Sarah Nelson, my academic advisor. She has been extremely helpful in not only planning a course of study, but also has provided guidance during the writing of this thesis.

Joseph Walker, a fellow graduate student, also provided significant help and support, specifically in helping to keep the computer systems running around the lab.

I would also like to thank my wife Amy for her emotional and financial support during this long and trying process. At times it seemed as if this thesis was as tough for her as it was for me. Without her support, I am not sure that I would have made it through this process. Additionally my parents were extremely supportive of my studies throughout my time as a graduate student. I am extremely thankful of them for their support over the past years.

My studies were supported by NIH grants R01 HL58759-03 (Dr. Guccione) and R01 HL63348-01A1 (Dr. Ratcliffe). The support from these grants was greatly appreciated.

ABSTRACT OF THE DISSERTATION

Experimental and Computational Analysis of Left Ventricular Aneurysm Mechanics

by

Scott Michael Moonly
Doctor of Philosophy in Bioengineering
University of California, San Francisco
University of California, Berkeley
2003
Julius Guccione, Ph.D. Chair

Left Ventricular (LV) aneurysm, a complication of myocardial infarction, is a subset of the single largest killer of residents in the United States, coronary heart disease. This thesis combines traditional mechanical testing techniques (biaxial material property testing), with state of the art computer simulations (Finite Element Method (FEM)) to analyze LV aneurysm. Specifically this thesis will show the effect of changing material properties on both the global and regional function of the left ventricle.

To obtain realistic material parameters for LV aneurysm tissue, an ovine model of LV aneurysm was used. Following harvest of the tissue, biaxial material property testing was preformed on the tissue. We found the aneurysm tissue to be stiffer than previously reported by other investigators.

The impact of these new LV aneurysm material properties was examined by creating a realistic finite element model of the left ventricle as a whole. The geometry for this model was obtained using a magnetic resonance imaging (MRI) scan of the ovine LV aneurysm model. The model predicted an increase in cardiac function as measured by

the Starling relation, a global decrease in fiber stress, and a global increase in cross-fiber stress. The results have important implications to the structural changes that might be occurring not only in the aneurysm region of the left ventricle, but also in the border zone and remote regions of the heart.

In an attempt to isolate the impact of each material parameter upon cardiac function, a series of simulations was conducted. The stiffness of the aneurysm was modeled in a number of ways. With all of the methods, cardiac function was improved as stiffness was increased. However, each method yielded different results for stress and strain predictions. This has important implications to the cellular response to changing stress and strain patterns following LV aneurysm and highlights the importance of choosing accurate material parameters.

Approved by:

Julius Guccione 6/15/02

Julius Guccione, Ph.D., Research Advisor Date

Table of Contents

Title Page ... i

Copyright Page ... ii

Acknowledgments ... iii

Abstract ... v

Table of Contents ... vii

List of Figures ... x

List of Tables ... xiii

1. Introduction 1

    An Introduction to the Finite Element Method ... 2

    The Current State of Heart Disease and Treatment Options ... 3

    Structure of the Thesis ... 4

    References ... 6

2. Physiology Review ... 8

    Introduction ... 9

    The Flow of Blood Throughout the Circulatory System ... 9

    The Cellular Basis of Muscle Contraction ... 10

    The Three Dimensional Microstructure of the Heart ... 11

    Common Indices Used to Describe Cardiac Function ... 13

    The Length Tension Relationship in Cardiac Muscle ... 14

    Means Used to Evaluate Cardiac Function ... 15

    References ... 31

3. The Application of FEM to Cardiac Mechanics 34

Introduction 35

Prolate Spheroidal Coordinate System 35

Coordinate Systems Used 36

Governing Equations of Finite Elasticity 40

Finite Element Equations 46

Diastolic Material Properties 48

Systolic Material Properties 49

References 54

4. Mechanical Properties of Left Ventricular Aneurysm 55

Abstract 56

Introduction 56

Methods 64

Results 74

Discussion 75

Conclusion 82

References 99

5. Finite Element Model of Left Ventricular Aneurysm 108

Abstract 109

Introduction 109

Methods 112

Results 122

Discussion 127

UCSF LIBRARY

Conclusion 130

References 154

6. The Effect of Changing Material Parameters on Left Ventricular Aneurysm.. 162

Abstract 163

Introduction 163

Methods 164

Results 168

Discussion 177

Conclusion 179

References 207

7. Conclusion 211

References 216

8. Bibliography 218

9. Appendix 257

UCSF LIBRARY

List of Figures

2.1 Sliding Filament Theory 25
2.2 Length Tension Relationship in Muscle 26
2.3 The Starling Relation 27
2.4 The Pressure Volume Relation for the Left Ventricle 28
2.5 Systolic Dysfunction 29
2.6 Diastolic Dysfunction 30
3.1 Prolate Spheroidal Coordinate System 52
3.2 Coordinate Systems Used 53
4.1 Biaxial Stretching System 90
4.2 Marker Locations 91
4.3 Mapping Transformation 92
4.4 Biaxial Testing Raw Data 93
4.5 Typical Stress Strain Plots 94
4.6 Typical Stress Strain Plots with Fitted Curve 95
4.7 Mean Predicted Stress Values 96
4.8 Comparison with Gupta Stress Results 97
4.9 Comparison with Normal Myocardium Stress Results 98
5.1 MRI Data Acquisition 141
5.2 MRI Data Fitting 142
5.3 168 Element Model Schematic 143
5.4 280 Element Model Schematic 144
5.5 Muscle Fiber Variation in the 280 Element Model 145

5.6 Predicted Pressure Volume Relations 146

5.7 Predicted Starling Relations 147

5.8 Diastolic Aneurysm Stress and Strain 148

5.9 Diastolic Border Zone Stress and Strain 149

5.10 Diastolic Remote Stress and Strain 150

5.11 Systolic Aneurysm Stress and Strain 151

5.12 Systolic Border Zone Stress and Strain 152

5.13 Systolic Remote Stress and Strain 153

6.1 MRI Data Acquisition 188

6.2 MRI Data Fitting 189

6.3 168 Element Model Schematic 190

6.4 Pressure Volume Relations (Variation of C) 191

6.5 Starling Relations (Variation of C) 192

6.6 End-Diastolic Mean Stress and Strain (Variation of C) 193

6.7 End-Systolic Mean Stress and Strain (Variation of C) 194

6.8 Pressure Volume Relations (Variation of Exponents) 195

6.9 Starling Relations (Variation of Exponents) 196

6.10 End-Diastolic Mean Stress and Strain (Variation of Exponents) 197

6.11 End-Systolic Mean Stress and Strain (Variation of Exponents) 198

6.12 Pressure Volume Relations (Variation of b_f) 199

6.13 Starling Relations (Variation of b_f) 200

6.14 End-Diastolic Mean Stress and Strain (Variation of b_f) 201

6.15 End-Systolic Mean Stress and Strain (Variation of b_f) 202

6.16 Pressure Volume Relations (Variation of b_t) 203

6.17 Starling Relations (Variation of b_t) 204

6.18 End-Diastolic Mean Stress and Strain (Variation of b_t) 205

6.19 End-Systolic Mean Stress and Strain (Variation of b_t) 206

List of Tables

2.I Cardiac Evaluation Indices 24

4.I Previous Myocardial Young's Modulus Estimation 84

4.II Summary of Fitted Parameters 85

4.III Predicted Stress Values 86

4.IV Summary of Previous LVA Material Property Estimates 87

4.V Gupta LVA Stress Results 88

4.VI Gupta LVA Stress Results 89

5.I Material Parameters Used in Model Simulations 132

5.II Systolic Elastance and Diastolic Compliance 133

5.III The Effect of Aneurysm Material Parameters on Cardiac Function 134

5.IV End-Diastolic Stress Strain Relationship in the Aneurysm Region 135

5.V End-Diastolic Stress Strain Relationship in the Border Zone Region 136

5.VI End-Diastolic Stress Strain Relationship in the Remote Region 137

5.VII End-Systolic Stress Strain Relationship in the Aneurysm Region 138

5.VIII End-Systolic Stress Strain Relationship in the Border Zone Region 139

5.IX End-Systolic Stress Strain Relationship in the Remote Region 140

6.I Elastance and Compliance Parameters (Variation of C) 180

6.II Global Function Parameters (Variation of C) 181

6.III Elastance and Compliance Parameters (Variation of Exponents) 182

6.IV Global Function Parameters (Variation of Exponents) 183

6.V Elastance and Compliance Parameters (Variation of b_f) 184

6.VI Global Function Parameters (Variation of b_f) 185

6.VII Elastance and Compliance Parameters (Variation of b_t) 186

6.VIII Global Function Parameters (Variation of b_t) 187

Chapter 1

Introduction

For many years the use of the finite element method (FEM) has provided much insight and guidance in the mechanical analysis of biologic systems and in recent years has become an everyday tool [1]. Prosthetics, implantable materials, and artificial limbs have all used the FEM in their development [2-4]. Even at the cellular level, stress and strain are being examined in relation to growth and healing of biological tissues [5-11]. In this dissertation the power of the FEM will be used to model and study left ventricular (LV) aneurysm. LV aneurysm has been a difficult problem to study for numerous reasons. The heart muscle is anisotropic with respect to muscle fiber orientation, which makes it more difficult to model than the nearly isotropic orthopedic materials. Furthermore, the heterogenous incompressible nonlinear time-dependent material properties of LV aneurysm are not well defined. The deformations associated with the heart are commonly large deformations resulting in more complex finite mechanics than the infinitesimal deformations associated with orthopedics. The complex muscle fiber angle variation also adds considerably to the difficulty in creation of finite element computer models of the heart. Finally, the changing material properties that result from active contraction of muscle need to be accounted for.

An Introduction to the Finite Element Method

The FEM is a numerical technique that is used to obtain an approximate solution to partial differential equations, such as the ones that define the stress and strain relationship in muscle. The first step in solving a FE problem is to divide the continuum you are analyzing into discrete elements. It is possible to use many shapes to define an element, but the most common are pyramidal and cubic based shapes [12]. The corners of these shapes are referred to as nodes. Next, interpolation functions are used to represent the variation between nodes of an element need to be selected. Although scalars, vectors, and higher order tensors may be used to interpolate, polynomials are the most commonly used functions. In this thesis linear interpolation in curvilinear coordinates is used between nodes. Next, the matrices that represent the changes in properties of individual elements will be set up. Then the individual element matrices will be assembled into a global matrix that represents the problem as a whole. Before solving the problem, boundary conditions need to be applied. This process consists of applying known loads upon elements, and specifying or limiting displacements of individual nodes. Finally the system of nonlinear equations will be solved, however, this solution does not always lead us to a correct answer. Often it is necessary to compute secondary properties from the output of the model in order to give useful results [1]. The details of the finite element method will be presented in Chapter 3.

The Current State of Heart Disease and Treatment Options

Currently almost 62 million Americans are suffering from some form of cardiovascular disease (CVD). In the year 2000, almost 1.5 million lives were lost to CVD, that is approximately 40% of deaths in the United States resulted from CVD. When compared to other major sources of death, CVD is more significant than other causes of death in the United States (Cancer 553,000; Accidents 98,000; and AIDS 14,000), in fact results in more deaths than the next five causes of death combined [13]. If all forms of CVD were eliminated, life expectancy would be raised by 7 years. In the year 2003, the estimated costs of CVD in the United States is $351.8 billion [13].

The research presented in this thesis is focused on the effect of changing LV aneurysm material properties on cardiac function. LV aneurysm results from myocardial infarction (MI), in which the local blood supply to a region of the heart is blocked and the tissue in that area subsequently dies. LV aneurysm is considered a subset of coronary heart disease (CHD), the single largest killer of residents in the United States, causing one out of every five deaths [13]. In the year 2000 the total mention mortality from CHD was 681,000, with MI being responsible for about 239,000 of these deaths [13]. It is estimated that about every 29 seconds an American will suffer a coronary event, and about every minute someone will die from one. In the year 2003 it is estimated that $129.9 billion will be spent fighting CHD in the United States [13].

Structure of the Thesis

Subsequent chapters of this thesis will first give a review of cardiovascular physiology (Chapter 2) and the FEM (Chapter 3). In Chapter 4, the technique of biaxial material property testing will be used to obtain accurate material parameters in constituitive relations (stress, strain) for ovine LV aneurysm. Chapter 5 will then incorporate these parameters into a highly detailed FEM model of the ovine LV determined from magnetic resonance imaging (MRI). The global and regional function results of the FEM model will then be compared to other methods of modeling LV aneurysm in order to elucidate the potential oversimplifications made in past modeling of LV aneurysm. Chapter 6 will then evaluate the effects of changing individual material parameters of LV aneurysm modeling upon global and regional function of the left ventricle. This process will allow us to link specific changes in stiffness within LV aneurysm with their respective changes in global and regional function.

References:

1. Huebner, K.H., E.A. Thornton, and T.G. Byrom, *The finite element method for engineers*. 3rd ed. 1995, New York: Wiley. xxvi, 627.
2. Huiskes, R. and E.Y. Chao, *A survey of finite element analysis in orthopedic biomechanics: the first decade.* J Biomech, 1983. **16**(6): p. 385-409.
3. Huiskes, R. and S.J. Hollister, *From structure to process, from organ to cell: recent developments of FE-analysis in orthopaedic biomechanics.* J Biomech Eng, 1993. **115**(4B): p. 520-7.
4. Gilbertson, L.G., et al., *Finite element methods in spine biomechanics research.* Crit Rev Biomed Eng, 1995. **23**(5-6): p. 411-73.
5. Ma, Y.H., S. Ling, and H.E. Ives, *Mechanical strain increases PDGF-B and PDGF beta receptor expression in vascular smooth muscle cells.* Biochem Biophys Res Commun, 1999. **265**(2): p. 606-10.
6. Hipper, A. and G. Isenberg, *Cyclic mechanical strain decreases the DNA synthesis of vascular smooth muscle cells.* Pflugers Arch, 2000. **440**(1): p. 19-27.
7. O'Callaghan, C.J. and B. Williams, *Mechanical strain-induced extracellular matrix production by human vascular smooth muscle cells: role of TGF-beta(1).* Hypertension, 2000. **36**(3): p. 319-24.
8. Collinsworth, A.M., et al., *Orientation and length of mammalian skeletal myocytes in response to a unidirectional stretch.* Cell Tissue Res, 2000. **302**(2): p. 243-51.

9. Sudhir, K., et al., *Mechanical strain stimulates a mitogenic response in coronary vascular smooth muscle cells via release of basic fibroblast growth factor.* Am J Hypertens, 2001. **14**(11 Pt 1): p. 1128-34.

10. Wakatsuki, T. and E.L. Elson, *Reciprocal interactions between cells and extracellular matrix during remodeling of tissue constructs.* Biophys Chem, 2003. **100**(1-3): p. 593-605.

11. Wakatsuki, T., R.B. Wysolmerski, and E.L. Elson, *Mechanics of cell spreading: role of myosin II.* J Cell Sci, 2003. **116**(Pt 8): p. 1617-25.

12. Reddy, J.N., *An introduction to the finite element method.* 2nd ed. McGraw-Hill series in mechanical engineering. 1993, New York: McGraw-Hill. xix, 684.

13. *2001 Heart and Stroke Statistical Update*. 2001, American Heart Association: Dallas, TX.

14. Guccione, J.M., K.D. Costa, and A.D. McCulloch, *Finite element stress analysis of left ventricular mechanics in the beating dog heart.* J Biomech, 1995. **28**(10): p. 1167-77.

Chapter 2

Physiology Review

Introduction

An understanding of basic cardiovascular physiology is important to the undertaking of any computational modeling of the heart. This chapter will serve to highlight the basics of the cardiovascular system, review myocyte structure and function, and to explain the indices used to evaluate cardiac function.

The Flow of Blood Throughout the Circulatory System

The heart is divided into two sides, the left and the right. Both sides consist of two chambers, an atrium and a ventricle. Outflow from the right ventricle (RV) goes to the lungs where the deoxygenated blood is oxygenated. Outflow of oxygenated blood from the left ventricle (LV) goes to all of the tissues of the body, and is known as the systemic circulation. The actual flow of blood through the circulation can be thought of starting with the return of deoxygenated blood to the right atrium from the venous circulation. From the right atrium, blood enters the right ventricle after passing through the tricuspid valve. As the right ventricle begins to contract, the tricuspid valve closes and right intraventricular pressure increases until the pressure developed is significant enough to open the pulmonic valve and propel the blood through the pulmonary artery into the pulmonary vascular bed. After the blood has been oxygenated in the lungs it returns through the pulmonary veins to the left atrium. When the mitral valve opens, blood in the left atrium passes through the mitral valve and enters the left ventricle. As in the right ventricle, the increased pressure that results from ventricular contraction causes the mitral valve to close. Once the left ventricular pressure increases to a sufficient level to open the aortic valve (when left ventricular pressure exceeds aortic pressure) the blood is ejected through the aorta and propelled throughout the systemic circulation [1, 2].

The Cellular Basis of Muscle Contraction

The individual unit of contraction is termed a sarcomere which is composed of both thin and thick filaments. The thick filaments are made of myosin. Myosin molecules have globular heads which can bind to actin molecules, and power the change in length of the muscle that results in contraction through ATP usage. The thin filaments have three components: actin, troponin, and tropomyosin. Actin provides binding sites for the myosin heads of the thick filaments. However, these binding sites are blocked with the molecule tropomyosin. Troponin has three subunits, of which the troponin C subunit can bind calcium. Upon binding of calcium, the troponin C molecule causes a conformational shift in the tropomyosin molecule which allows the binding of the myosin heads to actin. Muscle contraction occurs according to the sliding filament theory. This theory states that cross bridges form between myosin heads and actin binding sites. Removal of a phosphate from a bound ATP molecule results in the pivoting of the myosin head, and movement of the actin molecule. Subsequent binding of another ATP molecule restarts the process (Figure (2.1)) [3].

The process of excitation contraction coupling translates an incoming action potential into tension produced by the muscle. A cardiac action potential results in the depolarization of the cell membrane. The T-tubules spread this polarization to the inner part of the cell. Depolarization results in the entry of calcium from the extracellular fluid into the interior of the cell. This rise in calcium is not sufficient alone to create an action potential, but triggers the release of more calcium from internal stores in the sarcoplasmic reticulum. This calcium release is termed the calcium induced calcium release. As the intracellular calcium concentration rises, the calcium binds to more molecules of troponin C, which orients the molecules such that actin and myosin may interact. Cross-bridges are formed and broken requiring the metabolism of ATP between the thin and thick filaments as the molecules slide past each other. Cross bridge cycling results in the production of tension within the muscle. The strength of tension produced is proportional to the levels of intracellular calcium in the muscle cell. Relaxation, or the end of contraction, occurs when the calcium levels are returned to the resting state through the action of the calcium ATPase and the calcium-sodium exchangers, both of which pump calcium against an electrochemical gradient back from the intracellular space into the sarcoplasmic reticulum [1-3].

The Three Dimensional Microstructure of the Heart

The cylindrical cardiac myocytes are the main structural component of the muscle fibers that compose the heart. Myocytes have a length of about 100 μm, and a diameter of approximately 20μm. Myocytes connect to adjacent myocytes at points termed intercalated discs. Due to the large metabolic requirements of myocardium, there is a dense network of blood vessels present in the myocardium. The myocytes and blood vessels combine with an extra cellular matrix composed of collagen, elastin, glycosaminoglycans, and glycoproteins to form the three dimensional structure of the heart [4].

The heart also has a connective tissue matrix described by Caufield and Borg as having three components: (1) the interconnections between myocytes, (2) connections between myocytes and capillaries, and (3) a collagen weave that surrounds groups of myocytes [5]. Robinson further defined the components of the extracellular matrix into three groups [6]. The first being the endomysium, which consists of radial collagen cords and a pericellular network of fibers that surround the myocyte, combined with a lattice of collagen fibrils and microthreads. The second component was termed the perimysium. The term perimysium describes the connective tissue meshwork that surrounds cell bundles. The third level of organization is the epimysium, which is a sheath of connective tissue that surrounds entire muscles, such as the papillary muscles [6].

Cardiac muscle fiber angle varies from roughly longitudinal at the endocardium, to circumferential near the midwall, to nearly longitudinal at the epicardium [7]. The extensive meshwork of extracellular matrix components that surrounds the muscle fibers makes the tissue significantly stiffer in the muscle fiber direction [4]. Having different material properties in different coordinate axes causes the material to be labeled as anisotropic. The transmural variation in the orientation of muscle fibers is significant for FEM modelling because it contributes to anisotropy. When we model the heart we account for the change in muscle fiber orientation by creating a local muscle fiber axis that rotates through the ventricular wall as the muscle fibers do. The material properties are then defined with respect to this local muscle fiber axis so that the FEM model correctly accounts for the greater stiffness in the muscle fiber direction.

Common Indices Used to Describe Cardiac Function

Many indices have been developed to evaluate the function of the heart. Each has its own limitations. Stroke volume is the volume of blood ejected during one heart beat. If V_{ed} is the volume of the heart at the end of diastole or filling, and V_{es} is the volume in the heart at the end of systole or after ejection, then the Stroke Volume (SV) is defined as:

$$SV = V_{ed} - V_{es}. \tag{2.1}$$

The Ejection Fraction (EF) is then defined to be the relative portion of the end diastolic volume that is ejected during one heart beat or:

$$EF = \frac{SV}{V_{ed}}. \tag{2.2}$$

The cardiac output is then defined to be the volume of blood ejected per unit time. This is related to the heart rate (HR) as follows:

$$CO = SV \times HR, \tag{2.3}$$

where the heart rate is defined as the number of beats per minute.

For a normal healthy person we would expect to see a SV of around 45 ml/m^2 (the dimension of area is to account for the variation in size of individuals), an EF of about 67%, and a cardiac output of about 70 ml/kg/min [8].

The Length Tension Relationship in Cardiac Muscle

The maximal tension that a cardiac myocyte can develop is related to its resting length. The tension developed is directly proportional to the degree of overlap between actin and myosin molecules in the sarcomere. The point at which maximal tension occurs in the cardiac sarcomere is at a resting length of about 2.4 μm (Figure (2.2)) [1].

This idea can be extended to form a length tension relationship in the ventricle as a whole. Since the length of the individual muscle fibers just before contraction in either ventricle depends upon the ventricular volume at end diastole, and the ventricular pressure produced during systole is related to the tension in individual muscle fibers, we can form a ventricular length tension relationship in terms of ventricular pressure and end diastolic volume. Thus up to a point, as end diastolic volume increases so will the end diastolic ventricular pressure.

The Frank-Starling law of the heart states that the volume of blood ejected by the ventricle depends on the volume of blood in the ventricle at the end of diastole. This occurs because an increase in end diastolic volume results in an increase in ventricular pressure, which increases the tension in the muscle fibers, and thus increases the strength of contraction. There is a relationship between cardiac output or stroke volume and ventricular end diastolic pressure, which is commonly represented as a type of Frank Starling curve (Figure (2.3)).

Thus as the ventricular end diastolic volume increases, so does the output of the heart. This relationship occurs up to a point at which the heart can no longer keep up with the demand placed upon it, and the curve levels off. A positive inotrope, something that increases contractility of the myocardium, shifts the Starling relation up (See Figure (2.3), Positive Effect). This shift occurs because the heart is ejecting more blood at a given end diastolic volume, and thus functioning better. A negative inotrope, something that decreases myocardial contractility, causes a decrease in stroke volume and cardiac output, and thus shifts the Starling relation down (See Figure (2.3), Negative Effect).

Means Used to Evaluate Cardiac Function

Evaluation of cardiac performance can be thought of at three levels of integration: (1) myocardial function, (2) chamber pump performance, and (3) integrated cardiac output [9]. Each of these levels can be thought to exert influence upon the other, however, changes in one level do not specifically imply changes in the other levels of integration. It is important to be able to evaluate all of the levels in order to assess cardiac performance.

Myocardial performance is largely influenced by four factors: (1) preload, (2) afterload, (3) the myocardial contractile state, and (4) heart rate and cardiac rhythm [9]. The terms preload and afterload were originally used to describe the loading conditions in isolated muscle fiber experiments [10]. Preload is used to refer to the degree of stretch the myocardium is experiencing before contraction starts. Up to a certain point, due to the increased cross-bridge formations in the muscle fibers, increased preload results in an increased strength of contraction (Starling Relation) (Figure (2.2)) Afterload refers to the tension the muscle fiber experiences during the shortening phase of contraction [11]. Myocardial contractile state refers to the cellular basis of muscle contraction described above. Increases in heart rate result in increased in myocardial contractility due to the inability of the mechanisms for calcium exit to keep up with the increased rate of calcium entry produced by rapid stimulation [1].

The Left Ventricular Pressure-Volume Relationship

The pressure-volume relationship provides an important transition from muscle function to pump function in the left ventricle. The relationship between left ventricular pressure and left ventricular volume throughout the cardiac cycle forms a loop that is commonly broken into four phases (Figure (2.4)). The first of these phases is isovolumic contraction (Figure (2.4) points a to b). The beginning of this phase (Figure (2.4) point a) signals the end of diastole, and the beginning of contraction. The aortic and pulmonary valves in the heart are closed, thus as contraction begins ventricular pressure rises sharply, causing the mitral and tricuspid valves to shut. The volume in the ventricle at this time is the same as at the end of diastole. The second phase of the cardiac cycle is that of ventricular ejection (Figure (2.4) points b to c). This phase begins when the pressure developed during isovolumic systole in the ventricle is greater than the aortic pressure, which causes the aortic valve to open. The pressure in the ventricle continues to rise as the muscle is still contracting, but eventually begins to decline as the blood volume in the ventricle is reduced. The remaining volume at the end of contraction is termed the end systolic volume. Recall that the difference between the end diastolic volume and the end systolic volume is the stroke volume. When the ventricular pressure decreases below that in the aorta, the aortic valve closes and the ventricle enters the third phase of the cardiac cycle, that of isovolumic relaxation (Figure (2.4), points c to d). The volume in the ventricle remains constant during this phase, but the pressure decreases rapidly as the heart diastolic relaxation. Once the ventricular pressure falls below that of the left atrium, the mitral valve opens and the fourth phase of the cardiac cycle begins, that of ventricular filling (Figure (2.4) points d to a). During this phase blood enters into and fills the ventricle from the atrium [1, 2].

Pressure volume loops are useful for visualizing changes that can occur with the preload, afterload, or contractility of the heart. Changes in the preload reflect changes in the return of blood to the heart (end diastolic volume). If the preload is increased in healthy individuals, the stroke volume will also increase up to a point. The afterload is the pressure against which the ventricles must propel blood (aortic pressure). If aortic pressure is increased, the ventricle will have to reach a greater ventricular pressure to open the aortic valve. Similarly in the ejection phase of the cardiac cycle, the increased afterload will result in the closing of the aortic valve at a greater ventricular volume (increased end systolic volume). This increase in afterload will result in a decreased stroke volume. Contractility is the term used to define the force of muscular contraction. If the contractility of the ventricle is increased, the ventricle is able to expel a larger amount of blood during systole. Thus stroke volume increases, and end systolic volume decreases [1].

Figure (2.4) also shows the systolic elastance (end systolic pressure-volume relation (ESPVR)) and diastolic compliance curves (end diastolic pressure-volume relation (EDPVR)). The diastolic compliance curve determines the pressure-volume relationship during the filling phase of diastole. The systolic elastance curve is determined by calculating pressure-volume relations at end systole under variable loading conditions

The effects of both systolic and diastolic dysfunction can be observed in pressure volume loops. Systolic dysfunction shifts the systolic elastance curve to the right and decreases the slope (Figure (2.5)). The end systolic volume increases from c to c', which results in a decreased stroke volume. Diastolic dysfunction generally results in a shift of the diastolic compliance curve up and to the left (Figure (2.6)). The end diastolic volume is decreased from a to a', which causes the stroke volume to decrease [1].

The area of the pressure-volume loop for the left ventricle is termed the stroke work (SW). This is the external work performed by the left ventricle. The remaining area under the systolic elastance curve is the potential energy (PE) produced by the ventricle, but not resulting in external work. The sum of the SW and the PE is termed the pressure-volume area.

Assessment of Left Ventricular Function

$dP/dt_{\max}$

A common index used to measure the contractile state of the left ventricle is the maximum rate of rise of ventricular pressure ($dP/dt_{\max}$). This measure has been shown to be highly sensitive to acute changes in contractility [12]. $dP/dt_{\max}$ is usually observed immediately before the opening of the aortic valve, but this can be delayed in the presence of a severely diseased left ventricle. $dP/dt_{\max}$ is relatively independent of afterload, but has been shown to be extremely sensitive to preload [12]. Additionally, $dP/dt_{\max}$ shows wide variation between individuals, and is more useful for assessing directional changes in contractility associated with intervention [9].

Left Ventricular End Diastolic Pressure-Volume Relation

The LV EDPVR (diastolic compliance curve) relates the end diastolic pressure (P_{ED}) and volume (V_{ED}). This relationship is often fit to a quadratic polynomial:

$$P_{ED} = \beta_o + \beta_1 V_{ED} + \beta_2 V_{ED}^2 \tag{2.4}$$

where β_o, β_1, and β_2 are the stiffness parameters defining the EDPVR. This relationship does, however, only include the diastolic state of the ventricle and not the systolic state.

Left Ventricular End Systolic Pressure-Volume Relation

The left ventricular ESPVR defines the systolic elastance curve mentioned earlier. This curve, relating the end systolic pressure (P_{ES}) and volume (V_{ES}) can be approximated as a line, and thus described by a slope and intercept:

$$P_{ES} = E_{ES}\left(V_{ES} - V_o\right) \tag{2.5}$$

where E_{ES} is termed the end systolic elastance and V_o is the volume intercept. The end systolic elastance represents the stiffness of the left ventricle and shows how sensitive the ejection volume will be to changes in afterload. As contractility increases, so does the end systolic elastance. Similarly a decrease in contractility is represented by a decrease in the end systolic elastance. There are many clinical difficulties associated with the measurement of the ESPVR. To obtain an accurate ESPVR, a variety of loading conditions must be obtained. The methods used to obtain these loading conditions may themselves alter the ESPVR [13-15]. Another difficulty is the exact determination of end systole. The upper left corner of the pressure-volume loop may not exactly correlate with the closure of the aortic valve [16]. Finally the end systolic elastance is dependent upon the size of the ventricle, making it difficult to define a precise range E_{ES} [17].

$dP/dt_{\max}$ - End Diastolic Volume Relation

The relationship between $dP/dt_{\max}$ and the V_{ED} has been shown to be linearly related [12]. The slope of this relationship represents the maximum rate of change of ventricular elastance during contraction. This relation is, however, less stable than the ESPVR [18] and can only be defined by preload reductions, and not drug induced increases in load [19].

Stroke Work – End Diastolic Volume Relation

The relationship between the SW and V_{ED} has been shown to be linearly related and insensitive to arterial load under physiologic conditions [20-22]. The slope of this line has been termed the preload recruitable stroke work (PRSW). Since this measure is influence by both the ESPVR and EDPVR, it is a measure of the pump function of the left ventricle [18].

Maximum Power

The power generated by the left ventricle can be calculated as the product of the aortic flow and pressure. This value has been shown to be reflective of changes in contractile state, insensitive to changes in the arterial circulation and linearly related to the square of the end diastolic volume [23, 24]

Frank Starling Relations

Starling relations relate the input of the heart to its output. The output is typically measured using stroke volume, cardiac output or stroke work (as described above). The input is typically represented by end diastolic pressure. An upward shift in these curves represents positive effect on pump performance, while a downward shift represents a negative effect on pump performance.

Choice of index used to interpret finite element model results

In order to interpret the results predicted by finite element simulations used in this thesis, we must be able to isolate the most relevant cardiac function indices. Those that depend upon time (cardiac output, $dP/dt_{\max}$, and maximum power) are not applicable as the models we use are quasi-static, and thus the relation to the time domain is not available. The EF is used by many as an evaluation of cardiac function, but may not be as applicable as one of the variables being directly modified by the computer models is the end diastolic volume, the denominator of the EF calculation. The use of the stroke volume or stroke work alone ignores the influence of preload upon cardiac performance and diastolic function. Both the ESPVR (systolic elastance) and EDPVR (diastolic compliance) provide good information on systole and diastole respectively. These relations are, however, separate from one another and represent the emptying and filling of the left ventricle. In order to relate these two, the use of the stroke volume or stroke work in the form of a Starling relation provides the most useful information about the function of the left ventricle as a whole. These thoughts are summarized in Table 2.I. Although other indices will be presented throughout the thesis to focus on specifically diastolic or systolic function, the Starling relation will be used to evaluate the function of the ventricle as a whole.

Index	Comment
Systolic Function	
ESPVR	Only reflects the systolic performance of the ventricle
Ejection Fraction	The denominator of this value is the independent variable that is modified in the simulations
Stroke Volume	Stroke volume alone does not reflect preload dependence
Stroke Work	Stroke work alone does not reflect preload dependence
Cardiac Output	Depends upon time, not applicable to our models
dP/dt_{max}	Depends upon time, not applicable to our models
Maximum Power	Depends upon time, not applicable to our models
PRSW	Based upon the assumption that the relationship is linear, which does not hold true in all of our modeling
Diastolic Function	
EDPVR	Only reflects the diastolic performance of the ventricle
Global Function	
Starling Relations	Provides the best information on pump function for our use

Table 2.I Cardiac Evaluation Indices - Summary of indices used in the evaluation of cardiac function from finite element models.

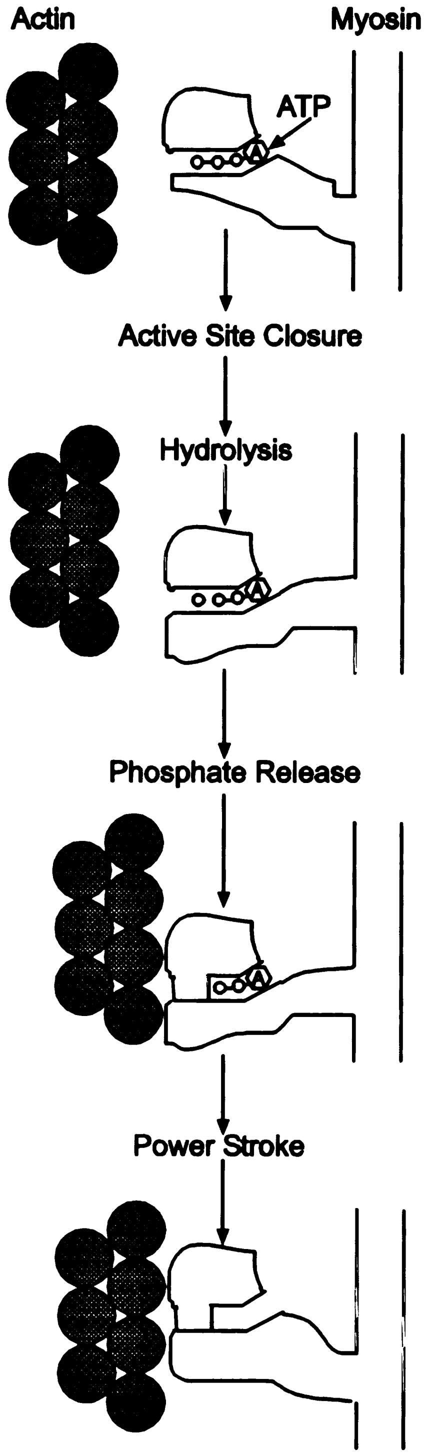
Actin
Myosin
ATP
A
Active Site Closure
Hydrolysis
Phosphate Release
Power Stroke

Figure 2.1 – Sliding Filament Theory – ATP hydrolysis causes a conformational shift in the myosin heads and closure of the active site. Following phosphate release myosin binds actin releasing ADP. This release triggers the power stroke which moves the myosin head along the actin molecule.

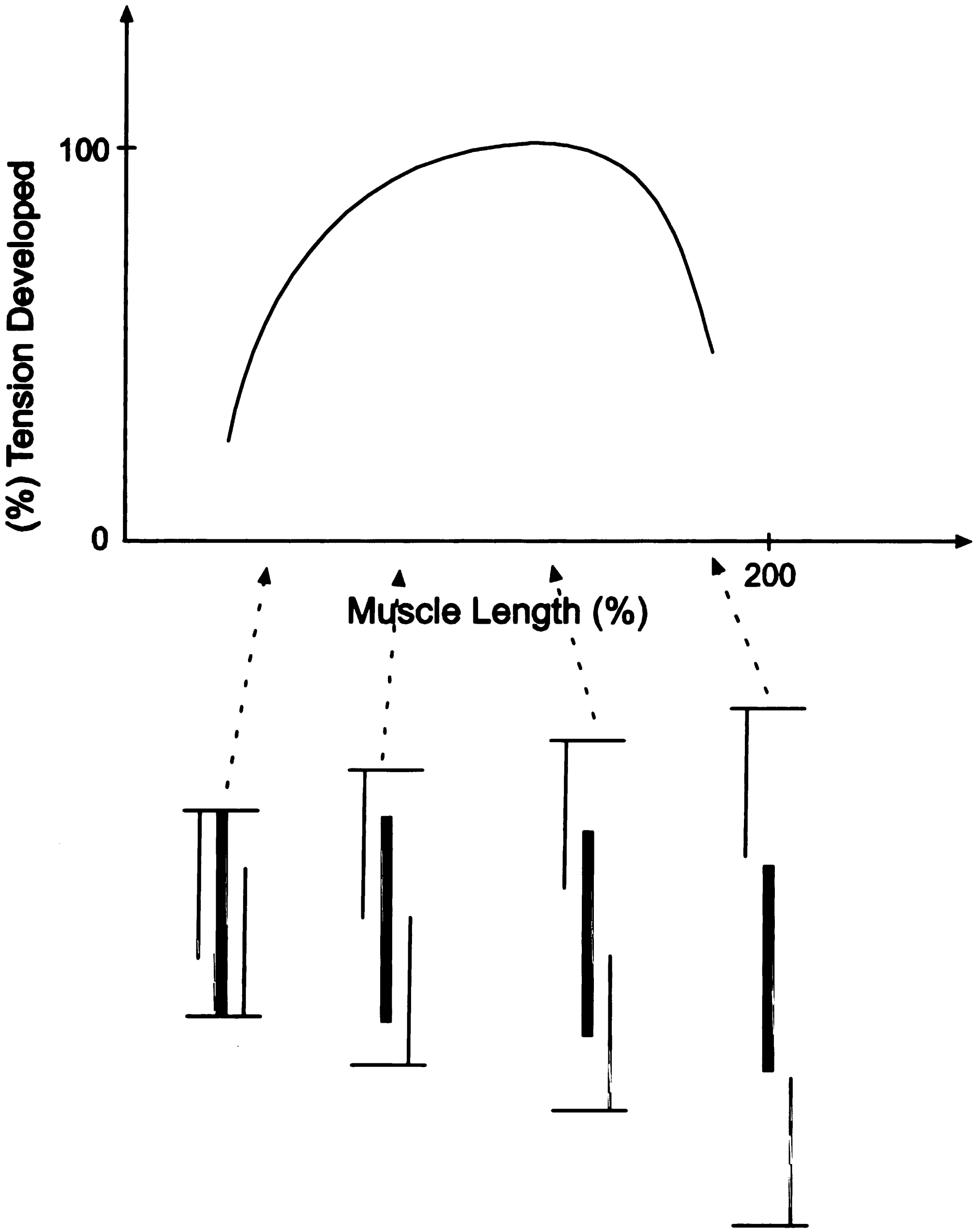

Figure 2.2 – Length Tension Relationship in Muscle – The degree of actin myosin overlap influences the developed tension in muscle. When the muscle length is short, ineffective crossbridge formation causes low developed tension. As the muscle length increases, developed tension increases until the point at which fewer cross bridges are formed because of the lack of overlap between actin and myosin.

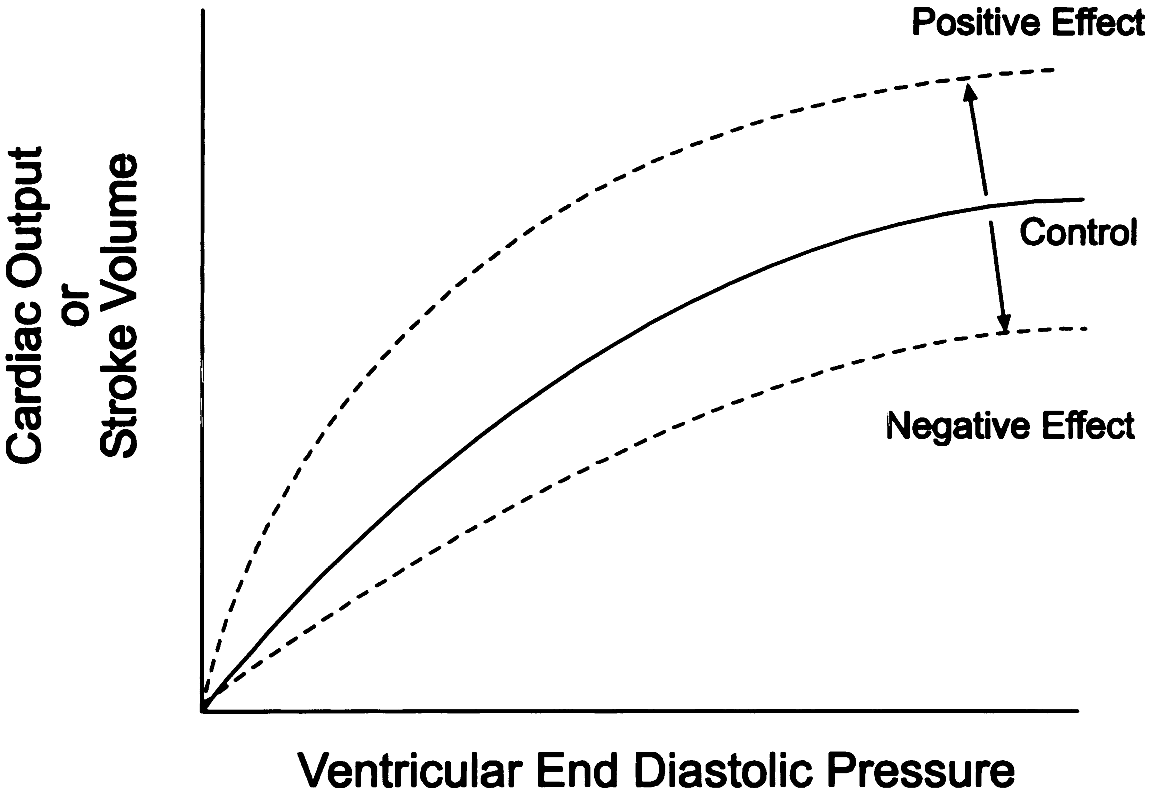

Figure 2.3. The Starling Relation. (Control) As the end diastolic pressure is increased, so is the Cardiac Output and Stroke Volume. This increase occurs up to a point at which the heart can no longer keep up with the demand placed upon it and the relation flattens. (Positive Effect) A treatment that has a positive effect shifts the Starling Relation up resulting in a greater Cardiac Output for a given end diastolic pressure compared to the control. (Negative Effect) A treatment that has a negative effect will result in a downwards shift of the Starling Relation. We see decreased Cardiac Output or Stroke Volume for a given end diastolic pressure when compared to a control.

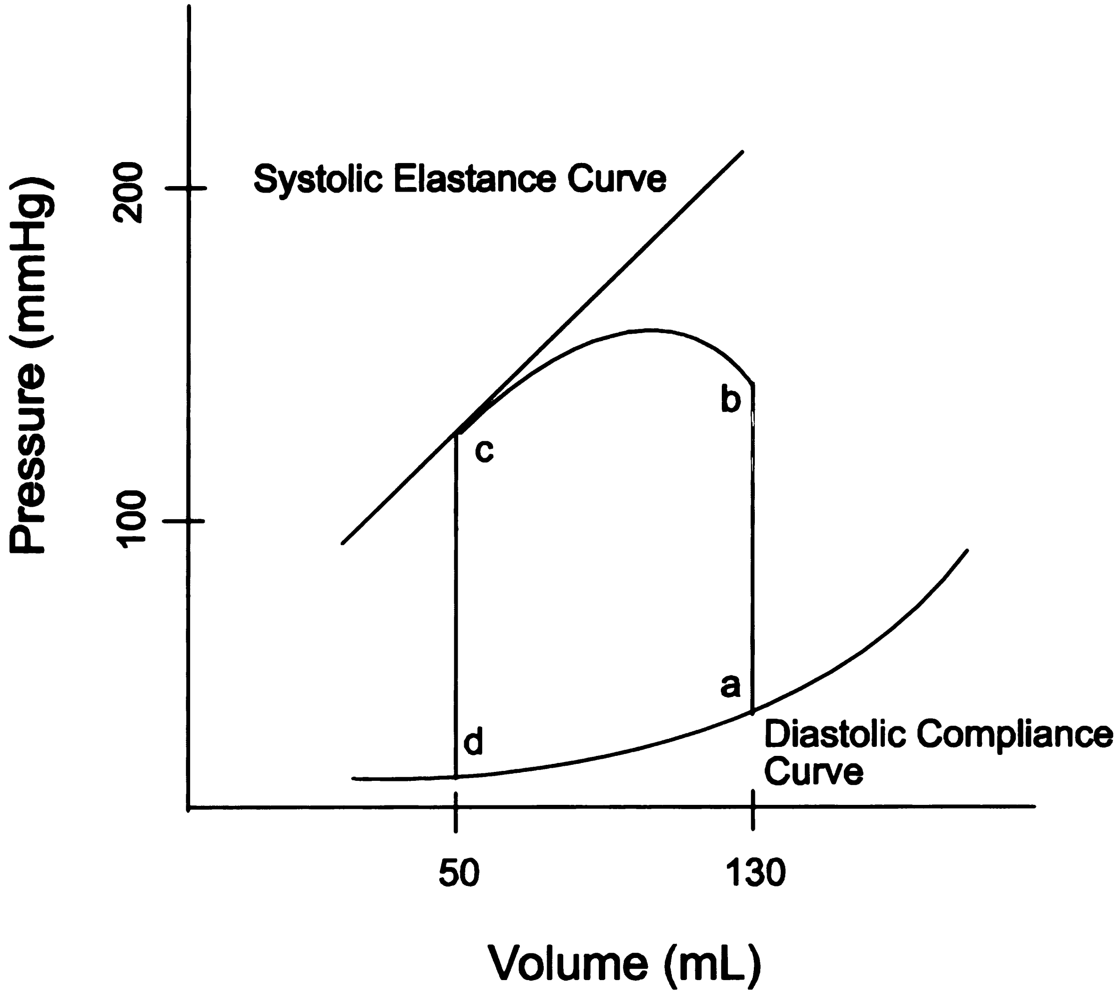
Pressure (mmHg)
200
100
Systolic Elastance Curve
b
c
a
d
Diastolic Compliance Curve
50
130
Volume (mL)

Figure 2.4. The Pressure Volume Relation for the Left Ventricle. Isovolumic contraction occurs between points a and b where we see an increase in left ventricular pressure with no change in volume. The ejection phase of systole is seen from points b to c. The pressure-volume relation at the end of this phase (point c) for varying load conditions forms the basis for the systolic elastance curve. The upper left hand corner of the loop represents one point on the end systolic elastance curve. The period of isovolumic relaxation is shown from points c to d. Diastolic filling is represented by points d to a.

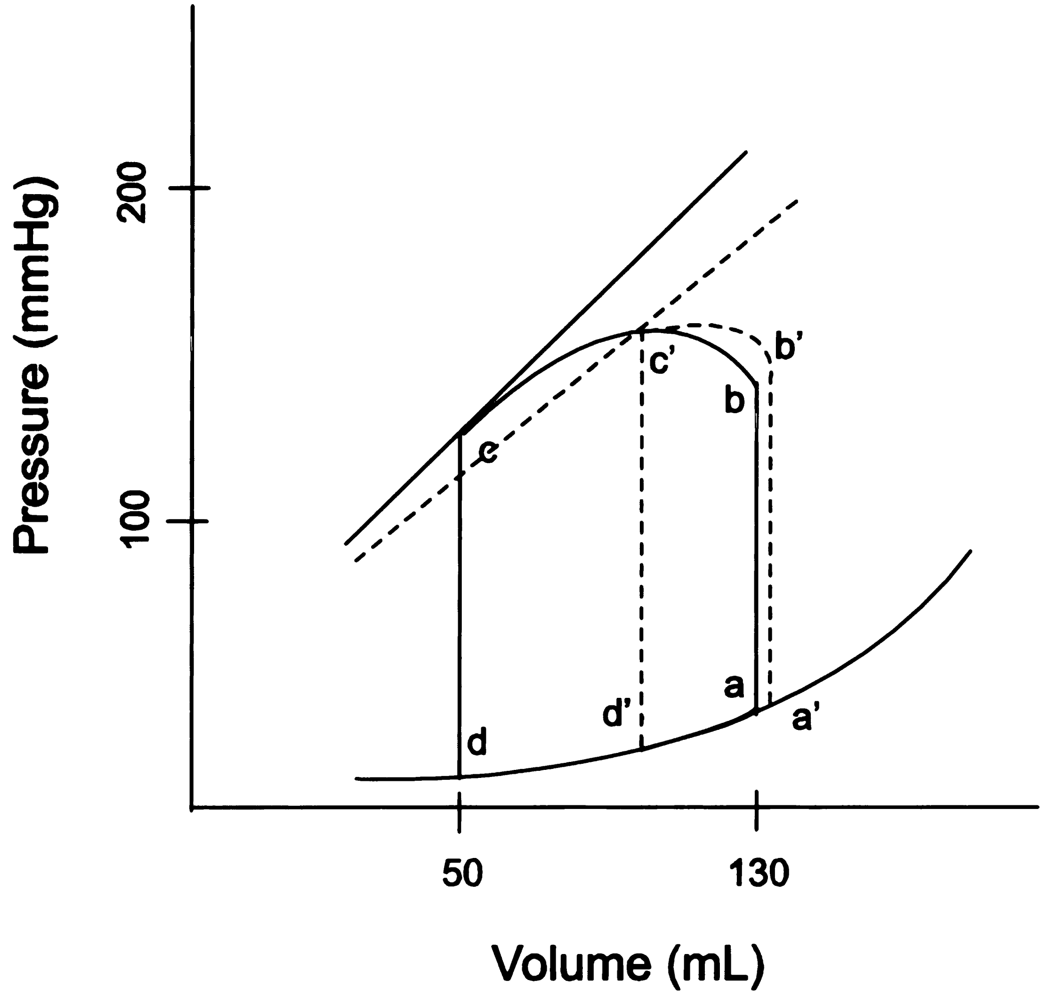

Figure 2.5. Systolic Dysfunction. The effects of systolic dysfunction are shown by the dashed lines. Systolic dysfunction shifts the systolic elastance curve to the right and decreases the slope. This results in a decrease of the stroke volume from the volume defined by points c and b to the volume defined by points c’ and b’.

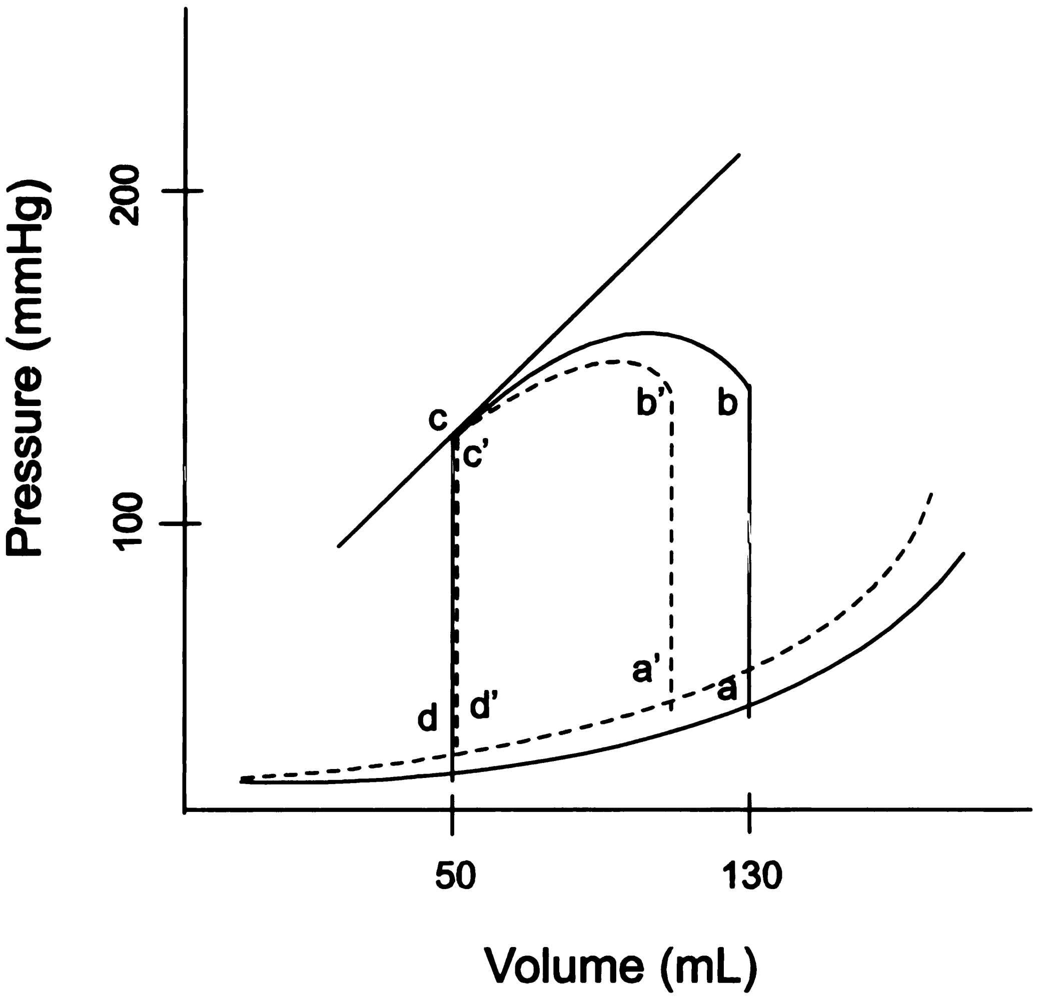

Figure 2.6. Diastolic Dysfunction. The effects of diastolic dysfunction are represented by the dashed lines. Diastolic dysfunction results in a shift of the diastolic compliance curve up and to left. This decreases the stroke volume by decreasing the end diastolic volume (points a and b are decreased to a' and b').

References:

1. Berne, R.M. and M.N. Levy, *Cardiovascular physiology*. 8th ed. The Mosby physiology monograph series. 2001, St. Louis, MO: Mosby. xiv, 312.
2. Guyton, A.C. and J.E. Hall, *Textbook of medical physiology*. 9th ed. 1996, Philadelphia: W.B. Saunders. xliii, 1148.
3. Lodish, H.F., *Molecular cell biology*. 2000, W.H. Freeman: New York.
4. Glass, L., et al., *Theory of heart : biomechanics, biophysics, and nonlinear dynamics of cardiac function*. 1991, New York: Springer-Verlag. xvii, 611.
5. Caulfield, J.B. and T.K. Borg, *The collagen network of the heart.* Lab Invest, 1979. **40**(3): p. 364-72.
6. Robinson, T.F., L. Cohen-Gould, and S.M. Factor, *Skeletal framework of mammalian heart muscle. Arrangement of inter- and pericellular connective tissue structures.* Lab Invest, 1983. **49**(4): p. 482-98.
7. Streeter, D.D., Jr., et al., *Fiber orientation in the canine left ventricle during diastole and systole.* Circ Res, 1969. **24**(3): p. 339-47.
8. Kennedy, J.W., et al., *Quantitative angiocardiography. I. The normal left ventricle in man.* Circulation, 1966. **34**(2): p. 272-8.
9. Little, W.C., *Assessment of Normal and Abnormal Cardiac Function*, in *Heart Disease*, E. Braunwald, Zipes, D., Libby, P., Editor. 2001, W.B. Saunders Company: Philadelphia, PA. p. 479-502.
10. Sonnenblick, E.H., *Force-velocity relations in mammalian heart muscle.* Am J Physiol, 1962. **202**: p. 931-939.

11. Sagawa, K., ,Maughan, W., Suga, H., Sunagawa, K. Cardiac Contraction and the Pressure-Volume Relationship. 1988, New York: Oxford University Press. 232-298.

12. Little, W.C., *The left ventricular dP/dtmax-end-diastolic volume relation in closed-chest dogs.* Circ Res, 1985. **56**(6): p. 808-15.

13. Crottogini, A.J., et al., *Left ventricular end-systolic elastance is incorrectly estimated by the use of stepwise afterload variations in conscious, unsedated, autonomically intact dogs.* Circulation, 1994. **90**(3): p. 1431-40.

14. Freeman, G.L., W.C. Little, and R.A. O'Rourke, *The effect of vasoactive agents on the left ventricular end-systolic pressure-volume relation in closed-chest dogs.* Circulation, 1986. **74**(5): p. 1107-13.

15. Sodums, M.T., et al., *Evaluation of left ventricular contractile performance utilizing end-systolic pressure-volume relationships in conscious dogs.* Circ Res, 1984. **54**(6): p. 731-9.

16. Brickner, M.E. and M.R. Starling, *Dissociation of end systole from end ejection in patients with long-term mitral regurgitation.* Circulation, 1990. **81**(4): p. 1277-86.

17. Hsia, H.H. and M.R. Starling, *Is standardization of left ventricular chamber elastance necessary?* Circulation, 1990. **81**(6): p. 1826-36.

18. Little, W.C., et al., *Comparison of measures of left ventricular contractile performance derived from pressure-volume loops in conscious dogs.* Circulation, 1989. **80**(5): p. 1378-87.

19. Noda, T., et al., *Curvilinearity of LV end-systolic pressure-volume and dP/dtmax-end-diastolic volume relations.* Am J Physiol, 1993. **265**(3 Pt 2): p. H910-7.

20. De Tombe, P.P., et al., *Ventricular stroke work and efficiency both remain nearly optimal despite altered vascular loading.* Am J Physiol, 1993. **264**(6 Pt 2): p. H1817-24.

21. Little, W.C. and C.P. Cheng, *Effect of exercise on left ventricular-arterial coupling assessed in the pressure-volume plane.* Am J Physiol, 1993. **264**(5 Pt 2): p. H1629-33.

22. Little, W.C. and C.P. Cheng, *Left ventricular-arterial coupling in conscious dogs.* Am J Physiol, 1991. **261**(1 Pt 2): p. H70-6.

23. Nakayama, M., et al., *Optimal preload adjustment of maximal ventricular power index varies with cardiac chamber size.* Am Heart J, 1998. **136**(2): p. 281-8.

24. Kass, D.A. and R. Beyar, *Evaluation of contractile state by maximal ventricular power divided by the square of end-diastolic volume.* Circulation, 1991. **84**(4): p. 1698-708.

Chapter 3

The Application of FEM to Cardiac Mechanics.

Introduction

The finite element method (FEM) has been used for analysis of biologic materials for a number of years. FEM has been shown to be valuable in the field of orthopedics. Its use in cardiovascular analysis has been more limited. In this chapter the formulation of the FEM will be presented in the context of cardiac mechanics. This is complicated by the fact that the FEM needs to account for finite elastic deformations of a nonlinear anisotropic soft tissue. Specific features of this derivation are aimed at easing the complexity of the model of the left ventricle. First the mathematics of the governing equations need to be developed in general curvilinear coordinates. This will ease the later transition into a prolate spheroidal coordinate system that represents the ventricular geometry and boundry conditions well. To accurately represent the left ventricle, the model needs to account for not only the anisotropy of the material properties, but also the changing material axis of this anisotropy along the muscle fiber direction.

Prolate Spheroidal Coordinate System

The prolate spheroidal coordinate system is chosen as the global curvilinear coordinate system for all of the simulations presented in this thesis (Figure (3.1)). This coordinate system is especially convenient for modeling of the heart as the truncated ellipsoids that are produced as volume elements in this system closely resemble the shape of the left ventricle. The following relations show the conversion between the Cartesian reference system and the prolate spheroidal system:

$$Y_1 = d \cosh \Lambda \cos \mathrm{M} \tag{3.1}$$

$$Y_2 = d \sinh \Lambda \sin \mathrm{M} \cos \Theta \tag{3.2}$$

$$Y_2 = d \sinh \Lambda \sin \mathrm{M} \sin \Theta \tag{3.3}$$

where d is the focal length of the ellipsoid.

Coordinate Systems Used

Of key importance in the development of this method is the ability to describe the deformation of an elastic body in which a point in the undeformed body B with position vector **R**, moves to the deformed body $\overline{\mathrm{B}}$ with position vector **r**. Generally, capital letters are used to represent the undeformed state while lower case letters are used to represent the deformed situation. In addition the base vectors **G** and **g** are used to represent the base vectors in the undeformed and deformed body respectively.

In order to formulate the finite element method for the problems presented in the remainder of this thesis, it is necessary to define four coordinate systems (Figure (3.2)). Most familiar is the Cartesian coordinate system $\{Y_1, Y_2, Y_3\}$. In the undeformed body B, the coordinates will be represented by Y_R, with the indices of R and S. The deformed body $\overline{\mathrm{B}}$ will have the coordinates of y_r, and the indices of r and s will be used. This serves as the global reference system. Second is an orthogonal curvilinear coordinate system $\{\Theta_1, \Theta_2, \Theta_3\}$ that is used to describe the geometry and deformation. In the undeformed body B, the coordinates will be represented by Θ_A, with the indices of A and B. The deformed body $\overline{B}$ will have the coordinates of θ_α, and the indices of α and β will be used. The curvilinear system is chosen as curvilinear systems more easily represent the shape of the left ventricle than Cartesian systems. For the purposes of the finite element method a normalized general curvilinear coordinate system is developed within a theoretical finite element $\{\xi_1, \xi_2, \xi_3\}$. In the undeformed body B, the coordinates will be represented by ξ_K, with the indices of K and L. Finally a local orthonormal body coordinate system is developed $\{X_1, X_2, X_3\}$ where the X_1 and X_2 axis are rotated about an angle η_1 that serves to represent the muscle fiber angle. In the undeformed body B, the coordinates will be represented by X_I, with the indices of I and J. The deformed body $\overline{B}$ will have the coordinates of x_i, and the indices of i and j will be used.

Given two position vectors in the global Cartesian reference system

$$\mathbf{R} = Y^R \mathbf{e_R} \tag{3.4}$$

and

$$\mathbf{r} = y^r \mathbf{e_r} \tag{3.5}$$

for the undeformed and deformed state respectively it is possible to define the base vectors in the more convenient curvilinear coordinate system as

$$\mathrm{G}_{\mathrm{A}}^{(\theta)} = \frac{\partial \mathrm{Y}^{\mathrm{R}}}{\partial \Theta^A} \mathbf{e}_{\mathrm{R}} \tag{3.6}$$

and

$$g_{\alpha}^{(\theta)} = \frac{\partial y^{r}}{\partial \Theta^{\alpha}} e_{r} \tag{3.7}$$

where the metric tensors are described by

$$G_{AB}^{(\theta)} = \frac{\partial Y^{R} \partial Y^{R}}{\partial \Theta^{A} \partial \Theta^{B}} \tag{3.8}$$

and

$$g_{\alpha\beta}^{(\theta)} = \frac{\partial y^{r} \partial y^{r}}{\partial \theta^{\alpha} \partial \theta^{\beta}}\,. \tag{3.9}$$

When working in a prolate spheroidal coordinate system it is important to have $G_{AB}^{(\theta)}$ defined explicitly:

$$G_{AB}^{(\theta)} = d^{2}\begin{bmatrix} \sinh^{2}\Lambda + \sin^{2}\mathrm{M} & 0 & 0 \\ 0 & \sinh^{2}\Lambda + \sin^{2}\mathrm{M} & 0 \\ 0 & 0 & \sinh^{2}\Lambda + \sin^{2}\mathrm{M} \end{bmatrix} \tag{3.10}$$

and similarly

$$G_{\alpha\beta}^{(\theta)} = d^{2}\begin{bmatrix} \sinh^{2}\lambda + \sin^{2}\mu & 0 & 0 \\ 0 & \sinh^{2}\lambda + \sin^{2}\mu & 0 \\ 0 & 0 & \sinh^{2}\lambda + \sin^{2}\mu \end{bmatrix} \tag{3.11}$$

Upon conversion to a finite element model and usage of the normalized coordinate system the base vectors become

$$\mathrm{G}_{\mathrm{K}}^{(\xi)} = \frac{\partial \Theta^{A}}{\partial \xi^{K}} \mathrm{G}_{\mathrm{A}}^{(\theta)} \tag{3.12}$$

and

$$\mathrm{g}_{K}^{(\xi)} = \frac{\partial \theta^{\alpha}}{\partial \xi^{K}} \mathrm{g}_{\alpha}^{(\theta)} \tag{3.13}$$

and the metric tensors become

$$\mathrm{G}_{\mathrm{KL}}^{(\xi)} = \frac{\partial \Theta^{A} \partial \Theta^{B}}{\partial \xi^{K} \partial \xi^{L}} \mathrm{G}_{\mathrm{AB}}^{(\theta)} \tag{3.14}$$

and

$$\mathrm{g}_{KL}^{(\xi)} = \frac{\partial \theta^{\alpha} \partial \theta^{\alpha}}{\partial \xi^{K} \partial \xi^{L}} \mathrm{g}_{\alpha\beta}^{(\theta)} . \tag{3.15}$$

In the fourth coordinate system, those with respect to the local fiber direction, the covariant base vectors and metric tensors are defined as:

$$\mathrm{G}_{\mathrm{I}}^{(x)} = \frac{\partial \xi^{K}}{\partial X^{I}} \mathrm{G}_{\mathrm{K}}^{(\xi)} \tag{3.16}$$

and

$$\mathrm{g}_{i}^{(x)} = \frac{\partial \xi^{K}}{\partial x^{i}} \mathrm{g}_{K}^{(\xi)} \tag{3.17}$$

or

$$g_I^{(x)} = \frac{\partial \xi^K}{\partial X^I} g_K^{(\xi)} \tag{3.18}$$

and

$$G_{IJ}^{(x)} = \frac{\partial \xi^K \partial \xi^L}{\partial X^I \partial X^J} G_{KL}^{(\xi)} = \delta_{IJ} \tag{3.19}$$

and

$$g_{ij}^{(x)} = \frac{\partial \xi^K \partial \xi^K}{\partial x^i \partial x^j} g_{KL}^{(\xi)} = \delta_{ij} \tag{3.20}$$

or

$$g_{IJ}^{(x)} = \frac{\partial \xi^K \partial \xi^L}{\partial x^i \partial x^j} g_{KL}^{(\xi)}, \tag{3.21}$$

where δ is the Kronecker Delta. The Kronecker Delta is defined as:

$$\delta_{11} = \delta_{22} = \delta_{33} = 1$$
$$\delta_{12} = \delta_{21} = \delta_{13} = \delta_{31} = \delta_{23} = \delta_{32} = 0$$

The above identities provide useful relations between the coordinate systems that will be used to our advantage in the derivations of the governing equations for Finite Elasticity.

Governing Equations of Finite Elasticity

Consider an arbitrary elastic body in B with surface A and volume V loaded with a surface traction **s**, at the boundary of B that is in equilibrium with **t** the internal traction vector. The traction vector can be expressed as a function of the second Piola-Kirchhoff stress tensor, **P**, the unit normal to the surface A, **N** and the deformation gradient tensor **F** as

$$t = t^i\, g_i^{(x)} = N_I P^{IJ} F_J^{\cdot i}\, g_i^{(x)} \tag{3.22}$$

where N_I is referred to the X_I coordinates in B, and **F** is defined as

$$F_J^{\cdot i} = \frac{\partial x^i}{\partial X^J}\,. \tag{3.23}$$

Thus we have defined the basis for a constitutive relation based upon a coordinate system that accurately simplifies the structure of the left ventricle, the local fiber coordinates. However, this coordinate system is not very convenient to represent the displacement vector between the two position vectors **r** and **R**:

$$u = r - R\,. \tag{3.24}$$

This vector is easily represented in the global curvilinear coordinate system, and so we will transform the traction vector in such a manner as it is defined in this coordinate system. This transformation is accomplished using the base vector relation defined in equation (3.22) above:

$$t = t^i \frac{\partial \theta^\alpha}{\partial x^i} g_\alpha^{(\theta)} = N_I P^{IJ} F_J^{\cdot\alpha}\, g_\alpha^{(\theta)} \tag{3.25}$$

where the deformation gradient tensor is now defined as

$$F_J^{\cdot\alpha} = \frac{\partial\theta^\alpha}{\partial X^J}\,. \tag{3.26}$$

When the body is subjected to an arbitrarily small displacement $\delta\mathbf{u}$ which satisfies compatibility and displacement boundary conditions on A the principle of virtual work requires that

$$\int_{A_2} \mathrm{s}\cdot\delta\,\mathrm{u}\,dA = \int_{A} \mathrm{t}\cdot\delta\,\mathrm{u}\,dA \tag{3.27}$$

If we plug in the definition for **t** defined in Equation (3.25) above and note that $\delta\,\mathrm{u} = \delta u_\beta\,\mathrm{g}^{(\theta)\beta}$ we get

$$\int_{A_2} \mathrm{s}\cdot\delta\,\mathrm{u}\,dA = \int_{A} \mathrm{N_I P^{IJ} F_J^{\cdot\alpha}}\,\delta u_\alpha\,dA \tag{3.28}$$

which after the use of Gauss' theorem becomes

$$\int_{A_2} \mathrm{s}\cdot\delta\,\mathrm{u}\,dA = \int_{V}\left\{\left(P^{IJ}F_J^{\cdot\alpha}\right)\Big|_I\,\delta u_\alpha + P^{IJ}F_J^{\cdot\alpha}\,\delta u_\alpha\big|_I\right\}dV\,. \tag{3.29}$$

The " $\big|_I$ " means covariant differentiation with respect to X_I:

$$\delta u_\alpha\big|_I = \frac{\partial \delta u_\alpha}{\partial X^I} - \Gamma^\beta_{\alpha I}\delta u_\beta . \tag{3.30}$$

The Christoffel symbol, $\Gamma^\beta_{\alpha I} = -\mathrm{g}^{(\theta)\beta}_{,I}\cdot \mathrm{g}^{(\theta)}_\alpha$, depends upon the choice of coordinate system. In the case of our prolate spheroidal coordinate system the Christoffel symbols are evaluated as:

$$\Gamma^1_{1I} = \frac{\sinh 2\lambda\cdot\lambda_{,I} + \sin 2\mu\cdot\lambda_{,I}}{2\left(\sinh^2\lambda + \sin^2\mu\right)} \tag{3.31}$$

$$\Gamma^2_{1I} = \frac{\sinh 2\lambda\cdot\lambda_{,I} - \sin 2\mu\cdot\lambda_{,I}}{2\left(\sinh^2\lambda + \sin^2\mu\right)} \tag{3.32}$$

$$\Gamma^3_{1I} = \coth\lambda\cdot\theta_{,I} \tag{3.33}$$

$$\Gamma^1_{2I} = -\Gamma^2_{1I} \tag{3.34}$$

$$\Gamma^2_{2I} = \Gamma^1_{1I} \tag{3.35}$$

$$\Gamma^3_{2I} = \cot\mu\cdot\theta_{,I} \tag{3.36}$$

$$\Gamma^1_{3I} = \frac{-\sinh 2\lambda\cdot\sin^2\mu}{2\left(\sinh^2\lambda + \sin^2\mu\right)}\cdot\theta_{,I} \tag{3.37}$$

$$\Gamma^2_{3I} = \frac{-\sinh^2\lambda\cdot\sin 2\mu}{2\left(\sinh^2\lambda + \sin^2\mu\right)}\cdot\theta_{,I} \tag{3.38}$$

$$\Gamma^3_{3I} = \coth\lambda\cdot\lambda_{,I} + \cot\mu\cdot\mu_{,I} \tag{3.39}$$

Usage of Cauchy's first law of motion further simplifies the integral expression in Equation (3.29). Cauchy's first law can be expressed as

$$\left(P^{IJ} F_J^\alpha\right)\Big|_I + \rho b^\alpha = \rho f^\alpha \tag{3.40}$$

where ρ is the material density, f is the acceleration and b is the body force per unit mass. Equation (3.29) now simplifies to

$$\int_V \left\{\left(P^{IJ} F_J^\alpha\right)\Big|_I \delta u_\alpha\right\} dV = \int_V \left\{\rho\left(b^\alpha - f^\alpha\right)\right\} \delta u_\alpha dV + \int_{A_2} \mathrm{s} \cdot \delta \mathrm{u}\, dA. \tag{3.41}$$

We seek a weak form of this equation for use in finite element analysis. This is accomplished by using a strain energy function to define the second Piola-Kirchhoff stress:

$$P^{IJ} = \frac{1}{2}\left(\frac{\partial W}{\partial E_{IJ}} + \frac{\partial W}{\partial E_{JI}}\right) \tag{3.42}$$

in which **E** is Green's Strain tensor defined with respect to the fiber coordinates:

$$E_{IJ} = \frac{1}{2}\left(g_{IJ}^{(x)} - \delta_{IJ}\right). \tag{3.43}$$

In this case $g_{IJ}^{(x)}$ is the right Cauchy-Green deformation tensor whose determinant $g^{(x)}$, is equal to one owing to incompressibility. This condition is enforced through the use of a Lagrange multiplier:

$$W(E) = \dot{W}(E) - \frac{p}{2}\left(g^{(x)} - 1\right), \tag{3.44}$$

then Equation (3.42) can be written as

$$P^{IJ} = \frac{1}{2}\left(\frac{\partial \dot{W}}{\partial E_{IJ}} + \frac{\partial \dot{W}}{\partial E_{JI}}\right) - pg^{(x)IJ} \tag{3.45}$$

where p is the hydrostatic pressure. The exact form of the strain energy function will be chosen to represent the nonlinear behavior of myocardium.

The Cauchy stress tensor **T** in the deformed state can then be computed from

$$T^{ij} = \frac{P^{IJ}}{\sqrt{g^{(x)}}} \frac{\partial x^i}{\partial X^I} \frac{\partial x^j}{\partial X^J}. \tag{3.46}$$

Finite Element Equations

The following approximation is used to represent the geometry of an element of the body B:

$$\Theta(\xi_1,\xi_2,\xi_3)=\sum_{n=1}^{n_{\max}}\sum_{\gamma=1}^{\gamma_{\max}}\psi^{\gamma}_{n(e)}(\xi_1,\xi_2,\xi_3)\cdot\Theta^{n(e)}_{A,\gamma}. \tag{3.47}$$

$\psi^{\gamma}_{n(e)}$ are the interpolation functions that can be tensor products of Lagrange and Hermite polynomials in each direction. $\Theta^{n(e)}_{A,\gamma}$ are the nodal coordinate generalized derivatives at local node n of element (e). $\gamma_{\max}$ is the number of nodal parameters used to interpolate Θ_A, including derivatives of Hermite polynomials. In all of the cases presented in this thesis, only linear interpolation is presented, thus $\gamma_{\max}=1$.

If we look adjust the expression for virtual work (Equation (3.41)) for the absence of accelerations and body forces we get

$$\int_V \left\{ \left(P^{IJ}F_J^{\alpha}\right)\Big|_I \delta u_\alpha \right\} dV = \int_{A_2} \mathrm{s}\cdot\delta\,\mathrm{u}\, dA. \tag{3.48}$$

Costa and Colleagues [1] present the following Galerkin finite element approximation to Equation (3.48) as

$$
\begin{aligned}
&\sum_{e=1}^{e_{\max}} \Omega_{\Delta}^{n(e)} \cdot S_{\gamma}^{n(e)} \cdot \int_{V_e} R_{n(e)}^{\gamma\alpha} \sqrt{G^{(\xi)}}\, d\xi^1 d\xi^2 d\xi^3 \\
&= \sum \Omega_{\Delta}^{n(e)} \cdot S_{\gamma}^{n(e)} \cdot \int_{A_{2_e}} q G^{(\xi)K3} \frac{\partial \theta^{\alpha}}{\partial \xi^{K}} \psi_{n(e)}^{\gamma} \sqrt{G^{(\xi)}}\, d\xi^1 d\xi^2
\end{aligned}
\tag{3.49}
$$

(no sum on λ or n) with $\alpha = 1,2,3$; $\Delta = 1, \ldots \Delta_{\max}$; $\gamma = 1, \ldots \gamma_{\max}$ (for linear interpolation $\gamma = 1$). $\Omega_{\Delta}^{n(e)}$ is a connectivity matrix to assemble the local element equations into a global system. $G^{(\xi)}$ is the determinant of the metric tensor $G_{KL}^{(\xi)}$. $R_{n(e)}^{\gamma\alpha}$ is defined as

$$
R_{n(e)}^{\gamma\alpha} = P^{IJ} \left[F_{J}^{\cdot\alpha} \psi_{n(e),I}^{\gamma} - \left(F_{J}^{\cdot\beta} \Gamma_{\beta I}^{\alpha} \right) \psi_{n(e)}^{\gamma} \right].
\tag{3.50}
$$

The $R_{n(e)}^{\gamma\alpha}$ terms evaluated in prolate spheroidal coordinates are:

$$
R_{n(e)}^{\gamma 1} = P^{IJ} \left\{ \begin{array}{l} \lambda_{,J} \left[\psi_{n(e),I}^{\gamma} - \left(D_1 \lambda_{,I} + D_2 \mu_{,I} \right) \psi_{n(e)}^{\gamma} \right] + \\ \mu_{,J} \left(D_1 \lambda_{,I} - D_2 \mu_{,I} \right) \psi_{n(e)}^{\gamma} + \theta_{,J} D_1 \sin^2 \mu \cdot \theta_{,I} \psi_{n(e)}^{\gamma} \end{array} \right\}
\tag{3.51}
$$

$$
R_{n(e)}^{\gamma 2} = P^{IJ} \left\{ \begin{array}{l} \lambda_{,J} \left[\psi_{n(e),I}^{\gamma} - \left(D_2 \lambda_{,I} + D_1 \mu_{,I} \right) \psi_{n(e)}^{\gamma} \right] + \\ \mu_{,J} \left[\psi_{n(e)}^{\gamma} - \left(D_1 \lambda_{,I} - D_2 \mu_{,I} \right) \psi_{n(e)}^{\gamma} \right] + \theta_{,J} D_2 \sinh^2 \lambda \cdot \theta_{,I} \psi_{n(e)}^{\gamma} \end{array} \right\}
\tag{3.52}
$$

$$
R_{n(e)}^{\gamma 3} = P^{IJ} \left\{ \begin{array}{l} -\lambda_{,J} \coth \lambda \cdot \theta_{,I} \psi_{n(e)}^{\gamma} - \mu_{J} \cot \mu \cdot \theta_{,I} \psi_{n(e)}^{\gamma} \\ +\theta_{,J} \left[\psi_{n(e)}^{\gamma} - \left(\coth \lambda \cdot \lambda_{,I} + \cot \mu \cdot \mu_{,I} \right) \psi_{n(e)}^{\gamma} \right] \end{array} \right\}
\tag{3.54}
$$

where

$$D_1 = \frac{(\cosh\lambda \sinh\lambda)}{(\sinh^2\lambda + \sin^2\mu)} \tag{3.55}$$

and

$$D_1 = \frac{(\cos\mu \sin\mu)}{(\sinh^2\lambda + \sin^2\mu)} \tag{3.56}$$

$S_\gamma^{n(e)}$ is a scaling factor that is constructed for each element to account for non-uniform spacing.

The integrals in Equation (3.49) are then evaluated using Gaussian quadrature creating a system of nonlinear elliptic finite element equations. This system of equations are then solved for the unknown nodal positions using the Newton-Raphson method [2].

Diastolic Material Properties

During the diastolic phase of ventricular contraction the following exponential strain energy function is used:

$$\overset{\bullet}{W} = \frac{C}{2}(\exp(Q) - 1) \tag{3.57}$$

with

$$Q = 2b_1\left(E_{11}+E_{22}+E_{33}\right)+b_2E_{11}^2+b_3\left(E_{22}^2+E_{33}^2+2E_{23}E_{32}\right)+2b_4\left(E_{12}E_{21}+E_{13}E_{31}\right) \qquad (3.58)$$

where $C = 0.88$ kPa, $b_1 = 0.0, b_2 = 18.5, b_3 = 3.58$, and $b_4 = 1.63$. The components of the Green's strain tensor **E** are with respect to the local fiber coordinate system. The constants used were determined experimentally by Guccione and colleagues[3] to cause a cylindrical model of the left ventricle to match experimentally determined strains from video tracking of epicardial markers.

Systolic Material Properties

A systolic constitutive relation is constructed by the addition an active force in the muscle fiber direction to the passive diastolic material properties that is a function of time (t), peak intracellular calcium concentration (Ca_o) and sarcomere length (l). The Second Piola-Kirchhoff stress systolic material properties is:

$$P^{IJ} = \frac{1}{2}\left(\frac{\partial \dot{W}}{\partial E_{IJ}}+\frac{\partial \dot{W}}{\partial E_{JI}}\right) - pg^{(x)IJ} + T_o\left(t, Ca_o, l\right)\delta_1^\alpha\delta_1^\beta. \qquad (3.59)$$

Work by Guccione and colleagues [4] has proposed the following form for T_o:

$$T_o = T_{\max}\frac{Ca_o^2}{Ca_o^2+ECa_{50}^2}C_t, \qquad (3.60)$$

where $T_{\max}$ is the isometric tension achieved at maximum sarcomere length and peak intracellular calcium concentration $(Ca_o)_{\max}$. The variable ECa_{50} gives the relation between intracellular calcium concentration and sarcomere length:

$$ECa_{50} = \frac{(Ca_o)_{\max}}{\sqrt{\exp\left[B\left(l - l_o\right)\right] - 1}} C_t \qquad (3.61)$$

where

$$C_t = \frac{1}{2}(1 - \cos\omega) \qquad (3.62)$$

and

$$\omega = \pi \frac{0.25 + t_r}{t_r} \qquad (3.63)$$

and

$$t_r = ml + b\,. \qquad (3.64)$$

In these equations l is the sarcomere length, l_o is the sarcomere length at which no active tension develops. B, b, and m are all constants. Guccione and colleagues [5] found the following values would allow a finite element model of the systolic heart based upon these measurements to accurately reproduce the strain in the left ventricular free wall:

$T_{\max} = 135.7\,\text{kPa}$, $Ca_o = 4.35\mu\text{mol}/L$, $(Ca_o)_{\max} = 4.35\mu\text{mol}/L$, $B = 4.75\mu m^{-1}$, $m = 1.0489\ \text{sec}\cdot\mu\text{m}^{-1}$, and $b = -1.429$ seconds. The sarcomere length, l, is a function of the strain in the left ventricular wall:

$$l = l_R\sqrt{2E_{11}+1} \tag{3.65}$$

where l_R is the sarcomere length in the unloaded state and E_{11} is the fiber strain. Rodriguez and colleagues [6] determined that there was a linear transmural variation in l_R from 1.78 μm at the endocardium to 1.96 μm at the epicardium.

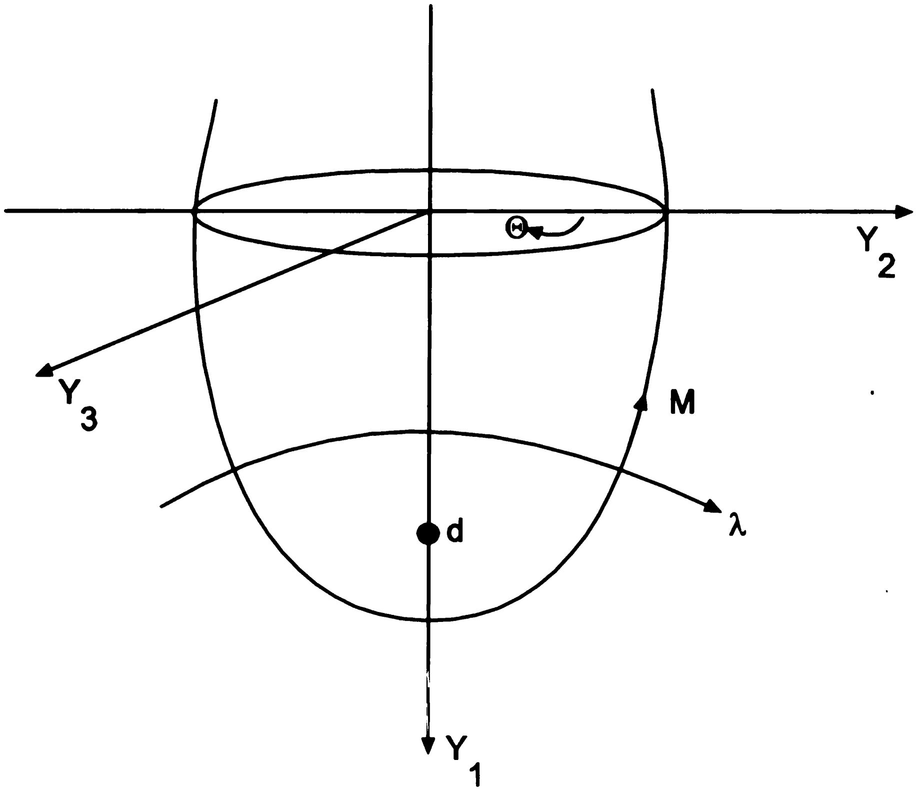
Y
2
Y
3
Θ
M
λ
d
Y
1

Figure 3.1 – Prolate Spheroidal Coordinate System

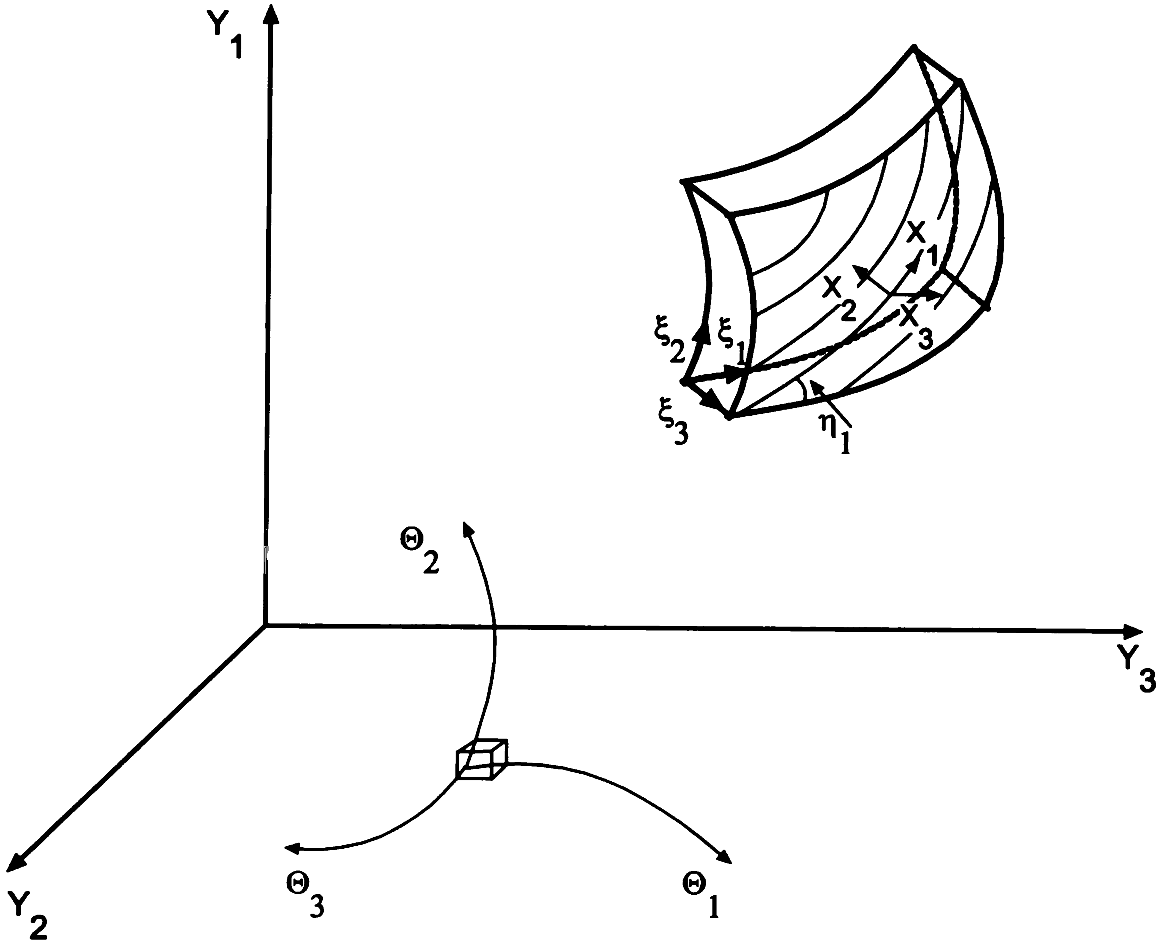
Y_1
ξ_2
ξ_1
ξ_3
X_1
X_2
X_3
η_1
Θ_2
Y_3
Y_2
Θ_3
Θ_1

Figure 3.2 – Coordinate Systems Used

References

1. Costa, K.D., et al., *A three-dimensional finite element method for large elastic deformations of ventricular myocardium: I--Cylindrical and spherical polar coordinates.* J Biomech Eng, 1996. **118**(4): p. 452-63.
2. Hoffman, J.D., *Numerical Methods for Engineers and Scientists*. 1992, New York: McGraw-Hill Inc.
3. Guccione, J.M., A.D. McCulloch, and L.K. Waldman, *Passive material properties of intact ventricular myocardium determined from a cylindrical model.* J Biomech Eng, 1991. **113**(1): p. 42-55.
4. Guccione, J.M. and A.D. McCulloch, *Mechanics of active contraction in cardiac muscle: Part I--Constitutive relations for fiber stress that describe deactivation.* J Biomech Eng, 1993. **115**(1): p. 72-81.
5. Guccione, J.M., L.K. Waldman, and A.D. McCulloch, *Mechanics of active contraction in cardiac muscle: Part II--Cylindrical models of the systolic left ventricle.* J Biomech Eng, 1993. **115**(1): p. 82-90.
6. Rodriguez, E.K., et al., *Effect of residual stress on transmural sarcomere length distributions in rat left ventricle.* Am J Physiol, 1993. **264**(4 Pt 2): p. H1048-56.

Chapter 4

Mechanical Properties of Left Ventricular Aneurysm

Abstract:

Biaxial mechanical property testing was performed on six adult Dorsett Sheep which had left ventricular (LV) aneurysm induced by ligation of the left anterior descending (LAD) coronary artery. Testing results suggested that the aneurysm tissue was significantly stiffer than previously reported. At a 15% equibiaxial stretch we found that the aneurysm tissue experienced a stress of 1,200 g/cm^2 in the circumferential direction and 1,400 g/cm^2 in the longitudinal direction. The results presented here correspond more closely than previous attempts with both stress and strain results obtained by computational modeling presented by other investigators studying this problem [1, 2].

Introduction:

The determination of material properties for soft biological tissues is of critical importance in the understanding of their function [3, 4]. This statement certainly is true for the investigation of LV aneurysm, a significant complication of myocardial infarction that may lead to LV remodeling with global and regional LV dysfunction, ventricular arrhythmias, or thrombolytic complications [5]. A key tool in the investigation of this disease is finite element modeling of LV mechanics [6-10]. These models are, however, limited by the accuracy of measurement of the material properties used to define the computer models. This study will attempt to determine accurate material properties of LV aneurysm in an attempt to develop more accurate finite element models of the disease.

Previous Methods of Determining Myocardial Material Properties

Early mechanical tests on myocardium were carried out using one-dimensional setups, which examined the mechanical properties of papillary muscle. Pinto and Fung used the methods of stress relaxation, creep, vibration, and stress-strain testing to arrive at a one-dimensional exponential constitutive relationship for papillary muscle in both the relaxed and stimulated state [11, 12]. Loeffler and Sagawa continued studies in this area showing that as the force was much greater at higher stretches [13], further suggesting an appropriate constitutive relationship was an exponential function. Przyklenk investigated the varying stiffness levels present through the ventricular wall [14], and found that the epicardium and endocardium were significantly stiffer than the midepicardium. One dimensional studies have been used more recently to investigate the difference in passive stiffness of papillary muscles from normal and hypertensive rats [15, 16], where it has been found that hypertensive rats have an increased passive stiffness. Allaart has examined the effects of perfusion pressure on the material properties of papillary muscles and found the increased perfusion pressure caused an increase of stress at large strains, and a decrease of stress at low strains [17]. Stuyvers has investigated the role of calcium in myocardial stiffness, and proposed that the calcium dependence of diastolic stiffness can be explained by the inverse relationship between calcium and the affinity of titin for actin [18].

Other investigators have chosen to examine the mechanical properties of myocardium by examining the properties of single cardiac myocytes [19]. Brady examined the difference in myocyte stiffness across mammalian species. In his studies it was found that the elastic modulus of the rat was greater than the rabbit, which is greater than the guinea pig [20]. Shroff used Atomic Force Microscopy (AFM), to examine the mechanical properties of rat atrial myocyte cells where he found that there was a two-fold increase in stiffness was observed with an increase in extracellular calcium from 0 to 5mM, and a 16-fold increase after formalin fixation [21]. Palmer found similar calcium dependent results using a pipette attachment system [22]. Kato used single cell studies to show that chronic overload hypertrophy did not alter relative passive cardiomyocyte stiffness [23]. Zile and colleagues used an agarose gel based stretching system to examine the role of cardiomyocyte material properties in the development of cardiac dysfunction. They found that changes in the viscous damping and myofilament activation may cause pressure hypertrophied cardiomyocytes to resist changes in shape during diastole and contribute to diastolic dysfunction. There was no significant change in the passive elastic spring seen between normal and pressure hypertrophied cardiomyocytes [24]. Heller assessed cardiac stiffness by measuring cardiomyocyte cell dimensions in varying osmotic conditions in copper deficient rats. A decrease in cardiomyocyte stiffness was found in copper deficient rats [25]. Harris and colleagues have investigated the relationship between changes in cardiomyocyte properties, with changes in the material properties of the muscle as a whole in hypertrophied myocardium. They found that pressure overload hypertrophy was associated with an increase in myocardial elastic stiffness [26].

It is well known in the biomechanics community that uniaxial tests are not sufficient to determine complete three-dimensional properties of biological soft tissues, however biaxial tests can characterize certain three dimensional relationships [27-41]. Uniaxial tests are also inaccurate when deformation is not measured at the center of the specimen, but rather by the displacement of the stretching device. Two-dimensional studies of pericardium and myocardium have been presented by many authors. Demer and Yin studied the behavior of canine myocardial sheets under biaxial loading [42]. They found that the material exhibited both non-linear elasticity and viscoelasticity with some strain rate dependence in the position of the stress strain relationships. They also found that the tissue exhibited anisotropic behavior along the fiber and cross-fiber directions. Sacks and Chuong examined the mechanical behavior of right ventricular free wall myocardium under biaxial loading [43]. They again found a highly nonlinear relationship between stress and strain, with strong anisotropy between the stiffer fiber and less stiff cross-fiber axes. Yin and colleagues reported biaxial testing results on canine pericardium in which they found again the tissue to be highly nonlinear and anisotropic [44]. In this study, a five parameter strain energy function was found to be optimal in reproducing experimental data. In a later biaxial study, this group found that a three parameter strain energy function more accurately reproduced their experimental results on left ventricular myocardium [45]. Again the data in this study was found to be highly nonlinear and anisotropic. All of these studies have presented data for myocardium that have a similar stiffness and anisotropy ratio. Shacklock then reported data showing a similar anisotropy ratio, but with lower stiffness than that measured by the Yin laboratory [46]. Humphrey, Strumpf and Yin, then proposed a new myocardial constituitive relation and showed its relation to biaxial stress strain data [47, 48]. The authors found a polynomial function of two coordinate invariant measures of finite deformation with five material parameters to fit their data well. They postulated that this relation was more applicable to broader classes of biaxial data than previously proposed relations. These investigators next examined differences in biaxial data from epicardial sections of the right and left ventricle and right and left atrium [49]. The investigators found no differences between the ventricular and atrial material properties, nor any difference between the left and right sides of the heart. They did, however, notice quantitative differences between the epicardial sections and noncontracting myocardium. They found the epicardium to be initially isotropic and compliant, but becomes increasingly stiff and anisotropic near the limits of its extensibility. Novak next examined the regional variation in myocardial material properties [50]. They found that anisotropy was similar in all regions of the heart, but that specimens from the left ventricular free wall tended to be stiffer than the other regions of the heart studied. A study of right ventricular free wall material properties was then undertaken by Sacks and colleagues [43]. They found an overall qualitative similarity in the mechanical behavior of the tissue when compared to left ventricular myocardium, with quantitative differences. Kang then examined the differences between epicardium and endocardium, and found that under biaxial testing the endocardium exhibited greater stiffness in the low strain range [51].

Hoffmeister and colleagues have proposed the use of quasilongitudinal-mode ultrasonic waves to determine the material stiffness of soft biologic tissue [52]. This method, when applied to sections of muscle with only one fiber direction, yielded a Young's modulus of 2.46 GPa in the direction of the fiber axis for formalin fixed myocardium. Baracca and colleagues proposed the use of the third heart sound to determine a stiffness coefficient and damping constant for both normal patients and those with ischemic heart disease [53]. In their studies it was found that those patients with ischemic heart disease showed an increase in both the stiffness coefficient and damping coefficient when compared to normal patients. Table 4.I shows the variability in the estimation of Young's Modulus by various investigators.

Ultrasonic dimension transducers have been used by multiple investigators as a means to determine myocardial material properties. Olsen and colleagues used this method to suggest that myocardial anisotropy contributes significantly to changes in ventricular shape during filling [54]. Omens and colleagues used this method to show a difference in anisotropy in the rat and dog at low loads, but at high loads this difference was minimized [55].

Passive Material Properties of Left Ventricular Aneurysm

Previous attempts at the characterization of the material parameters of LV aneurysm have been limited. Parmley used uniaxial testing methods to arrive at simplistic characterization of material parameters of LV aneurysm [56]. Gupta improved upon this by applying biaxial testing methods to the characterization of LV aneurysm [1, 2].

For the present study we will define passive material properties of the LV aneurysm using a strain energy function similar to that presented for diastolic myocardium in Chapter 3. The strain energy function that we will use is

$$W = \frac{C}{2}\left(e^{Q} - 1\right), \tag{4.1}$$

where the Green strain components, $E_{\alpha\beta}$, are referred to the orthogonal axes of the biaxial stretcher and are chosen such that they lie in the circumferential and axial coordinates (v^{α}):

$$E_{\alpha\beta} = \left(\frac{\partial x^k}{\partial v^\alpha}\frac{\partial x^k}{\partial v^\beta} - \delta_{\alpha\beta}\right) \tag{4.2}$$

and

$$Q = b_c E_{11}^2 + b_l\left(E_{22}^2 + E_{33}^2 + E_{23}^2 + E_{32}^2\right) + b_{lr}(E_{12}^2 + E_{21}^2 + E_{13}^2 + E_{31}^2), \tag{4.3}$$

where x^k are the deformed rectangular Cartesian coordinates and $\delta_{\alpha\beta}$ is the Kronecker delta. E_{11} is the circumferential strain, E_{22} is the longitudinal strain, E_{33} is the radial strain, E_{23} is the shear strain in the transverse plane, and E_{12} and E_{13} are shear strain in the circumferential longitudinal coordinate plane, circumferential radial plane.

The second Piola-Kirchhoff stress tensor referred to the global coordinates v^α is calculated according to:

$$t^{\alpha\beta} = \frac{1}{2}\left(\frac{\partial W}{\partial E_{\alpha\beta}} + \frac{\partial W}{\partial E_{\beta\alpha}}\right) - pg^{\alpha\beta} \tag{4.4}$$

where the contravariant metric tensor referred to global coordinates is

$$g^{\alpha\beta} = \frac{\partial v^\alpha}{\partial x^k}\frac{\partial v^\beta}{\partial x^k} \tag{4.5}$$

After deformation, the Cauchy stress tensor with reference to a new coordinate system in the deformed body, $\hat{v}^i$, is related to the second Piola-Kirchhoff stress tensor by:

$$T^{ij} = \frac{\partial x^k}{\partial v^\alpha}\frac{\partial x^l}{\partial v^\beta}\frac{\partial \hat{v}^i}{\partial x^k}\frac{\partial \hat{v}^j}{\partial x^l} t^{\alpha\beta}\frac{1}{\sqrt{I_3}} \tag{4.6}$$

Methods:

A total of six adult Dorsett sheep were studied in this experiment. All animals were studied in compliance with the animal welfare regulations and the "Guide for the Care and Use of Laboratory Animals"[57]. Material property testing was performed on excised sections of the diseased left ventricular free wall following creation of LV aneurysm.

Creation of the Left Ventricular Aneurysm

LV aneurysm was induced according to the method described by Markovitz and colleagues [58]. Briefly adult Dorsett Sheep were sedated using an intramuscular injection of ketamine (15 mg/kg), masked, then intubated and ventilated using an isoflurane and oxygen mixture. Arterial pressure and a surface electrocardiogram were monitored using a continuous oscilloscope display. Access to the heart was gained using a left thoracotomy in the fifth intercostal space. During this incision a lidocaine infusion was started (1.5 mg • kg^{-1} • min^{-1}). Following opening of the pericardium, the distal left anterior descending (LAD) coronary was ligated using 2-0 silk sutures at a point 40% of the distance from the apex to the base of the heart. Additionally a suture was placed around the second diagonal of the LAD coronary artery at it's inception from the LAD. Before the sutures were secured the animal received a bolus of lidocaine (2 mg/kg), and the lidocaine infusion rate was increased (3 mg • kg^{-1} • min^{-1}). Following ligation the animal was watched for 45 minutes for the occurrence of ventricular tachycardia. When ventricular tachycardia was observed an additional bolus of lidocaine (1.5 mg/kg each) and bretylium (50 mg each) were given. Following the period of monitoring, the thoracotomy was closed in layers and a 28F chest tube was inserted. The lidocaine infusion was stopped 10 minutes postoperatively. The chest tube was removed before extubation. The animal received Naxcel (ceftiofur sodium, 1mg/pound per day intramuscularly) for three days following the operation and was allowed to recover for 10 weeks.

Harvest of Left Ventricular Aneurysm

After allowing the LV aneurysm to mature for a period of ten weeks, the animals were sacrificed, and the LV aneurysm was excised for testing. Anesthesia was induced as described above. Through the use of a median sternotomy the heart was exposed. Potassium Chloride (saturated) was then injected into the left ventricle to induce asystolic arrest. The hearts were then immediately excised and placed in a cold (0 to 5 °C) cardioplegic solution (14 mmol/L H_2PO_4, 11 mmol/L KOH, 15 mmol/L KCl, 220 mmol/L glucose, 0.1 mmol/L EGTA, 75 μmol/L, adenosine pH 7.4) and transported to the biaxial stretcher. 2,3-butanedine monoxime (BDM) was added to the solution (10 mM) to prevent systolic contracture.

Biaxial Stretching Apparatus

The biaxial stretching device used here has been described elsewhere [44, 45, 47, 59], and is displayed schematically in Figure (4.1). Briefly, two independent linear motors and worm gears drive two pairs of orthogonally oriented carriages. One of the carriages in each pair contains a force transducer. The LV aneurysm tissue was connected to the carriage using a continuous stand of 0-0 silk suture looped 6-10 times through the specimen near the edges. Between tests the specimen was kept in a thermally regulated (20 °C), oxygen-perfused, cardioplegic solution.

Deformations in the central portion of the sample were continuously monitored using a video camera based system [59]. Briefly small vanilla chips were glued to the specimen to form a rectangle (approximately 4 mm by 4 mm). A light source illuminated the marked area, and a computer based system allowed on-line monitoring to material deformation. Distances between the vanilla chips were continuously measured in order to provide a real time estimate of the local strain in the center of the specimen. These measurements were used to drive the system in real time to predefined stretching lengths.

Testing Protocol

Prior to the mounting of the tissue, the force transducers were calibrated. Weights with known values were attached to the carriages with force transducers using sutures. Three points were calibrated, zero, a low (500 g) and a high value (1 Kg) weight.

After initial mounting of the tissue, stress free dimensions were determined by stretching the sample 10-20 times under 100 gram equivalent loads, followed by a period of five minutes during which the tissue was allowed to rest in a stress free configuration. The reference state was checked three to five times against previous tests following equibiaxial stretches of 5%. The reference state was considered acceptable once subsequent states differed by only a few percent. Specimen dimensions were measured using a ruler, and thickness was measured by using a digital caliper and two microscope slides.

Following pre-stretching of the material, a stress-free state was obtained by monitoring the point at which the sutures exhibited a downward "slack." We assumed that at the point where this was first evident, the material was not experiencing any load. After obtaining this stress-free state, each sample was subjected to equibiaxial stretches beginning at 5%, and increasing by 5% if the tissue did not show signs of tearing at the suture locations. Between each stretch the no load state was ensured by verifying that the sutures were just beginning to exhibit a downward "slack." Real time feedback controlled the displacement of the carriages to ensure the tissue was deforming to the proper length. Force and displacement data were saved to disk for subsequent analysis after the experiment.

The markers used for strain analysis were placed on the sample in the manner shown in Figure (4.2). Strain analysis was completed using the method originally described by Humphrey [27], with the assumption of homogenous strain in the central area. Interpolation functions were used to map the actual marker locations onto a square region. For our tests it was assumed that:

$$\begin{aligned} u &= \sum f_i(s,r)u_i \\ v &= \sum f_i(s,r)v_i \\ X &= \sum f_i(s,r)X_i \\ Y &= \sum f_i(s,r)Y_i \end{aligned}, \qquad (4.7)$$

where

$$f_i(s,r) = (1+ss_i)(1+rr_i)/4 \quad i=1, 2, 3, 4 \qquad (4.8)$$

and u_i and v_i were particle displacements, X_i and Y_i were initial particle locations, s and r were mapping coordinates, and u and v were approximate displacements in the X and Y directions respectively (r_i and s_i correspond to the r and s coordinates of the ith corner of the box depicted in Figure 4.3).

This biaxial stretching problem, can be assumed to be a plane stress problem in which the only non-zero Green strains are E_{XX}, E_{YY}, E_{XY} and E_{ZZ}. The strains are calculated in the following manner. Since we are interested in the strain at the center of the marked region in Figure (4.3), we assume that:

$$\begin{aligned} s &= 0 \\ r &= 0 \end{aligned} \tag{4.9}$$

The derivatives of the mapping function are calculated with respect to s and r:

$$\begin{aligned} \frac{\partial f}{\partial s} &= \frac{s_i(1+rr_i)}{4} \\ \frac{\partial f}{\partial r} &= \frac{(1+ss_i)r_i}{4} \end{aligned} \tag{4.10}$$

Using (4.7), the derivatives of the displacements can be calculated:

$$\begin{aligned} \frac{\partial u}{\partial s} &= u\frac{\partial f}{\partial s} \\ \frac{\partial u}{\partial r} &= u\frac{\partial f}{\partial r} \\ \frac{\partial v}{\partial s} &= v\frac{\partial f}{\partial s} \\ \frac{\partial v}{\partial r} &= v\frac{\partial f}{\partial r} \end{aligned} \tag{4.11}$$

The derivatives of x and y with respect to s and r are calculated using the chain rule:

$$\begin{aligned}\frac{\partial X}{\partial s} &= X\frac{\partial f}{\partial s}\\ \frac{\partial X}{\partial r} &= X\frac{\partial f}{\partial r}\\ \frac{\partial Y}{\partial s} &= Y\frac{\partial f}{\partial s}\\ \frac{\partial Y}{\partial r} &= Y\frac{\partial f}{\partial r}\end{aligned} \tag{4.12}$$

The derivatives of the displacements with respect to the marker coordinates can then be calculated by solving the following equations:

$$\begin{aligned}\begin{Bmatrix}\dfrac{\partial u}{\partial s}\\ \dfrac{\partial u}{\partial r}\end{Bmatrix} &= \begin{bmatrix}\dfrac{\partial X}{\partial s} & \dfrac{\partial Y}{\partial s}\\ \dfrac{\partial X}{\partial r} & \dfrac{\partial Y}{\partial r}\end{bmatrix}\begin{Bmatrix}\dfrac{\partial u}{\partial X}\\ \dfrac{\partial u}{\partial Y}\end{Bmatrix}\\ \begin{Bmatrix}\dfrac{\partial v}{\partial s}\\ \dfrac{\partial v}{\partial r}\end{Bmatrix} &= \begin{bmatrix}\dfrac{\partial X}{\partial s} & \dfrac{\partial Y}{\partial s}\\ \dfrac{\partial X}{\partial r} & \dfrac{\partial Y}{\partial r}\end{bmatrix}\begin{Bmatrix}\dfrac{\partial v}{\partial X}\\ \dfrac{\partial v}{\partial Y}\end{Bmatrix}\end{aligned} \tag{4.13}$$

The strains can then be calculated according to:

$$
\begin{aligned}
E_{XX} &= \frac{\partial u}{\partial X} + \left[\left(\frac{\partial u}{\partial X} \right)^2 + \left(\frac{\partial v}{\partial X} \right)^2 \right] \Big/ 2 \\
E_{YY} &= \frac{\partial v}{\partial Y} + \left[\left(\frac{\partial u}{\partial Y} \right)^2 + \left(\frac{\partial v}{\partial Y} \right)^2 \right] \Big/ 2 \\
2E_{XY} &= \frac{\partial u}{\partial Y} + \frac{\partial v}{\partial X} + \frac{\partial u}{\partial X}\frac{\partial u}{\partial Y} + \frac{\partial v}{\partial X}\frac{\partial v}{\partial Y}
\end{aligned}
\tag{4.14}
$$

The shear strain, E_{XY}, was monitored to ensure that the values were close to zero, so that the number could be excluded in the nonlinear fitting calculations.

Stretch ratios and shear factors can be calculated from:

$$
\begin{aligned}
\lambda_X &= 1 + \frac{\partial u}{\partial X} \\
\lambda_Y &= 1 + \frac{\partial v}{\partial Y} \\
k_1 &= \frac{\partial u}{\partial Y} \\
k_2 &= \frac{\partial v}{\partial X}
\end{aligned}
\tag{4.15}
$$

If we assume the tissue to be incompressible, the stretch ratios relate according to:

$$
\lambda_X \lambda_Y \lambda_Z = 1 \tag{4.16}
$$

Forces were converted into Cauchy stresses by dividing the measured force with the measured cross sectional area of the specimen.

Simplification of the Strain Energy Function

The exponential portion of the strain energy function described in (4.3) was modified owing to the absence of shear strain.

$$\begin{aligned} W &= \frac{C}{2}\left(e^{Q}-1\right) \\ Q &= b_c E_{11}^2 + b_l\left(E_{22}^2 + E_{33}^2\right) \end{aligned} \tag{4.17}$$

after removal of all of the shear terms. This simplification results in the calculation of Cauchy stress as follows. The strains are related to the stretch ratios according to:

$$\begin{aligned} E_{XX} &= \frac{1}{2}\left(\lambda_X^2 - 1\right) \\ E_{YY} &= \frac{1}{2}\left(\lambda_Y^2 - 1\right) \\ E_{ZZ} &= \frac{1}{2}\left(\lambda_Z^2 - 1\right) \end{aligned} \tag{4.18}$$

The Cauchy stress is then given by

$$T_{XX} = \lambda_X^2 \frac{\partial W}{\partial E_{XX}} - p$$
$$T_{YY} = \lambda_Y^2 \frac{\partial W}{\partial E_{YY}} - p \qquad (4.19)$$

Using the assumption of no stress in the Z direction, the hydrostatic pressure is given by

$$p = \lambda_Z^2 \frac{\partial W}{\partial E_{ZZ}} \qquad (4.20)$$

Parameter Estimation

The experimental data yielded both the stress and strain values necessary to represent Equation (4.19) with only the material constants unknown. The Levenberg-Marquardt method was then used to solve this system of non-linear equations [60]. The method was implemented using the MATLAB optimization toolbox nonlinear least squares fitting function. Equation (4.19) was set to zero, then each part was squared. A minimum was found by imputing the measured stress and strain values and simultaneously optimizing both parts of the modified Equation (4.19).

For each biaxial stretch, a series of three loading cycles were recorded. Forces in the circumferential and longitudinal anatomical directions were recorded (Figure (4.4(a)), Figure (4.4(b))). The motor displacements were also recorded (Figure (4.4(b)), Figure (4.4(c))), while strain estimates were also calculated to drive the motors.

Results:

In all of the experiments the second cycle was chosen for analysis. Stress strain results were calculated for both the circumferential (Figure (4.5(a))) and longitudinal (Figure (4.5(b))) directions. A nonlinear least squares fit was then preformed to obtain the parameters described in Equation (4.17). The results for a typical experiment are presented in Figure (4.6). Table 4.II summarizes the fitted parameters for this study. The stiffness constant, C, varied from 0.1 kPa to .77 kPa with a mean of .29 kPa. The exponential constant in the circumferential direction, b_c, varied from 1.64 to 208.58 with a mean of 33.17. The exponential constant in the longitudinal direction, b_l, varied from 25.45 to 55.05 with a mean of 41.56.

One measure of the degree of anisotropy of the aneurysm is the ratio of b_l to b_c, which gives a measure of the relative stiffness of the longitudinal and circumferential directions respectively. This ratio varied from .17 to 28.03 with a mean of 7.92, indicating that longitudinal direction is stiffer than the circumferential direction.

Predicted stress values from the fitted parameters at the corresponding stretch ratios are presented in Table 4.III. Figure (4.7) displays a graphical representation of this data. When the LV aneurysm were stretched 10%, the mean circumferential Cauchy stress was 1,448 g/cm^2 while the longitudinal Cauchy stress was 1,304 g/cm^2. For a 15% stretch, the mean circumferential Cauchy Stress was 1,196 g/cm^2 and the mean longitudinal Cauchy stress was 1,399 g/cm^2. At 20% stretch, the mean circumferential Cauchy stress was 13,847 g/cm^2, and the mean longitudinal Cauchy stress was 23,741 g/cm^2.

A second measure of anisotropy would be to compare the longitudinal Cauchy stress, T_{XX}, with the circumferential Cauchy stress, T_{YY}. The ratio of these stresses was 1.03, 1.38, and 1.57 for a 10%, 15% and 20% stretch respectively (Figure (4.7)). This again indicates that the longitudinal direction is stiffer than the circumferential direction.

Discussion:

Comparison with Other LV Aneurysm Material Property Data

Gupta and colleagues previously reported material property information for LV aneurysm induced in sheep at various time points following infarction [1, 2]. Briefly the Gupta system consisted of two orthogonal stepper motors that move according to a predefined protocol, without feedback from the actual deformation of the tissue. The LV aneurysm was affixed to the device through a series of stainless steel orthodontic wires (0.7 mm diameter) that ride on rollers to allow lateral motion while being displaced in the direction of the orthogonal axes. Strain was measured using two pairs of brightly colored stainless steel pins (0.024 inches, diameter), placed through the tissue along to two orthogonal axes of the stretcher. The motions of the pins were tracked using a video camera, and analyzed at a later time.

Gupta and colleagues chose to use a strain energy function defined in terms of principle extensions for convenience based upon the suggestion by Needleman [10]. Although both isotropic and anisotropic strain energy functions were presented [1], the anisotropic function was shown to have best fit. The strain energy function chosen was:

$$W = \mu\left[\frac{\lambda_1^{k_1}}{k_1} + \frac{\lambda_2^{k_2}}{k_2} + \frac{\lambda_3^{k_a}}{k_a} - 3\right] \tag{4.21}$$

$$k_a = \frac{k_1 + k_2}{2} \tag{4.22}$$

where λ_i are the extension ratios, and μ and k_i are the material constants. For a rectangular shape, the principal stresses are then given by:

$$T_i = \mu\left[\lambda_i^{k_i} - \lambda_3^{k_a}\right] \tag{4.23}$$

The fitted parameters from their study are reproduced in Table 4.IV. The ratio of k_l to k_c was shown to decrease as the infarct age increased. This ratio also changed from being greater than 1 (indicating stiffer tissue in the longitudinal direction of the aneurysm), to less than one (indicating stiffer tissue in the circumferential direction of the aneurysm) as the infarct age increased. The authors chose to represent the stress in the aneurysm while undergoing a 15% equibiaxial stretch by averaging the predicted stress levels in each experiment based upon the predicted stiffness parameters in each experiment (Table 4.V). These results indicate that the stress levels in circumferential direction ranged from 19.4 gm/cm^2 to 338.5 gm/cm^2 showing a decrease at the 6 week time point. The stresses in the longitudinal direction ranged from 53.2 gm/cm^2 to 310.7 gm/cm^2, showing a decrease at the 2 and 6 week time points. The mean stresses were 140.3 and 177.5 gm/cm^2 for the circumferential and longitudinal directions respectively. The ratio of the longitudinal to circumferential stress ranged from 0.5 to 3.7 with a mean of 1.9.

If the authors would have chosen to calculate predictive stresses based upon the averages of the model parameters for the 15% stretch, they would have obtained the results presented in Table 4.VI. The most notable change in these results is seen at the 6 week time points, when compared to the results presented in Table 4.V. We see the circumferential stress is increased in comparison to the 2 week time point, and the longitudinal stress is only decreased by 7% as compared to 80%.

It is difficult to directly compare the parameter results of the Gupta study with the ones presented here. However, a direct comparison of the stress values can be conducted. If we look at the data presented for the six week time point under a 15% equibiaxial stretch, we see that the results obtained here are significantly stiffer. Gupta reported values of 115.6 gm/cm^2 and 53.2 gm/cm^2 for the circumferential and longitudinal stresses respectively at the 6 week time point, which most closely agrees with the time scale reported here. The values of the circumferential and longitudinal stresses found in this study were 1,197 gm/cm^2 and 1,400 gm/cm^2. Although the tissue was found to be significantly stiffer in this study when compared to Gupta's, the qualitative similarity of the longitudinal direction being stiffer still exists.

Figure (4.8) shows the stress strain predictions from the Gupta 15% equibiaxial fit constants, with data predicted from the 15% biaxial presented here. It is clearly evident that the material properties reported here, produce significantly higher stresses than those described by Gupta.

Biaxial Stretcher Design

Many of the differences between our results and those of Gupta can be attributed to differences in stretcher design. The first difference is in the method of attachment to the stretcher. In our studies we have used long sutures wrapped around a metal pole. This allowed lateral movement (which is dependent upon suture to metal friction, as Gupta observed), while applying the forces in the direction of the orthogonal axes. In Gupta's system, the tissue is attached to the stretcher using thin aluminum pins (0.024 inches, diameter) that are placed perpendicular to the direction of stretching. The corner pins in this set up are actually driven by both sets of orthogonal axes. Thus deformation in one direction is restricted by the motion of the second direction. This could result in the creation of shear strain, which was not accounted for in the Gupta study. The study presented in this paper was monitored to ensure that the shears were minimal. Not only can significant shearing affect the assumptions of equibiaxial stretching, but also it can have an affect upon the accuracy of the force measured by the load cells.

Another source of discrepancy could be the method used to measure strain. Gupta placed small optical wires through the center of the tissue to accomplish this. As pointed out by Downs [59], this method is questionable due to the restraining effects of the fibers on the specimen, the stress concentration induced by the newly created hole, and the nonlinearity of the photodiode system used to measure displacements.

Additionally the motor control design is different between the two designs. Our study employed a system that monitored central tissue displacement in real time. This allowed us to stretch the tissue until the central region arrived at the prescribed stretch ratio. In Gupta's study the prescribed displacement was generated by motor motion only, irregardless of the strain delivered to the center of the tissue specimen. While, the parameters were fit to the appropriate extension ratios, the predicted stress values were calculated based upon the stretch ratio delivered to the motors.

Comparison to Other Methodologies of Stress Determination

Calculation of the in-vivo stretch ratio experienced by LV aneurysm has proven difficult. The relative thinness of the aneurysm has made use of tagged MRI difficult. Jackson and colleagues have used sonomicrometry crystals to examine this problem in sheep that have undergone the same surgical procedure as the subjects in this study. In their work they have found end systolic stretch ratios approaching 10% [61]. Other studies based upon finite element models of tagged MRI data of left ventricular aneurysm have suggested that the stretch ratio approached 13% during the end of isovolumic systole [7]. Moustakidis has recently used the combination of finite element modeling and tagged MRI to predict peak aneurysm stress levels in sheep that have had left ventricular aneurysm induced. They found a peak stress level of approximately 1,100 g/cm^2 [6]. In the study presented here, in order for the aneurysm to experience that stress level it would be required to experience a 13% or 14% stretch in the circumferential and longitudinal directions respectively. In the experiments presented by Gupta, the tissue would be required to experience a 19% stretch in the circumferential direction and a 23% stretch in the longitudinal direction in order to experience the same level of stress. Clearly, the results from the present study correspond more closely with those presented by other investigators. It is likely that Gupta is underestimating the stress 10 fold.

Comparison with Normal Myocardial Material Properties

Guccione and colleagues used a cylindrical model of the left ventricle to obtain material properties in combination with strain data obtained by bi plane x-ray [62]. Based on previous research, they proposed the following anisotropic strain energy function:

$$W = \frac{C}{2}\left(e^{Q} - 1\right) \tag{4.24}$$

$$Q = b_f E_{11}^2 + b_t\left(E_{22}^2 + E_{33}^2 + E_{23}^2 + E_{32}^2\right) + b_{fs}(E_{12}^2 + E_{21}^2 + E_{13}^2 + E_{31}^2) \tag{4.25}$$

where E_{11} is the fiber strain, E_{22} is the cross fiber strain, E_{33} is the radial strain, E_{23} is the shear strain in the transverse plane, and E_{12} and E_{13} are shear strain in the fiber cross fiber coordinate plane, fiber radial plane. Their study found that the following material constants allowed the cylindrical model to match the measured epicardial strains:

$$\begin{aligned} C &= 0.876\ kPa \\ b_f &= 18.48 \\ b_t &= 3.58 \\ b_{fs} &= 1.627 \end{aligned} \tag{4.26}$$

Although these constants are measured with respect the fiber axis, which changes through the ventricular wall, and our study determined constants with respect to geometric axes (longitudinal, circumferential) it is possible to compare the stress developed over a reasonable strain range. Figure (4.9) demonstrates that the material properties measured in left ventricular aneurysm are significantly stiffer than those measured in normal myocardium.

Conclusion:

The present study has presented some discrepancies with previously reported material property testing of LV aneurysm. We found that the LV aneurysm is significantly stiffer than previously proposed. Previous experimental systems could have introduced error into measurement of strain, which would have adversely affected the predicted material property parameters. Furthermore, the results presented here better correlate to stress values in left ventricular aneurysm as determined by tagged MRI [6, 7].

The results obtained here could be improved upon with the use of new experimental modalities. Previously the use of a combination of imaging and finite element modeling as a method to determine material properties has been examined [63, 64]. Unfortunately, these early studies were limited by the resolution of the imaging modality. Currently, MRI is being investigated for use in this capacity [65], however, since the aneurysm tissue is so thin (2 mm) tagging will not be possible to this region. A more rigorous use of sonomicrometry [61, 66-73] could be applied to measure strain. Also Dokos, has recently begun the use of a triaxial testing system to determine material properties [74, 75]. The Dokos system utilizes a device capable of applying simple shear deformations in two orthogonal directions while simultaneously measuring the resulting forces in three axes. This triaxial system will be especially useful in examining the material properties of biological tissue under shear strain.

To further investigate the implications of the stiffer material properties, finite element studies of left ventricular aneurysm will be conducted. These studies will help to understand the importance of changing aneurysm material parameters upon the global and regional function of the LV.

Investigator	Year	Animal	Young's Modulus (mN/mm^2)
Allaart	1995	Rat	30
Brady	1991	Guinea Pig	16.4
		Rabbit	22.4
		Rat	25.8
Shroff	1995	Rat	500
Hoffmeister	1994	Human	2.46

Table 4.I – Variation in measurement of Young's Modulus of myocardium as reported by previous investigators.

Experiment	% Stretch	bc	bl	C (bar)	C(g.cm2)
36061	10%	19.93	49.60	0.0014	1.4271
	15%	11.05	55.05	0.0010	1.0194
36068	10%	208.58	36.83	0.0036	3.6697
36075	20%	34.16	25.45	0.0020	2.0387
36190	15%	1.64	44.06	0.0027	2.7523
	20%	6.86	39.43	0.0029	2.9562
36210	15%	41.02	44.91	0.0024	2.4465
	20%	31.15	43.03	0.0029	2.9562
36217	10%	4.39	31.75	0.0030	3.0581
	20%	1.87	52.49	0.0022	2.2426
	25%	4.19	34.56	0.0077	7.8491

Minimum	1.64	25.45	0.0010	1.0194
Mean	33.17	41.56	0.0029	2.9469
Standard Deviation	59.86	9.04	0.0018	1.79
Maximum	208.58	55.05	0.0077	7.8491

Table 4.II – Summary of fitted parameters. Results of all biaxial testing studies when fit to Equation (4.24) using the Levenberg-Marquardt method. The results show that the longitudinal direction is stiffer than the transverse direction, verifying anisotropy in the LV aneurysm tissue.

Experiment	% Stretch	T_{XX}(g/cm^2)	T_{YY}(g/cm^2)	T_{XX}/T_{YY}
36061	10%	84.41	90.37	1.07
	15%	645.81	929.53	1.44
36068	10%	4,223.83	3,776.54	0.89
36075	20%	2,812.21	2,476.33	0.88
36190	15%	390.97	653.29	1.67
	20%	2,769.08	5,209.73	1.88
36210	15%	2,553.00	2,616.35	1.02
	20%	29,214.57	33,588.56	1.15
36217	10%	40.40	45.60	1.13
	20%	7,502.70	17,703.91	2.36
	25%	20,594.42	53,690.12	2.61
10% Stretch Mean		1,449.54	1,304.17	1.03
15% Stretch Mean		1,196.59	1,399.72	1.38
20% Stretch Mean		13,847.57	23,741.18	1.57

Table 4.III – Predicted Stress Values – Predicted stress values of the LV aneurysm tissue when an exact stretch of 10%, 15% or 20% is applied. The ratio of longitudinal to circumferential stresses is presented as an indication of anisotropy.

Infract Age	Stretch	μ	k_c	k_l	k_l/k_c
Control	10%	1.01	21.99	28.34	1.29
	15%	0.76	23.30	28.03	1.20
4 Hours	10%	2.12	26.33	38.99	1.48
	15%	1.78	24.00	34.36	1.43
1 Week	10%	4.99	31.61	38.50	1.22
	15%	5.13	26.18	27.94	1.07
2 Weeks	10%	3.74	38.27	35.26	0.92
	15%	3.64	32.08	30.23	0.94
6 Weeks	10%	2.24	26.73	19.61	0.73
	15%	9.87	27.27	22.60	0.83

Table 4.IV – Summary of Previous LV Aneurysm Material Property Estimates. Parameters as reported by Gupta [1, 2]. Stress and Stretch Data were fit to Equation (4.21).

	Stress Based On Average of Individual Studies		
Infarct Age	T_{XX}	T_{YY}	T_{XX}/T_{YY}
Control	19.4	54.8	2.82
4 Hours	54.6	203.9	3.73
1 Week	173.6	310.7	1.79
2 Weeks	338.5	264.8	0.78
6 Weeks	115.6	53.2	0.46

Table 4.V – Gupta LV aneurysm Stress Results – LV aneurysm stress results for a simulated exact 15% equibiaxial stretch as reported by Gupta [1, 2]. Results are determined by calculated material parameters for each study, then producing estimated stress values for each study. These results were then averaged to produce the values shown above.

	Stress Based On Model Averages		
Infarct Age	T_{XX}	T_{YY}	T_{XX}/T_{YY}
Control	19.7	38.2	1.94
4 Hours	51.0	216.8	4.25
1 Week	199.2	254.7	1.28
2 Weeks	322.3	248.9	0.77
6 Weeks	446.2	232.3	0.52

Table 4.VI – Gupta LV aneurysm Stress Results – LV aneurysm stress results for an exact simulated 15% equibiaxial stretch from data presented in [1, 2]. Results were obtained by calculating material property constants for each study, then averaging their value. The average value was then used to predict a stress value when a simulated equibiaxial stretch of 15% was performed.

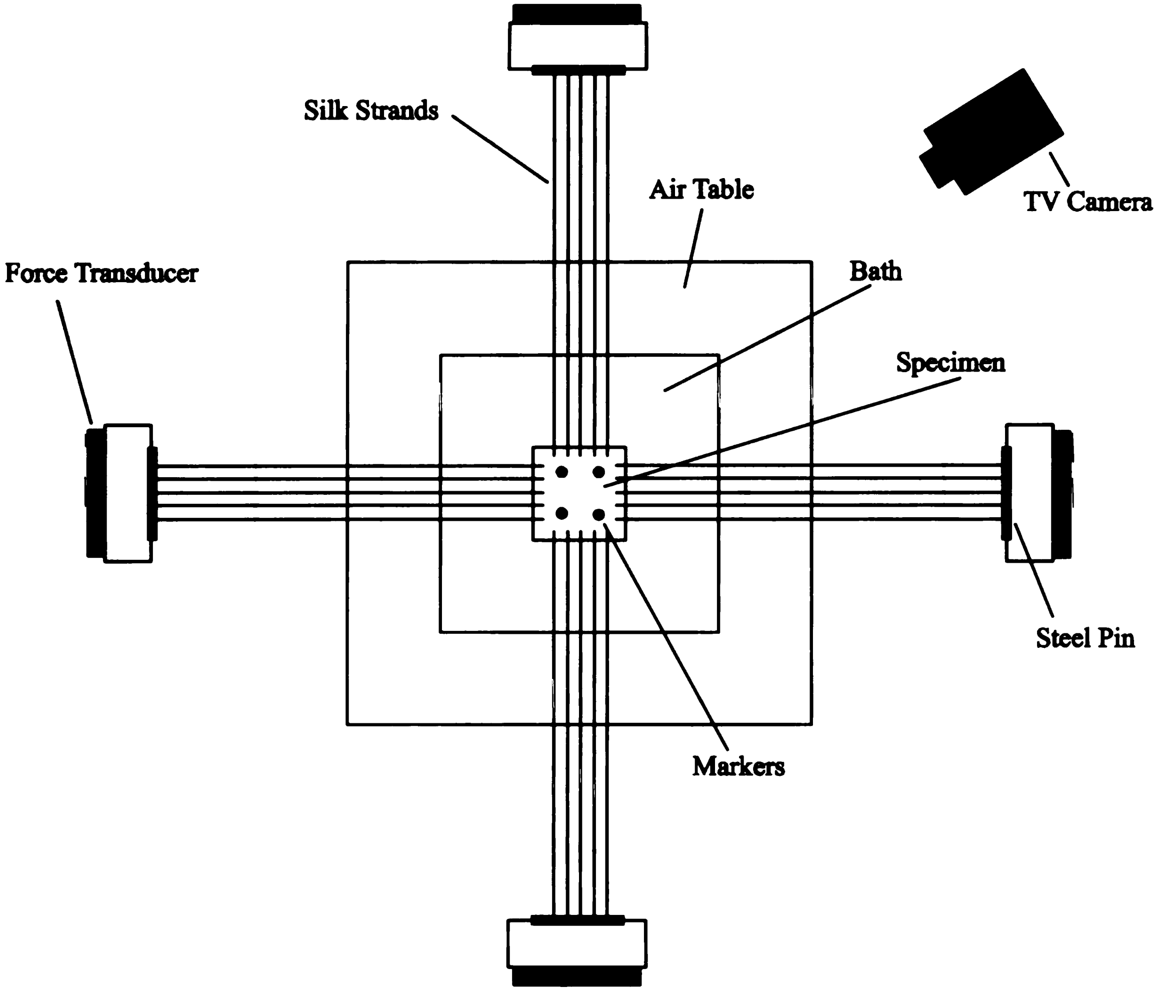
Silk Strands
Air Table
TV Camera
Force Transducer
Bath
Specimen
Steel Pin
Markers

Figure 4.1 –Biaxial Stretching System. The biaxial stretching device consisted of two orthogonal motor axes that drive the displacement of tissue which is attached using sutures. Motor displacement is controlled using a video system that monitors tissue displacement at the center of the specimen to assure that the sample is being stretched to the appropriate length. Forces are measures using a force transducer on each orthogonal axis.

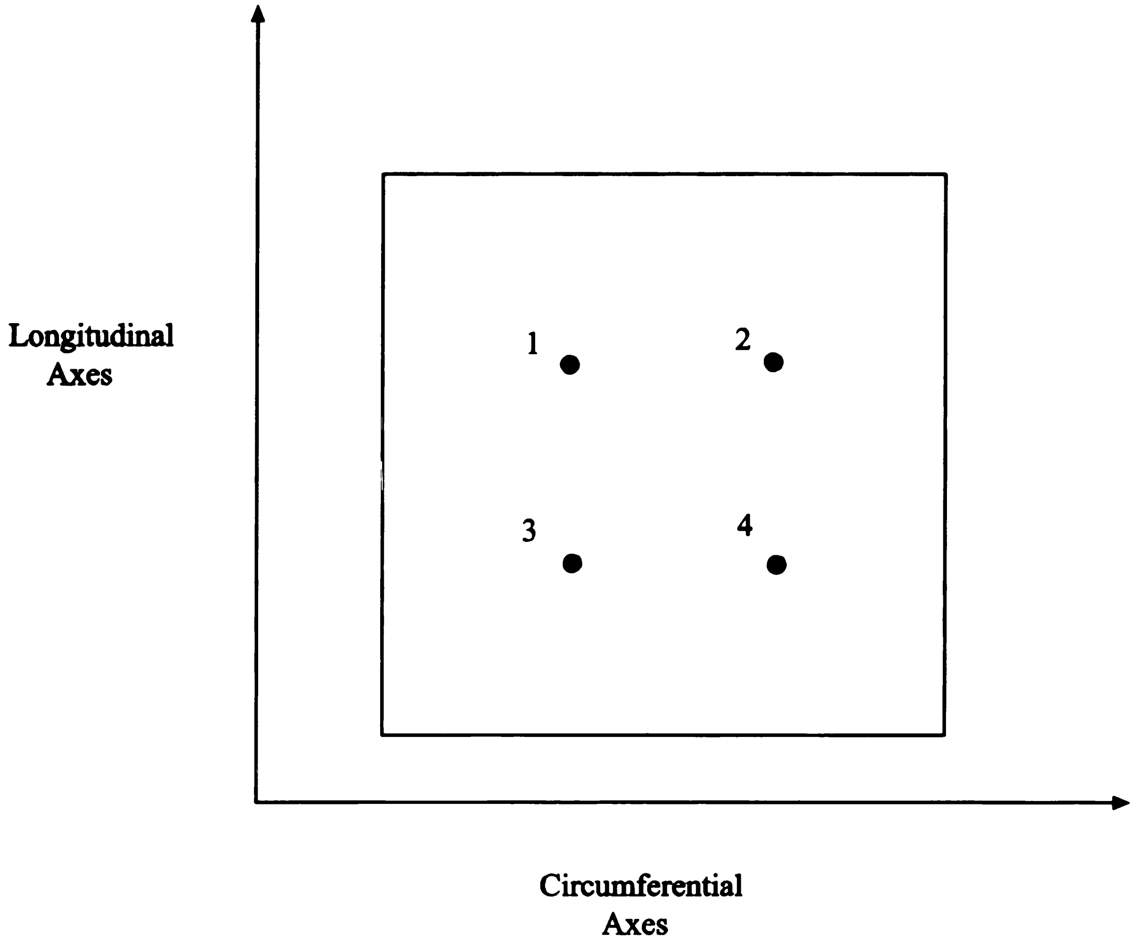
Longitudinal Axes
1
2
3
4
Circumferential Axes

Figure 4.2 – Marker Locations – Four markers are placed in the center of the tissue sample in an approximate square pattern. The video tracking system monitors the displacement of these markers to determine both stretch ratios and strain.

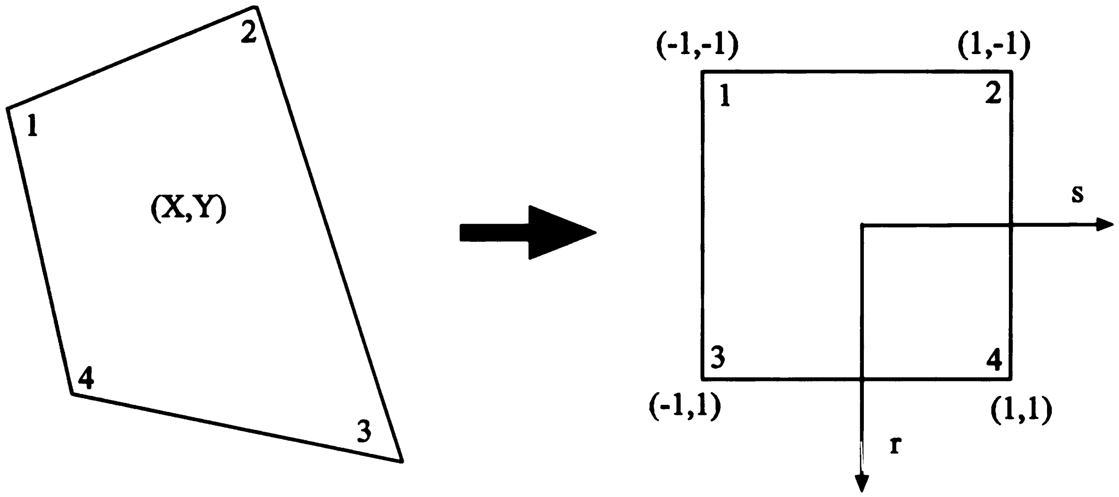
1
2
(X,Y)
4
3
(-1,-1)
(1,-1)
1
2
s
3
4
(-1,1)
(1,1)
r

Figure 4.3 – Mapping Transformation – Schematic of mapping transformation used with Equation (4.7). Coordinates measured in the arbitrary (X,Y) plane are mapped to the normalized (s,r) plane.

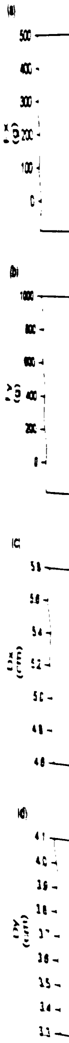

Figure
stretchi
(c, d) t

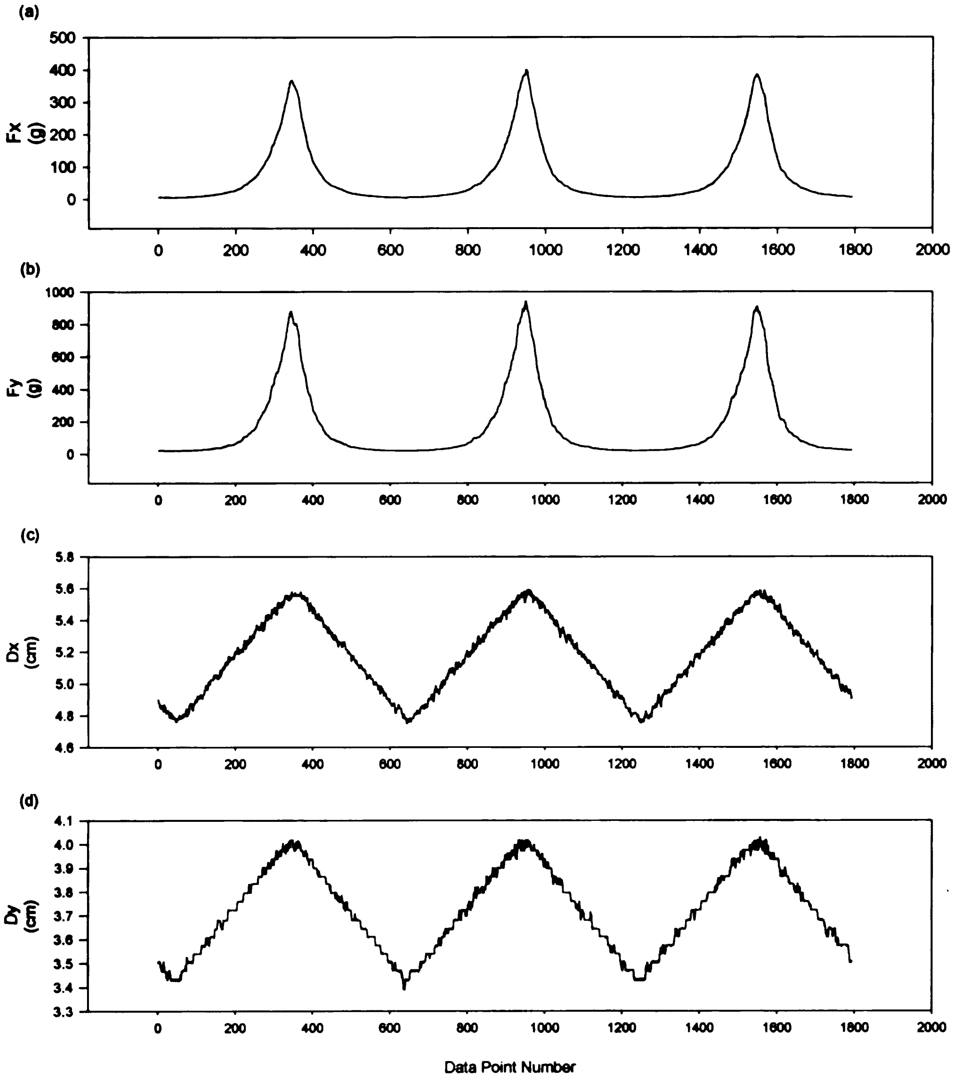

Figure 4.4 – Biaxial Testing Raw Data – Data from representative biaxial stretching test that shows the force measurements (a, b) and displacements (c, d) that were recorded.

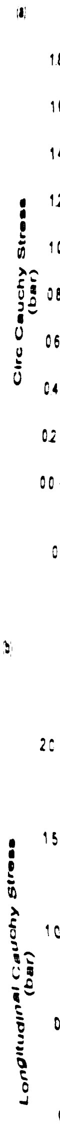
(a)
Circ Cauchy Stress (bar)
0.6
0.4
0.2
0.0
(b)
Longitudinal Cauchy Stress (bar)
2.0
1.5

Figu
and l

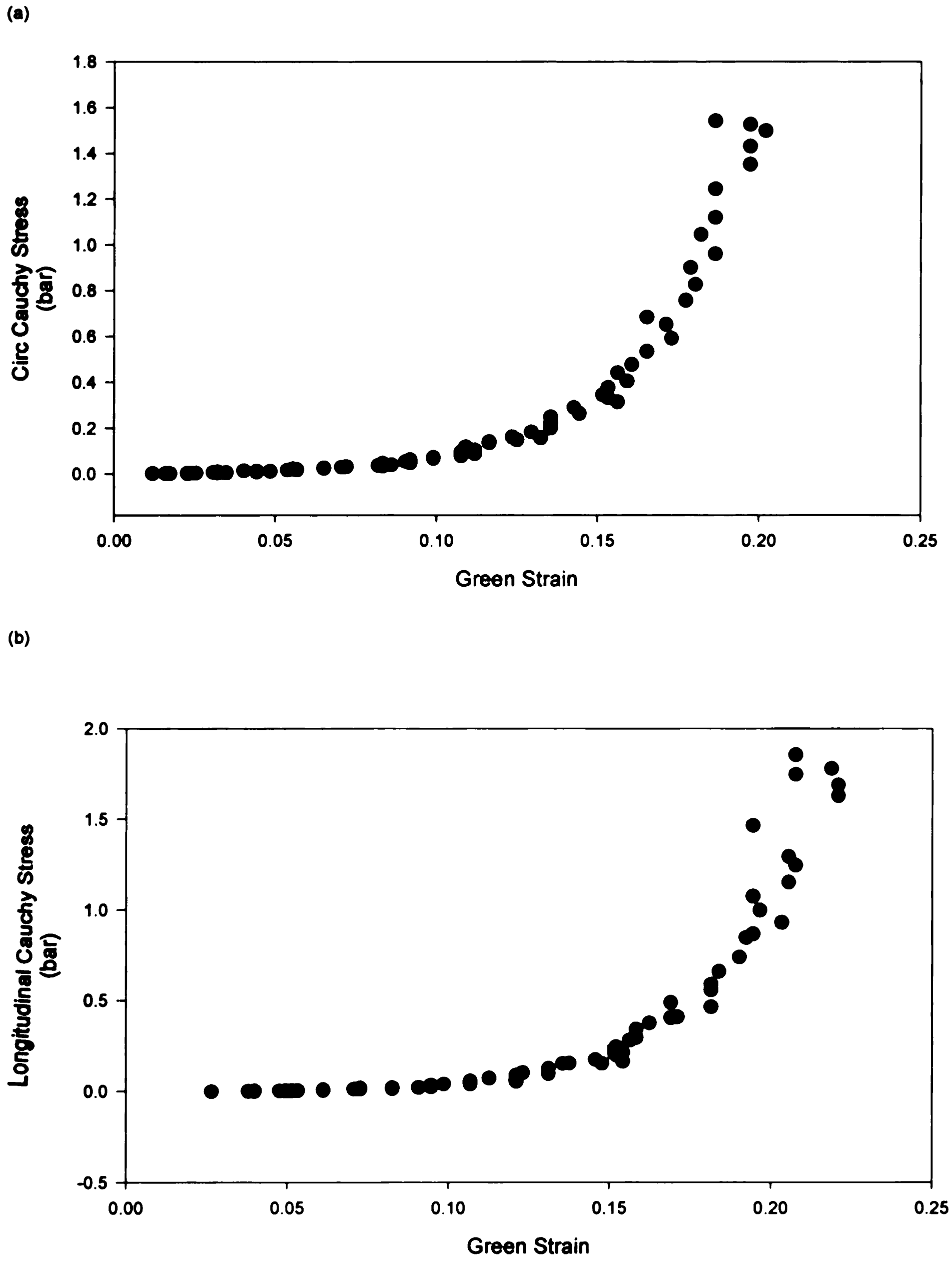

Figure 4.5 – Typical stress versus strain plots for the circumferential (a) and longitudinal (b) directions for a 20% equibiaxial stretch.

Figure
circumf
valued (
are pres
presente
respecti
respecti

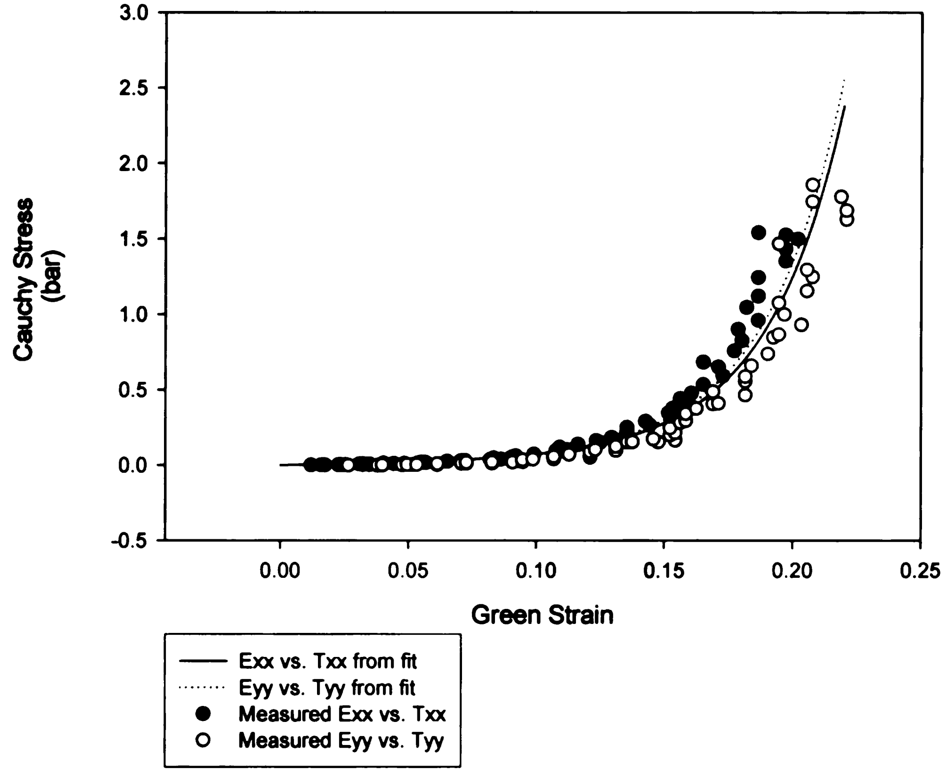

Figure 4.6 – Stress stain results plotted for a typical 20% equibiaxial stretch. Measured circumferential stress and strain values (solid circles) and longitudinal stress and strain valued (open circles) are plotted. The results from the corresponding material property fit are presented in the circumferential (solid line) and longitudinal (dashed line) are presented. E_{cc} and E_{ll} are the strains in the circumferential and longitudinal directions respectively. T_{cc} and T_{ll} are the stresses in the circumferential and longitudinal directions respectively.

Cauchy Stress

Fig
equ
long

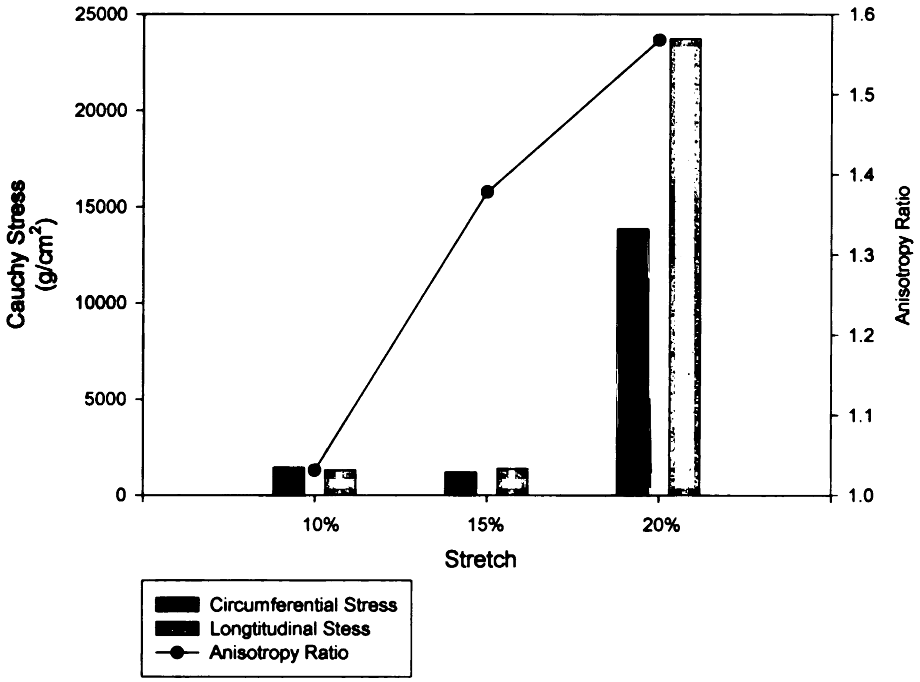

Figure 4.7 – Mean predicted stress values at 10%, 15% and 20% equibiaxial stretched are presented. The corresponding ratio of longitudinal to circumferential stressed is also plotted.

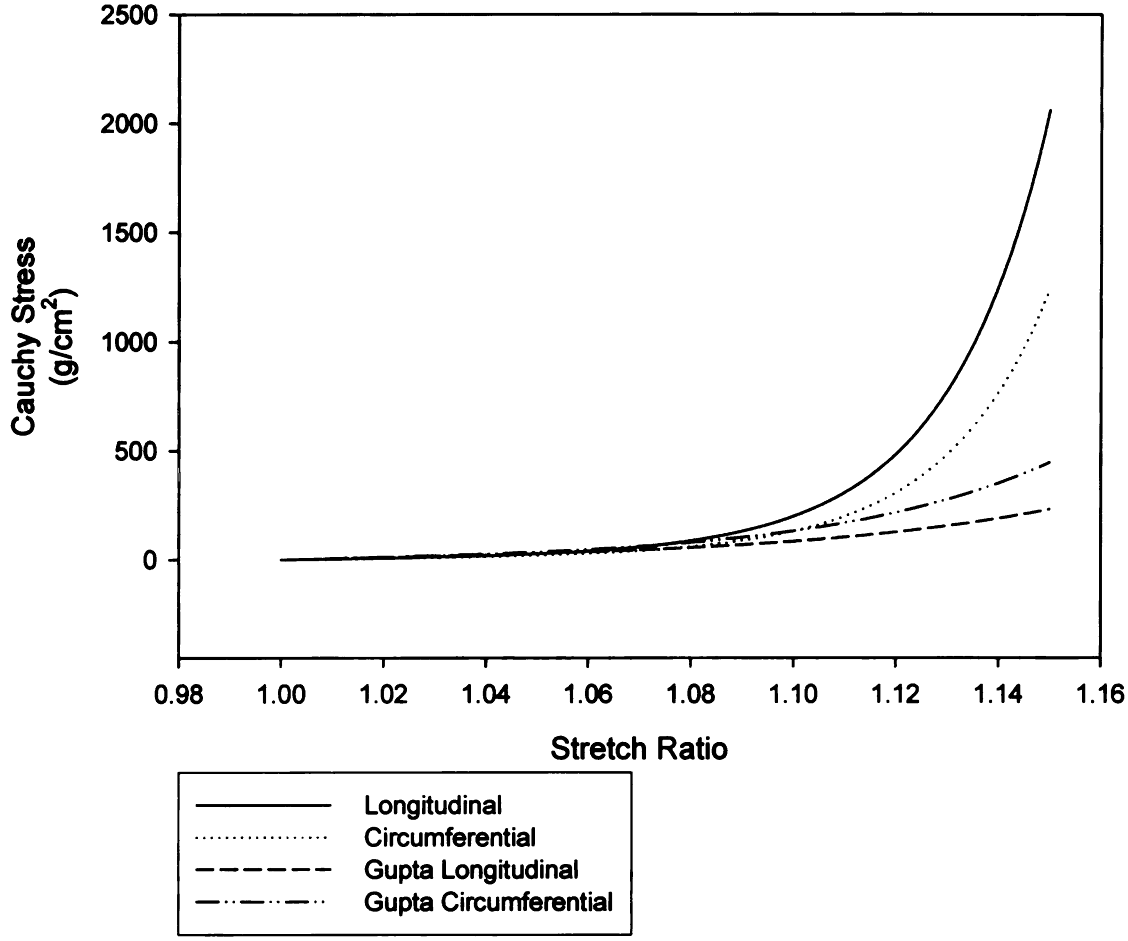

Figure 4.8 – Comparison of the predicted stress strain relationship for the data presented in this study and the one presented by Gupta [1, 2].

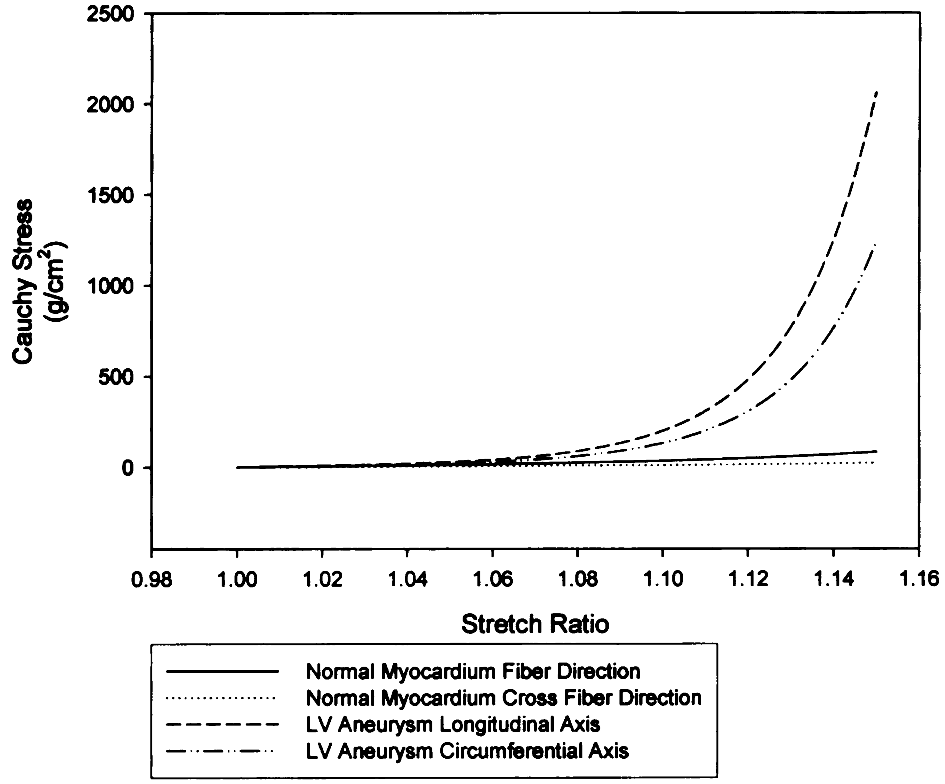

Figure 4.9 – Comparison of the predicted stress strain relationships for the LV aneurysm data presented in this study with that of normal myocardium as presented by Guccione [62]. The LV aneurysm data is defined with respect to the global circumferential and longitudinal directions, while the normal myocardium data is with respect to the local muscle fiber coordinate system.

eferenc

. G

E

. (

v

. V

4.

5.

6.

7.

8.

9.

References:

1. Gupta, K.B., *Functional and Structural Changes in Left Ventricular Aneurysm*, in *Bioengineeing*. 1991, University of Pennsylvania: Philadelphia. p. 310.
2. Gupta, K.B., et al., *Changes in passive mechanical stiffness of myocardial tissue with aneurysm formation.* Circulation, 1994. **89**(5): p. 2315-26.
3. Fung, Y.C., *Biomechanics : mechanical properties of living tissues*. 2nd ed. 1993, New York: Springer-Verlag. xviii, 568 p.
4. Fung, Y.C., *Biomechanics : motion, flow, stress, and growth*. 1990, New York: Springer-Verlag. xv, 569 p.
5. Grondin, P., et al., *Natural history of saccular aneurysms of the left ventricle.* J Thorac Cardiovasc Surg, 1979. **77**(1): p. 57-64.
6. Moustakidis, P., et al., *Altered left ventricular geometry changes the border zone temporal distribution of stress in an experimental model of left ventricular aneurysm: a finite element model study.* Circulation, 2002. **106**(12 Suppl 1): p. I168-75.
7. Guccione, J.M., et al., *Mechanism underlying mechanical dysfunction in the border zone of left ventricular aneurysm: a finite element model study.* Ann Thorac Surg, 2001. **71**(2): p. 654-62.
8. Bogen, D.K., A. Needleman, and T.A. McMahon, *An analysis of myocardial infarction. The effect of regional changes in contractility.* Circ Res, 1984. **55**(6): p. 805-15.
9. Bogen, D.K., et al., *An analysis of the mechanical disadvantage of myocardial infarction in the canine left ventricle.* Circ Res, 1980. **47**(5): p. 728-41.

10. Needleman, A., et al., *A finite element model of the infarcted left ventricle.* J Biomech, 1983. **16**(1): p. 45-58.

11. Pinto, J.G. and Y.C. Fung, *Mechanical properties of the heart muscle in the passive state.* J Biomech, 1973. **6**(6): p. 597-616.

12. Pinto, J.G. and Y.C. Fung, *Mechanical properties of the stimulated papillary muscle in quick-release experiments.* J Biomech, 1973. **6**(6): p. 617-30.

13. Loeffler, L., 3rd and K. Sagawa, *A one-dimensional viscoelastic model of cat heart muscle studied by small length perturbations during isometric contraction.* Circ Res, 1975. **36**(4): p. 498-512.

14. Przyklenk, K., et al., *Effect of myocyte necrosis on strength, strain, and stiffness of isolated myocardial strips.* Am Heart J, 1987. **114**(6): p. 1349-59.

15. Conrad, C.H., et al., *Myocardial fibrosis and stiffness with hypertrophy and heart failure in the spontaneously hypertensive rat.* Circulation, 1995. **91**(1): p. 161-70.

16. Okoshi, M.P., et al., *Comparative mechanical study of isolated papillary muscle from Wistar-Kyoto and Wistar rats.* Jpn Heart J, 1994. **35**(3): p. 333-43.

17. Allaart, C.P., P. Sipkema, and N. Westerhof, *Effect of perfusion pressure on diastolic stress-strain relations of isolated rat papillary muscle.* Am J Physiol, 1995. **268**(3 Pt 2): p. H945-54.

18. Stuyvers, B.D., M. Miura, and H.E. ter Keurs, *Diastolic viscoelastic properties of rat cardiac muscle; involvement of Ca2+.* Adv Exp Med Biol, 1997. **430**: p. 13-28.

19. Brady, A.J., *Mechanical properties of isolated cardiac myocytes.* Physiol Rev, 1991. **71**(2): p. 413-28.

20. Brady, A.J., *Length dependence of passive stiffness in single cardiac myocytes.* Am J Physiol, 1991. **260**(4 Pt 2): p. H1062-71.

21. Shroff, S.G., D.R. Saner, and R. Lal, *Dynamic micromechanical properties of cultured rat atrial myocytes measured by atomic force microscopy.* Am J Physiol, 1995. **269**(1 Pt 1): p. C286-92.

22. Palmer, R.E., A.J. Brady, and K.P. Roos, *Mechanical measurements from isolated cardiac myocytes using a pipette attachment system.* Am J Physiol, 1996. **270**(2 Pt 1): p. C697-704.

23. Kato, S., et al., *Effects of pressure- or volume-overload hypertrophy on passive stiffness in isolated adult cardiac muscle cells.* Am J Physiol, 1996. **271**(6 Pt 2): p. H2575-83.

24. Zile, M.R., et al., *Constitutive properties of adult mammalian cardiac muscle cells.* Circulation, 1998. **98**(6): p. 567-79.

25. Heller, L.J., D.E. Mohrman, and J.R. Prohaska, *Decreased passive stiffness of cardiac myocytes and cardiac tissue from copper-deficient rat hearts.* Am J Physiol Heart Circ Physiol, 2000. **278**(6): p. H1840-7.

26. Harris, T.S., et al., *Constitutive properties of hypertrophied myocardium: cellular contribution to changes in myocardial stiffness.* Am J Physiol Heart Circ Physiol, 2002. **282**(6): p. H2173-2182.

27. Humphrey, J.D., D.L. Vawter, and R.P. Vito, *Quantification of strains in biaxially tested soft tissues.* J Biomech, 1987. **20**(1): p. 59-65.

28. Humphrey, J.D., D.L. Vawter, and R.P. Vito, *Mechanical behavior of excised canine visceral pleura.* Ann Biomed Eng, 1986. **14**(5): p. 451-66.

29.

30.

31.

32.

33.

34.

35.

36.

37.

38.

29. Hoffman, A.H. and P. Grigg, *A method for measuring strains in soft tissue.* J Biomech, 1984. **17**(10): p. 795-800.

30. Humphrey, J.D., D.L. Vawter, and R.P. Vito, *Pseudoelasticity of excised visceral pleura.* J Biomech Eng, 1987. **109**(2): p. 115-20.

31. Lin, D.H. and F.C. Yin, *A multiaxial constitutive law for mammalian left ventricular myocardium in steady-state barium contracture or tetanus.* J Biomech Eng, 1998. **120**(4): p. 504-17.

32. Fung, Y.C., *Biorheology of soft tissues.* Biorheology, 1973. **10**(2): p. 139-55.

33. Fung, Y.C., K. Fronek, and P. Patitucci, *Pseudoelasticity of arteries and the choice of its mathematical expression.* Am J Physiol, 1979. **237**(5): p. H620-31.

34. May-Newman, K. and F.C. Yin, *Biaxial mechanical behavior of excised porcine mitral valve leaflets.* Am J Physiol, 1995. **269**(4 Pt 2): p. H1319-27.

35. Strumpf, R.K., J.D. Humphrey, and F.C. Yin, *Biaxial mechanical properties of passive and tetanized canine diaphragm.* Am J Physiol, 1993. **265**(2 Pt 2): p. H469-75.

36. Nielsen, P.M., P.J. Hunter, and B.H. Smaill, *Biaxial testing of membrane biomaterials: testing equipment and procedures.* J Biomech Eng, 1991. **113**(3): p. 295-300.

37. Lanir, Y., *Constitutive equations for fibrous connective tissues.* J Biomech, 1983. **16**(1): p. 1-12.

38. Gou, P.F., *Strain energy function for biological tissues.* J Biomech, 1970. **3**(6): p. 547-50.

39. Lee, A.A. and A.D. McCulloch, *Multiaxial myocardial mechanics and extracellular matrix remodeling: mechanochemical regulation of cardiac fibroblast function.* Adv Exp Med Biol, 1997. **430**: p. 227-40.

40. Humphrey, J.D. and F.C. Yin, *Constitutive relations and finite deformations of passive cardiac tissue II: stress analysis in the left ventricle.* Circ Res, 1989. **65**(3): p. 805-17.

41. Humphrey, J.D. and F.C. Yin, *A new constitutive formulation for characterizing the mechanical behavior of soft tissues.* Biophys J, 1987. **52**(4): p. 563-70.

42. Demer, L.L. and F.C. Yin, *Passive biaxial mechanical properties of isolated canine myocardium.* J Physiol, 1983. **339**: p. 615-30.

43. Sacks, M.S. and C.J. Chuong, *A constitutive relation for passive right-ventricular free wall myocardium.* J Biomech, 1993. **26**(11): p. 1341-5.

44. Chew, P.H., F.C. Yin, and S.L. Zeger, *Biaxial stress-strain properties of canine pericardium.* J Mol Cell Cardiol, 1986. **18**(6): p. 567-78.

45. Yin, F.C., et al., *Quantification of the mechanical properties of noncontracting canine myocardium under simultaneous biaxial loading.* J Biomech, 1987. **20**(6): p. 577-89.

46. Shacklock, A., *Biaxial Testing of Cardiac Tissue.* 1987, University of Auckland, New Zealand: Auckland.

47. Humphrey, J.D., R.K. Strumpf, and F.C. Yin, *Determination of a constitutive relation for passive myocardium: I. A new functional form.* J Biomech Eng, 1990. **112**(3): p. 333-9.

48. Humphrey, J.D., R.K. Strumpf, and F.C. Yin, *Determination of a constitutive relation for passive myocardium: II. Parameter estimation.* J Biomech Eng, 1990. **112**(3): p. 340-6.

49. Humphrey, J.D., R.K. Strumpf, and F.C. Yin, *Biaxial mechanical behavior of excised ventricular epicardium.* Am J Physiol, 1990. **259**(1 Pt 2): p. H101-8.

50. Novak, V.P., F.C. Yin, and J.D. Humphrey, *Regional mechanical properties of passive myocardium.* J Biomech, 1994. **27**(4): p. 403-12.

51. Kang, T., J.D. Humphrey, and F.C. Yin, *Comparison of biaxial mechanical properties of excised endocardium and epicardium.* Am J Physiol, 1996. **270**(6 Pt 2): p. H2169-76.

52. Hoffmeister, B.K., et al., *Estimation of the elastic stiffness coefficient c13 of fixed tendon and fixed myocardium.* J Acoust Soc Am, 1995. **97**(5 Pt 1): p. 3171-6.

53. Baracca, E., et al., *Non-invasive estimation of the diastolic elastic and viscoelastic properties of the left ventricle.* Eur Heart J, 1991. **12**(2): p. 249-61.

54. Olsen, C.O., et al., *Diastolic anisotropic properties of the left ventricle in the conscious dog.* Circ Res, 1991. **69**(3): p. 765-78.

55. Omens, J.H., D.A. MacKenna, and A.D. McCulloch, *Measurement of strain and analysis of stress in resting rat left ventricular myocardium.* J Biomech, 1993. **26**(6): p. 665-76.

56. Parmley, W.W., et al., *In vitro length-tension relations of human ventricular aneurysms. Relation of stiffness to mechanical disadvantage.* Am J Cardiol, 1973. **32**(7): p. 889-94.

57. Institute of Laboratory Animal Resources (U.S.), *Guide for the care and use of laboratory animals*. 7th ed. 1996, Washington, D.C.: National Academy Press. xii, 125.

58. Markovitz, L.J., et al., *Large animal model of left ventricular aneurysm.* Ann Thorac Surg, 1989. **48**(6): p. 838-45.

59. Downs, J., et al., *An improved video-based computer tracking system for soft biomaterials testing.* IEEE Trans Biomed Eng, 1990. **37**(9): p. 903-7.

60. Marquardt, D., *An Algorithm for Least-Squares Estimation of Nonlinear Parameters.* SIAM J. Appl. Math., 1963. **11**: p. 431-441.

61. Jackson, B.M., et al., *Extension of borderzone myocardium in postinfarction dilated cardiomyopathy.* J Am Coll Cardiol, 2002. **40**(6): p. 1160-7; discussion 1168-71.

62. Guccione, J.M., A.D. McCulloch, and L.K. Waldman, *Passive material properties of intact ventricular myocardium determined from a cylindrical model.* J Biomech Eng, 1991. **113**(1): p. 42-55.

63. Han, G.J., et al., *Application of finite-element analysis with optimisation to assess the in vivo non-linear myocardial material properties using echocardiographic imaging.* Med Biol Eng Comput, 1993. **31**(5): p. 459-67.

64. Yettram, A.L. and M.C. Beecham, *An analytical method for the determination of along-fibre to cross-fibre elastic modulus ratio in ventricular myocardium--a feasibility study.* Med Eng Phys, 1998. **20**(2): p. 103-8.

65. Okamoto, R.J., et al., *Epicardial suction: a new approach to mechanical testing of the passive ventricular wall.* J Biomech Eng, 2000. **122**(5): p. 479-87.

66. Sebbag, L., et al., *Protection of ischemic myocardium in dogs using intracoronary 2,3-butanedione monoxime (BDM).* J Mol Cell Cardiol, 2003. **35**(2): p. 165-76.

67. Crottogini, A.J., et al., *Left ventricular end-systolic elastance is incorrectly estimated by the use of stepwise afterload variations in conscious, unsedated, autonomically intact dogs.* Circulation, 1994. **90**(3): p. 1431-40.

68. Brown, M.A., et al., *Post-systolic shortening: a marker of potential for early recovery of acutely ischaemic myocardium in the dog.* Cardiovasc Res, 1987. **21**(10): p. 703-16.

69. Savage, E.B., et al., *Repair of left ventricular aneurysm. Changes in ventricular mechanics, hemodynamics, and oxygen consumption.* J Thorac Cardiovasc Surg, 1992. **104**(3): p. 752-62.

70. Ratcliffe, M.B., et al., *Radio frequency heating of chronic ovine infarct leads to sustained infarct area and ventricular volume reduction.* J Thorac Cardiovasc Surg, 2000. **119**(6): p. 1194-204.

71. Toombs, C.F., et al., *Nonlinearity of indexes of left ventricular performance: effects on estimation of slope and diameter axis intercepts.* Am J Physiol, 1991. **260**(6 Pt 2): p. H1802-9.

72. Little, W.C., et al., *Comparison of measures of left ventricular contractile performance derived from pressure-volume loops in conscious dogs.* Circulation, 1989. **80**(5): p. 1378-87.

73. Noda, T., et al., *Curvilinearity of LV end-systolic pressure-volume and dP/dtmax-end-diastolic volume relations.* Am J Physiol, 1993. **265**(3 Pt 2): p. H910-7.

74.

75.

74. Dokos, S., et al., *A triaxial-measurement shear-test device for soft biological tissues.* J Biomech Eng, 2000. **122**(5): p. 471-8.

75. Dokos, S., et al., *Shear properties of passive ventricular myocardium.* Am J Physiol Heart Circ Physiol, 2002. **283**(6): p. H2650-9.

Chapter 5

Finite Element Model of Left Ventricular Aneurysm

Abstract:

A highly detailed finite element model was used to examine the presence of left ventricular (LV) aneurysm in the ovine heart. Through a series of simulations, the choice of material parameters used to model LV aneurysm was found to have a large effect upon both the global and regional function of the heart. Simply reducing the contractility and increasing the stiffness of the aneurysm region were found to produce different results than using material parameters measured from biaxial testing. This highlights the importance of using accurate material parameter predictions applied to a realistic model rather than simply increasing the "stiffness" of the tissue in a generalized model as other investigators have done in the past. Furthermore, our model predicted an increase in cross-fiber stress and a decrease in fiber stress at all regions of the left ventricle at end systole. This result could have significant importance in understanding the mechanism behind collagen expression in the diseased left ventricle.

Introduction:

In the previous chapter, we used a biaxial testing apparatus to arrive at material parameter estimation for ovine LV aneurysm. The next logical step is to understand the effects that these material parameters have on both the global and regional function of the left ventricle. This goal will be accomplished by developing a finite element model of LV aneurysm based upon these measured parameters. Furthermore, we will compare the results predicted by this data to other means of simulating LV aneurysm and normal my

by

app

The

the

dev

car

forn

pov

bas

Rad

stra

ellip

myo

geor

reso

mod

relat

of th

cardi

basec

previ

myocardium. The global function predictions, and detailed stress strain results, predicted by these models will allow us to understand the importance of selecting the most appropriate material parameters when creating computer models of the left ventricle.

There have been many attempts by other investigators to use mathematical modeling in the past. One of the first was an analytical thin shelled sphere model of the heart developed by Vayo [2] that was used to predict relations between aneurysm shape and cardiac function. Bogen developed a finite element model based upon membrane formulation that was applied to an initially spherical model of the left ventricle [3-5]. A power law strain energy function was used by Bogen to describe systole and diastole was based upon the Law of Laplace. In order to study the mechanics of LV aneurysm rupture Radhakrishnan used a thin shelled ellipsoidal model of the left ventricle with linear stress strain relations [6]. Reif and colleagues continued study in this area using a three layered ellipsoidal model of the left ventricle with linear stress strain relationships for the myocardium and aneurysm tissue [7]. Recently, investigators have used realistic geometries determined from imaging modalities (echocardiography and magnetic resonance imaging) to construct finite element models of LV aneurysm [8-10]. These models are all based upon infinitesimal deformation theory, and use linear stress strain relations, that do not accurately match the realistic deformations and material properties of the heart. The models presented previously are based upon numerous assumptions of cardiac mechanics that do not necessarily hold true. Some of the earliest models were based upon simple geometries that do not accurately model the left ventricle. The previous models all use either a power law strain energy function or a linear stress strain

relation. Both the myocardium [11-25] and aneurysm [26-28] have been shown by many investigators to be highly nonlinear and may best be described by an exponential strain energy function [29-32]. The use of the Law of Laplace has also been shown to inaccurately predict LV mechanics [33]. None of the above studies define special material properties for the border zone region. Recent studies have suggested that the systolic material properties in the border zone are depressed compared to normal myocardium [1]. It has also been established by other investigators that large deformation theory is superior in describing the function of the left ventricle, however, computational resources previously limited its application [34, 35]. Finally, none of the above models account for the muscle fiber structure of the left ventricle [36], and the subsequent impact upon LV mechanics [37-39].

In the present study, we will present a model that addresses many of these concerns. Specifically, our model will have: (1) a realistic geometry measured from magnetic resonance imaging, (2) incorporate myocardial material properties defined with respect to the local muscle fiber direction, (3) have aneurysm material properties measured from biaxial stretching, (4) define separate material properties in the border zone that incorporate an appropriate decrease in systolic function, (5) use exponential strain energy functions derived from experimental data and (6) be solved using large deformation finite element method techniques. This analysis should allow us to produce the most realistic computer model of LV aneurysm to date.

Methods:

Creation of the Left Ventricular Aneurysm

LV aneurysm was induced according to the method described Chapter 4.

Preparation for Magnetic Resonance Imaging

Ten weeks following creation of the LV aneurysm, the animal was prepared for magnetic resonance imaging (MRI). Sedation was accomplished using an intramuscular injection of ketamine (15 mg/kg). After sedation, the animal was intubated and ventilated using a mixture of isoflurane and oxygen. To monitor hemodynamic data nonferromagnetic catheters (Mikro-Tip, 5F, model SPC-350 MR; Millar Instruments Inc, Houston, TX) were inserted into the left ventricle, right ventricle and aortic root using the left carotid artery, jugular vein and femoral artery, respectively. The animal was then positioned in the supine position within the MRI machine (Magnetom Vision, Siemens Medical Systems, Iselin, NJ), with a Helmholtz coil centered on the chest. Following imaging, the animal was sacrificed using pentobarbital (120 mg/kg intravenously), and heparin (5000 U intravenously) followed by rapid infusion of KCl (80 mEq intravenously).

Magnetic Resonance Image Acquisition and Processing

Multiple scout images were used to identify the position of the heart, and to locate the true short and long-axis planes. After the preliminary image set up, a series of eight short-axis image planes (8 mm thick) were obtained parallel to the true short-axis plane at 8 mm intervals starting at the level of the mitral valve and continuing until the image contained only LV epicardium, with no LV or right ventricular endocardium visible. Additionally, four long-axis images were obtained at 45 degree intervals, orthogonal to the true short-axis plane, and intersecting the LV centroid.

The R wave of the electrocardiogram was used to synchronize the image acquisition. The ventilator (Hallowell 2000, Hallowell EMC, Pittsfield, MA) was stopped at maximum inspiration for 20 to 30 seconds during the image acquisition to minimize respiratory motion and the associated motion artifacts in the images. During the period of paused ventilation a series of images was acquired at 29 ms intervals until the approximate completion of the cardiac cycle. Total data acquisition time was approximately 45 minutes. Imaging variables were a repetition time equal to the cardiac cycle (RR duration), an echo time of 29 ms, an excitation angle of 15 degrees, and an acquisition matrix of 256 x 256. The field of view was set to 350 x 350 mm^2 and 400 x 400 mm^2 for the short-axis and long-axis images, respectively. The raw images were then transferred to a Silicon Graphics Workstation (Silicon Graphics Inc., Mountain View, CA), and converted to the .rgb format using custom software [1]. The images were then cropped and scaled by 300% (Figure 5.1).

The border zone region was identified by isolating the region where the LV wall thickness changed from normal (12 to 15 mm) to very thin (3 mm). Thus, we used anatomical, rather than functional means to identify the border zone.

Biaxial Material Property Determination

Biaxial material properties were obtained as described in Chapter 4. Briefly six animals with LV aneurysm were studied. After the aneurysm was allowed to mature for six weeks, the animal was sacrificed and the aneurysm was excised for testing. Testing was performed using a biaxial stretcher previously described by others [18, 40-42]. The resulting stress strain results were fit using the Levenberg-Marquardt method [43] to obtain parameters for the strain energy function described below.

Creation of Model Geometry

The images obtained previously from MRI were examined to isolate the time point which most closely was associated with the beginning of diastolic filling. The eight short-axis and four long-axis slices associated with this time point were then digitized to obtain the locations of the endocardium and epicardium. Using the method of Nielson [44], a high order finite element (FE) model of the left ventricle (including the aneurysm) was created in prolate spheroidal coordinates (focal length, 41.0 mm). This model was then fit to smooth bicubic Hermite finite elements [45] to the epicardial (304 points) and

endocardial (247 points) data sets (Figure 5.2). For the original 16 element model, the root mean square errors of the surface fits were 0.8 mm and 1.2 mm for the endocardium and epicardium respectively. The wall thickness of the model ranged from 15 mm near the base to 3 mm near the apex. The wall and cavity volumes of the model were 104.8 mL and 198.1 mL respectively.

In order to accurately model the variation of the material properties seen in the three different sections of the model (remote, border zone, and aneurysm), the 16 element bicubic model was refined into a 168 element trilinear model, with 12 elements circumferentially and 14 elements longitudinally (Figure 5.3) with constant hydrostatic pressure within each element. Then normal, border zone, and aneurysm regions of the model occupied approximately 76%, 14%, and 10 % of the total wall volume respectively. The fiber angles were assumed to vary linearly from 83 degrees at the endocardium to -37 degrees at the epicardium, in accordance with previous measurements [46].

In order to incorporate the material properties measured from the previously described biaxial measurements, it was necessary to create a second, more complex model. The parameters obtained from the biaxial stretching experiments are defined with respect to the circumferential longitudinal axes, whereas the material properties used in the border zone and remote sections are defined with respect to the muscle fiber orientation. In order to accommodate this, a "window pane" region was created in the existing border zone region of the model. To prevent discontinuities in the circumferential direction, it was necessary to refine the circumferential elements that formed a border between aneurysm and border zone (Figure 5.4). The refining was done in such a manner that the closest 10% of the elements next to the aneurysm were placed in the new "window pane region." In this new 280 element model there are three different fiber orientation schemes used. In the remote and border zone regions of the model, the fiber angles were assumed to vary linearly from 83 degrees at the endocardium to -37 degrees at the epicardium. In the window pane region, the fibers vary from their value in the border zone (i.e. -37 degrees at the epicardium), to 0 degrees at the border with the aneurysm region. In the aneurysm region, the fibers show no transmural variation and are aligned with the circumferential direction (i.e. zero degrees) (Figure 5.5), which is in approximate agreement with histological measures of collagen fiber angle variation [47].

Finite Element Model

The finite element methods used for the simulation are similar to that described by Costa and colleagues [37]. The mathematical descriptions (stress strain relationships) for systolic and diastolic material properties were originally described by Guccione [32]. These methods are described in Chapter 3, but will be briefly summarized here.

The use of two different local coordinate systems necessitates the use of two similar, yet different strain energy functions. In the remote, border zone and aneurysm regions the following strain energy function was used:

$$W = \frac{C}{2}\{\exp[b_f E_{11}^2 + b_t(E_{22}^2 + E_{33}^2 + E_{23}^2 + E_{32}^2) + b_{fs}(E_{12}^2 + E_{21}^2 + E_{13}^2 + E_{31}^2)] - 1\} \quad (5.1)$$

where E_{11} is fiber strain, E_{22} is cross-fiber in-plane strain, E_{33} is radial strain, E_{23} is shear in the transverse plane, and E_{12} and E_{13} are shear strain in the fiber-cross fiber and fiber-radial coordinate planes. Guccione and colleagues previously found that the material constants $C = 0.88$ kPa, $b_f = 18.48$, $b_t = 3.58$, $b_{fs} = 1.63$ allowed a cylindrical model of the left ventricle to match strains measured during passive ventricular filling in an intact canine heart preparation [29]. Equation (5.1), also has been shown to allow an FE model of the beating dog heart [32] to predict end diastolic finite strain distributions from a midventricular region of the anterior LV free wall consistent with three-dimensional strain measurements for passive inflation [46].

For the aneurysm region of the left ventricle, the following strain energy function will be used:

$$W = \frac{C}{2}\{\exp[b_c E_{11}^2 + b_l(E_{22}^2 + E_{33}^2 + E_{23}^2 + E_{32}^2) + b_{cs}(E_{12}^2 + E_{21}^2 + E_{13}^2 + E_{31}^2)] - 1\} \quad (5.2)$$

where E_{11} is circumferential strain, E_{22} is longitudinal strain, E_{33} is radial strain, E_{23} is shear in the transverse plane, and E_{12} and E_{13} are shear strain in the circumferential-longitudinal and circumferential-radial coordinate planes. Biaxial measurements from 10 week old ovine LV aneurysm presented in Chapter 4 yielded the following parameter va

m

Sy

wa

se

of

(5.

fu

[3

In

50

co

ov

re

be

pro

values: $C = 0.29$ kPa, $b_c = 33.17$ and $b_l = 41.56$. The shear term, b_{cs}, was not measured, so the value for normal myocardium, 1.63, was used.

Systolic contraction was modeled in three different ways. In the remote region, systole was assumed to function in a normal manner, as described in Chapter 3. Briefly, the second Piola-Kirchhoff stress tensor was defined referred to fiber coordinates as the sum of passive three-dimensional stress derived from the strain energy function (Equation (5.1)) and an active fiber stress component T_o (oriented along the fiber axis) that is a function of time t, peak intracellular calcium concentration Ca_o, and sarcomere length l [31]:

$$t^{\alpha\beta} = \frac{1}{2}\left(\frac{\partial W}{\partial E_{\alpha\beta}} + \frac{\partial W}{\partial E_{\beta\alpha}}\right) - pg^{\alpha\beta} + T_o\left(t, Ca_o, l\right)\delta_1^{\alpha}\delta_1^{\beta}, \tag{5.3}$$

In the border zone region (and window pane sub region), the contractility was reduced by 50%, at the suggestion of previous studies [1] that have shown this reduction in contractility reproduces the observed circumferential lengthening in the border zone of ovine LV aneurysm models [48]. The remainder of the systolic contraction model remained the same as in the remote region. In the aneurysm, the tissue was assumed to be noncontractile, and thus the systolic properties were the same as the diastolic material properties described above.

The two models described above (the 168 element, and 280 element) were used to create four separate simulations. The 168 element model was used to simulate a control case, an aneurysm with normal material properties (i.e. normal diastolic properties, but no contraction in the aneurysm region, 50% contractility in the border zone region), and a "stiff" aneurysm (increased diastolic stiffness, no active contraction in the aneurysm region, 50% contraction in the border zone region). The control case was used to provide a comparison situation with normal myocardial material properties applied to a diseased geometry. This case serves to isolate only the changes that occur with material property variation and not geometry change. The 280 element model was used to model an aneurysm with material properties based on those measured by the biaxial stretcher. A summary of these parameters is presented in Table 5.I.

Each of the models was placed through the same simulated cardiac cycle. The initial shape, with diastolic material properties was inflated from an intracavity pressure of 0 mmHg to 37.5 mmHg. Stress, strain, and volume measurements were made at 3.75 mmHg increments. After the diastolic filling phase, contractility was increased from 0% to 100% while LV cavity pressure was increased to 120 mmHg. Intracavity pressure was decreased from 120 mmHg to 0 mmHg while contractility was held at 100%. Stress, strain, and volume measurements were made at 7.5 mmHg increments. In this manner pressure-volume relationships were created with the corresponding stress and strain values for each simulation.

Calculation of Diastolic and Systolic Pressure-Volume Relationships

Volume solutions were obtained at end diastolic (0-40 mmHg), and end systolic (0-120 mmHg) pressures. Owing to the non-linearity of the produced systolic pressure-volume relations, the end systolic pressure (P_{ES}) and end systolic volume (V_{ES}) from the finite element model were fit to the following quadratic relationship:

$$P_{ES} = \beta_{o,EES} + \beta_{1,EES} V_{ES} + \beta_{2,EES} V_{ES}^2 \qquad (5.4)$$

where $\beta_{o,EES}$, $\beta_{1,EES}$ and $\beta_{2,EES}$ are the stiffness parameters of the LV end systolic elastance. The relationship between the end diastolic pressure (P_{ED}) and the end diastolic volume (V_{ED}) was then fit to the following quadratic equation:

$$P_{ED} = \beta_{o,DC} + \beta_{1,DC} V_{ED} + \beta_{2,DC} V_{ED}^2 \qquad (5.5)$$

where β_o, β_1 and β_2 are the diastolic stiffness parameters.

Calculation of Stroke Volume/P_{ED} (Starling) Relationship

For each set of material parameters, a stroke volume/P_{ED} (Starling relation) was calculated by constructing a series of pressure-volume loops that were bound by the end systolic and end diastolic pressure-volume loops produced by the simulation. V_{ED} was

initially set to 40 mmHg, and then decreased for subsequent loops. In order to calculate the end systolic pressure-volume point on each loop arterial elastance (E_A) was set to a fixed value of 3.2 mmHg/ml, a value that has been reported by two investigators studying the ovine infarct model presented here [49, 50]. Since the end systolic pressure-volume relation was significantly non-linear, the following equation was used to find the intersection between the arterial elastance line and the end systolic pressure-volume relationship:

$$0=\left(\beta_{o,EES}+E_A V_{ED}\right)+\left(\beta_{1,EES}-E_A\right)V_{ES}+\beta_{2,EES}V_{ES}^2, \tag{5.6}$$

where V_{ED} is the volume intercept of the arterial elastance. V_{ES} was then calculated by obtaining roots of Equation (5.6). The stroke volume was then calculated by taking the difference between V_{ED} and V_{ES}.

Calculation of Stress and Strain Values

For each simulation, stress and strain were calculated at the same pressure points that volume was calculated. Stress and strain values were calculated at the central Gauss point within each element, the point at which the values are most accurate. Stress and strain values were calculated with respect to the unloaded model configuration. These results were then averaged across the three respective sections (Remote, Border Zone, and Aneurysm) to provide a representation of the stress or strain in each region.

Results:

Aneurysm Material Property Influence on Global Function

For each of the four simulations conducted, pressure-volume relations were constructed (Figure 5.6). Compared to the control case, the case in which normal aneurysm material properties were used showed that the diastolic pressure-volume relation was unchanged as the diastolic material properties were the same. The systolic pressure-volume relation showed an increase in linearity, and was shifted to the right. The "stiff" aneurysm case showed a leftward shift in the diastolic pressure-volume relation when compared to the control case. The systolic pressure-volume relation showed an increase in linearity, was similar to the control case at high ventricular volumes, and a rightward shift at low ventricular volumes when compared to the control case. When the material properties for the aneurysm were those measured by biaxial stretching, the greatest leftward shift in the diastolic pressure-volume relation compared to the control case was seen. The systolic pressure-volume relation was shifted to the left at high ventricular volumes, and to the right at low ventricular volumes when compared to the control case. The systolic and diastolic stiffness parameters are presented in Table 5.II. Volume solutions from these parameters at pressures corresponding to end systole (100 mmHg) and end diastole (20 mmHg) are presented in Table 5.III. This analysis shows that the stroke volume decreased from 32.0 mL in the control case to 26.6 mL and 26.8 mL in the normal

aneurysm material property case and "stiff" aneurysm cases, respectively. The stoke volume only decreased to 27.6 mL in the biaxial material properties case.

The effect of aneurysm material parameters on the Starling relationship is presented in Figure 5.7. In all cases the Starling relation was depressed when compared to the control case. The normal aneurysm material properties case and the "stiff" aneurysm material property case were largely similar, while the material properties determined from biaxial material property testing showed the least depression from the control case.

Aneurysm Material Property Influence on Regional Function

Strain and Stress Analysis During Diastole

The strain and stress results in the aneurysm region of each model are presented in Figure 5.8. The control case and normal aneurysm stiffness case produced the same results, as the only difference is seen in systole. The strain results show a reduction in fiber and radial strain for the biaxial material property case, but a slight increase in cross-fiber strain compared to the other simulations. The stress results show a decrease in fiber stress and an increase in cross-fiber stress for the biaxial material property case compared to the other simulations. Table 5.IV presents the strain and stress results in the aneurysm region at end diastole (20 mmHg). Fiber stress and strain were shown to be lowest in the case where the material properties were chosen from biaxial testing. In this case the strain was reduced from 0.165 in the control case to 0.112 (32% decrease), while the

stress was reduced from 14.5 kPa in the control case to 8.8 kPa (39% decrease). Cross-fiber stress and strain were increased in the biaxial testing material property case when compared to the control case. Cross-fiber strain increased from 0.23 in the control case to .25 (5% increase), and cross-fiber stress increased from 4.4 kPa to 5.5 kPa (23% increase).

Figure 5.9 shows the strain and stress results for the border zone region of each model. The fiber strain in the border zone region is similar to that predicted by the "stiff" aneurysm model, which was less than that predicted by the control case. The cross-fiber strain and radial strain decreased from the control model to the "stiff" aneurysm model, to the biaxial material property model. The stress results predicted that the lowest border zone stress was shown in the model defined with material properties determined by biaxial stretching. Table 5.V presents the strain and stress results in the border zone region at end diastole (20 mmHg). At end diastole all of the border zone stress and strain calculations predicted by the model with material properties determined from biaxial testing showed a decrease when compared to the control case. Fiber stress and strain produced by the biaxial material property model were 21% and 18% lower than the same components predicted by the control model. Cross-fiber stress and strain produced by the biaxial material property model were 19% and 29% lower than the same components predicted by the control model. Radial stress and strain produced by the biaxial material property model were 18% and 25% lower than the same components predicted by the control model.

Figure 5.10 shows the strain and stress results in the remote region predicted by each of the models. The remote region fiber and radial strain were shown to be reduced in the biaxial material property model compared to the other simulations. This reduction in strain resulted in decreased fiber stress and increased radial strain in the region. Table 5.VI presents the strain and stress results in the remote region at end diastole (20 mmHg). Fiber stress and strain produced by the biaxial material property model were 15% lower than the same components predicted by the control model. The cross-fiber stress and strain were increased by 1% and 2% respectively. The radial strain was decreased by 12%, while the radial strain showed and increase of 10%

Strain and Stress Analysis During Systole

Figure 5.11 shows the strain and stress results for the aneurysm region. The largest difference is seen in the cross-fiber direction, where fiber strain predicted by the biaxial material properties model was shown to be greater in the aneurysm region when compared to the other simulations. This resulted in an increase in cross-fiber stress in the case where material properties were determined by biaxial testing when compared to the other simulations. Table 5.VII presents the strain and stress results for the aneurysm at end systole (100 mmHg). In the aneurysm region at end systole fiber strain predicted by the model with biaxial material properties was increased by 7% when compared to the control model, while fiber stress showed a 20% decrease. Cross-fiber strain predicted by the biaxial material property model was increased by 20% compared to the control case,

while cross-fiber stress was increased by nearly 3,500% (from -0.7 kPa to 22.4 kPa). Radial strain showed very little difference between the two cases.

The strain and stress results for the border zone region during systole are shown in Figure 5.12. All of the simulations in which an aneurysm is modeled (no active contraction in the aneurysm region) showed an increase in fiber strain in the border zone region. Only the simulation defined by biaxial material properties showed a predicted decrease in fiber stress in the border zone when compared to the control case, the other simulations predicted the opposite. All simulations predicted an increase in cross-fiber stress in the border zone. Table 5.VIII presents the strain and stress results for the border zone region at end systole. At end systole fiber strain predicted from the model with aneurysm material properties determined from biaxial testing showed a 45% increase in strain when compared to the control model, while stress was decreased by 29%. Cross-fiber strain predicted by the model with aneurysm material properties determined by biaxial testing was 27% less than that predicted by the control model, while stress was increased by 206%. Radial strain was reduced by 46% in the biaxial material property model compared to the control model, while stress was decreased by 26%.

The strain and stress results for the remote region are presented in Figure 5.13. Again only the simulation defined by material properties determined by biaxial testing predicted a decrease in fiber stress. All simulations predicted an increase in cross-fiber stress. Table 5.IX presents the strain and stress results for the remote region at end systole. At end systole, the fiber strain predicted by the biaxial material property model was

decreased by 91% when compared to the control case, while fiber stress was reduced by 12%. Cross-fiber strain predicted in the biaxial material property model was increased by 6% when compared to the control case, while cross-fiber stress was increased by 12%. Radial strain predicted by the biaxial material property model was increased by 131% when compared to the control model, while radial stress was increased by 9%.

Discussion:

The results presented here represent the most realistic computational model of LV aneurysm presented to date. We have provided a detailed analysis of not only cardiac function during LV aneurysm, but also a regional stress and strain analysis. We have shown that by using the material properties measured from biaxial testing, rather than simply altering the stiffness of the myocardial aneurysm, allows our model to predict an optimal cardiac function when compared to simply increasing the "stiffness" of the aneurysm. These studies have also shown that the choice of material parameters used to define the aneurysm can have significant impact upon the global and regional function of the left ventricle. In nearly every case, simply modeling the aneurysm region by increasing the stiffness component (C in Equation (5.1)), and/or removing the contractility produced drastically different results than actually using measured material parameters that model stiffness realistically.

In all regions of the heart (aneurysm, border zone, remote), the use of our biaxially determined material properties predicted decreased fiber stress of at least 15% at both end

diastole and end systole. Simply increasing the bulk stiffness (C in Equation (5.1)) predicted an increase in fiber stiffness. The aneurysm and remote region showed a corresponding increase in cross-fiber stress at end diastole, while the border zone region showed a decrease in cross-fiber stress at end diastole. At end systole, all regions showed an increase in cross-fiber stress when compared to the control case. The same increase in cross-fiber stress was not seen in the other models based upon a generic increase in stiffness.

The studies by Bogen [3-5], based upon a spherical shell model of the left ventricle, produced similar global results to those obtained here. However, there were some differences. The systolic pressure-volume relationships presented by Bogen show no overlap between non-infarcted tissue and infarcted tissue. Our results (Figure 5.6), show that this lack of overlap is not the case, and in fact at high ventricular pressure, the systolic pressure-volume loop for the biaxial material property data is shifted further to the left than the control case. Furthermore, the Bogen model is not able to reproduce the non-linear systolic stress strain relationship that our models produce.

One of the shortcomings that the Bogen model had was, as the authors noted, its inability to predict the stress and strain present in the border zone region. Their model contained a discontinuity at this junction whereas the present model shows a gradual shift in material properties (both fiber angle distribution and contractility). Discontinuity in the Bogen model certainly invalidates the results at the junction between infarct and residual myocardium, and may serve to skew the remainder of the results as well.

The Bogen model has also predicted the existence of higher stresses in the remote myocardium away from the border zone junction during diastole. Our model predicts the opposite, namely that the remote region experiences less stress during diastole than the aneurysm tissue.

In the study by Moustakidis and colleagues regional stress values similar to the ones reported here are presented [9]. However, they did not make use of fiber angle distributions and could not report the difference between fiber and cross-fiber stress. Our results were similar in magnitude to the Moustakidis results in that during both systole and diastole the aneurysm region experiences the largest stress value followed by the border zone region, then the remote region. Their model does not reveal the intricacies that our model is able to, such as the changes in fiber and cross fiber stress.

One of the key results presented here is the change in stresses produced not only in the aneurysm itself, but also the border zone and remote region. It has been well established by others that regional changes in collagen content and cross-linking following myocardial infarction could have an effect upon LV mechanics and performance [51-62]. It is quite possible that the increase in cross-fiber stress coupled with the decrease in fiber stress throughout the heart during systole could be a mechanical signal to alter the extra cellular matrix collagen content. Certainly more experiments need to be done to verify this theory. It should also be noted that during diastole, the border zone region showed a decrease in both fiber and cross-fiber stress when compared to the control case. These

results highlight the need to examine the expression of collagen in response to changing stress and strain.

Future Improvements:

The computer model could be improved in a number of ways. First, new techniques such as tagged MRI [63], could be used to optimize material parameters in the border zone and remote regions of the ventricle. Diffusion tensor MRI [64] could also be employed to give more accurate measurements of the true fiber angle distribution throughout the remote and border zone regions. MRI techniques are generally limited in the aneurysm region, as the relative thickness of the region is too small to allow analysis by current means.

Conclusion:

The results presented here illustrate two important points. First, the choice of material properties used to study LV aneurysm is not a trivial one. By examining different material properties that can all model LV aneurysm through increased stiffness, we have shown that each can produce drastically different results. Therefore, it is of utmost importance to select material parameters that are as close to reality as possible. Second, we have shown that models of LV aneurysm show a relative increase in cross-fiber stress and a decrease in fiber stress when compared to healthy tissue.

Of cri

param

we sh

aneur

Of critical importance in the future is the identification of how the change in material parameters can affect the global and regional function of the left ventricle. Furthermore, we should identify the importance of changing the local fiber angle system in the aneurysm to more closely associate with reality.

	Anuerysm Region	Border Zone Region	Remote Region
Control			
C (kPa)	0.88	0.88	0.88
bf	18.48	18.48	18.48
bt	3.58	3.58	3.58
bfs	1.63	1.63	1.63
Contractility	100%	100%	100%
Model Elements	168		
Normal Anuerysm Material Properties			
C (kPa)	0.88	0.88	0.88
bf	18.48	18.48	18.48
bt	3.58	3.58	3.58
bfs	1.63	1.63	1.63
Contractility	0%	50%	100%
Model Elements	168		
"Stiff" Anuerysm			
C (kPa)	8.8	0.88	0.88
bf	18.48	18.48	18.48
bt	3.58	3.58	3.58
bfs	1.63	1.63	1.63
Contractility	0%	50%	100%
Model Elements	168		
Anuerysm Material Properties from Biaxial Testing			
C (kPa)	0.29	0.88	0.88
bf*	33.17	18.48	18.48
bt*	41.56	3.58	3.58
bfs*	1.63	1.63	1.63
Contractility	0%	50%	100%
Model Elements	280		

Table 5.I – Material Parameters Used In Model Simulations – For each of the four cases, the material parameters used in the stress strain relations are presented. In the control case all material parameters are "normal" in all regions. The normal aneurysm material property case has "normal" material properties in all three sections; however, contractility is reduced to 50% in the border zone and 0% in the aneurysm. The "stiff" aneurysm has the same material properties as the "normal" aneurysm, with the exception of the stiffness parameter C, which was increased by a factor of 10. The last case has material parameters in the aneurysm region defined by biaxial material property testing, and the remote and border zone regions have normal material parameters with 100% and 50% contractility respectively.

	End Systolic Elastance			End Diastolic Compliance		
	$\beta_{o,EES}$	$\beta_{1,EES}$	$\beta_{2,EES}$	$\beta_{o,DC}$	$\beta_{1,DC}$	$\beta_{2,DC}$
Control	-111.1253	1.6329	-0.0028	59.0928	-0.8138	0.0028
Normal Aneurysm Material Properties	-52.0667	0.4674	0.0010	59.0928	-0.8138	0.0028
"Stiff" Aneurysm	-85.8411	0.9903	-0.0003	60.2605	-0.8854	0.0033
Material Properties from Biaxial Testing	-87.6375	0.8398	0.0008	89.4227	-1.2819	0.0046

Table 5.II – Systolic Elastance and Diastolic Compliance – Fitted quadratic parameters to the systolic elastance (Equation (5.4)) and diastolic compliance (Equation (5.5)) relations for each of the four cases.

	ED Volume (mL)	ES Volume (mL)	SV (mL)	EF
Control	231.86	199.85	32.01	13.8%
Normal Aneurysm Material Properties	231.86	205.28	26.58	11.5%
"Stiff" Aneurysm	211.67	184.87	26.81	12.7%
Material Properties from Biaxial Testing	205.94	178.36	27.58	13.4%

Table 5.III – The effect of aneurysm material parameters on global indices of cardiac function. ED (20 mmHg) and ES (100 mmHg) volumes determined from equation (5.5) and equation (5.4) respectively. Note the increase in SV shown by the biaxial material property case compare to the other diseased cases.

	Aneurysm Region					
	ED Mean Strain			ED Mean Stress (kPa)		
	Fiber	Cross-Fiber	Radial	Fiber	Cross-Fiber	Radial
Control	0.165	0.234	-0.223	14.484	4.424	-0.700
Normal Aneurysm Material Properties	0.165	0.234	-0.223	14.484	4.424	-0.700
"Stiff" Aneurysm	0.137	0.216	-0.204	10.531	4.030	-0.602
Material Properites from Biaxial Testing	0.112	0.246	-0.170	8.842	5.475	-0.665

Table 5.IV – End Diastolic Stress Strain Results in the Aneurysm Region – Stress and strain results for each case in the aneurysm region at end diastole (20 mmHg). In the material properties determined from biaxial testing case, the fiber angle orientation is constant thought the ventricular wall, as opposed to the normal fiber angle variation seen in the other cases. Note that the biaxial material parameter model shows the lowest fiber stress and strain.

Border Zone Region

ED Mean Strain			ED Mean Stress (kPa)		
			Fiber	Cross-Fiber	Radial
					-0.778

	Border Zone Region					
	ED Mean Strain			ED Mean Stress (kPa)		
	Fiber	Cross-Fiber	Radial	Fiber	Cross-Fiber	Radial
Control	0.153	0.235	-0.221	11.435	3.600	-0.778
Normal Aneurysm Material Properties	0.153	0.235	-0.221	11.435	3.600	-0.778
"Stiff" Aneurysm	0.126	0.194	-0.190	11.463	3.356	-0.917
Material Properites from Biaxial Testing	0.126	0.168	-0.164	9.057	2.920	-0.641

Table 5.V – End Diastolic Stress Strain Results in the Border Zone Region – Stress and strain results for each case in the border zone region at end diastole (20 mmHg). Note that the material properties determined from biaxial stretching show the lowest stress and strain values.

Remote Region
ED Mean Stress (kPa)
Radial

	Remote Region					
	ED Mean Strain			ED Mean Stress (kPa)		
	Fiber	Cross-Fiber	Radial	Fiber	Cross-Fiber	Radial
Control	0.122	0.205	-0.193	6.035	2.028	-0.679
Normal Aneurysm Material Properties	0.122	0.205	-0.193	6.035	2.028	-0.679
"Stiff" Aneurysm	0.120	0.209	-0.194	5.774	2.059	-0.673
Material Properites from Biaxial Testing	0.104	0.210	-0.169	5.158	2.012	-0.744

Table 5.VI – End Diastolic Stress Strain Results in the Remote Region – Stress and strain results for each case in the remote region at end diastole (20 mmHg).

Aneurysm Region			
ES Mean Strain	ES Mean Stress (kPa)		
Radial	Fiber	Cross-Fiber	Radial
		0.662	-6.972

	Aneurysm Region					
	ES Mean Strain			ES Mean Stress (kPa)		
	Fiber	Cross-Fiber	Radial	Fiber	Cross-Fiber	Radial
Control	0.082	0.249	-0.054	83.181	-0.662	-6.972
Normal Aneurysm Material Properties	0.141	0.244	-0.107	87.174	7.919	-6.415
"Stiff" Aneurysm	0.114	0.233	-0.095	73.441	6.482	-6.138
Material Properites from Biaxial Testing	0.088	0.300	-0.054	66.464	22.417	-6.971

Table 5.VII – End Systolic Stress Strain Results in the Aneurysm Region – Stress and strain results for each case in the aneurysm region at end systole (100 mmHg). In the material properties determined from biaxial testing case, the fiber angle orientation is constant thought the ventricular wall, as opposed to the normal fiber angle variation seen in the other cases. Note the decrease in end systolic fiber stress and increase in end-systolic cross-fiber stress.

Border Zone Region			
Strain	ES Mean Stress (kPa)		
	Fiber	Cross-Fiber	Radial
			7.213

	Border Zone Region					
	ES Mean Strain			ES Mean Stress (kPa)		
	Fiber	Cross-Fiber	Radial	Fiber	Cross-Fiber	Radial
Control	0.056	0.247	-0.087	68.908	-3.315	-7.213
Normal Aneurysm Material Properties	0.115	0.251	-0.122	62.210	2.583	-6.410
"Stiff" Aneurysm	0.087	0.213	-0.099	61.501	2.562	-6.729
Material Properites from Biaxial Testing	0.081	0.180	-0.047	49.091	3.517	-5.366

Table 5.VIII – End Systolic Stress Strain Results in the Border Zone Region – Stress and strain results for each case in the border zone region at end systole (100 mmHg). Note the decrease in end systolic fiber stress and increase in end systolic cross-fiber stress.

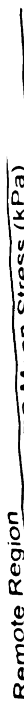
Remote Region
Stress (kPa)

	Remote Region					
	ES Mean Strain			ES Mean Stress (kPa)		
	Fiber	Cross-Fiber	Radial	Fiber	Cross-Fiber	Radial
Control	0.011	0.138	0.013	46.506	-6.723	-7.772
Normal Aneurysm Material Properties	0.016	0.129	0.019	48.929	-7.033	-7.947
"Stiff" Aneurysm	0.012	0.133	0.018	47.179	-6.901	-7.868
Material Properites from Biaxial Testing	0.001	0.146	0.030	40.864	-7.269	-8.469

Table 5.IX – End Systolic Stress Strain Results in the Remote Region – Stress and strain results for each case in the remote region at end systole (100 mmHg). Note the decrease in end systolic fiber stress and increase in end systolic cross-fiber stress.

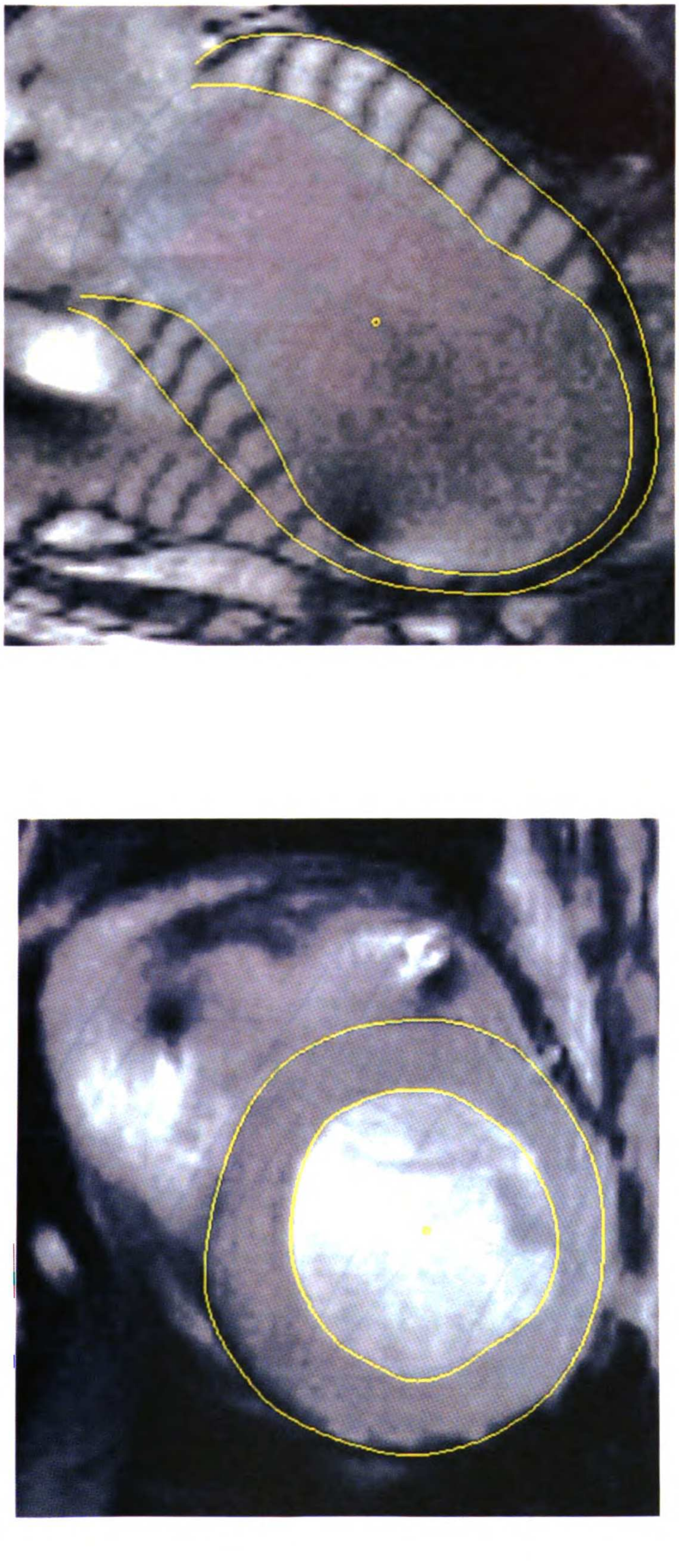

Figure 5.1 – MRI Data acquisition (Images reproduced from Guccione [1])

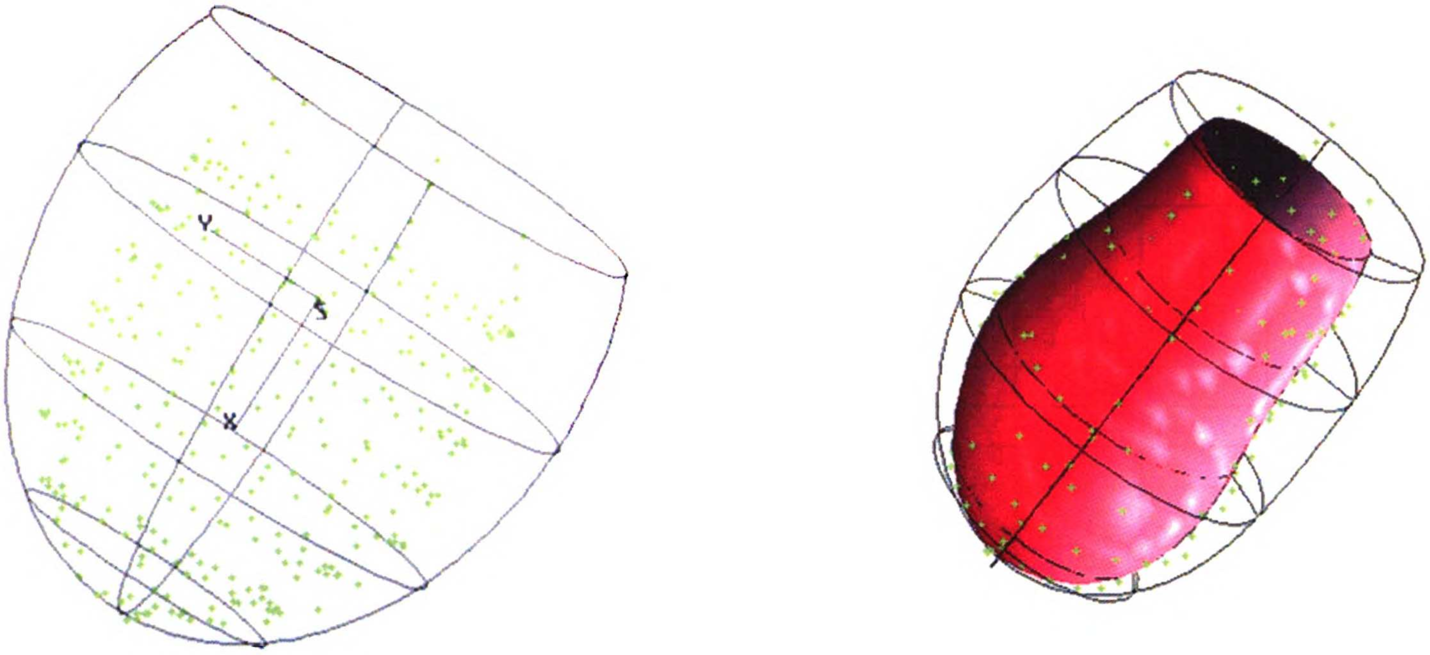

Figure 5.2 – MRI Data Fitting – (Left) Initial unfit model shown with solid line, green points show MRI data points. (Right) – Fitted model is shown with the solid lines, and endocardial surface is shown in red. (Images reproduced from Guccione [1])

UCSF LIBRARY

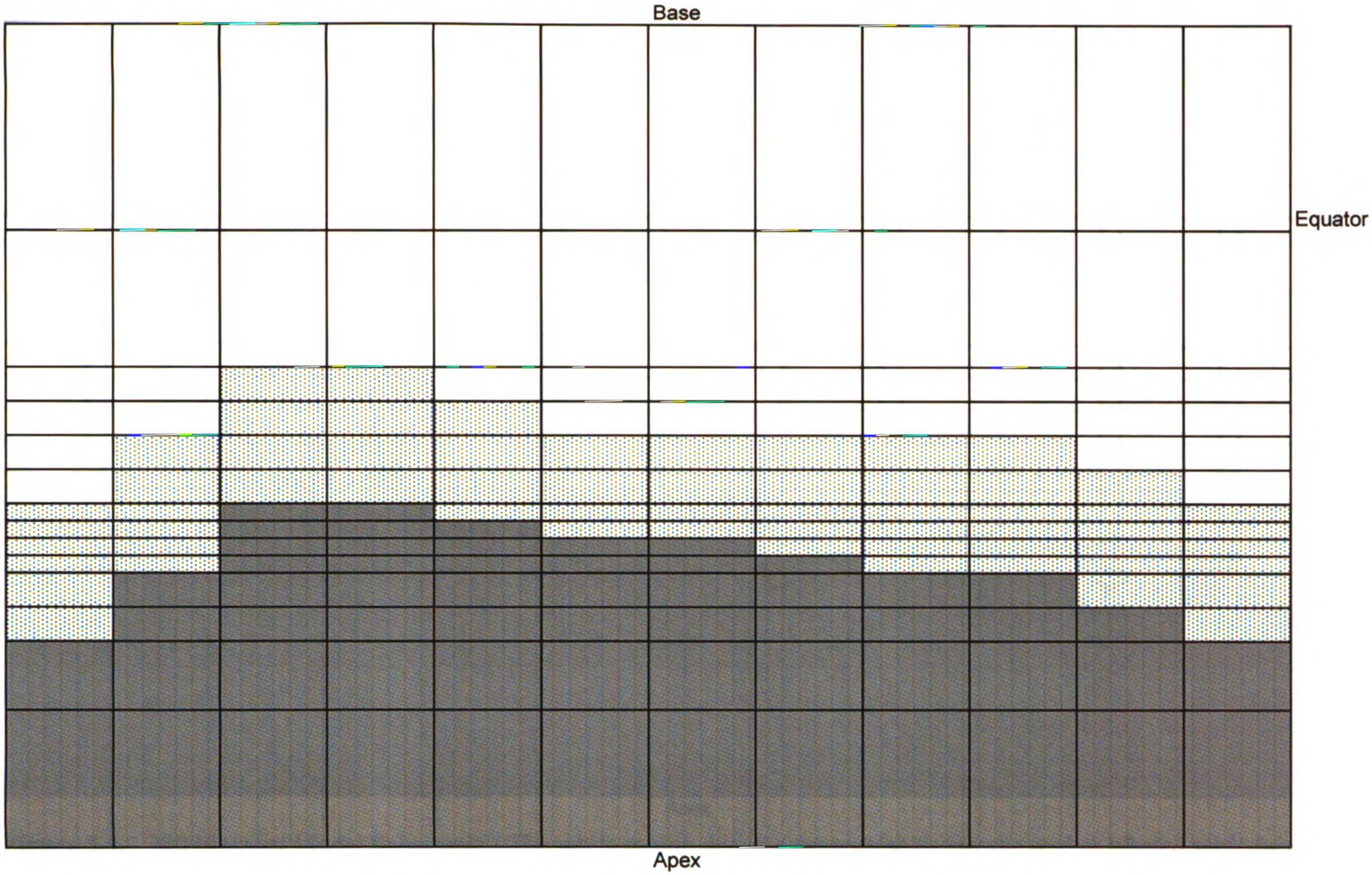

Figure 5.3 – 168 Element Model Schematic – The white region denotes the remote tissue, the region labeled with grey dots denotes the border zone region, and the solid region denotes aneurysm tissue.

UCSF LIBRARY

Base

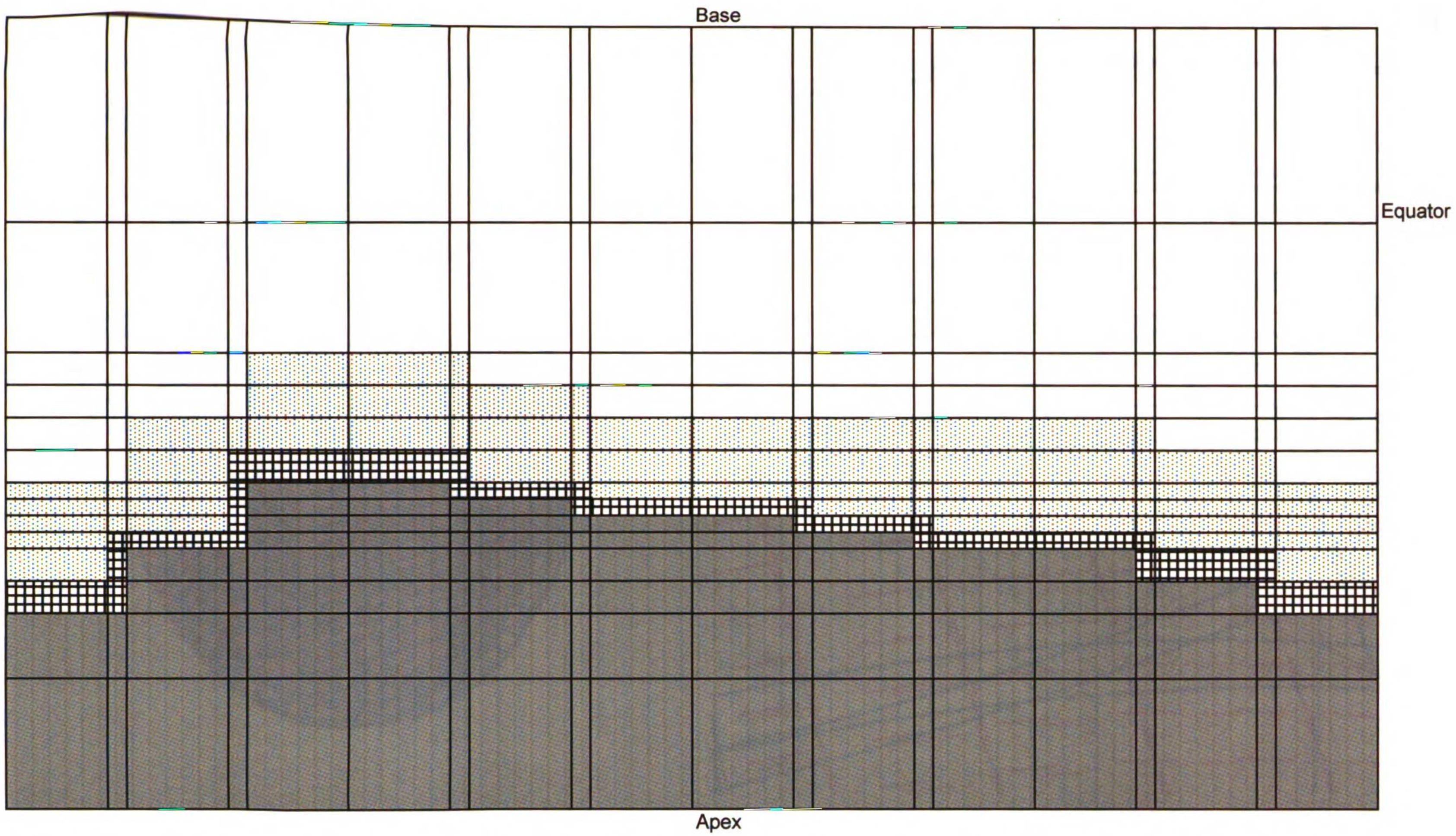

Figure 5.4 – 280 Element Model Schematic - The white region denotes the remote tissue, the region labeled with grey dots denotes the border zone region, and the solid region denotes aneurysm tissue. The hatched region is the “window pane” region where material parameters are the same as the border zone region, but fiber angles change from their border zone value to zero at the beginning of the aneurysm region across this area.

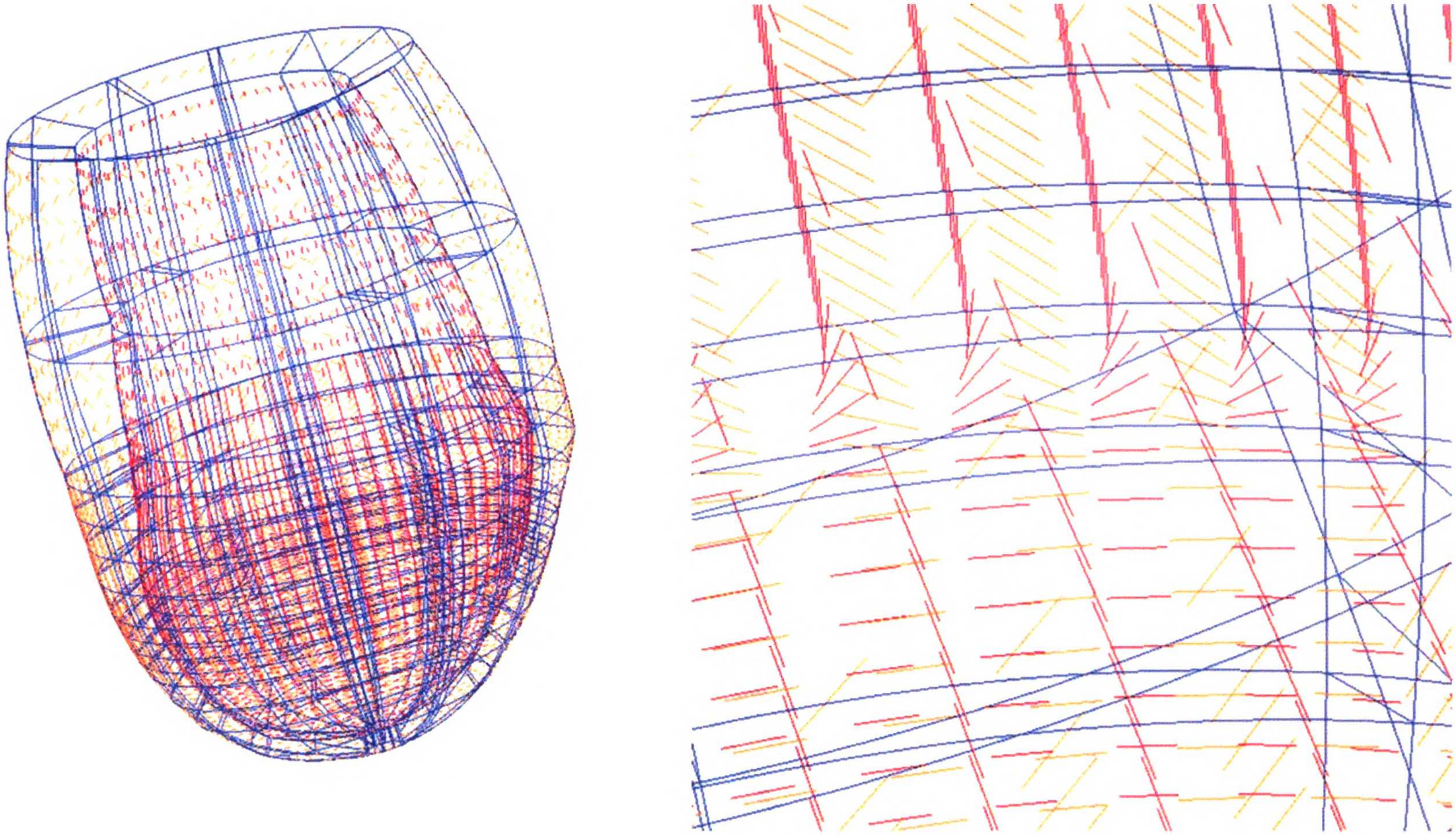

Figure 5.5 – Muscle Fiber Variation in the 280 Element Model – (Left) Global finite element model - Epicardial fiber angles are shown in orange, endocardial fiber angles are shown in red. (Right) Close up of the “window pane” region where fiber angles shift to zero degrees to be in agreement with the aneurysm region.

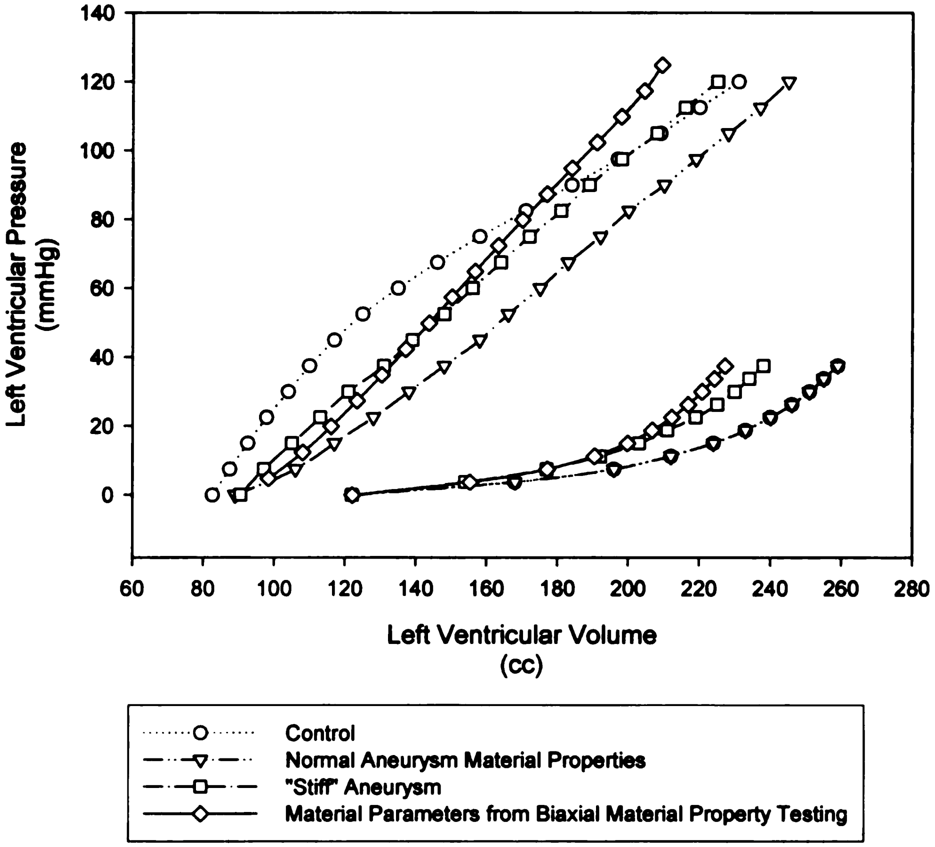

Figure 5.6 – Predicted Pressure-Volume Relations

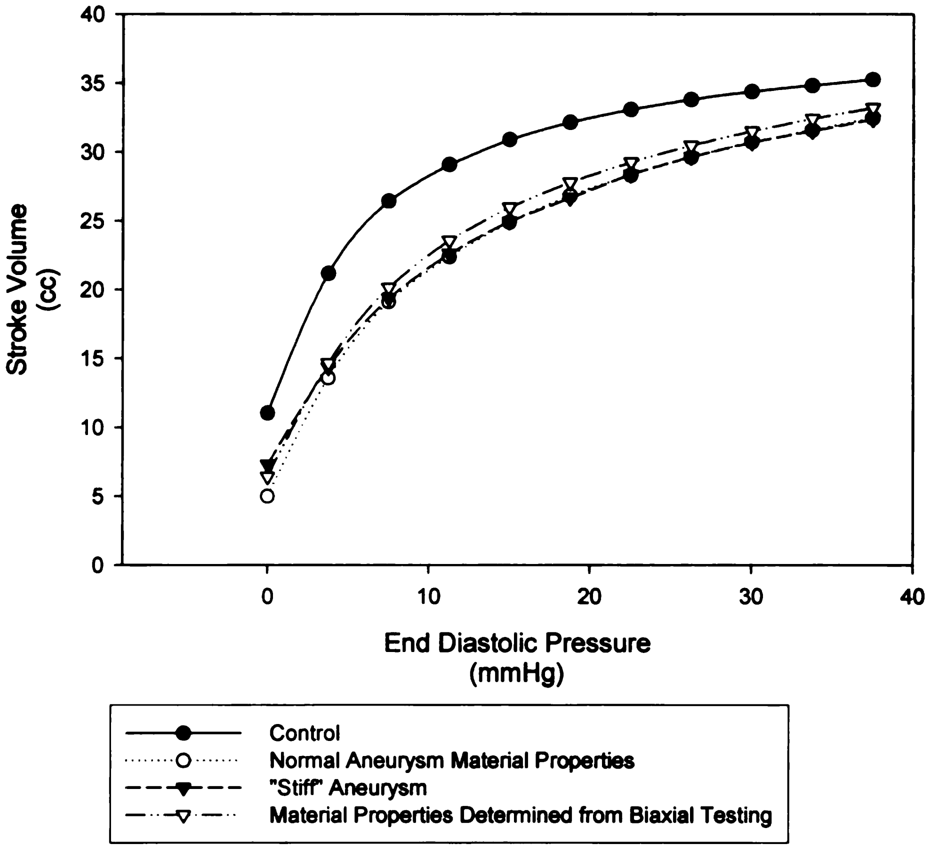

Figure 5.7 – Predicted Starling Relation – The control case and normal aneurysm material property case are the same as their respective properties only differ during active contraction.

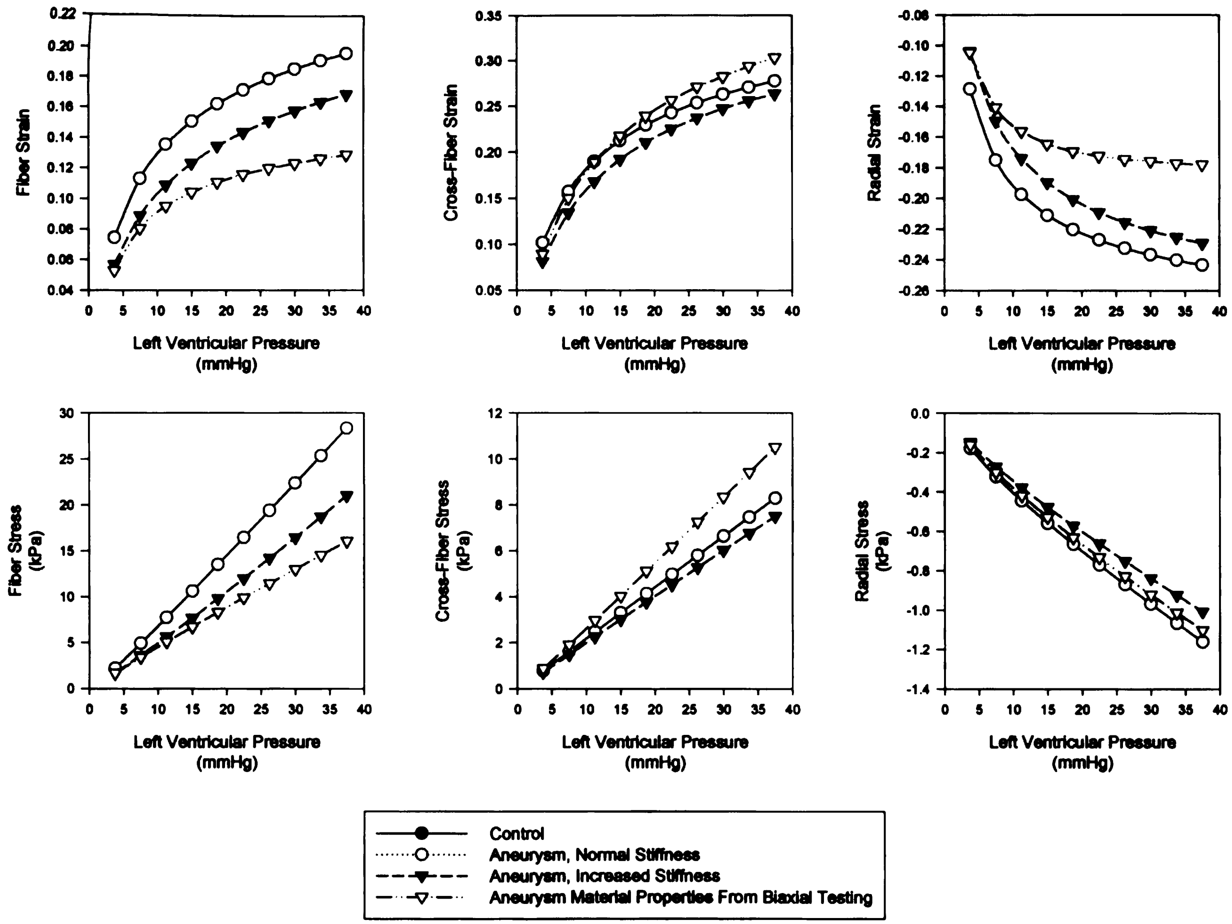

Figure 5.8 – Diastolic Aneurysm Stress and Strain - The control case and normal aneurysm material property case are the same as their respective properties only differ during active contraction.

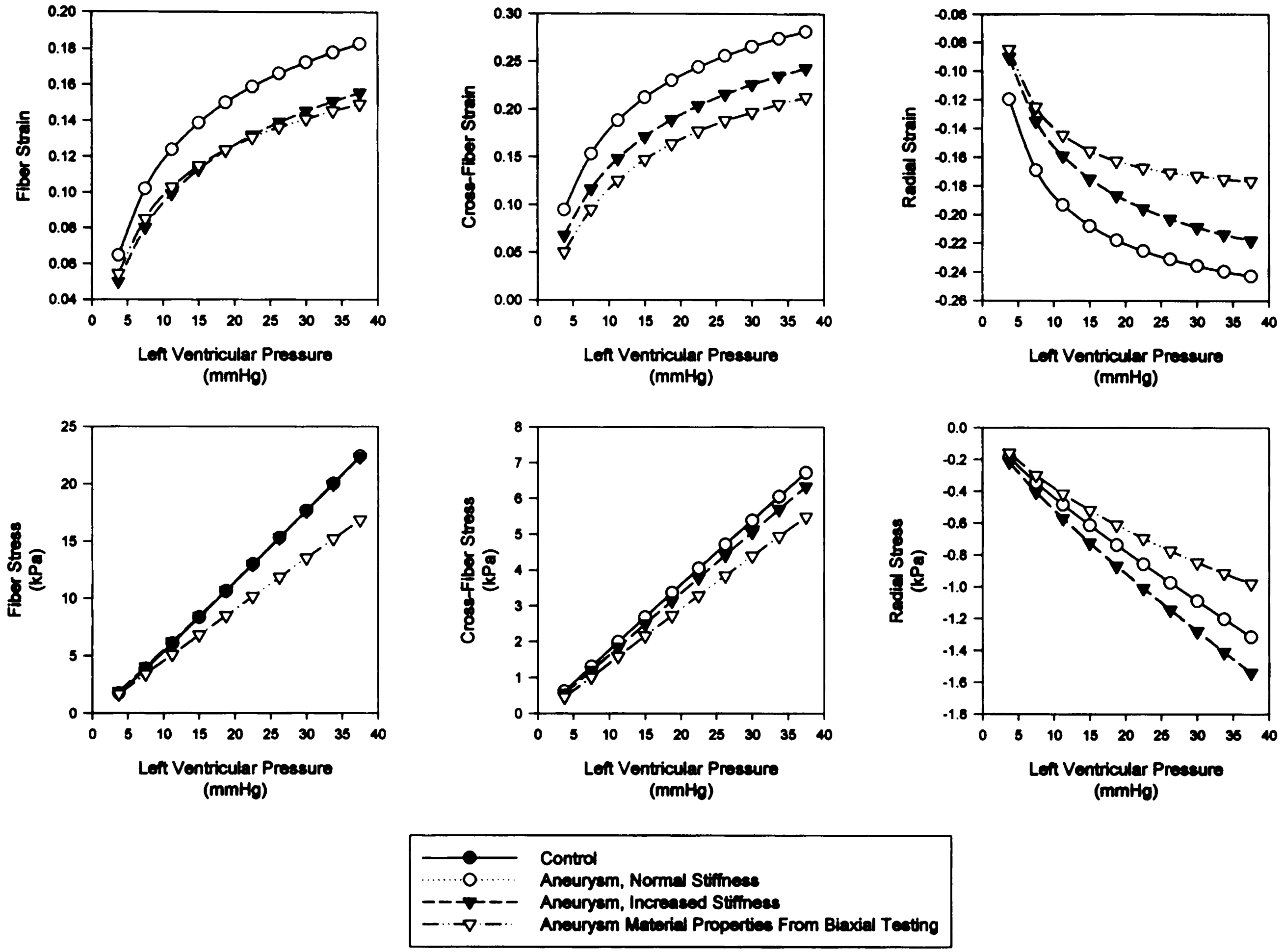

Figure 5.9 – Diastolic Border Zone Stress and Strain - The control case and normal aneurysm material property case are the same as their respective properties only differ during active contraction.

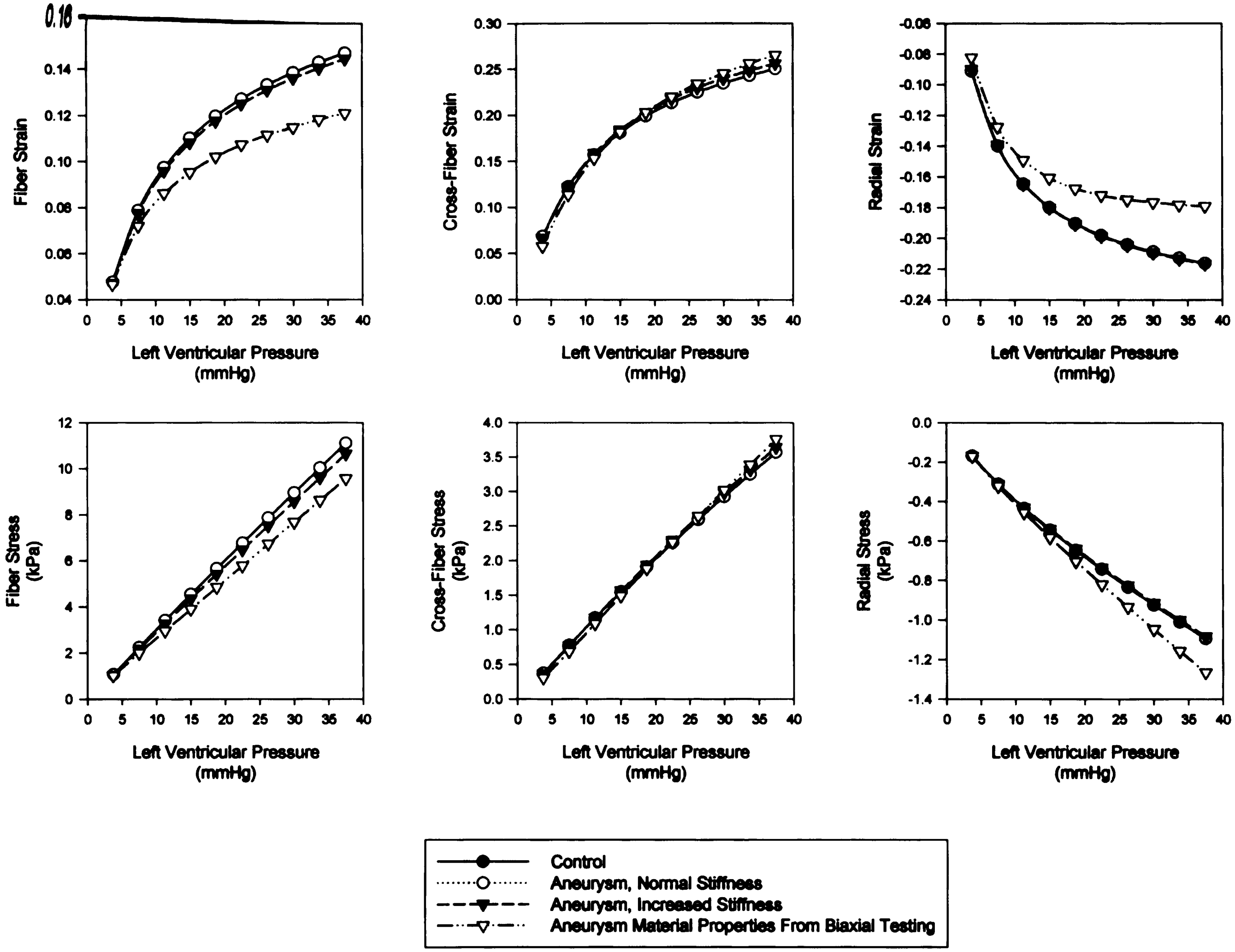

Figure 5.10 – Diastolic Remote Stress and Strain - The control case and normal aneurysm material property case are the same as their respective properties only differ during active contraction

0 26

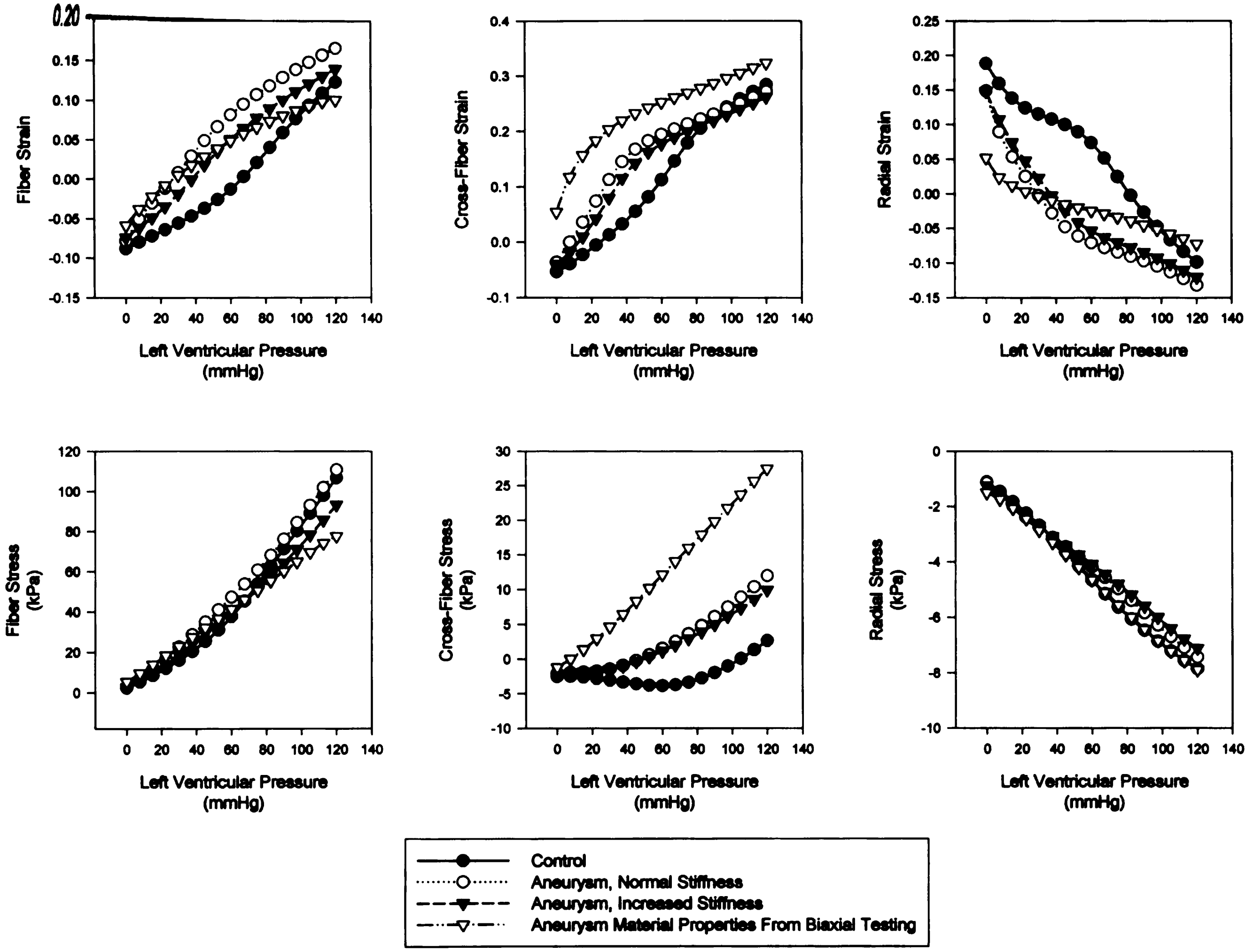

Figure 5.11 – Systolic Aneurysm Stress and Strain

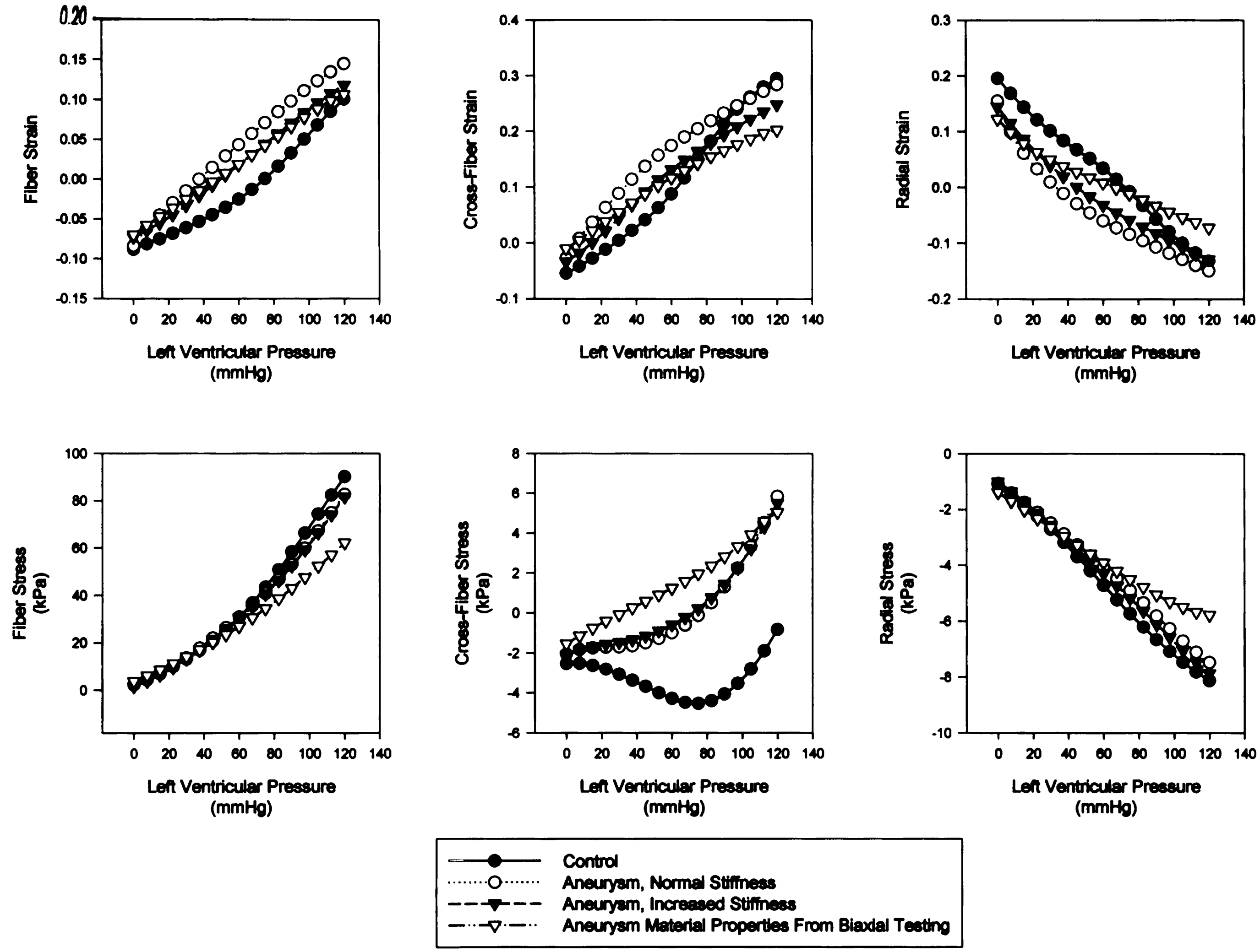

Figure 5.12 – Systolic Border Zone Stress and Strain

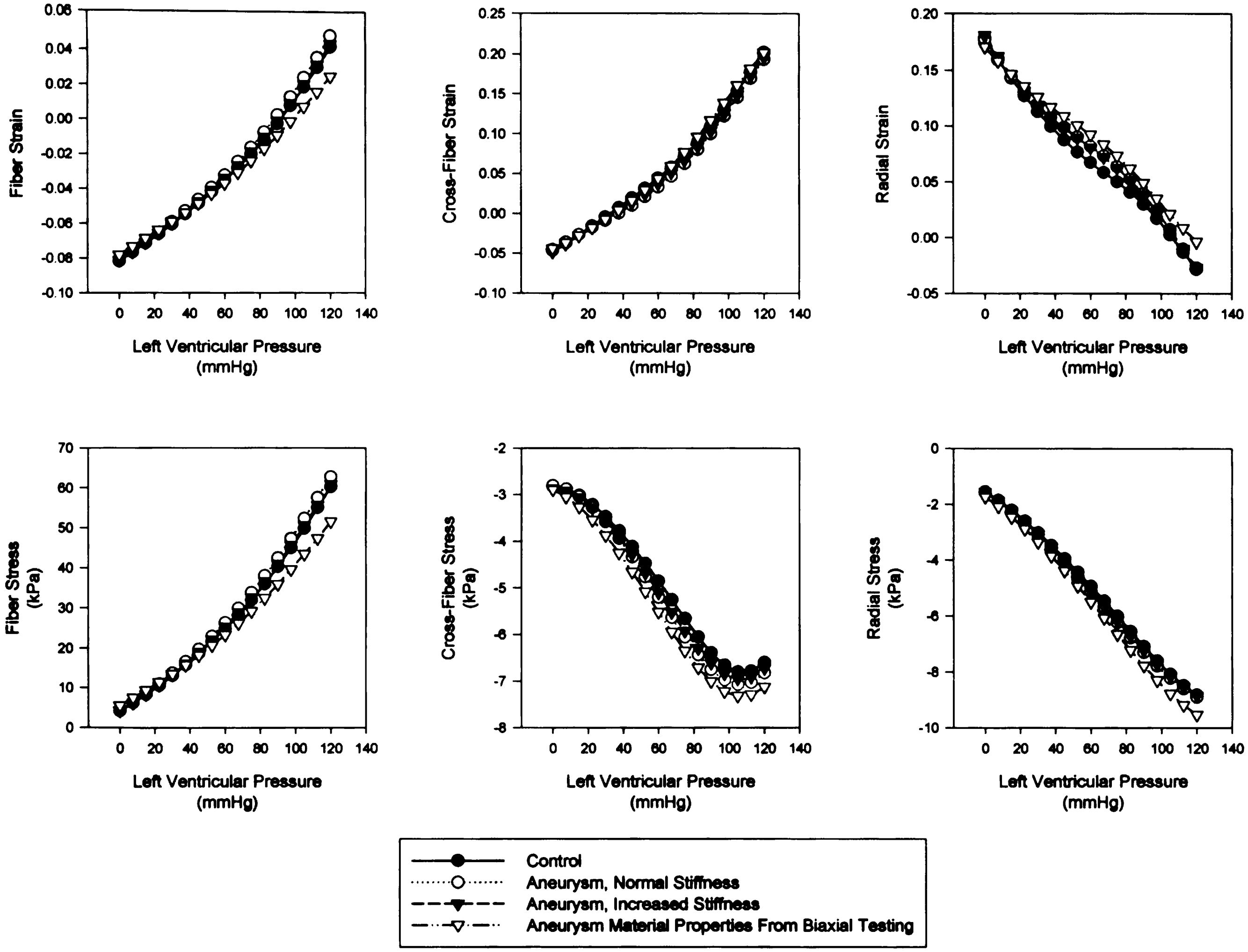

Figure 5.13 – Systolic Remote Stress and Strain

References:

1. Guccione, J.M., et al., *Mechanism underlying mechanical dysfunction in the border zone of left ventricular aneurysm: a finite element model study.* Ann Thorac Surg, 2001. **71**(2): p. 654-62.
2. Vayo, H.W., *The theory of the left ventricular aneurysm.* Bull Math Biophys, 1966. **28**(3): p. 363-70.
3. Bogen, D.K., A. Needleman, and T.A. McMahon, *An analysis of myocardial infarction. The effect of regional changes in contractility.* Circ Res, 1984. **55**(6): p. 805-15.
4. Bogen, D.K., et al., *An analysis of the mechanical disadvantage of myocardial infarction in the canine left ventricle.* Circ Res, 1980. **47**(5): p. 728-41.
5. Needleman, A., et al., *A finite element model of the infarcted left ventricle.* J Biomech, 1983. **16**(1): p. 45-58.
6. Radhakrishnan, S., D.N. Ghista, and G. Jayaraman, *Mechanics of left ventricular aneurysm.* J Biomed Eng, 1986. **8**(1): p. 9-23.
7. Reif, T.H. and M.D. Silver, *Role of stress concentration in the pathogenesis of cardiac rupture following acute myocardial infarction.* Can J Cardiol, 1995. **11**(9): p. 757-62.
8. Aikawa, Y., et al., *Regional wall stress predicts ventricular remodeling after anteroseptal myocardial infarction in the Healing and Early Afterload Reducing Trial (HEART): an echocardiography-based structural analysis.* Am Heart J, 2001. **141**(2): p. 234-42.

10.

11.

12.

13.

14

9. Moustakidis, P., et al., *Altered left ventricular geometry changes the border zone temporal distribution of stress in an experimental model of left ventricular aneurysm: a finite element model study.* Circulation, 2002. **106**(12 Suppl 1): p. I168-75.

10. Solomon, S.D., et al., *Assessment of regional left ventricular wall stress after myocardial infarction by echocardiography-based structural analysis.* J Am Soc Echocardiogr, 1998. **11**(10): p. 938-47.

11. Brady, A., *Passive Elastic Properties of Cardiac Myocytes Relative to Intact Cardiac Tissue*, in *Cardiac Myocyte-Connective Tissue Interactions in Health and Disease*, K.R. Tobinson TF, Editor. 1990, Krager: Basel. p. 37-52.

12. Brady, A.J., *Mechanical properties of isolated cardiac myocytes.* Physiol Rev, 1991. **71**(2): p. 413-28.

13. Chaudhry, H.R., *Passive material properties of intact ventricular myocardium determined from a cylindrical model.* J Biomech Eng, 1996. **118**(2): p. 262-3.

14. Demer, L.L. and F.C. Yin, *Passive biaxial mechanical properties of isolated canine myocardium.* J Physiol, 1983. **339**: p. 615-30.

15. Harris, T.S., et al., *Constitutive properties of hypertrophied myocardium: cellular contribution to changes in myocardial stiffness.* Am J Physiol Heart Circ Physiol, 2002. **282**(6): p. H2173-2182.

16. Humphrey, J.D., R.K. Strumpf, and F.C. Yin, *Determination of a constitutive relation for passive myocardium: II. Parameter estimation.* J Biomech Eng, 1990. **112**(3): p. 340-6.

17. Humphrey, J.D., R.K. Strumpf, and F.C. Yin, *Determination of a constitutive relation for passive myocardium: I. A new functional form.* J Biomech Eng, 1990. **112**(3): p. 333-9.

18. Humphrey, J.D., R.K. Strumpf, and F.C. Yin, *Biaxial mechanical behavior of excised ventricular epicardium.* Am J Physiol, 1990. **259**(1 Pt 2): p. H101-8.

19. Horowitz, A., et al., *Structural three-dimensional constitutive law for the passive myocardium.* J Biomech Eng, 1988. **110**(3): p. 200-7.

20. Humphrey, J.D. and F.C. Yin, *Biaxial mechanical behavior of excised epicardium.* J Biomech Eng, 1988. **110**(4): p. 349-51.

21. Humphrey, J.D. and F.C. Yin, *Constitutive relations and finite deformations of passive cardiac tissue II: stress analysis in the left ventricle.* Circ Res, 1989. **65**(3): p. 805-17.

22. Lin, D.H. and F.C. Yin, *A multiaxial constitutive law for mammalian left ventricular myocardium in steady-state barium contracture or tetanus.* J Biomech Eng, 1998. **120**(4): p. 504-17.

23. Pinto, J.G. and Y.C. Fung, *Mechanical properties of the stimulated papillary muscle in quick-release experiments.* J Biomech, 1973. **6**(6): p. 617-30.

24. Pinto, J.G. and Y.C. Fung, *Mechanical properties of the heart muscle in the passive state.* J Biomech, 1973. **6**(6): p. 597-616.

25. Shacklock, A., *Biaxial Testing of Cardiac Tissue.* 1987, University of Auckland, New Zealand: Auckland.

26. Yamaguchi, A., et al., *Left ventricular volume predicts postoperative course in patients with ischemic cardiomyopathy.* Ann Thorac Surg, 1998. **65**(2): p. 434-8.

27. Gupta, K.B., *Functional and Structural Changes in Left Ventricular Aneurysm*, in *Bioengineeing*. 1991, University of Pennsylvania: Philadelphia. p. 310.

28. Gupta, K.B., et al., *Changes in passive mechanical stiffness of myocardial tissue with aneurysm formation.* Circulation, 1994. **89**(5): p. 2315-26.

29. Guccione, J.M., A.D. McCulloch, and L.K. Waldman, *Passive material properties of intact ventricular myocardium determined from a cylindrical model.* J Biomech Eng, 1991. **113**(1): p. 42-55.

30. Guccione, J.M. and A.D. McCulloch, *Mechanics of active contraction in cardiac muscle: Part I--Constitutive relations for fiber stress that describe deactivation.* J Biomech Eng, 1993. **115**(1): p. 72-81.

31. Guccione, J.M., L.K. Waldman, and A.D. McCulloch, *Mechanics of active contraction in cardiac muscle: Part II--Cylindrical models of the systolic left ventricle.* J Biomech Eng, 1993. **115**(1): p. 82-90.

32. Guccione, J.M., K.D. Costa, and A.D. McCulloch, *Finite element stress analysis of left ventricular mechanics in the beating dog heart.* J Biomech, 1995. **28**(10): p. 1167-77.

33. Moriarty, T.F., *The law of Laplace. Its limitations as a relation for diastolic pressure, volume, or wall stress of the left ventricle.* Circ Res, 1980. **46**(3): p. 321-31.

34. Yin, F.C., *Ventricular wall stress.* Circ Res, 1981. **49**(4): p. 829-42.

35. Mirsky, I., et al., *Passive elastic wall stiffness of the left vertnicle: a comparison between linear theory and large deformation theory.* Bull Math Biol, 1976. **38**(3): p. 239-51.

36. Streeter, D.D., Jr. and W.T. Hanna, *Engineering mechanics for successive states in canine left ventricular myocardium. II. Fiber angle and sarcomere length.* Circ Res, 1973. **33**(6): p. 656-64.

37. Costa, K.D., et al., *A three-dimensional finite element method for large elastic deformations of ventricular myocardium: I--Cylindrical and spherical polar coordinates.* J Biomech Eng, 1996. **118**(4): p. 452-63.

38. Costa, K.D., et al., *A three-dimensional finite element method for large elastic deformations of ventricular myocardium: II--Prolate spheroidal coordinates.* J Biomech Eng, 1996. **118**(4): p. 464-72.

39. McCulloch, A., et al., *Large-scale finite element analysis of the beating heart.* Crit Rev Biomed Eng, 1992. **20**(5-6): p. 427-49.

40. Chew, P.H., F.C. Yin, and S.L. Zeger, *Biaxial stress-strain properties of canine pericardium.* J Mol Cell Cardiol, 1986. **18**(6): p. 567-78.

41. Yin, F.C., et al., *Quantification of the mechanical properties of noncontracting canine myocardium under simultaneous biaxial loading.* J Biomech, 1987. **20**(6): p. 577-89.

42. Downs, J., et al., *An improved video-based computer tracking system for soft biomaterials testing.* IEEE Trans Biomed Eng, 1990. **37**(9): p. 903-7.

43. Marquardt, D., *An Algorithm for Least-Squares Estimation of Nonlinear Parameters.* SIAM J. Appl. Math., 1963. **11**: p. 431-441.

44. Nielsen, P.M., et al., *Mathematical model of geometry and fibrous structure of the heart.* Am J Physiol, 1991. **260**(4 Pt 2): p. H1365-78.

45. Reddy, J.N., *An introduction to the finite element method.* 2nd ed. McGraw-Hill series in mechanical engineering. 1993, New York: McGraw-Hill. xix, 684.

46. Omens, J.H., K.D. May, and A.D. McCulloch, *Transmural distribution of three-dimensional strain in the isolated arrested canine left ventricle.* Am J Physiol, 1991. **261**(3 Pt 2): p. H918-28.

47. Holmes, J.W., Covell, J.W., *Collagen Fiber Orientation in Myocardial Scar Tissue.* Cardiovascular Pathobiology, 1996. **1**(1): p. 15-22.

48. Moulton, M.J., et al., *Mechanical dysfunction in the border zone of an ovine model of left ventricular aneurysm.* Ann Thorac Surg, 1995. **60**(4): p. 986-97; discussion 998.

49. Ratcliffe, M.B., et al., *Ventricular volume, chamber stiffness, and function after anteroapical aneurysm plication in the sheep.* J Thorac Cardiovasc Surg, 2000. **119**(1): p. 115-24.

50. Savage, E.B., et al., *Repair of left ventricular aneurysm. Changes in ventricular mechanics, hemodynamics, and oxygen consumption.* J Thorac Cardiovasc Surg, 1992. **104**(3): p. 752-62.

51. McCormick, R.J., et al., *Regional differences in LV collagen accumulation and mature cross-linking after myocardial infarction in rats.* Am J Physiol, 1994. **266**(1 Pt 2): p. H354-9.

52. MacKenna, D.A., et al., *Contribution of collagen matrix to passive left ventricular mechanics in isolated rat hearts.* Am J Physiol, 1994. **266**(3 Pt 2): p. H1007-18.

53. Omens, J.H., D.A. MacKenna, and A.D. McCulloch, *Measurement of strain and analysis of stress in resting rat left ventricular myocardium.* J Biomech, 1993. **26**(6): p. 665-76.

54. Weber, K.T., et al., *Collagen network of the myocardium: function, structural remodeling and regulatory mechanisms.* J Mol Cell Cardiol, 1994. **26**(3): p. 279-92.

55. Weber, K.T., *Cardiac interstitium in health and disease: the fibrillar collagen network.* J Am Coll Cardiol, 1989. **13**(7): p. 1637-52.

56. Whittaker, P., D.R. Boughner, and R.A. Kloner, *Role of collagen in acute myocardial infarct expansion.* Circulation, 1991. **84**(5): p. 2123-34.

57. Whittaker, P., et al., *Stunned myocardium and myocardial collagen damage: differential effects of single and repeated occlusions.* Am Heart J, 1991. **121**(2 Pt 1): p. 434-41.

58. Weis, S.M., et al., *Myocardial Mechanics and Collagen Structure in the Osteogenesis Imperfecta Murine (oim).* Circ Res, 2000. **87**(8): p. 663-669.

59. Bowen, F.W., et al., *Restraining acute infarct expansion decreases collagenase activity in borderzone myocardium.* Ann Thorac Surg, 2001. **72**(6): p. 1950-6.

60. Jugdutt, B.I. and R.W. Amy, *Healing after myocardial infarction in the dog: changes in infarct hydroxyproline and topography.* J Am Coll Cardiol, 1986. **7**(1): p. 91-102.

61. Cleutjens, J.P., et al., *Collagen remodeling after myocardial infarction in the rat heart.* Am J Pathol, 1995. **147**(2): p. 325-38.

62. Jugdutt, B.I., M.J. Joljart, and M.I. Khan, *Rate of collagen deposition during healing and ventricular remodeling after myocardial infarction in rat and dog models.* Circulation, 1996. **94**(1): p. 94-101.

63. Gerber, B.L., et al., *Microvascular obstruction and left ventricular remodeling early after acute myocardial infarction.* Circulation, 2000. **101**(23): p. 2734-41.

64. Geerts, L., et al., *Characterization of the normal cardiac myofiber field in goat measured with MR-diffusion tensor imaging.* Am J Physiol Heart Circ Physiol, 2002. **283**(1): p. H139-45.

Chapter 6

The Effect of Changing Material Parameters on Left Ventricular Aneurysm

Abstract:

Previously we established that computer models of left ventricular (LV) aneurysm resulted in global increases of cross-fiber stress and decreases of fiber stress at end systole. This study attempts to isolate the cause of this observation. Through extensive modelling of varying material parameters of LV aneurysm it was discovered that all methods of globally increasing the stiffness of the aneurysm tissue resulted in the increase in cardiac function as measured by the Starling relation. However, only an increase in transverse stiffness (b_t in Equation 5.1), rather than a change in the local aneurysm fiber angle, could reproduce the observed global stress results.

Introduction:

The results presented in Chapter 5 justified the need to identify both the global and regional results of altering the material properties of LV aneurysm. As described before there have been many attempts at creating a mathematical model of LV aneurysm [2-10]. These models, however, are limited in their application owing to simplified geometry, simplified material properties and/or simplified solution method. In Chapter 5 we developed a highly sophisticated model of the left ventricle based upon MRI imaging modalities, and used the finite element method (Chapter 3) to arrive at detailed global and regional function performance indices of the left ventricle. In this chapter we will extend this study to examine a wide variety of material parameters for LV aneurysm and the potential effect that they might have upon cardiac performance.

Methods:

Creation of the LV aneurysm was accomplished using the methods described in Chapter 4. MRI imaging, image processing and model creation were done using the methods described in Chapter 5.

Finite Element Model

The finite element methods used for the simulation are similar to that described by Costa and colleagues [11]. The mathematical descriptions (stress strain relationships) for systolic and diastolic material properties were originally described by Guccione [12]. These methods are described in Chapter 3, but will be briefly summarized here.

The following strain energy function was used for all regions of the left ventricle:

$$W = \frac{C}{2}\{\exp[b_f E_{11}^2 + b_t(E_{22}^2 + E_{33}^2 + E_{23}^2 + E_{32}^2) + b_{fs}(E_{12}^2 + E_{21}^2 + E_{13}^2 + E_{31}^2)] - 1\} \qquad (6.1)$$

where E_{11} is fiber strain, E_{22} is cross-fiber in-plane strain, E_{33} is radial strain, E_{23} is shear in the transverse plane, and E_{12} and E_{13} are shear strain in the fiber-cross fiber and fiber-radial coordinate planes. Guccione and colleagues previously found that the material constants $C = 0.88$ kPa, $b_f = 18.48$, $b_t = 3.58$, $b_{fs} = 1.63$ allowed a cylindrical model of the left ventricle to match strains measured during passive ventricular filling in an intact

canine heart preparation [13]. Equation (6.1), also has been shown to allow an FE model of the beating dog heart [12] to predict end diastolic finite strain distributions from a midventricular region of the anterior LV free wall consistent with three-dimensional strain measurements for passive inflation [14]. Variation in the constants described in Equation (6.1) will be used to model the effects of changing stiffness in the aneurysm region.

Systolic contraction was modeled in three different ways. In the remote region, systole was assumed to function in a normal manner, as described in Chapter 3. Briefly, the second Piola-Kirchhoff stress tensor was defined referred to fiber coordinates as the sum of passive three-dimensional stress derived from the strain energy function (Equation (6.1)) and an active fiber stress component T_o (oriented along the fiber axis) that is a function of time t, peak intracellular calcium concentration Ca_o, and sarcomere length l [15]:

$$t^{\alpha\beta} = \frac{1}{2}\left(\frac{\partial W}{\partial E_{\alpha\beta}} + \frac{\partial W}{\partial E_{\beta\alpha}}\right) - pg^{\alpha\beta} + T_o\left(t, Ca_o, l\right)\delta_1^{\alpha}\delta_1^{\beta}, \qquad (6.2)$$

In the border zone region (and window pane sub region), the contractility was reduced by 50%, at the suggestion of previous studies [1] that have shown this reproduces the observed circumferential lengthening in the border zone of ovine LV aneurysm models [16]. The remainder of the systolic contraction model remained the same as in the remote

region. In the aneurysm, the tissue was assumed to be noncontractile, and thus the systolic properties were the same as the diastolic material properties described above.

A "control case" was presented, identical to that in Chapter 5, which serves as a point of comparison for functional relations. This control case has normal myocardial material properties (both systolic and diastolic) throughout all regions of the heart. The geometry for this case is the same as the rest of the simulations, that of an ovine left ventricle with LV aneurysm. Again these simulations serve to highlight the effect of changing material parameters on cardiac function rather than changes in geometry.

Calculation of Diastolic and Systolic Pressure-Volume Relationships

Volume solutions were obtained at end diastolic (0-40 mmHg), and end systolic (0-120 mmHg) pressures. Owing to the non-linearity of the produced systolic pressure-volume relations, the end systolic pressure (P_{ES}) and end systolic volume (V_{ES}) from the finite element model were fit to the following quadratic relationship:

$$P_{ES} = \beta_{o,EES} + \beta_{1,EES} V_{ES} + \beta_{2,EES} V_{ES}^2 \tag{6.3}$$

where $\beta_{o,EES}$, $\beta_{1,EES}$ and $\beta_{2,EES}$ are the stiffness parameters of the LV end systolic elastance. The relationship between the end diastolic pressure (P_{ED}) and the end diastolic volume (V_{ED}) was then fit to the following quadratic equation:

$$P_{ED} = \beta_{o,DC} + \beta_{1,DC} V_{ED} + \beta_{2,DC} V_{ED}^2 \tag{6.4}$$

where β_o, β_1 and β_2 are the diastolic stiffness parameters.

Calculation of Stroke Volume/P_{ED} (Starling) Relationship

For each set of material parameters, a stroke volume/P_{ED} (Starling relation) was calculated by constructing a series of pressure-volume loops that were bound by the end systolic and end diastolic pressure-volume loops produced by the simulation. V_{ED} was initially set to 40 mmHg, and then decreased for subsequent loops. In order to calculate the end systolic pressure-volume point on each loop arterial elastance (E_A) was set to a fixed value of 3.2, a value that has been reported by two investigators studying the ovine infarct model presented here [17, 18]. Since the end systolic pressure-volume relation was significantly non-linear, the following equation was used to find the intersection between the arterial elastance line and the end systolic pressure-volume relationship:

$$0 = \left(\beta_{o,EES} + E_A V_{ED}\right) + \left(\beta_{1,EES} - E_A\right) V_{ES} + \beta_{2,EES} V_{ES}^2, \tag{6.5}$$

where V_{ED} is the volume intercept of the arterial elastance. V_{ES} was then calculated by obtaining roots of Equation (6.5). The stroke volume was then calculated by taking the difference between V_{ED} and V_{ES}.

Calculation of Stress and Strain Values

For each simulation, stress and strain were calculated at end diastole (20 mmHg) and end systole (100 mmHg). Stress and strain values were calculated at the central Gauss point within each element, the point at which the values are most accurate. Stress and strain values were calculated with respect to the unloaded model configuration. These results were then averaged across the three respective sections (Remote, Border Zone, and Aneurysm) to provide a representation of the stress or strain in each region.

Results:

The Effects of Changing Global Stiffness

The effects changing global stiffness were modeled by varying parameter C in Equation (6.1). The value of C used in the simulations ranged from 0.876 kPa, the value in normal myocardium [13], to 876 kPa, a factor of 1000. The constants that describe end systolic elastance and end diastolic compliance (Equations (6.3) and (6.4)) are shown in Table 6.I. Figure 6.4 shows the predicted pressure-volume relations from the simulations. Table 6.II shows the predicted end diastolic (20 mmHg) and end systolic (100 mmHg) LV volumes, stroke volumes and ejection fractions. As the value of C was increased from 0.876 kPa to 876 kPa the end diastolic volume decreased from 231 mL to 184 mL while the end systolic volume was decreased from 205 mL to 155 mL. As the end systolic volume was reduced to a greater degree, the corresponding stroke volumes increased

from 27 mL to 29 mL as the parameter C was increased. The ejection fraction was similarly increased from 11.5% to 15.7%. The control case resulted in the highest stroke volume (32 mL). The Starling relation for variation of the parameter C is presented in Figure 6.5. As the stiffness of the aneurysm was increased, an improvement in function as measured by the Starling relation was seen. This improvement was, however, attenuated at higher stiffness values.

At end diastole (20 mmHg), strain and stress results are presented in Figure 6.6. Mean fiber strain was initially reduced by increasing the value of C, however when the value of C reached 876 kPa mean fiber strain was beginning to increase again in all regions of the heart. Also, the greatest fiber strain was seen in the aneurysm region at low values of aneurysm stiffness, but was shifted to the remote region as the aneurysm grew stiffer. Mean fiber stress in the remote and aneurysm regions followed a similar trend to the mean fiber stress, but the border zone region mean fiber stress was seen to globally increase as the value of C was increased. The largest values of fiber stress were seen initially in the aneurysm region; however, the location of the largest fiber stress value was shifted to the border zone region as the aneurysm grew stiffer. Mean cross-fiber strain was seen to decrease as the value of C was increased in all regions of the heart. Mean cross-fiber stress globally decreased as the value of C was increased. The largest value of cross-fiber stress was initially seen in the aneurysm region, but the largest cross-fiber stress value was shifted to the border zone region as the stiffness of the aneurysm was increased. Radial strain was seen to globally increase throughout the heart as the value of C was increased. Radial stress decreased in the aneurysm and border zone

regions of the heart, while radial stress in the remote region remained relatively constant. Again, a shift in the largest value of the radial stress was seen from the aneurysm region to the border zone region at high values of C.

End systolic fiber strain and stress results are presented in Figure 6.7. At end systole (100 mmHg) all the fiber, cross-fiber and remote mean strain values were relatively constant in the remote region across all values of C tested. The aneurysm and border zone regions, however, showed a decrease in strain as the stiffness parameter was increased. This decrease in strain resulted in a substantial decrease in the fiber stress as the value of C was increased. The border zone region showed little change in stress until the value of C was increased to 876 kPa, when a slight increase was observed. The remote region showed a slight decrease as the stiffness was increased. The cross-fiber stress was relatively constant in the remote region as the value of C was increased, whereas the border zone and aneurysm regions saw decreases in cross-fiber stress. The radial stress was shown to decrease in the aneurysm and remote regions, while an increase in radial stress was seen in the border zone.

The Effects of Changing Exponential Stiffness

The effects of changing the exponential stiffness components of Equation (6.1) were modeled by multiplying all of the exponential components (b_f, b_t, and b_{fs}) by a factor of between 0.5 and 20. Table 6.III presents the fitted end systolic and end diastolic parameters as described in Equations (6.3) and (6.4) respectively. Figure 6.8 shows the

pressure-volume relations predicted by the model. As shown in Table 6.IV, reducing all of the exponential terms in the aneurysm by 50% results in an increase in end diastolic volume (232 mL to 248 mL) and end systolic volume (206 mL to 222 mL), with a corresponding decrease in stroke volume (26.6 mL to 25.5 mL) and ejection fraction (11.5% to 10.3%) when compared to the case in which aneurysm material properties are those of normal myocardium. Conversely, increasing the exponential components by a factor of 20 from their normal values resulted in decreases in end diastolic volume (232 mL to 199 mL) and end systolic volume (206 mL to 170 mL). However, stroke volume (26.5 mL to 29.5 mL) and ejection fraction (11.5% to 14.8%) were increased. Figure 6.9 shows the effects of changing the exponential parameters on the Starling relation. Decreasing the exponential parameters resulted in the decrease in the cardiac performance as measured by the Starling relation. Increasing the exponential parameters resulted in an improvement in cardiac performance. This effect became greatly attenuated as the scale of the exponential parameters was increased.

The effect of altering the exponential components of the strain energy function on strain and stress at end diastole can be seen in Figure 6.10. As the exponential parameters were increased the aneurysm and border zone regions of the left ventricle saw a decrease in all fiber, cross-fiber and radial strain components. At higher values of the exponential strain components, the fiber and radial strain was slightly increased in the remote region. As the exponential component was increased the aneurysm fiber stress saw a decrease in value while the border zone stress increased slightly. The fiber stress in the remote region remained relatively constant at end diastole. As the exponential parameters were

increased, cross-fiber stress was reduced in all regions. The radial stress in the border zone region was increased, however was decreased in the aneurysm region as the exponential parameters were increased.

The effect of altering the exponential components of the strain energy function on strain and stress at end diastole can be seen in Figure 6.11. Fiber, cross-fiber and radial strain were all decreased as the exponential ratio was increased. Corresponding to this decrease, the fiber and cross-fiber stress values were decreased as the exponential values were increased. Radial stress was decreased in the remote and aneurysm regions, but slightly increased in the border zone region.

The Effects of Changing Fiber Stiffness

The effects of changing fiber stiffness on cardiac mechanics and performance were modeled by decreasing the value of b_f in equation (6.1) by as much as 40% (the lowest value at which converged solutions were obtained) and increasing by as much as 1000% (the highest value at which converged solutions were obtained) from its normal value of 18.48. Table 6.V displays the fitted end systolic elastance and end diastolic compliance parameters as described by Equations (6.3) and Equation (6.4) respectively. Table 6.VI shows that decreasing the fiber stiffness by 40% increased the end diastolic volume from 232 mL in the control case to 239 mL, while the end systolic volume was increased from 200 mL to 213 mL. This decrease in fiber stiffness resulted in the stroke volume

decreasing from 32 mL in the control case to 26 mL, and a decrease in ejection fraction from 13.8% to 10.9%. Increasing the fiber stress up to 1000% resulted in a decrease in end diastolic volume (208 mL) when compared to the control case (232 mL). Similarly the end systolic volume was also reduced from 200 mL in the control case to 179 mL. When the fiber stiffness was decreased by 1000%, the stroke volume was reduced from 32 mL in the control case to 29 mL, however, the ejection fraction remained relatively constant (13.8% in the control case vs. 13.9% when the fiber stiffness was increased by 1000%. Figure 6.12 shows the predicted pressure-volume relations from the model. Decreasing the fiber stress in the aneurysm regions resulted in rightward shifts in both the end diastolic and end systolic pressure-volume relations. Figure 6.13 shows the predicted Starling relations from the models. All of modeled aneurysm cases resulted in a decrement of cardiac function as measured by the Starling relation, however as the fiber stiffness was increased, better function was observed. This affect is attenuated at high values as the difference between an increase of 500% and an increase of 1000% in small.

The effects of changing fiber stiffness in the aneurysm region at end diastole on strain and stress are seen in Figure 6.14. As fiber stiffness was increased the mean fiber strain in the aneurysm and border zone region was reduced, while the fiber strain in the remote region was slightly increased at large fiber stiffness values. Cross-fiber strain was reduced in all regions of the left ventricle as the value of b_f was increased. Radial strain, however, was increased in all regions of the left ventricle at end diastole. End diastolic fiber stress was reduced in the aneurysm region as b_f was increased, slightly increased in the border zone region, and relatively constant in the remote region. Cross-fiber stress

was reduced in all regions as the value of b_f was increased. Radial stress was relatively constant in the remote region, increased in the border zone region and reduced in the aneurysm region as b_f was increased at end diastole.

The effects of changing fiber stiffness on end systolic strain and stress are shown in Figure 6.15. End systolic fiber strain was reduced in the aneurysm and border zone region, while the remote region fiber strain remained relatively constant as the fiber stiffness was increased. The end systolic cross-fiber strain was reduced significantly in the aneurysm and border zone regions, but only slightly in the remote region. The end systolic radial strain was also reduced in the border zone region and aneurysm regions while the remote region radial strain was increased slightly. As fiber stiffness was increased the fiber stress in the aneurysm region was reduced greatly as the fiber stress in the border zone and aneurysm regions remained relatively constant. The cross fiber stress at end systole was reduced in the aneurysm region as fiber stiffness was increased. The cross-fiber stress was also reduced, but then switched from a positive stress value to an increasing negative stress value as fiber stiffness was increased. The cross-fiber stress in the remote region remained essentially constant. The end systolic radial stress was reduced in the aneurysm and remote regions but increased in the border zone region as fiber stiffness was increased.

The Effects of Changing Cross-Fiber Stiffness

The effects of altering cross-fiber stiffness in LV aneurysm were modeled by varying the value of b_t in equation (6.1). The value of b_t was varied between a decrease of 80% and an increase of 2000% from its value of 3.58 in normal myocardium. Table 6.VII displays the fitted end systolic elastance and end diastolic compliance parameters as described by Equations (6.3) and Equation (6.4) respectively. Table 6.VIII shows that decreasing the value of b_t by 80% results in an increase in the end diastolic volume (238 mL) when compared to the control case (232 mL). Similarly, the end systolic volume was increased to 212 mL from 200 mL when the value of b_t is decreased by 80%. The changes in the end diastolic and end systolic volumes lead to a decrease in stroke volume, from 32 mL in the control case to 26 mL when the value of b_t is decreased by 80%. Figure 6.16 shows the change in the predicted pressure-volume relations as the value of b_t is altered. Decreasing the value of b_t causes a rightward shift in the diastolic and systolic pressure-volume relations. Increasing the value of b_t causes a leftward shift in the diastolic and systolic pressure-volume relations. Figure 6.17 shows the effect of changing b_t upon the Starling relationship. All cases in which an aneurysm was modeled showed a decrease in cardiac function when compared to the control case. As the value of b_t is increased, the Starling relation is also shifted upwards. This increase in function does, however, approach a limit as the difference between an increase of 1000% and 2000% is negligible.

The effects of altering b_t upon end diastolic strain and stress are presented in Figure 6.18. Increasing the value of b_t resulted in decreases of end diastolic mean fiber strain in all regions of the left ventricle. Cross-fiber strain was also decreased in the aneurysm and border zone regions, but increased in the remote regions as the value of b_t was increased. End diastolic radial strain was decreased in the aneurysm and border zone regions, but remained relatively constant in the remote region. End diastolic fiber stress was reduced in the aneurysm and border zone regions, but remained relatively constant in the remote region. End diastolic cross-fiber stress was initially increased in the border zone region as the value of b_t was increased, but began to decrease as the value of b_t approached 20. The cross-fiber stress was increased in the remote region, but remained constant in the aneurysm region. The end diastolic radial stress was initially increased in the border zone region as b_t was increased, but decreased as the value of b_t surpassed 10. The radial stress in the aneurysm region was reduced, and the remote region radial stress remained nearly constant as the value of b_t was increased.

The effects of altering b_t upon end systolic strain and stress are presented in Figure 6.19. End systolic mean fiber strain was reduced in all regions as the value of b_t was increased. Similarly, the value of cross-fiber strain was reduced in the aneurysm and border zone regions as the value of b_t was increased, however, the cross-fiber strain was increased in the remote regions. End systolic radial strain was reduced in the border zone and aneurysm regions, but remained relatively constant in the remote region. End systolic mean fiber stress was reduced greatly in the border zone and aneurysm regions and

slightly in the remote regions as the value of b_t was increased. Cross fiber stress at end systole was increased in all regions of the left ventricle as the value of b_t was increased. End systolic radial stresses were reduced in all regions of the left ventricle.

Discussion:

Throughout all of the simulations it was found that generally increasing the stiffness of the aneurysm tissue resulted in improved performance. This improvement of performance generally reached a limit, and an increase of 1000% in stiffness produced little change in global function. This result is largely in agreement with the results presented by Bogen [4], with the exception that our model predicts improvement in performance at all end diastolic pressures, while the Bogen model shows crossing over of the Starling relations as the end diastolic pressure is increased. The increase in performance occurred in all manners of increasing infarct stiffness, and could not be attributed to any one component of the stress-strain relation.

Perhaps the most interesting result presented in Chapter 5 was that computer models of LV aneurysm predicted global decreases in fiber stress and increases in cross-fiber stress at end systole. Because the model was constructed in such a manner as to have differing fiber angles in the aneurysm region, one could ask the question if this change in fiber angles was the cause of this observation. Additionally, all of the material parameters were changed from "normal" values. If a change in fiber angle could not reproduce these results, then which material parameter could reproduce these observations? The results

of these simulations show that the observed global decrease in fiber stress and increase in cross-fiber stress can be reproduced by our computer models without the reconstruction of a local aneurysm fiber angle. As Figure 6.19 shows, altering the transverse stiffness component, b_t, can reproduce this observation. Alterations to the global stiffness parameter (C), fiber stiffness parameters (b_f), and all exponential stiffness parameters failed to reproduce the results predicted by material properties determined from biaxial testing.

This observation has importance in understanding the process of ventricular remodeling following LV aneurysm. Others have established that collagen expression following LV aneurysm plays a significant role in ventricular remodeling [19-30]. We have established that LV aneurysm alters the material properties of the affected tissue in such a manner as to increase the local transverse stiffness of the aneurysm tissue. This local change in aneurysm stiffness has global mechanical effects upon the left ventricle, specifically a decrease in muscle fiber stress and increase in cross-fiber stress. Understanding the implications of this to global collagen expression will certainly provide clues into the process of ventricular remodeling in response to LV aneurysm.

This study is limited by a number of factors. The computer model could be improved in a number of ways. First, new techniques such as tagged MRI [31], could be used to optimize material parameters in the border zone and remote regions of the ventricle. Diffusion tensor MRI [32] could also be employed to give more accurate measurements of the true fiber angle distribution throughout the remote and border zone regions. MRI

techniques are generally limited in the aneurysm region, as the relative thickness of the region is too small to allow analysis by current means.

Conclusion:

This study serves to illustrate two important points. The first is the observed increase in cardiac performance can be reproduced by globally increasing the stiffness of the LV aneurysm in any number of ways. However, each of these methods has important consequences upon the stress and strain of the left ventricle. One must take great care in selecting the most appropriate material parameters in order to begin to fully understand the disease as a whole. Simply judging cardiac performance by global function indices only reveals part of the story, and can lead to incorrect assumptions about cardiac mechanics.

The second point is that the observed global decrease in end systolic fiber stress and decrease in end systolic cross-fiber stress is not a result of a change in the local fiber system of the aneurysm, but rather an increase in transverse aneurysm stiffness. This not only provides insight into the mechanics behind ventricular remodeling, but also potential extracellular matrix targets to stop this remodeling from happening.

	End Systolic Elastance			End Diastolic Compliance		
	$\beta_{o,EES}$	$\beta_{1,EES}$	$\beta_{2,EES}$	$\beta_{o,DC}$	$\beta_{1,DC}$	$\beta_{2,DC}$
Control	-111.1253	1.6329	-0.0028	59.0928	-0.8138	0.0028
Normal Aneurysm Material Properties	-52.0667	0.4674	0.0010	59.0928	-0.8138	0.0028
C=8.76 kPa	-85.8411	0.9903	-0.0003	60.2605	-0.8854	0.0033
C=87.6 kPa	-153.0002	1.9505	-0.0029	85.6315	-1.2824	0.0048
C=876 kPa	-211.7323	2.7158	-0.0049	114.0330	-1.7419	0.0067

Table 6.I – End systolic elastance and end diastolic compliance parameters for equations (6.3) and (6.4) as the value of C in Equation (6.1) is adjusted over a wide range.

	ED Volume (mL)	ES Volume (mL)	SV (mL)	EF
Control	231.86	199.85	32.01	13.8%
Normal Aneurysm Material Properties	231.86	205.28	26.58	11.5%
C=8.76 kPa	211.67	184.87	26.81	12.7%
C=87.6 kPa	196.23	167.49	28.74	14.6%
C=876 kPa	184.42	155.42	29.00	15.7%

Table 6.II – The change in global functional parameters as the value of C in Equation (6.1) is adjusted over a wide range.

	End Systolic Elastance			End Diastolic Compliance		
	$\beta_{o,EES}$	$\beta_{1,EES}$	$\beta_{2,EES}$	$\beta_{o,DC}$	$\beta_{1,DC}$	$\beta_{2,DC}$
Control	-111.1253	1.6329	-0.0028	59.0928	-0.8138	0.0028
Normal Aneurysm Material Properties	-52.0667	0.4674	0.0010	59.0928	-0.8138	0.0028
Exponential Terms Decreased by 50%	-31.2744	0.1953	0.0014	51.3667	-0.6877	0.0023
Exponential Terms Increased by 50%	-63.5499	0.6221	0.0007	64.2207	-0.8957	0.0031
Exponential Terms Increased by 500%	-97.4806	1.0968	-0.0003	80.9887	-1.1597	0.0042
Exponential Terms Increased by 1000%	-114.2134	1.3340	-0.0008	90.3274	-1.3052	0.0047
Exponential Terms Increased by 2000%	-128.2970	1.5294	-0.0013	99.2162	-1.4439	0.0053

Table 6.III - End systolic elastance and end diastolic compliance parameters for equations (6.3) and (6.4) as the value of the exponential parameters in Equation (6.1) are adjusted over a wide range.

	ED Volume (mL)	ES Volume (mL)	SV (mL)	EF
Control	231.86	199.85	32.01	13.8%
Normal Aneurysm Material Properties	231.86	205.28	26.58	11.5%
Exponential Terms Decreased by 50%	247.68	222.22	25.46	10.3%
Exponential Terms Increased by 50%	224.54	197.33	27.21	12.1%
Exponential Terms Increased by 500%	209.12	180.49	28.63	13.7%
Exponential Terms Increased by 1000%	203.45	174.30	29.15	14.3%
Exponential Terms Increased by 2000%	198.97	169.50	29.47	14.8%

Table 6.IV - The change in global functional parameters as the value of the exponential parameters in Equation (6.1) are adjusted over a wide range.

	End Systolic Elastance			End Diastolic Compliance		
	$\beta_{o,EES}$	$\beta_{1,EES}$	$\beta_{2,EES}$	$\beta_{o,DC}$	$\beta_{1,DC}$	$\beta_{2,DC}$
Control	-111.1253	1.6329	-0.0028	59.0928	-0.8138	0.0028
Normal Aneurysm Material Properties	-52.0667	0.4674	0.0010	59.0928	-0.8138	0.0028
b_f Decreased by 40%	-41.5801	0.3294	0.0012	54.0056	-0.7353	0.0025
b_f Increased by 40%	-58.7936	0.5545	0.0008	62.1439	-0.8629	0.0030
b_f Increased by 500%	-85.6101	0.9273	0.0001	75.1245	-1.0709	0.0038
b_f Increased by 1000%	-96.9730	1.0954	-0.0002	84.7059	-1.2146	0.0043

Table 6.V - End systolic elastance and end-diastolic compliance parameters for equations (6.3) and (6.4) as the value of b_f in Equation (6.1) is adjusted over a wide range.

	ED Volume (mL)	ES Volume (mL)	SV (mL)	EF
Control	231.86	199.85	32.01	13.8%
Normal Aneurysm Material Properties	231.86	205.28	26.58	11.5%
b_f Decreased by 40%	239.20	213.21	25.99	10.9%
b_f Increased by 40%	227.45	200.44	27.01	11.9%
b_f Increased by 500%	213.20	184.89	28.31	13.3%
b_f Increased by 1000%	207.59	178.76	28.83	13.9%

Table 6.VI – The change in global function parameters as the value of b_f in Equation (6.1) is adjusted over a wide range.

	End Systolic Elastance			End Diastolic Compliance		
	$\beta_{o,EES}$	$\beta_{1,EES}$	$\beta_{2,EES}$	$\beta_{o,DC}$	$\beta_{1,DC}$	$\beta_{2,DC}$
Control	-111.1253	1.6329	-0.0028	59.0928	-0.8138	0.0028
Normal Aneurysm Material Properties	-52.0667	0.4674	0.0010	59.0928	-0.8138	0.0028
b_t Decreased by 80%	-41.8439	0.3333	0.0012	56.5878	-0.7711	0.0026
b_t Increased by 500%	-75.4263	0.7917	0.0003	68.0287	-0.9616	0.0034
b_t Increased by 1000%	-88.9927	0.9885	-0.0001	74.2963	-1.0621	0.0038
b_t Increased by 2000%	-105.3593	1.2245	-0.0007	81.2750	-1.1700	0.0042

Table 6.VII - End systolic elastance and end diastolic compliance parameters for equations (6.3) and (6.4) as the value of b_t in Equation (6.1) is adjusted over a wide range.

	ED Volume (mL)	ES Volume (mL)	SV (mL)	EF
Control	231.86	199.85	32.01	13.8%
Normal Aneurysm Material Properties	231.86	205.28	26.58	11.5%
b_t Decreased by 80%	237.79	211.50	26.29	11.1%
b_t Increased by 500%	218.39	190.88	27.51	12.6%
b_t Increased by 1000%	212.32	184.17	28.16	13.3%
b_t Increased by 2000%	207.50	178.73	28.77	13.9%

Table 6.VIII - The change in global function parameters as the value of b_t in Equation (6.1) is adjusted over a wide range.

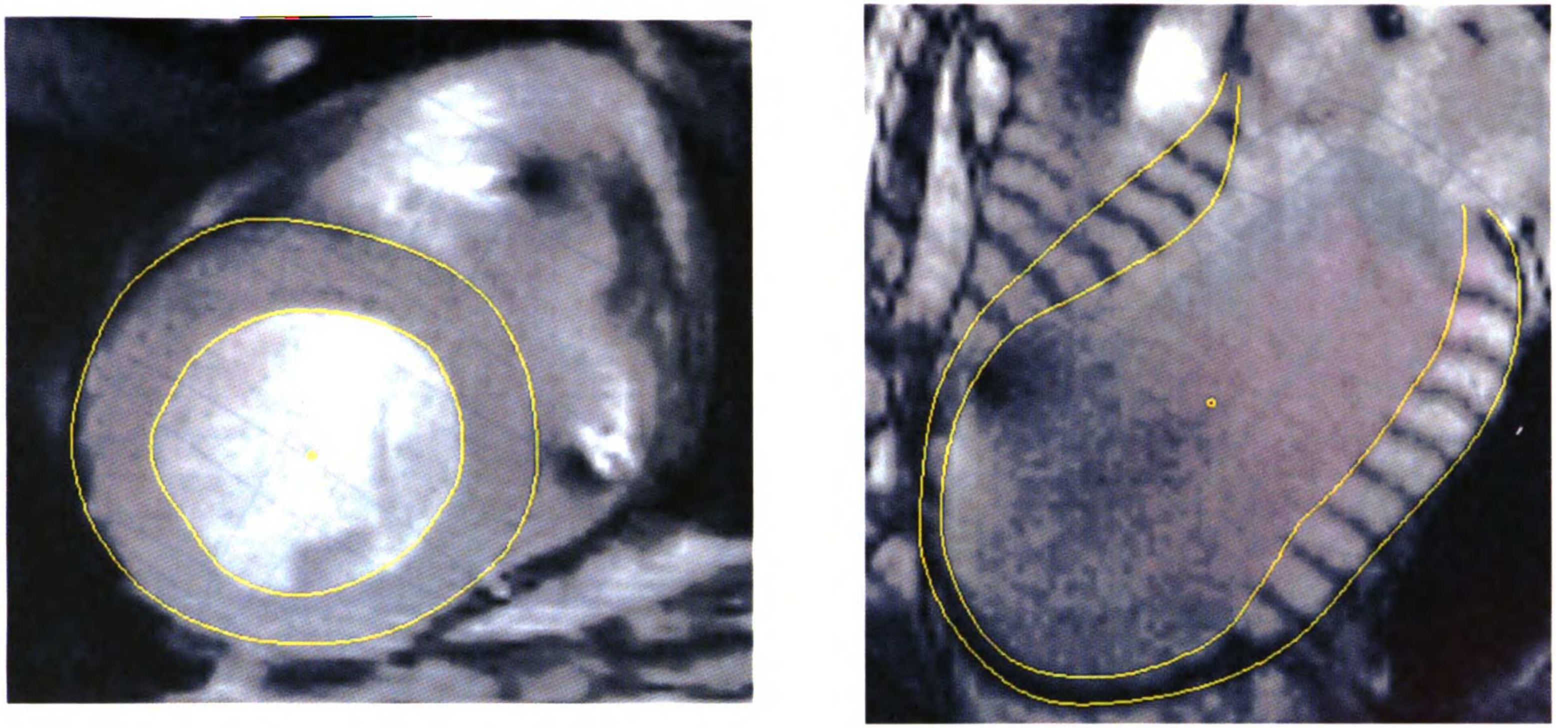

Figure 6.1 – MRI Data acquisition (Images reproduced from Guccione [1])

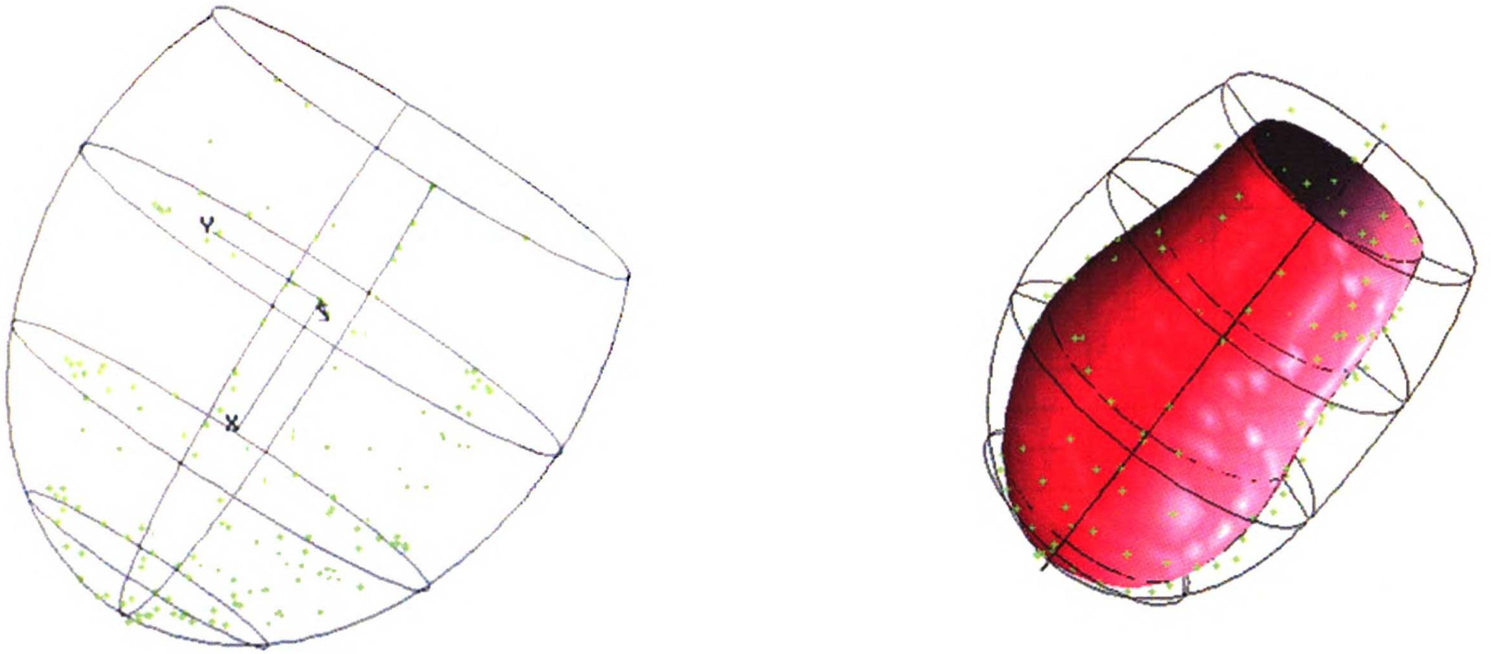

Figure 6.2 – MRI Data Fitting – (Left) Initial unfit model shown with solid line, green points show MRI data points. (Right) – Fitted model is shown with the solid lines, and endocardial surface is shown in red. (Images reproduced from Guccione [1])

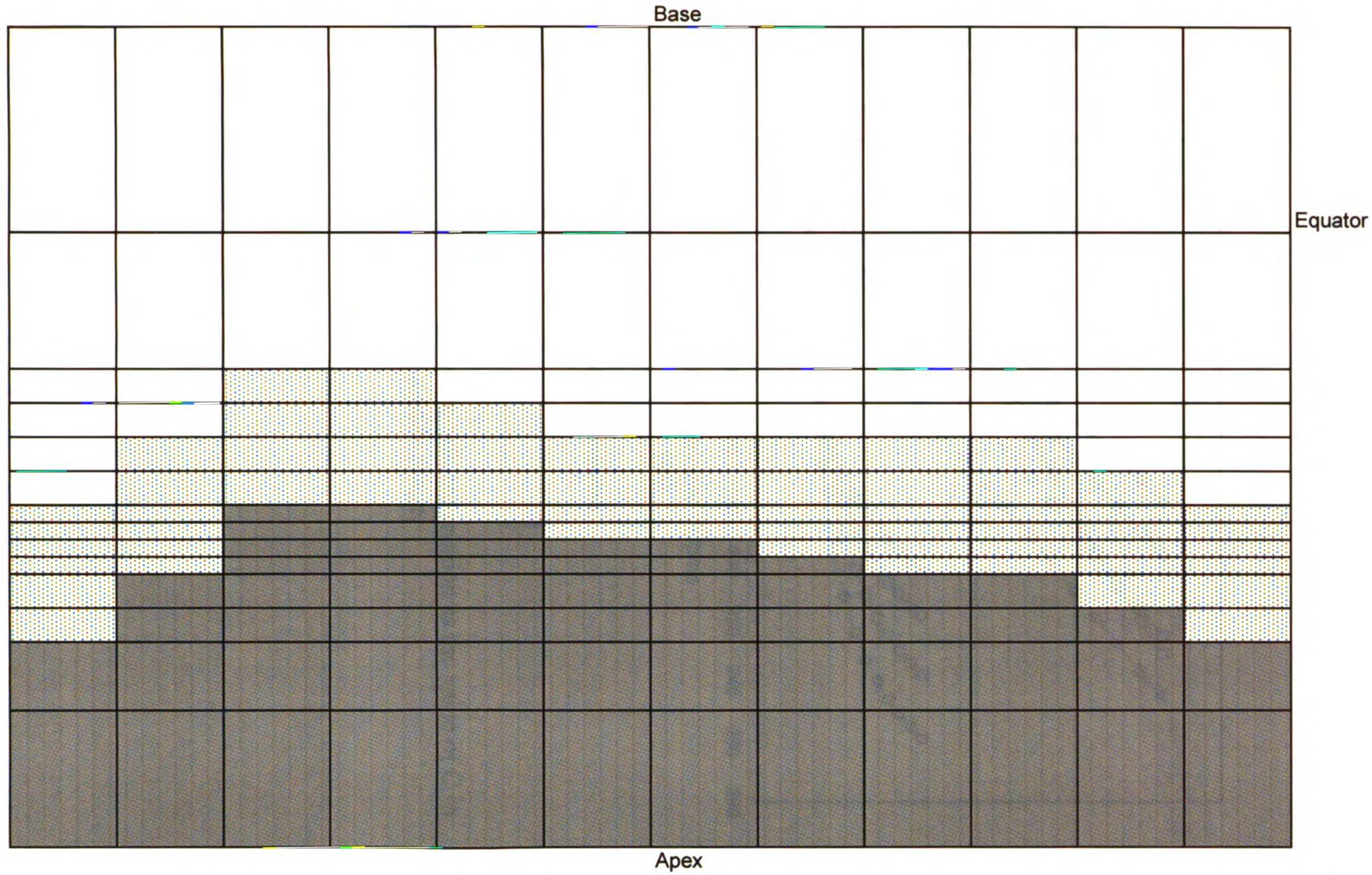

Figure 6.3 – 168 Element Model Schematic – The white region denotes the remote tissue, the region labeled with grey dots denotes the border zone region, and the solid region denotes aneurysm tissue.

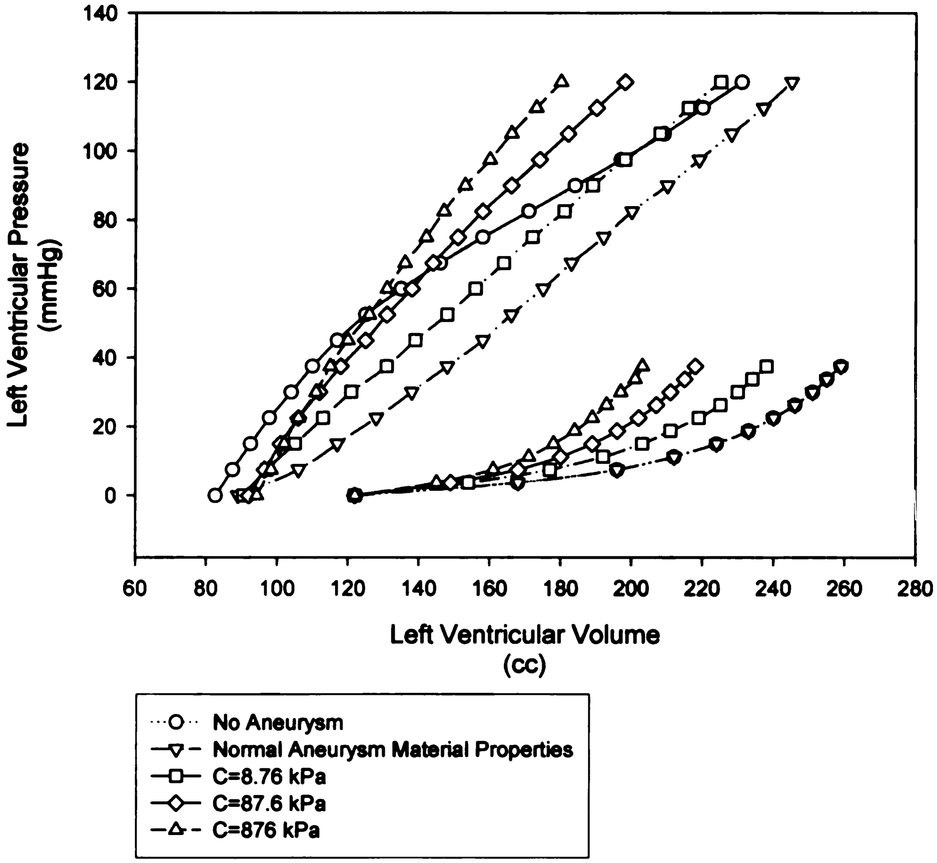

Figure 6.4 – Change in the pressure-volume relation as the value of C in Equation (6.1) is increased over a wide range.

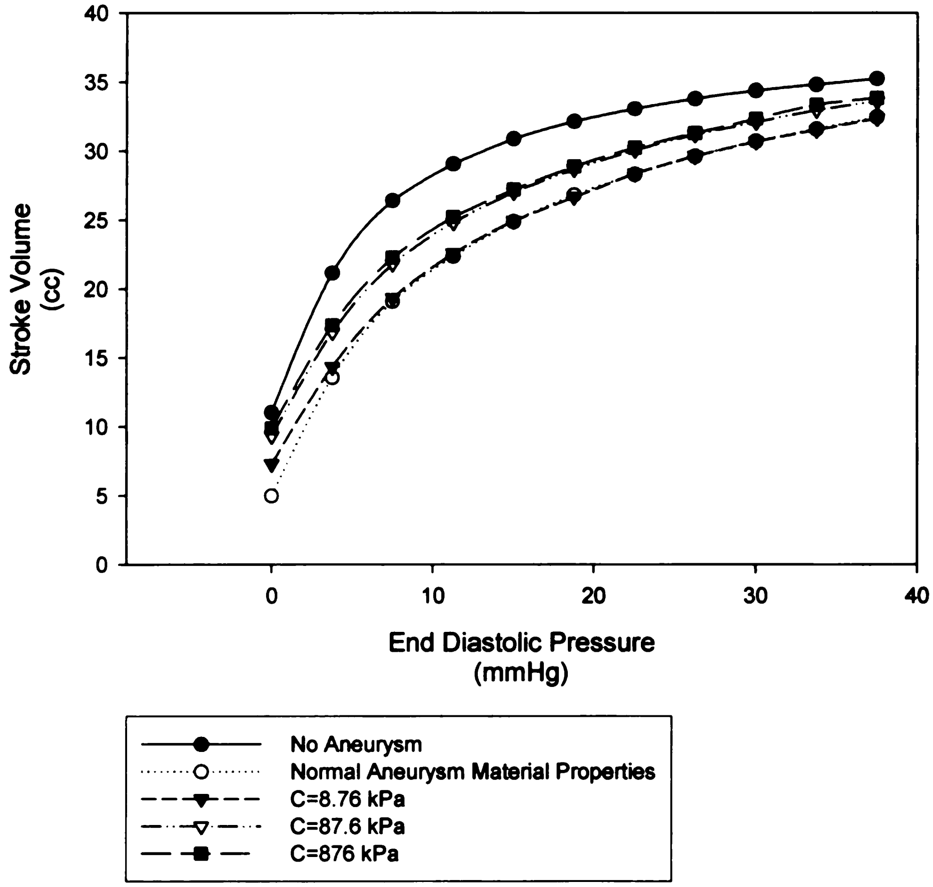

Figure 6.5 - Change in the Starling relation as the value of C in Equation (6.1) is increased over a wide range.

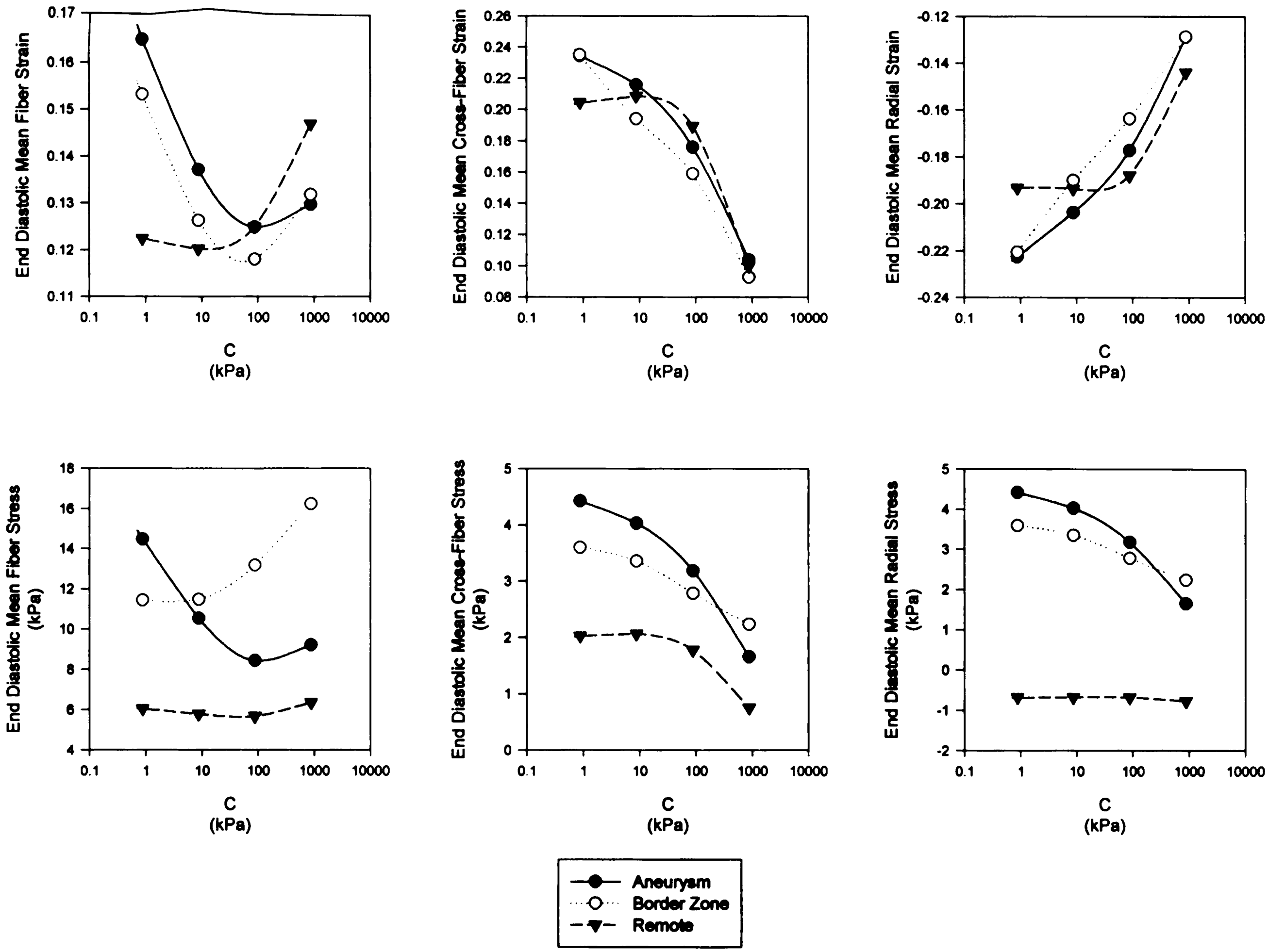

Figure 6.6 - Change in the end diastolic mean stress and strain as the value of C in Equation (6.1) is increased over a wide range.

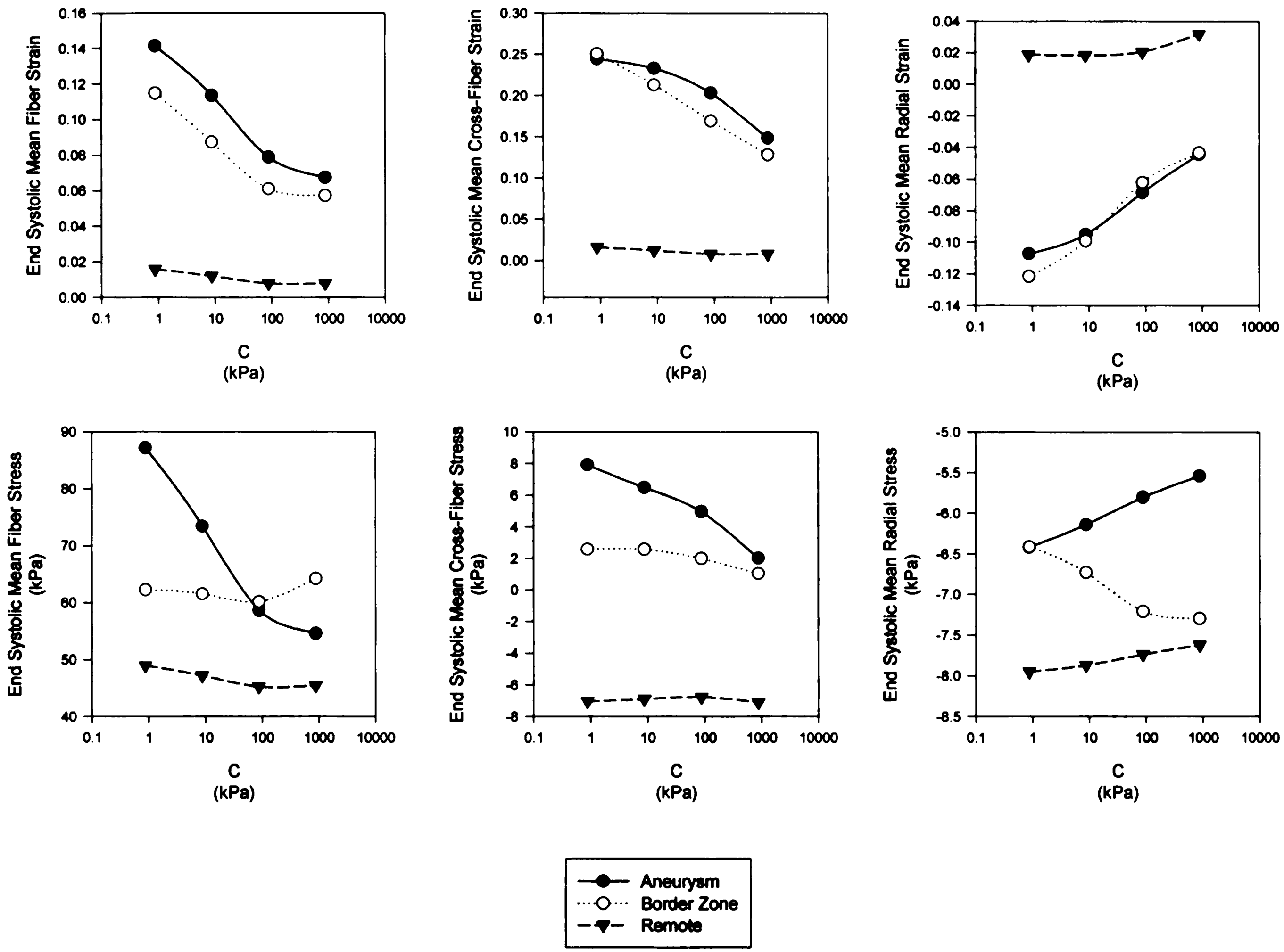

Figure 6.7 - Change in the end systolic mean stress and strain as the value of C in Equation (6.1) is increased over a wide range.

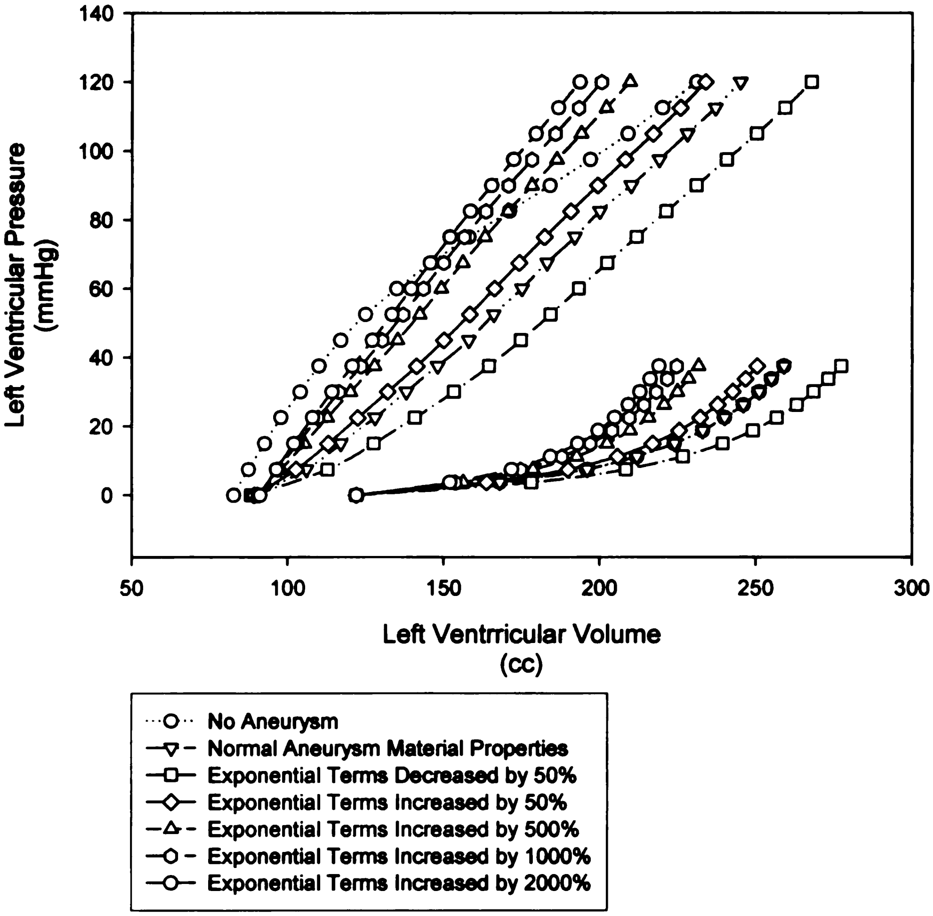

Figure 6.8 - Change in the pressure-volume relation as the exponential parameters in Equation (6.1) are varied over a wide range.

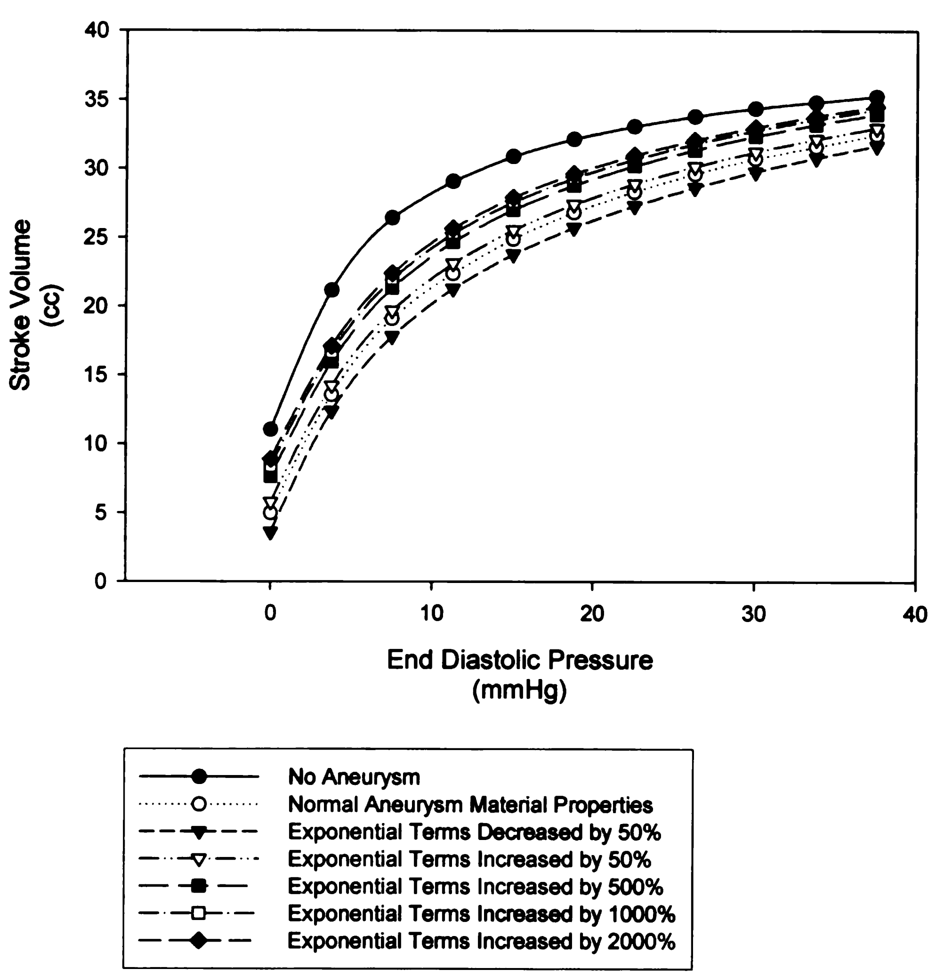

Figure 6.9 - Change in the Starling relation as the exponential parameters in Equation (6.1) are varied over a wide range.

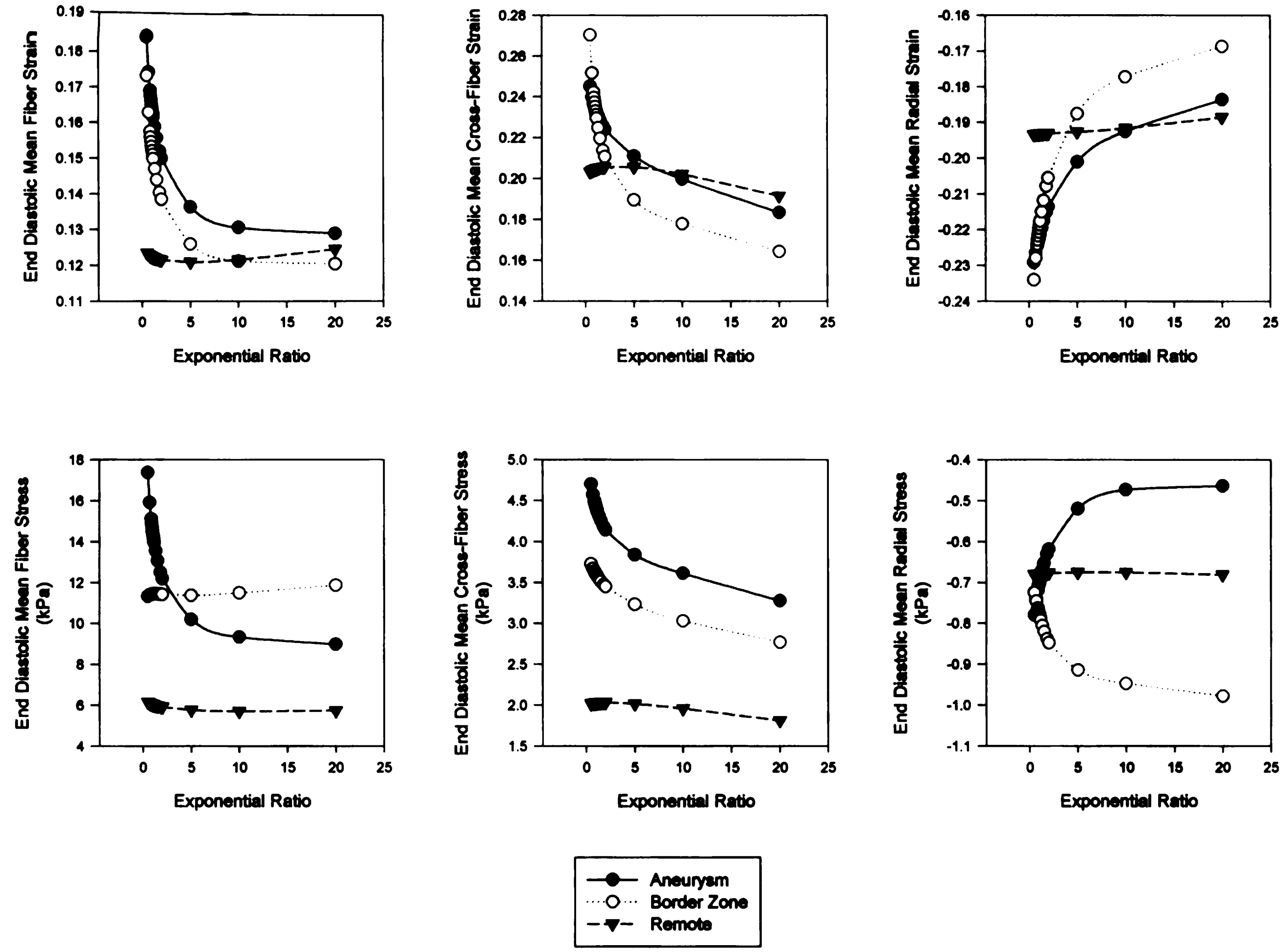

Figure 6.10 - Change in the end diastolic mean stress and strain as the exponential parameters in Equation (6.1) are varied over a wide range.

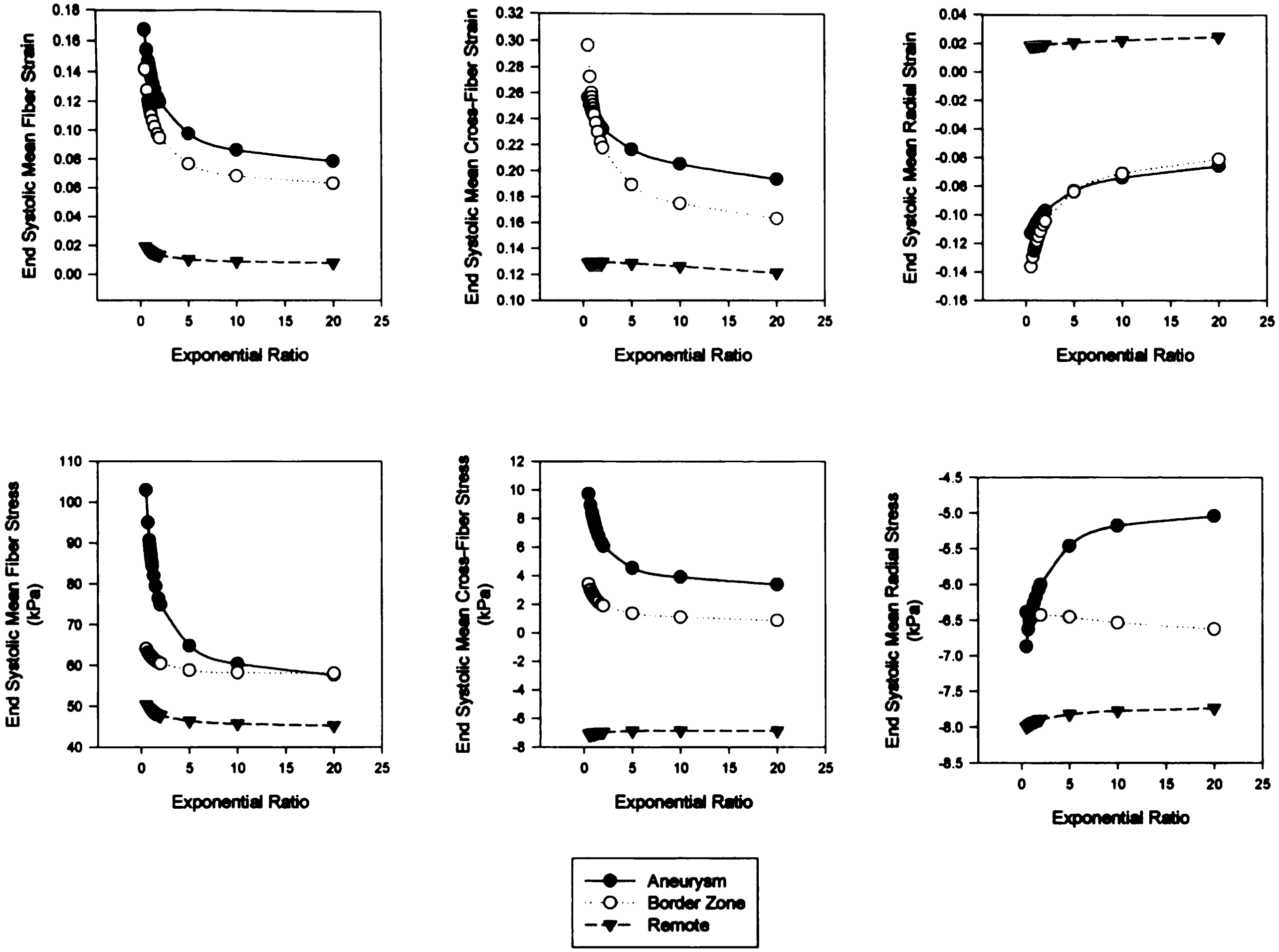

Figure 6.11 - Change in the end systolic mean stress and strain as the exponential parameters in Equation (6.1) are varied over a wide range.

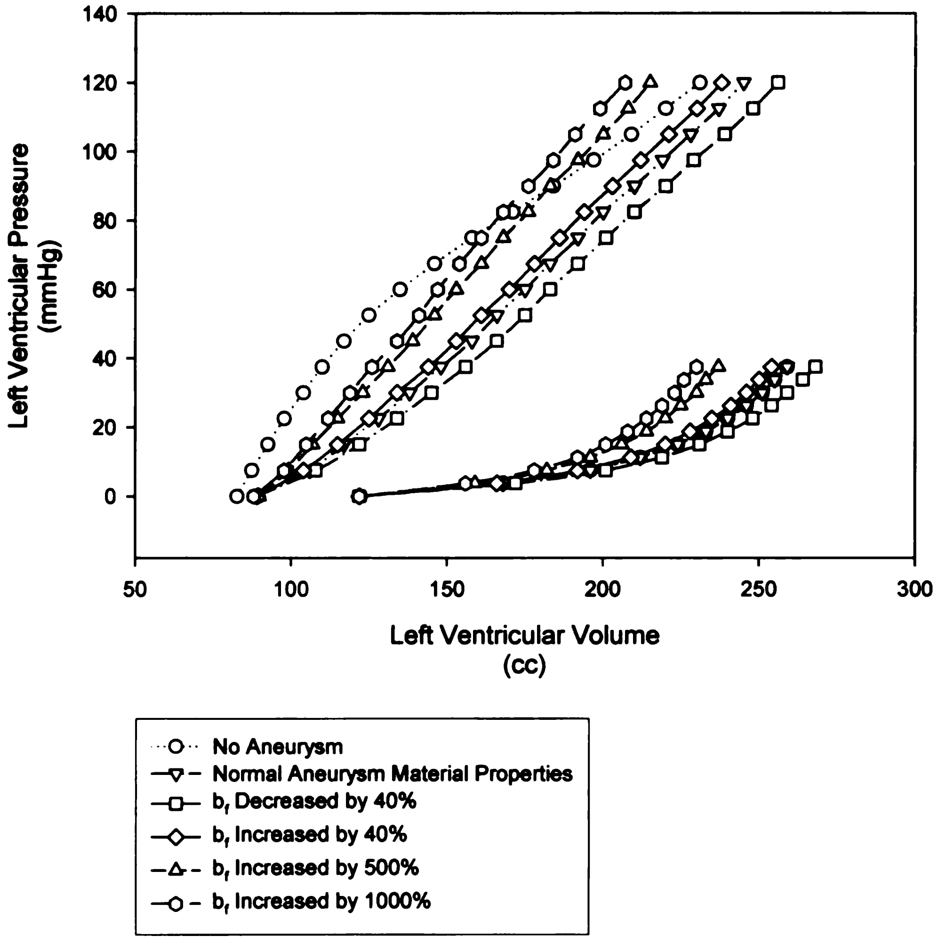

Figure 6.12 - Change in the pressure-volume relation as the value of b_f in Equation (6.1) is varied over a wide range.

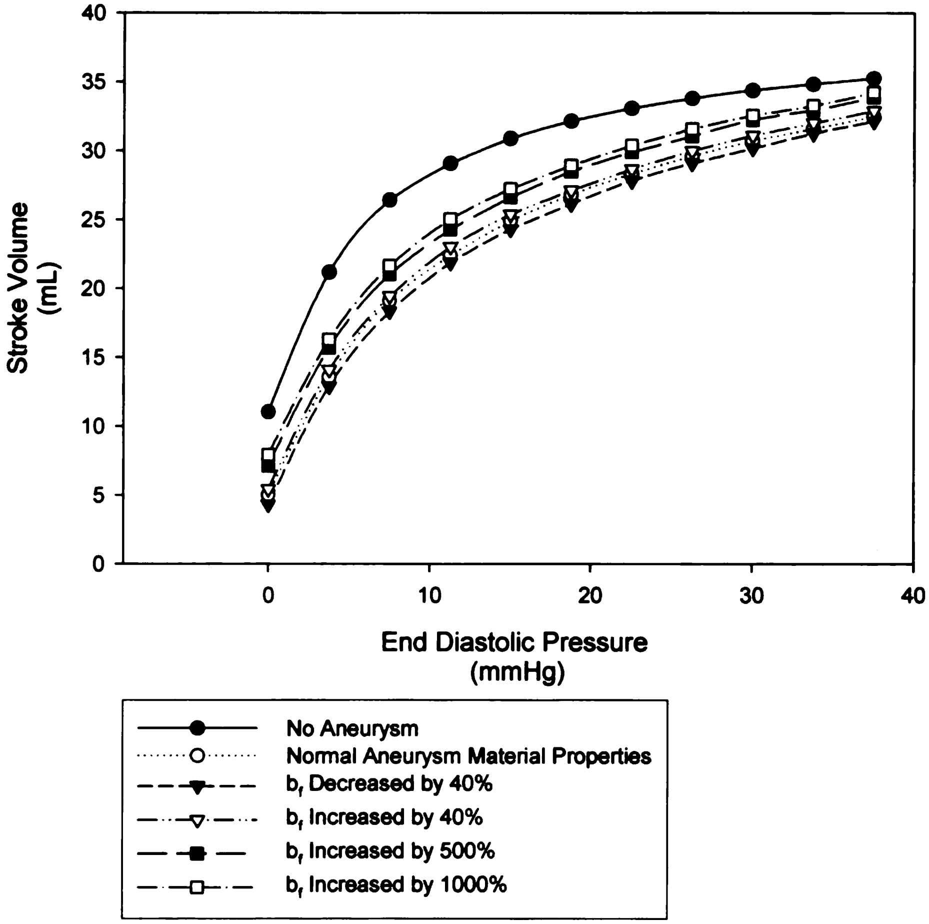

Figure 6.13 - Change in the pressure-volume relation as the value of b_f in Equation (6.1) is varied over a wide range.

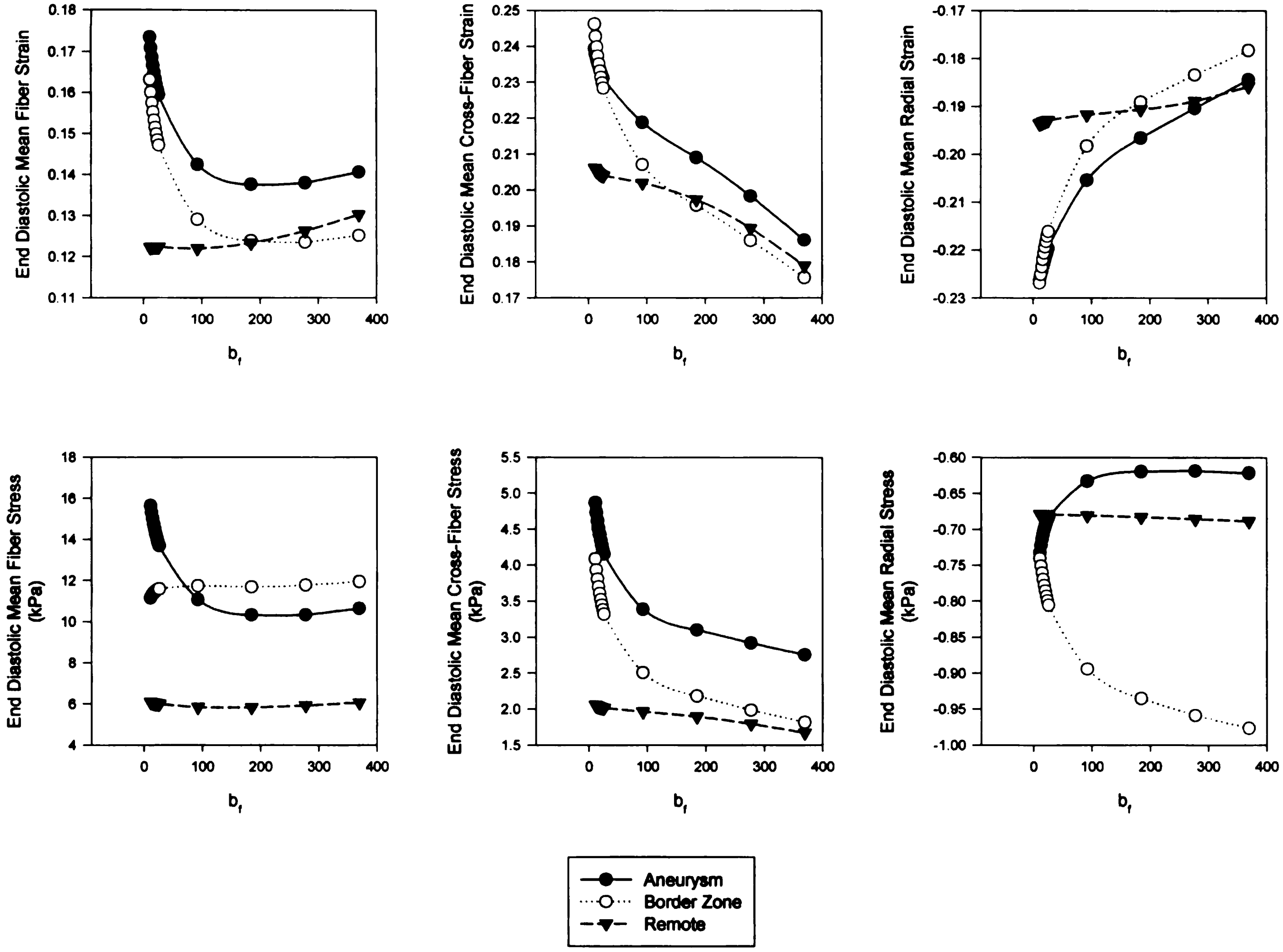

Figure 6.14 - Change in the end diastolic mean stress and strain as the value of b_f in Equation (6.1) is varied over a wide range.

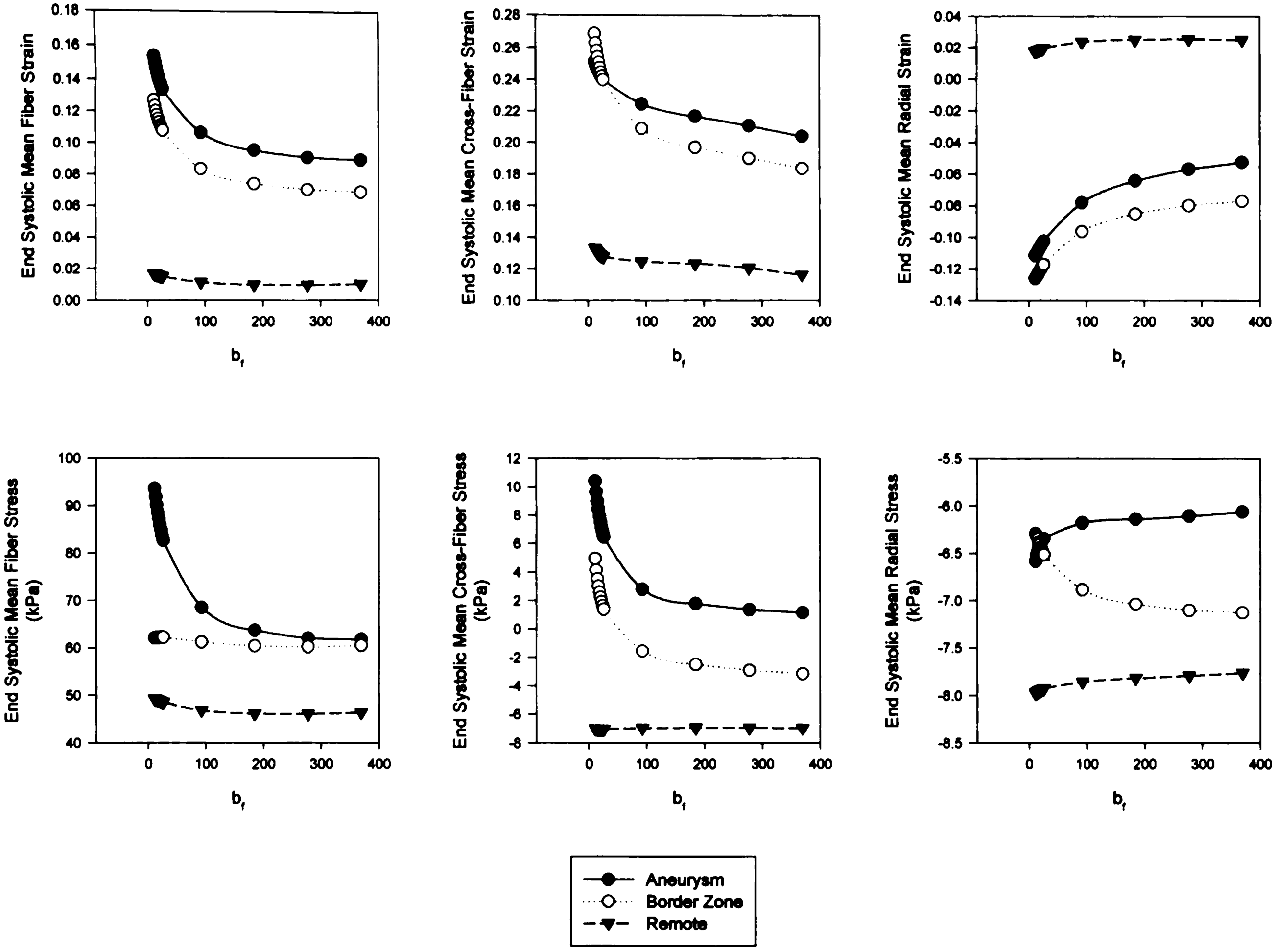

Figure 6.15 - Change in the end systolic mean stress and strain as the value of b_f in Equation (6.1) is varied over a wide range.

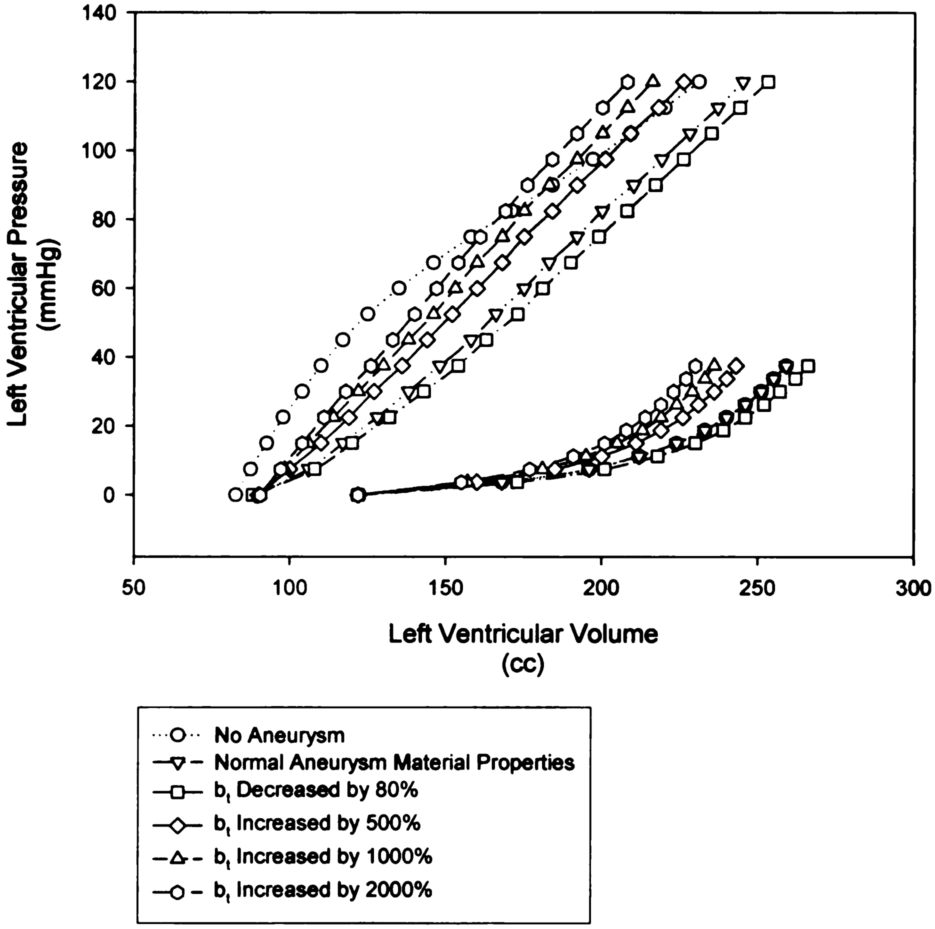

Figure 6.16 - Change in the pressure-volume relation as the value of b_t in Equation (6.1) is varied over a wide range.

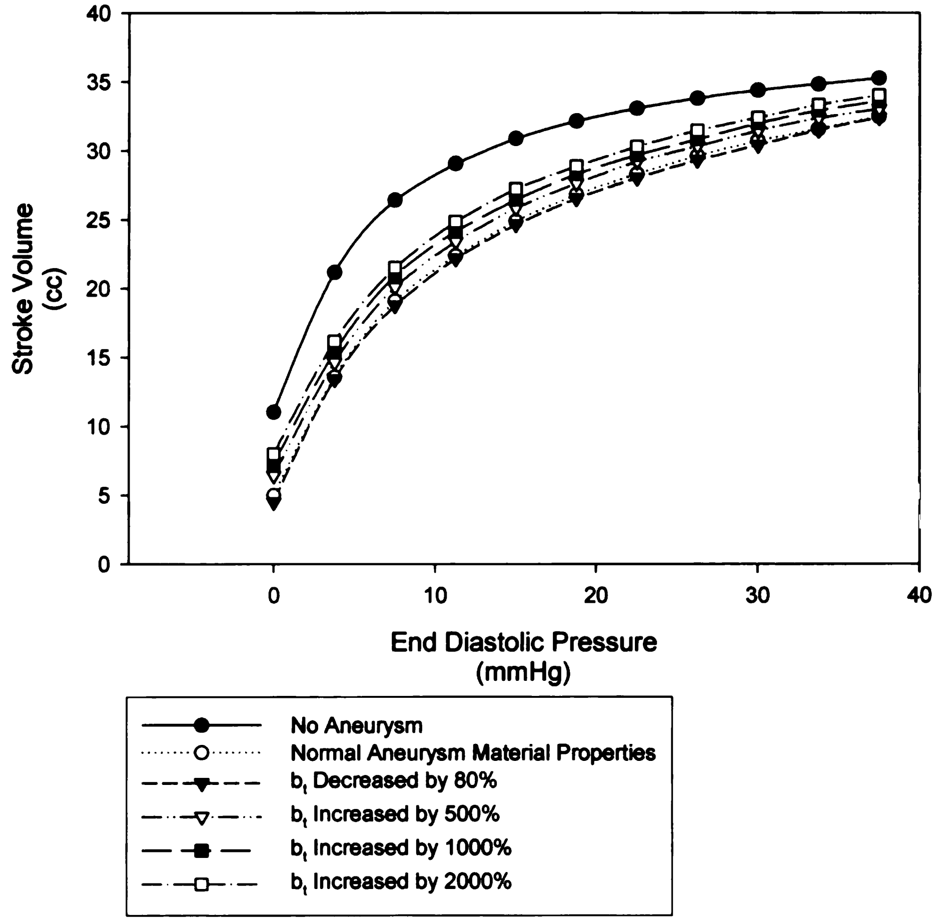

Figure 6.17 - Change in Starling relation as the value of b_t in Equation (6.1) is varied over a wide range.

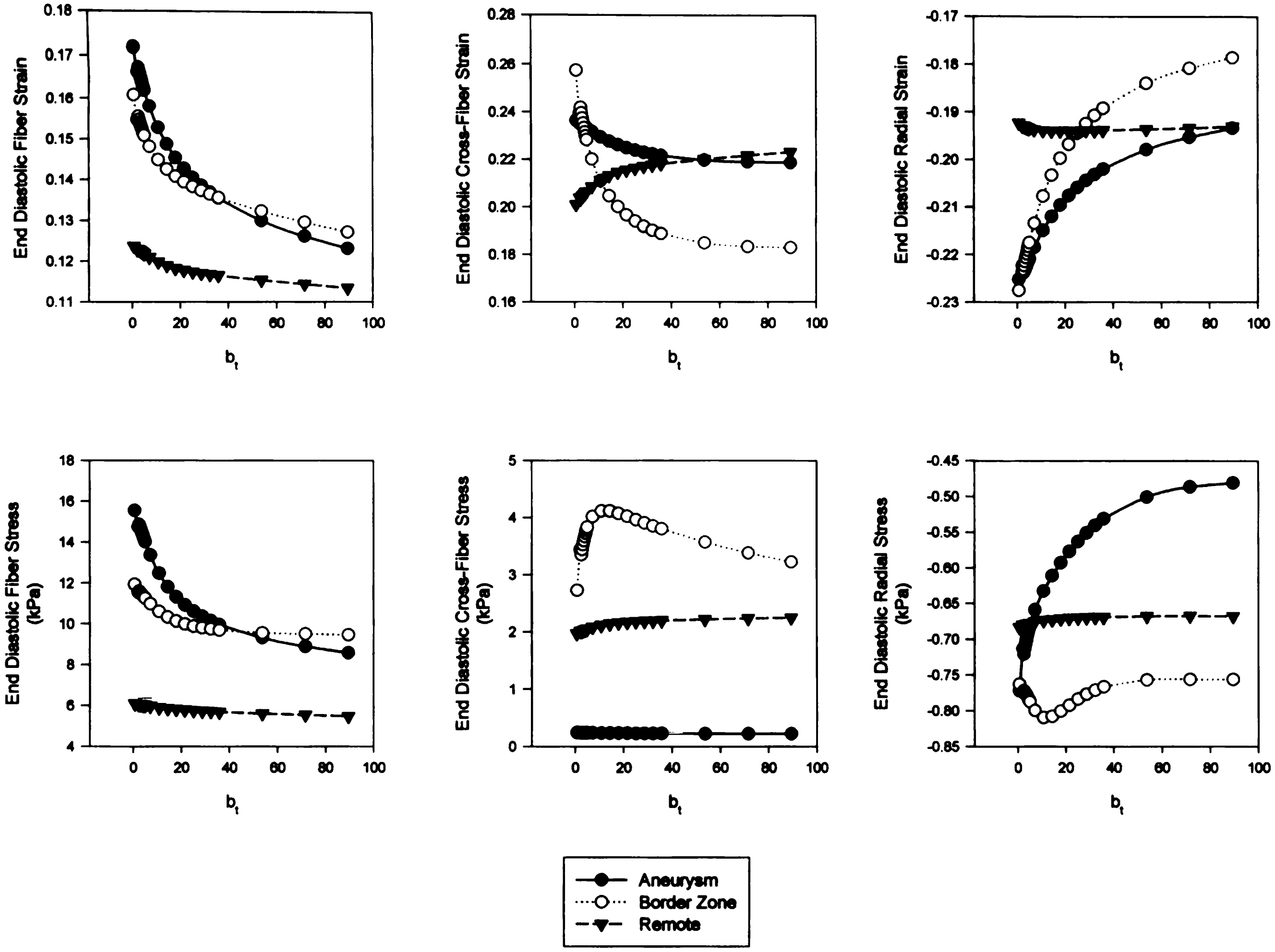

Figure 6.18 - Change in the end diastolic mean stress and strain as the value of b_t in Equation (6.1) is varied over a wide range.

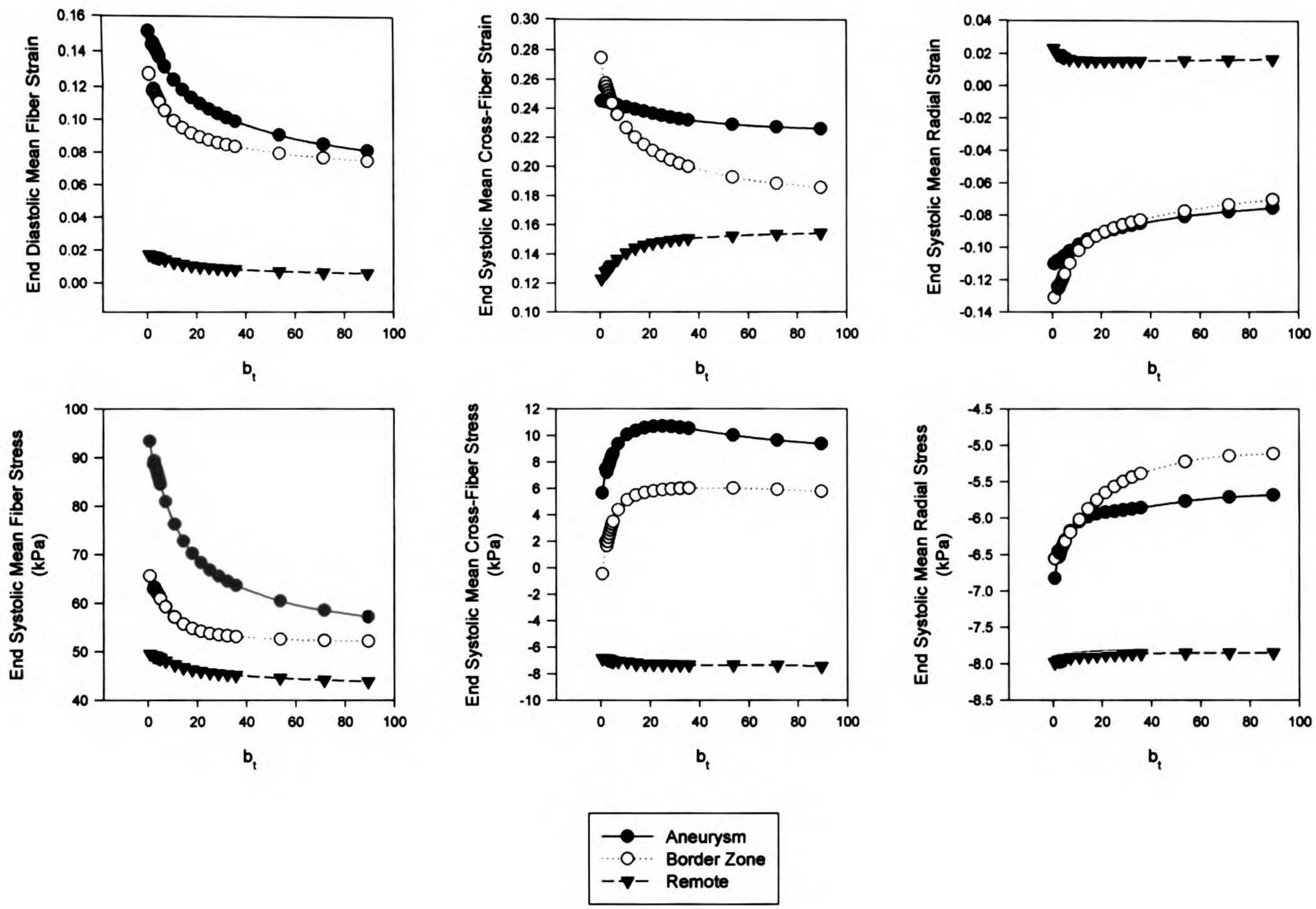

Figure 6.19 - Change in the end systolic mean stress and strain as the value of b_t in Equation (6.1) is varied over a wide range.

References:

1. Guccione, J.M., et al., *Mechanism underlying mechanical dysfunction in the border zone of left ventricular aneurysm: a finite element model study.* Ann Thorac Surg, 2001. 71(2): p. 654-62.
2. Radhakrishnan, S., D.N. Ghista, and G. Jayaraman, *Mechanics of left ventricular aneurysm.* J Biomed Eng, 1986. 8(1): p. 9-23.
3. Bogen, D.K., A. Needleman, and T.A. McMahon, *An analysis of myocardial infarction. The effect of regional changes in contractility.* Circ Res, 1984. 55(6): p. 805-15.
4. Bogen, D.K., et al., *An analysis of the mechanical disadvantage of myocardial infarction in the canine left ventricle.* Circ Res, 1980. 47(5): p. 728-41.
5. Vayo, H.W., *The theory of the left ventricular aneurysm.* Bull Math Biophys, 1966. 28(3): p. 363-70.
6. Needleman, A., et al., *A finite element model of the infarcted left ventricle.* J Biomech, 1983. 16(1): p. 45-58.
7. Reif, T.H. and M.D. Silver, *Role of stress concentration in the pathogenesis of cardiac rupture following acute myocardial infarction.* Can J Cardiol, 1995. 11(9): p. 757-62.
8. Aikawa, Y., et al., *Regional wall stress predicts ventricular remodeling after anteroseptal myocardial infarction in the Healing and Early Afterload Reducing Trial (HEART): an echocardiography-based structural analysis.* Am Heart J, 2001. 141(2): p. 234-42.

9. Moustakidis, P., et al., *Altered left ventricular geometry changes the border zone temporal distribution of stress in an experimental model of left ventricular aneurysm: a finite element model study.* Circulation, 2002. 106(12 Suppl 1): p. I168-75.

10. Solomon, S.D., et al., *Assessment of regional left ventricular wall stress after myocardial infarction by echocardiography-based structural analysis.* J Am Soc Echocardiogr, 1998. 11(10): p. 938-47.

11. Costa, K.D., et al., *A three-dimensional finite element method for large elastic deformations of ventricular myocardium: I--Cylindrical and spherical polar coordinates.* J Biomech Eng, 1996. 118(4): p. 452-63.

12. Guccione, J.M., K.D. Costa, and A.D. McCulloch, *Finite element stress analysis of left ventricular mechanics in the beating dog heart.* J Biomech, 1995. 28(10): p. 1167-77.

13. Guccione, J.M., A.D. McCulloch, and L.K. Waldman, *Passive material properties of intact ventricular myocardium determined from a cylindrical model.* J Biomech Eng, 1991. 113(1): p. 42-55.

14. Omens, J.H., K.D. May, and A.D. McCulloch, *Transmural distribution of three-dimensional strain in the isolated arrested canine left ventricle.* Am J Physiol, 1991. 261(3 Pt 2): p. H918-28.

15. Guccione, J.M., L.K. Waldman, and A.D. McCulloch, *Mechanics of active contraction in cardiac muscle: Part II--Cylindrical models of the systolic left ventricle.* J Biomech Eng, 1993. 115(1): p. 82-90.

16. Moulton, M.J., et al., *Mechanical dysfunction in the border zone of an ovine model of left ventricular aneurysm.* Ann Thorac Surg, 1995. 60(4): p. 986-97; discussion 998.

17. Ratcliffe, M.B., et al., *Ventricular volume, chamber stiffness, and function after anteroapical aneurysm plication in the sheep.* J Thorac Cardiovasc Surg, 2000. 119(1): p. 115-24.

18. Savage, E.B., et al., *Repair of left ventricular aneurysm. Changes in ventricular mechanics, hemodynamics, and oxygen consumption.* J Thorac Cardiovasc Surg, 1992. 104(3): p. 752-62.

19. McCormick, R.J., et al., *Regional differences in LV collagen accumulation and mature cross-linking after myocardial infarction in rats.* Am J Physiol, 1994. 266(1 Pt 2): p. H354-9.

20. MacKenna, D.A., et al., *Contribution of collagen matrix to passive left ventricular mechanics in isolated rat hearts.* Am J Physiol, 1994. 266(3 Pt 2): p. H1007-18.

21. Omens, J.H., D.A. MacKenna, and A.D. McCulloch, *Measurement of strain and analysis of stress in resting rat left ventricular myocardium.* J Biomech, 1993. 26(6): p. 665-76.

22. Weber, K.T., et al., *Collagen network of the myocardium: function, structural remodeling and regulatory mechanisms.* J Mol Cell Cardiol, 1994. 26(3): p. 279-92.

23. Weber, K.T., *Cardiac interstitium in health and disease: the fibrillar collagen network.* J Am Coll Cardiol, 1989. 13(7): p. 1637-52.

24. Whittaker, P., D.R. Boughner, and R.A. Kloner, *Role of collagen in acute myocardial infarct expansion.* Circulation, 1991. 84(5): p. 2123-34.

25. Whittaker, P., et al., *Stunned myocardium and myocardial collagen damage: differential effects of single and repeated occlusions.* Am Heart J, 1991. 121(2 Pt 1): p. 434-41.

26. Weis, S.M., et al., *Myocardial Mechanics and Collagen Structure in the Osteogenesis Imperfecta Murine (oim).* Circ Res, 2000. 87(8): p. 663-669.

27. Bowen, F.W., et al., *Restraining acute infarct expansion decreases collagenase activity in borderzone myocardium.* Ann Thorac Surg, 2001. 72(6): p. 1950-6.

28. Jugdutt, B.I. and R.W. Amy, *Healing after myocardial infarction in the dog: changes in infarct hydroxyproline and topography.* J Am Coll Cardiol, 1986. 7(1): p. 91-102.

29. Cleutjens, J.P., et al., *Collagen remodeling after myocardial infarction in the rat heart.* Am J Pathol, 1995. 147(2): p. 325-38.

30. Jugdutt, B.I., M.J. Joljart, and M.I. Khan, *Rate of collagen deposition during healing and ventricular remodeling after myocardial infarction in rat and dog models.* Circulation, 1996. 94(1): p. 94-101.

31. Gerber, B.L., et al., *Microvascular obstruction and left ventricular remodeling early after acute myocardial infarction.* Circulation, 2000. 101(23): p. 2734-41.

32. Geerts, L., et al., *Characterization of the normal cardiac myofiber field in goat measured with MR-diffusion tensor imaging.* Am J Physiol Heart Circ Physiol, 2002. 283(1): p. H139-45.

Chapter 7

Conclusion

This thesis has focused on the combination of traditional mechanical testing techniques (biaxial material property testing) with state of the art computer modeling (Finite Element Method (FEM)) to study and evaluate left ventricular aneurysm (LVA). The combination of these tools allows us to gain a greater understanding into this disease.

In Chapter 3, an ovine LVA model [1] was used to obtain realistic material property values for LVA. After allowing the aneurysms to mature for ten weeks, the tissue was harvested then stretched on a biaxial testing device. Our results found that the tissue was significantly stiffer than previously reported [2, 3]. We feel that the discrepancy lies in the difference in the design of the two different biaxial stretching machines, with ours being superior.

The impact of these new LVA material properties was examined by creating a realistic finite element model of the left ventricle as a whole. The geometry for this model was obtained using a magnetic resonance imaging (MRI) scan of the Markovitz [1] ovine LVA model. The model predicted an increase in cardiac function as measured by the Starling relation, a global decrease in fiber stress, and a global increase in cross-fiber stress. The results have important implications to the structural changes that might be occurring not only in the aneurysm region of the left ventricle, but also in the border zone and remote regions of the heart. This study also illuminated another interesting result, that the choice of material parameters used to model LVA had significant impact upon the output of the models. While there are many different approaches to increasing the

stiffness of the aneurysm, each yielded unique and different results in terms of global and regional function of the left ventricle.

In an attempt to isolate the impact of each material parameter upon cardiac function, a series of simulations was conducted. The stiffness of the aneurysm was changed by altering the bulk stiffness of the aneurysm (C in Eqn 6.1), all of the exponential terms in Equation 6.1, the fiber stiffness (b_f in Equation 6.1), and the cross-fiber stiffness (b_t in Equation 6.1). With all of the methods, cardiac function was improved as stiffness was increased. However, each method yielded different results for stress and strain predictions. This has important implications to the cellular response to changing stress and strain patterns following LVA. These calculations are all static. Before definitive effects of changing material parameters can be made, the effects on veno-cardiac, and cardio-arterial impedence matching must also be considered.

One of the most important lessons to be learned from this experience is that the choice of material parameters in FEM simulations is of the utmost importance. Many investigators, ourselves included, have in the past simply modeled an increase in stiffness by modifying one component of the strain energy function [4]. The results of this assumption will be the inaccurate prediction of stress and strain. This realization will be of increasing importance as the relationship between stress/strain and cellular expression begins to be uncovered [5-8]. This idea also underlies the importance of developing models such as ours that are able to predict stress and strain along fiber and cross-fiber axes. Previous models of LVA have lacked this ability [9-11].

Future Directions

Currently work is being done to greatly improve the accuracy of the models presented in this paper. Tagged magnetic resonance imaging (MRI) is currently being applied to the left ventricle [12, 13]. The results from experiments such as these can yield many useful results. First, they could be used, in combination with left ventricular pressures and computational modeling, to provide an accurate in-vivo method of determining left ventricular material properties. Second, they could be used to measure in-vivo the strain of the left ventricle in nearly all regions.

Another advance currently being applied to the study of the left ventricle is the use of diffusion tensor MRI [14]. This method allows us to accurately map the muscle fiber orientation of the left ventricle. Inclusion of a regionally accurate model of LV muscle fiber orientation into the model would allow a highly accurate FEM model to be developed. Calculations of the effects of changing material parameters on impedence matching and efficiency also need to be performed.

The end goal of all of these tools would be their combination into an individual specific computational model of the left ventricle. If for an individual all of these methods could be combined it would be possible to create computational model with a new level of detail. The creation of such a model would allow us with an even higher order of

accuracy to predict the effects of surgical repairs of the ventricle, medical devices and cell transplantation upon the left ventricle.

Referneces:

1. Markovitz, L.J., et al., *Large animal model of left ventricular aneurysm.* Ann Thorac Surg, 1989. **48**(6): p. 838-45.
2. Gupta, K.B., *Functional and Structural Changes in Left Ventricular Aneurysm*, in *Bioengineeing*. 1991, University of Pennsylvania: Philadelphia. p. 310.
3. Gupta, K.B., et al., *Changes in passive mechanical stiffness of myocardial tissue with aneurysm formation.* Circulation, 1994. **89**(5): p. 2315-26.
4. Guccione, J.M., et al., *Mechanism underlying mechanical dysfunction in the border zone of left ventricular aneurysm: a finite element model study.* Ann Thorac Surg, 2001. **71**(2): p. 654-62.
5. Thomas, C.H., et al., *Engineering gene expression and protein synthesis by modulation of nuclear shape.* Proc Natl Acad Sci U S A, 2002. **99**(4): p. 1972-7.
6. Holmes, J.W., Covell, J.W., *Collagen Fiber Orientation in Myocardial Scar Tissue.* Cardiovascular Pathobiology, 1996. **1**(1): p. 15-22.
7. Holmes, J.W., J.A. Nunez, and J.W. Covell, *Functional implications of myocardial scar structure.* Am J Physiol, 1997. **272**(5 Pt 2): p. H2123-30.
8. Song, G., et al., *Altered mechanical properties and intracellular calcium signaling in cardiomyocytes from annexin 6 null-mutant mice.* Faseb J, 2002. **16**(6): p. 622-4.
9. Moustakidis, P., et al., *Altered left ventricular geometry changes the border zone temporal distribution of stress in an experimental model of left ventricular

aneurysm: a finite element model study. Circulation, 2002. **106**(12 Suppl 1): p. I168-75.

10. Bogen, D.K., A. Needleman, and T.A. McMahon, *An analysis of myocardial infarction. The effect of regional changes in contractility.* Circ Res, 1984. **55**(6): p. 805-15.

11. Bogen, D.K., et al., *An analysis of the mechanical disadvantage of myocardial infarction in the canine left ventricle.* Circ Res, 1980. **47**(5): p. 728-41.

12. Kramer, C.M., et al., *Reverse remodeling and improved regional function after repair of left ventricular aneurysm.* J Thorac Cardiovasc Surg, 2002. **123**(4): p. 700-6.

13. Kramer, C.M., et al., *Regional differences in function within noninfarcted myocardium during left ventricular remodeling.* Circulation, 1993. **88**(3): p. 1279-88.

14. Geerts, L., et al., *Characterization of the normal cardiac myofiber field in goat measured with MR-diffusion tensor imaging.* Am J Physiol Heart Circ Physiol, 2002. **283**(1): p. H139-45.

Chapter 8

Bibliography

Bibliography:

1. *2001 Heart and Stroke Statistical Update*. 2001, American Heart Association: Dallas, TX.
2. Aikawa, Y., et al., *Regional wall stress predicts ventricular remodeling after anteroseptal myocardial infarction in the Healing and Early Afterload Reducing Trial (HEART): an echocardiography-based structural analysis.* Am Heart J, 2001. **141**(2): p. 234-42.
3. Allaart, C.P., P. Sipkema, and N. Westerhof, *Effect of perfusion pressure on diastolic stress-strain relations of isolated rat papillary muscle.* Am J Physiol, 1995. **268**(3 Pt 2): p. H945-54.
4. Arrighi, J.A. and R. Soufer, *Left ventricular diastolic function: physiology, methods of assessment, and clinical significance.* J Nucl Cardiol, 1995. **2**(6): p. 525-43.
5. Artrip, J.H., M.C. Oz, and D. Burkhoff, *Left ventricular volume reduction surgery for heart failure: a physiologic perspective.* J Thorac Cardiovasc Surg, 2001. **122**(4): p. 775-82.
6. Ba'albaki, H.A. and S.D. Clements, Jr., *Left ventricular aneurysm: a review.* Clin Cardiol, 1989. **12**(1): p. 5-13.
7. Baracca, E., et al., *Non-invasive estimation of the diastolic elastic and viscoelastic properties of the left ventricle.* Eur Heart J, 1991. **12**(2): p. 249-61.

8. Barratt-Boyes, B.G., et al., *The results of surgical treatment of left ventricular aneurysms. An assessment of the risk factors affecting early and late mortality.* J Thorac Cardiovasc Surg, 1984. **87**(1): p. 87-98.

9. Berne, R.M. and M.N. Levy, *Cardiovascular physiology.* 8th ed. The Mosby physiology monograph series. 2001, St. Louis, MO: Mosby. xiv, 312.

10. Bogen, D.K. and T.A. McMahon, *Do cardiac aneurysms blow out?* Biophys J, 1979. **27**(2): p. 301-16.

11. Bogen, D.K., A. Needleman, and T.A. McMahon, *An analysis of myocardial infarction. The effect of regional changes in contractility.* Circ Res, 1984. **55**(6): p. 805-15.

12. Bogen, D.K., et al., *An analysis of the mechanical disadvantage of myocardial infarction in the canine left ventricle.* Circ Res, 1980. **47**(5): p. 728-41.

13. Bowen, F.W., et al., *Restraining acute infarct expansion decreases collagenase activity in borderzone myocardium.* Ann Thorac Surg, 2001. **72**(6): p. 1950-6.

14. Brady, A., *Passive Elastic Properties of Cardiac Myocytes Relative to Intact Cardiac Tissue*, in *Cardiac Myocyte-Connective Tissue Interactions in Health and Disease*, K.R. Tobinson TF, Editor. 1990, Krager: Basel. p. 37-52.

15. Brady, A.J., *Length dependence of passive stiffness in single cardiac myocytes.* Am J Physiol, 1991. **260**(4 Pt 2): p. H1062-71.

16. Brady, A.J., *Mechanical properties of isolated cardiac myocytes.* Physiol Rev, 1991. **71**(2): p. 413-28.

17. Brickner, M.E. and M.R. Starling, *Dissociation of end systole from end ejection in patients with long-term mitral regurgitation.* Circulation, 1990. **81**(4): p. 1277-86.

18. Brown, M.A., et al., *Post-systolic shortening: a marker of potential for early recovery of acutely ischaemic myocardium in the dog.* Cardiovasc Res, 1987. **21**(10): p. 703-16.

19. Buckberg, G.D., *Congestive heart failure: treat the disease, not the symptom--return to normalcy.* J Thorac Cardiovasc Surg, 2001. **121**(4): p. 628-37.

20. Burton, N.A., et al., *Left ventricular aneurysm. Preoperative risk factors and long-term postoperative results.* J Thorac Cardiovasc Surg, 1979. **77**(1): p. 65-75.

21. Capasso, J.M., T.F. Robinson, and P. Anversa, *Alterations in collagen cross-linking impair myocardial contractility in the mouse heart.* Circ Res, 1989. **65**(6): p. 1657-64.

22. Castiglioni, A., et al., *Surgical restoration of the left ventricle for postinfarction aneurysm.* Ital Heart J, 2002. **3**(6): p. 370-4.

23. Caulfield, J.B. and T.K. Borg, *The collagen network of the heart.* Lab Invest, 1979. **40**(3): p. 364-72.

24. Chaudhry, H.R., *Passive material properties of intact ventricular myocardium determined from a cylindrical model.* J Biomech Eng, 1996. **118**(2): p. 262-3.

25. Cherniavsky, A.M., et al., *Preoperative modeling of an optimal left ventricle volume for surgical treatment of ventricular aneurysms.* Eur J Cardiothorac Surg, 2001. **20**(4): p. 777-82.

26. Chew, P.H., F.C. Yin, and S.L. Zeger, *Biaxial stress-strain properties of canine pericardium.* J Mol Cell Cardiol, 1986. **18**(6): p. 567-78.

27. Cleutjens, J.P., et al., *Collagen remodeling after myocardial infarction in the rat heart.* Am J Pathol, 1995. **147**(2): p. 325-38.

28. Cohen, A.J., et al., *Ventricular aneurysm repair: a new approach.* J Card Surg, 2000. **15**(3): p. 209-16.

29. Collinsworth, A.M., et al., *Orientation and length of mammalian skeletal myocytes in response to a unidirectional stretch.* Cell Tissue Res, 2000. **302**(2): p. 243-51.

30. Coltharp, W.H., et al., *Ventricular aneurysmectomy. A 25-year experience.* Ann Surg, 1994. **219**(6): p. 707-13; discussion 713-4.

31. Connelly, C.M., et al., *Reversible and irreversible elongation of ischemic, infarcted, and healed myocardium in response to increases in preload and afterload.* Circulation, 1991. **84**(1): p. 387-99.

32. Connelly, C.M., et al., *Effects of reperfusion after coronary artery occlusion on post-infarction scar tissue.* Circ Res, 1985. **57**(4): p. 562-77.

33. Conrad, C.H., et al., *Myocardial fibrosis and stiffness with hypertrophy and heart failure in the spontaneously hypertensive rat.* Circulation, 1995. **91**(1): p. 161-70.

34. Cooley, D.A., *Ventricular endoaneurysmorrhaphy: a simplified repair for extensive postinfarction aneurysm.* J Card Surg, 1989. **4**(3): p. 200-5.

35. Cooley, D.A., et al., *Intracavitary repair of ventricular aneurysm and regional dyskinesia.* Ann Surg, 1992. **215**(5): p. 417-23; discussion 423-4.

36. Cosgrove, D.M., et al., *Ventricular aneurysm resection. Trends in surgical risk.* Circulation, 1989. **79**(6 Pt 2): p. I97-101.

37. Costa, K.D., et al., *A three-dimensional finite element method for large elastic deformations of ventricular myocardium: I--Cylindrical and spherical polar coordinates.* J Biomech Eng, 1996. **118**(4): p. 452-63.

38. Costa, K.D., et al., *A three-dimensional finite element method for large elastic deformations of ventricular myocardium: II--Prolate spheroidal coordinates.* J Biomech Eng, 1996. **118**(4): p. 464-72.

39. Crottogini, A.J., et al., *Left ventricular end-systolic elastance is incorrectly estimated by the use of stepwise afterload variations in conscious, unsedated, autonomically intact dogs.* Circulation, 1994. **90**(3): p. 1431-40.

40. De Tombe, P.P., et al., *Ventricular stroke work and efficiency both remain nearly optimal despite altered vascular loading.* Am J Physiol, 1993. **264**(6 Pt 2): p. H1817-24.

41. Demer, L.L. and F.C. Yin, *Passive biaxial mechanical properties of isolated canine myocardium.* J Physiol, 1983. **339**: p. 615-30.

42. Di Donato, M., et al., *Early hemodynamic results of left ventricular reconstructive surgery for anterior wall left ventricular aneurysm.* Am J Cardiol, 1992. **69**(9): p. 886-90.

43. Di Donato, M., et al., *Effects of the Dor procedure on left ventricular dimension and shape and geometric correlates of mitral regurgitation one year after surgery.* J Thorac Cardiovasc Surg, 2001. **121**(1): p. 91-6.

44. Di Donato, M., et al., *Outcome of left ventricular aneurysmectomy with patch repair in patients with severely depressed pump function.* Am J Cardiol, 1995. **76**(8): p. 557-61.

45. Di Donato, M., et al., *Regional myocardial performance of non-ischaemic zones remote from anterior wall left ventricular aneurysm. Effects of aneurysmectomy.* Eur Heart J, 1995. **16**(9): p. 1285-92.

46. Dokos, S., et al., *A triaxial-measurement shear-test device for soft biological tissues.* J Biomech Eng, 2000. **122**(5): p. 471-8.

47. Dokos, S., et al., *Shear properties of passive ventricular myocardium.* Am J Physiol Heart Circ Physiol, 2002. **283**(6): p. H2650-9.

48. Dor, V., et al., *Left ventricular aneurysm: a new surgical approach.* Thorac Cardiovasc Surg, 1989. **37**(1): p. 11-9.

49. Dor, V., et al., *Endoventricular patch plasties with septal exclusion for repair of ischemic left ventricle: technique, results and indications from a series of 781 cases.* Jpn J Thorac Cardiovasc Surg, 1998. **46**(5): p. 389-98.

50. Dor, V., et al., *Late hemodynamic results after left ventricular patch repair associated with coronary grafting in patients with postinfarction akinetic or dyskinetic aneurysm of the left ventricle.* J Thorac Cardiovasc Surg, 1995. **110**(5): p. 1291-9; discussion 1300-1.

51. Dor, V., et al., *Efficacy of endoventricular patch plasty in large postinfarction akinetic scar and severe left ventricular dysfunction: comparison with a series of large dyskinetic scars.* J Thorac Cardiovasc Surg, 1998. **116**(1): p. 50-9.

52. Doss, M., et al., *Long term follow up of left ventricular function after repair of left ventricular aneurysm. A comparison of linear closure versus patch plasty.* Eur J Cardiothorac Surg, 2001. **20**(4): p. 783-5.

53. Downs, J., et al., *An improved video-based computer tracking system for soft biomaterials testing.* IEEE Trans Biomed Eng, 1990. **37**(9): p. 903-7.

54. Drzewiecki, G., et al., *Modeling of mechanical dysfunction in regional stunned myocardium of the left ventricle.* IEEE Trans Biomed Eng, 1996. **43**(12): p. 1151-63.

55. Ertl, G., et al., *Cardiac dysfunction and development of heart failure.* Eur Heart J, 1993. **14 Suppl A**: p. 33-7.

56. Factor, S.M., et al., *The effects of acutely increased ventricular cavity pressure on intrinsic myocardial connective tissue.* J Am Coll Cardiol, 1988. **12**(6): p. 1582-9.

57. Fallert, M.A., et al., *Myocardial electrical impedance mapping of ischemic sheep hearts and healing aneurysms.* Circulation, 1993. **87**(1): p. 199-207.

58. Faxon, D.P., et al., *The influence of surgery on the natural history of angiographically documented left ventricular aneurysm: the Coronary Artery Surgery Study.* Circulation, 1986. **74**(1): p. 110-8.

59. Feneley, M.P., et al., *Comparison of preload recruitable stroke work, end-systolic pressure-volume and dP/dtmax-end-diastolic volume relations as indexes of left ventricular contractile performance in patients undergoing routine cardiac catheterization.* J Am Coll Cardiol, 1992. **19**(7): p. 1522-30.

60. Fishbein, M.C., D. Maclean, and P.R. Maroko, *The histopathologic evolution of myocardial infarction.* Chest, 1978. **73**(6): p. 843-9.

61. Fishbein, M.C., D. Maclean, and P.R. Maroko, *Experimental myocardial infarction in the rat: qualitative and quantitative changes during pathologic evolution.* Am J Pathol, 1978. **90**(1): p. 57-70.

62. Fletcher, P.J., et al., *Left ventricular diastolic pressure-volume relations in rats with healed myocardial infarction. Effects on systolic function.* Circ Res, 1981. **49**(3): p. 618-26.

63. Freeman, G.L., W.C. Little, and R.A. O'Rourke, *The effect of vasoactive agents on the left ventricular end-systolic pressure-volume relation in closed-chest dogs.* Circulation, 1986. **74**(5): p. 1107-13.

64. Freiburg, A., et al., *Series of exon-skipping events in the elastic spring region of titin as the structural basis for myofibrillar elastic diversity.* Circ Res, 2000. **86**(11): p. 1114-21.

65. Fung, Y.C., *Biorheology of soft tissues.* Biorheology, 1973. **10**(2): p. 139-55.

66. Fung, Y.C., *Biomechanics : mechanical properties of living tissues.* 1981, New York: Springer-Verlag. xii, 433 p.

67. Fung, Y.C., *Biomechanics : motion, flow, stress, and growth.* 1990, New York: Springer-Verlag. xv, 569 p.

68. Fung, Y.C., *Biomechanics : motion, flow, stress, and growth.* 1990, New York: Springer-Verlag. xv, 569.

69. Fung, Y.C., *Biomechanics : mechanical properties of living tissues.* 2nd ed. 1993, New York: Springer-Verlag. xviii, 568 p.

70. Fung, Y.C., *Biomechanics : mechanical properties of living tissues*. 2nd ed. 1993, New York: Springer-Verlag. xviii, 568.

71. Fung, Y.C., *Biomechanics : circulation*. 2nd ed. 1997, New York: Springer. xvii, 571 p.

72. Fung, Y.C., *Selected works on biomechanics and aeroelasticity*. Advanced series in biomechanics ; vol. 1. 1997, Singapore ; New Jersey: World Scientific. 2 v., pts. A & B (xxxiv, 1934 p.).

73. Fung, Y.C. and American Society of Mechanical Engineers. Applied Mechanics Division., *Biomechanics; proceedings of a symposium sponsored by the Applied Mechanics Division of the ASME, at the annual meeting, November 30, 1966, New York, N.Y.* 1966, New York,: American Society of Mechanical Engineers. 204 p.

74. Fung, Y.C. and S. Chien, *Introduction to bioengineering*. Advanced series in biomechanics ; vol. 2. 2001, Singapore ; River Edge, NJ: World Scientific. xvii, 293 p.

75. Fung, Y.C., K. Fronek, and P. Patitucci, *Pseudoelasticity of arteries and the choice of its mathematical expression.* Am J Physiol, 1979. **237**(5): p. H620-31.

76. Fung, Y.C., et al., *Biomechanics in China, Japan, and U.S.A. : proceedings of an international conference held in Wuhan, China, in May, 1983*. 1984, Beijing, China: Science Press. viii, 526 p.

77. Fung, Y.C., et al., *Biomechanics, its foundations and objectives*. 1972, Englewood Cliffs, N.J.,: Prentice-Hall. xiii, 641 p.

78. Fung, Y.C., et al., *Frontiers in biomechanics*. 1986, New York: Springer-Verlag. xviii, 395 p.

79. Geerts, L., et al., *Characterization of the normal cardiac myofiber field in goat measured with MR-diffusion tensor imaging.* Am J Physiol Heart Circ Physiol, 2002. **283**(1): p. H139-45.

80. Gerber, B.L., et al., *Microvascular obstruction and left ventricular remodeling early after acute myocardial infarction.* Circulation, 2000. **101**(23): p. 2734-41.

81. Gilbertson, L.G., et al., *Finite element methods in spine biomechanics research.* Crit Rev Biomed Eng, 1995. **23**(5-6): p. 411-73.

82. Glass, L., et al., *Theory of heart : biomechanics, biophysics, and nonlinear dynamics of cardiac function*. 1991, New York: Springer-Verlag. xvii, 611.

83. Gou, P.F., *Strain energy function for biological tissues.* J Biomech, 1970. **3**(6): p. 547-50.

84. Granzier, H., et al., *Mechanical properties of titin isoforms.* Adv Exp Med Biol, 2000. **481**: p. 283-300; discussion 300-4.

85. Grondin, P., et al., *Natural history of saccular aneurysms of the left ventricle.* J Thorac Cardiovasc Surg, 1979. **77**(1): p. 57-64.

86. Grossi, E.A., et al., *Endoventricular remodeling of left ventricular aneurysm. Functional, clinical, and electrophysiological results.* Circulation, 1995. **92**(9 Suppl): p. II98-100.

87. Guccione, J.M., K.D. Costa, and A.D. McCulloch, *Finite element stress analysis of left ventricular mechanics in the beating dog heart.* J Biomech, 1995. **28**(10): p. 1167-77.

88. Guccione, J.M. and A.D. McCulloch, *Mechanics of active contraction in cardiac muscle: Part I--Constitutive relations for fiber stress that describe deactivation.* J Biomech Eng, 1993. **115**(1): p. 72-81.

89. Guccione, J.M., A.D. McCulloch, and L.K. Waldman, *Passive material properties of intact ventricular myocardium determined from a cylindrical model.* J Biomech Eng, 1991. **113**(1): p. 42-55.

90. Guccione, J.M., et al., *Mechanism underlying mechanical dysfunction in the border zone of left ventricular aneurysm: a finite element model study.* Ann Thorac Surg, 2001. **71**(2): p. 654-62.

91. Guccione, J.M., et al., *Residual stress produced by ventricular volume reduction surgery has little effect on ventricular function and mechanics: a finite element model study.* J Thorac Cardiovasc Surg, 2001. **122**(3): p. 592-9.

92. Guccione, J.M., L.K. Waldman, and A.D. McCulloch, *Mechanics of active contraction in cardiac muscle: Part II--Cylindrical models of the systolic left ventricle.* J Biomech Eng, 1993. **115**(1): p. 82-90.

93. Gupta, K.B., *Functional and Structural Changes in Left Ventricular Aneurysm*, in *Bioengineeing*. 1991, University of Pennsylvania: Philadelphia. p. 310.

94. Gupta, K.B., et al., *Changes in passive mechanical stiffness of myocardial tissue with aneurysm formation.* Circulation, 1994. **89**(5): p. 2315-26.

95. Guyton, A.C. and J.E. Hall, *Textbook of medical physiology*. 9th ed. 1996, Philadelphia: W.B. Saunders. xliii, 1148.

96. Hadland, P.H., et al., *The effects of simulated akinetic and dyskinetic aneurysms on left ventricular systolic function: clinical implications.* Eur J Cardiothorac Surg, 1997. **12**(4): p. 642-7.

97. Hahn, E.A., et al., *The Myocarditis Treatment Trial: design, methods and patients enrollment.* Eur Heart J, 1995. **16 Suppl O**: p. 162-7.

98. Han, G.J., et al., *Application of finite-element analysis with optimisation to assess the in vivo non-linear myocardial material properties using echocardiographic imaging.* Med Biol Eng Comput, 1993. **31**(5): p. 459-67.

99. Harris, T.S., et al., *Constitutive properties of hypertrophied myocardium: cellular contribution to changes in myocardial stiffness.* Am J Physiol Heart Circ Physiol, 2002. **282**(6): p. H2173-2182.

100. Heller, L.J., D.E. Mohrman, and J.R. Prohaska, *Decreased passive stiffness of cardiac myocytes and cardiac tissue from copper-deficient rat hearts.* Am J Physiol Heart Circ Physiol, 2000. **278**(6): p. H1840-7.

101. Hipper, A. and G. Isenberg, *Cyclic mechanical strain decreases the DNA synthesis of vascular smooth muscle cells.* Pflugers Arch, 2000. **440**(1): p. 19-27.

102. Hochman, J.S. and B.H. Bulkley, *Pathogenesis of left ventricular aneurysms: an experimental study in the rat model.* Am J Cardiol, 1982. **50**(1): p. 83-8.

103. Hochman, J.S. and B.H. Bulkley, *Expansion of acute myocardial infarction: an experimental study.* Circulation, 1982. **65**(7): p. 1446-50.

104. Hoffman, A.H. and P. Grigg, *A method for measuring strains in soft tissue.* J Biomech, 1984. **17**(10): p. 795-800.

105. Hoffman, J.D., *Numerical Methods for Engineers and Scientists*. 1992, New York: McGraw-Hill Inc.

106. Hoffmeister, B.K., et al., *Estimation of the elastic stiffness coefficient c13 of fixed tendon and fixed myocardium.* J Acoust Soc Am, 1995. **97**(5 Pt 1): p. 3171-6.

107. Holmes, J.W., Covell, J.W., *Collagen Fiber Orientation in Myocardial Scar Tissue.* Cardiovascular Pathobiology, 1996. **1**(1): p. 15-22.

108. Holmes, J.W., J.A. Nunez, and J.W. Covell, *Functional implications of myocardial scar structure.* Am J Physiol, 1997. **272**(5 Pt 2): p. H2123-30.

109. Horowitz, A., et al., *Structural three-dimensional constitutive law for the passive myocardium.* J Biomech Eng, 1988. **110**(3): p. 200-7.

110. Hsia, H.H. and M.R. Starling, *Is standardization of left ventricular chamber elastance necessary?* Circulation, 1990. **81**(6): p. 1826-36.

111. Huebner, K.H., E.A. Thornton, and T.G. Byrom, *The finite element method for engineers*. 3rd ed. 1995, New York: Wiley. xxvi, 627.

112. Huiskes, R. and E.Y. Chao, *A survey of finite element analysis in orthopedic biomechanics: the first decade.* J Biomech, 1983. **16**(6): p. 385-409.

113. Huiskes, R. and S.J. Hollister, *From structure to process, from organ to cell: recent developments of FE-analysis in orthopaedic biomechanics.* J Biomech Eng, 1993. **115**(4B): p. 520-7.

114. Humphrey, J.D., R.K. Strumpf, and F.C. Yin, *Biaxial mechanical behavior of excised ventricular epicardium.* Am J Physiol, 1990. **259**(1 Pt 2): p. H101-8.

115. Humphrey, J.D., R.K. Strumpf, and F.C. Yin, *Determination of a constitutive relation for passive myocardium: I. A new functional form.* J Biomech Eng, 1990. **112**(3): p. 333-9.

116. Humphrey, J.D., R.K. Strumpf, and F.C. Yin, *Determination of a constitutive relation for passive myocardium: II. Parameter estimation.* J Biomech Eng, 1990. **112**(3): p. 340-6.

117. Humphrey, J.D., R.K. Strumpf, and F.C. Yin, *A constitutive theory for biomembranes: application to epicardial mechanics.* J Biomech Eng, 1992. **114**(4): p. 461-6.

118. Humphrey, J.D., D.L. Vawter, and R.P. Vito, *Mechanical behavior of excised canine visceral pleura.* Ann Biomed Eng, 1986. **14**(5): p. 451-66.

119. Humphrey, J.D., D.L. Vawter, and R.P. Vito, *Pseudoelasticity of excised visceral pleura.* J Biomech Eng, 1987. **109**(2): p. 115-20.

120. Humphrey, J.D., D.L. Vawter, and R.P. Vito, *Quantification of strains in biaxially tested soft tissues.* J Biomech, 1987. **20**(1): p. 59-65.

121. Humphrey, J.D. and F.C. Yin, *On constitutive relations and finite deformations of passive cardiac tissue: I. A pseudostrain-energy function.* J Biomech Eng, 1987. **109**(4): p. 298-304.

122. Humphrey, J.D. and F.C. Yin, *A new constitutive formulation for characterizing the mechanical behavior of soft tissues.* Biophys J, 1987. **52**(4): p. 563-70.

123. Humphrey, J.D. and F.C. Yin, *Biaxial mechanical behavior of excised epicardium.* J Biomech Eng, 1988. **110**(4): p. 349-51.

124. Humphrey, J.D. and F.C. Yin, *Constitutive relations and finite deformations of passive cardiac tissue II: stress analysis in the left ventricle.* Circ Res, 1989. **65**(3): p. 805-17.

125. Humphrey, J.D. and F.C. Yin, *Biomechanical experiments on excised myocardium: theoretical considerations.* J Biomech, 1989. **22**(4): p. 377-83.

126. Hunter, P.J., *Myocardial constitutive laws for continuum mechanics models of the heart.* Adv Exp Med Biol, 1995. **382**: p. 303-18.

127. Hunter, P.J., A.D. McCulloch, and H.E. ter Keurs, *Modelling the mechanical properties of cardiac muscle.* Prog Biophys Mol Biol, 1998. **69**(2-3): p. 289-331.

128. Hunter, P.J., et al., *An anatomical heart model with applications to myocardial activation and ventricular mechanics.* Crit Rev Biomed Eng, 1992. **20**(5-6): p. 403-26.

129. Inoue, T., et al., *Features of coronary artery lesions related to left ventricular aneurysm formation in anterior myocardial infarction.* Angiology, 1993. **44**(8): p. 593-8.

130. Institute of Laboratory Animal Resources (U.S.), *Guide for the care and use of laboratory animals*. 7th ed. 1996, Washington, D.C.: National Academy Press. xii, 125.

131. Jackson, B.M., et al., *Extension of borderzone myocardium in postinfarction dilated cardiomyopathy.* J Am Coll Cardiol, 2002. **40**(6): p. 1160-7; discussion 1168-71.

132. Janz, R.F. and R.J. Waldron, *Predicted effect of chronic apical aneurysms on the passive stiffness of the human left ventricle.* Circ Res, 1978. **42**(2): p. 255-63.

133. Jatene, A.D., *Left ventricular aneurysmectomy. Resection or reconstruction.* J Thorac Cardiovasc Surg, 1985. **89**(3): p. 321-31.

134. Jugdutt, B.I., *Left ventricular rupture threshold during the healing phase after myocardial infarction in the dog.* Can J Physiol Pharmacol, 1987. **65**(3): p. 307-16.

135. Jugdutt, B.I. and R.W. Amy, *Healing after myocardial infarction in the dog: changes in infarct hydroxyproline and topography.* J Am Coll Cardiol, 1986. **7**(1): p. 91-102.

136. Jugdutt, B.I., M.J. Joljart, and M.I. Khan, *Rate of collagen deposition during healing and ventricular remodeling after myocardial infarction in rat and dog models.* Circulation, 1996. **94**(1): p. 94-101.

137. Jugdutt, B.I., et al., *Effect of prolonged inotropic stimulation on ventricular remodeling during healing after myocardial infarction in the dog: mechanistic insights.* J Am Coll Cardiol, 1996. **27**(7): p. 1787-95.

138. Kang, T., J.D. Humphrey, and F.C. Yin, *Comparison of biaxial mechanical properties of excised endocardium and epicardium.* Am J Physiol, 1996. **270**(6 Pt 2): p. H2169-76.

139. Kantrowitz, A., et al., *A prosthetic myocardium for repair of localized defects of the left ventricle: concept and hemodynamic feasibility.* Int J Artif Organs, 1980. **3**(3): p. 173-9.

140. Kass, D.A. and R. Beyar, *Evaluation of contractile state by maximal ventricular power divided by the square of end-diastolic volume.* Circulation, 1991. **84**(4): p. 1698-708.

141. Kato, S., et al., *Effects of pressure- or volume-overload hypertrophy on passive stiffness in isolated adult cardiac muscle cells.* Am J Physiol, 1996. **271**(6 Pt 2): p. H2575-83.

142. Kaufman, W.R. and B.I. Jugdutt, *Left ventricular catecholamines during acute myocardial infarction in the dog.* Can J Physiol Pharmacol, 1987. **65**(2): p. 172-8.

143. Kawata, T., et al., *Systolic and diastolic function after patch reconstruction of left ventricular aneurysms.* Ann Thorac Surg, 1995. **59**(2): p. 403-7.

144. Kellermayer, M.S., et al., *Mechanical manipulation of single titin molecules with laser tweezers.* Adv Exp Med Biol, 2000. **481**: p. 111-26; discussion 127-8.

145. Kelley, S.T., et al., *Restraining infarct expansion preserves left ventricular geometry and function after acute anteroapical infarction.* Circulation, 1999. **99**(1): p. 135-42.

146. Kennedy, J.W., et al., *Quantitative angiocardiography. I. The normal left ventricle in man.* Circulation, 1966. **34**(2): p. 272-8.

147. Kesler, K.A., et al., *Anterior wall left ventricular aneurysm repair. A comparison of linear versus circular closure.* J Thorac Cardiovasc Surg, 1992. **103**(5): p. 841-7; discussion 847-8.

148. Kim, C.B. and E. Braunwald, *Potential benefits of late reperfusion of infarcted myocardium. The open artery hypothesis.* Circulation, 1993. **88**(5 Pt 1): p. 2426-36.

149. Kiseleva, I., et al., *Mechanoelectric feedback after left ventricular infarction in rats.* Cardiovasc Res, 2000. **45**(2): p. 370-8.

150. Klein, M.D., M.V. Herman, and R. Gorlin, *A hemodynamic study of left ventricular aneurysm.* Circulation, 1967. **35**(4): p. 614-30.

151. Kofidis, T., et al., *In vitro engineering of heart muscle: artificial myocardial tissue.* J Thorac Cardiovasc Surg, 2002. **124**(1): p. 63-9.

152. Komeda, M., et al., *Operative risks and long-term results of operation for left ventricular aneurysm.* Ann Thorac Surg, 1992. **53**(1): p. 22-8; discussion 28-9.

153. Kramer, C.M., et al., *Angiotensin-converting enzyme inhibition limits dysfunction in adjacent noninfarcted regions during left ventricular remodeling.* J Am Coll Cardiol, 1996. **27**(1): p. 211-7.

154. Kramer, C.M., et al., *Regional differences in function within noninfarcted myocardium during left ventricular remodeling.* Circulation, 1993. **88**(3): p. 1279-88.

155. Kramer, C.M., et al., *Reverse remodeling and improved regional function after repair of left ventricular aneurysm.* J Thorac Cardiovasc Surg, 2002. **123**(4): p. 700-6.

156. Lanir, Y., *Constitutive equations for fibrous connective tissues.* J Biomech, 1983. **16**(1): p. 1-12.

157. Lapeyre, A.C., 3rd, et al., *Systemic embolism in chronic left ventricular aneurysm: incidence and the role of anticoagulation.* J Am Coll Cardiol, 1985. **6**(3): p. 534-8.

158. Lee, A.A. and A.D. McCulloch, *Multiaxial myocardial mechanics and extracellular matrix remodeling: mechanochemical regulation of cardiac fibroblast function.* Adv Exp Med Biol, 1997. **430**: p. 227-40.

159. Levenberg, K., *A Method for the Solution of Certain Problems in Least Squares.* Quart. Appl. Math., 1944. **2**: p. 164-168.

160. Li, P., et al., *Myocardial infarction alters myofilament calcium sensitivity and mechanical behavior of myocytes.* Am J Physiol, 1997. **272**(1 Pt 2): p. H360-70.

161. Lin, D.H. and F.C. Yin, *A multiaxial constitutive law for mammalian left ventricular myocardium in steady-state barium contracture or tetanus.* J Biomech Eng, 1998. **120**(4): p. 504-17.

162. Little, W.C., *The left ventricular dP/dtmax-end-diastolic volume relation in closed-chest dogs.* Circ Res, 1985. **56**(6): p. 808-15.

163. Little, W.C., *Assessment of Normal and Abnormal Cardiac Function*, in *Heart Disease*, E. Braunwald, Zipes, D., Libby, P., Editor. 2001, W.B. Saunders Company: Philadelphia, PA. p. 479-502.

164. Little, W.C. and R.J. Applegate, *Congestive heart failure: systolic and diastolic function.* J Cardiothorac Vasc Anesth, 1993. **7**(4 Suppl 2): p. 2-5.

165. Little, W.C. and C.P. Cheng, *Left ventricular-arterial coupling in conscious dogs.* Am J Physiol, 1991. **261**(1 Pt 2): p. H70-6.

166. Little, W.C. and C.P. Cheng, *Effect of exercise on left ventricular-arterial coupling assessed in the pressure-volume plane.* Am J Physiol, 1993. **264**(5 Pt 2): p. H1629-33.

167. Little, W.C., et al., *Comparison of measures of left ventricular contractile performance derived from pressure-volume loops in conscious dogs.* Circulation, 1989. **80**(5): p. 1378-87.

168. Lodish, H.F., *Molecular cell biology*. 2000, W.H. Freeman: New York.

169. Loeffler, L., 3rd and K. Sagawa, *A one-dimensional viscoelastic model of cat heart muscle studied by small length perturbations during isometric contraction.* Circ Res, 1975. **36**(4): p. 498-512.

170. Lu, P., et al., *Comparison of tomographic and planar radionuclide ventriculography in the assessment of regional left ventricular function in patients with left ventricular aneurysm before and after surgery.* J Nucl Cardiol, 1994. **1**(6): p. 537-45.

171. Lumia, F.J., et al., *Left ventricular function after elective aneurysmectomy.* Clin Cardiol, 1985. **8**(7): p. 385-90.

172. Ma, Y.H., S. Ling, and H.E. Ives, *Mechanical strain increases PDGF-B and PDGF beta receptor expression in vascular smooth muscle cells.* Biochem Biophys Res Commun, 1999. **265**(2): p. 606-10.

173. MacKenna, D.A., et al., *Contribution of collagen matrix to passive left ventricular mechanics in isolated rat hearts.* Am J Physiol, 1994. **266**(3 Pt 2): p. H1007-18.

174. MacKenna, D.A., S.M. Vaplon, and A.D. McCulloch, *Microstructural model of perimysial collagen fibers for resting myocardial mechanics during ventricular filling.* Am J Physiol, 1997. **273**(3 Pt 2): p. H1576-86.

175. Maclean, D., et al., *Long-term preservation of ischemic myocardium after experimental coronary artery occlusion.* J Clin Invest, 1978. **61**(3): p. 541-51.

176. Magovern, G.J., et al., *Surgical therapy for left ventricular aneurysms. A ten-year experience.* Circulation, 1989. **79**(6 Pt 2): p. I102-7.

177. Mariotti, R., et al., *Left ventricular aneurysm: clinical and hemodynamic data.* Clin Cardiol, 1990. **13**(12): p. 845-50.

178. Markovitz, L.J., et al., *Large animal model of left ventricular aneurysm.* Ann Thorac Surg, 1989. **48**(6): p. 838-45.

179. Marquardt, D., *An Algorithm for Least-Squares Estimation of Nonlinear Parameters.* SIAM J. Appl. Math., 1963. **11**: p. 431-441.

180. Mason, J.W., et al., *A clinical trial of immunosuppressive therapy for myocarditis. The Myocarditis Treatment Trial Investigators.* N Engl J Med, 1995. **333**(5): p. 269-75.

181. Mathur, A.B., et al., *Endothelial, cardiac muscle and skeletal muscle exhibit different viscous and elastic properties as determined by atomic force microscopy.* J Biomech, 2001. **34**(12): p. 1545-53.

182. May-Newman, K. and F.C. Yin, *Biaxial mechanical behavior of excised porcine mitral valve leaflets.* Am J Physiol, 1995. **269**(4 Pt 2): p. H1319-27.

183. May-Newman, K. and F.C. Yin, *Biaxial mechanical behavior of excised porcine mitral valve leaflets.* Am J Physiol, 1995. **269**(4 Pt 2): p. H1319-27.

184. McCormick, R.J., et al., *Regional differences in LV collagen accumulation and mature cross-linking after myocardial infarction in rats.* Am J Physiol, 1994. **266**(1 Pt 2): p. H354-9.

185. McCulloch, A., et al., *Large-scale finite element analysis of the beating heart.* Crit Rev Biomed Eng, 1992. **20**(5-6): p. 427-49.

186. McCulloch, A.D., B.H. Smaill, and P.J. Hunter, *Left ventricular epicardial deformation in isolated arrested dog heart.* Am J Physiol, 1987. **252**(1 Pt 2): p. H233-41.

187. McCulloch, A.D., B.H. Smaill, and P.J. Hunter, *Regional left ventricular epicardial deformation in the passive dog heart.* Circ Res, 1989. **64**(4): p. 721-33.

188. McKay, R.G., et al., *Left ventricular remodeling after myocardial infarction: a corollary to infarct expansion.* Circulation, 1986. **74**(4): p. 693-702.

189. McNulty, P.H., et al., *Left ventricular aneurysm as a consequence of hypertrophic obstructive cardiomyopathy.* Catheter Cardiovasc Interv, 2002. **55**(3): p. 385-8.

190. Meizlish, J.L., et al., *Functional left ventricular aneurysm formation after acute anterior transmural myocardial infarction. Incidence, natural history, and prognostic implications.* N Engl J Med, 1984. **311**(16): p. 1001-6.

191. Mickleborough, L.L., S. Carson, and J. Ivanov, *Repair of dyskinetic or akinetic left ventricular aneurysm: results obtained with a modified linear closure.* J Thorac Cardiovasc Surg, 2001. **121**(4): p. 675-82.

192. Miller, J.M., et al., *Subendocardial resection for ventricular tachycardia: predictors of surgical success.* Circulation, 1984. **70**(4): p. 624-31.

193. Mills, N.L., C.T. Everson, and D.R. Hockmuth, *Technical advances in the treatment of left ventricular aneurysm.* Ann Thorac Surg, 1993. **55**(3): p. 792-800.

194. Mirsky, I., et al., *Passive elastic wall stiffness of the left vertnicle: a comparison between linear theory and large deformation theory.* Bull Math Biol, 1976. **38**(3): p. 239-51.

195. Miyawaki, H., et al., *The response of left ventricular regional function to afterload stress in patients with old myocardial infarction and ventricular aneurysm.* Jpn Circ J, 1991. **55**(12): p. 1211-23.

196. More, J.J., *The Levenberg-Marquardt Algorithm: Implementation and Theory*, in *Numerical Analysis*, G.A. Watson, Editor. 1977, Springer Verlag. p. 105-116.

197. Moriarty, T.F., *The law of Laplace. Its limitations as a relation for diastolic pressure, volume, or wall stress of the left ventricle.* Circ Res, 1980. **46**(3): p. 321-31.

198. Moss, R.L., *Ca2+ regulation of mechanical properties of striated muscle. Mechanistic studies using extraction and replacement of regulatory proteins.* Circ Res, 1992. **70**(5): p. 865-84.

199. Moulton, M.J., et al., *Mechanical dysfunction in the border zone of an ovine model of left ventricular aneurysm.* Ann Thorac Surg, 1995. **60**(4): p. 986-97; discussion 998.

200. Moustakidis, P., et al., *Altered left ventricular geometry changes the border zone temporal distribution of stress in an experimental model of left ventricular aneurysm: a finite element model study.* Circulation, 2002. **106**(12 Suppl 1): p. I168-75.

201. Nagel, E., et al., *Cardiac rotation and relaxation after anterolateral myocardial infarction.* Coron Artery Dis, 2000. **11**(3): p. 261-7.

202. Nakayama, M., et al., *Optimal preload adjustment of maximal ventricular power index varies with cardiac chamber size.* Am Heart J, 1998. **136**(2): p. 281-8.

203. Needleman, A., et al., *A finite element model of the infarcted left ventricle.* J Biomech, 1983. **16**(1): p. 45-58.

204. Nielsen, P.M., P.J. Hunter, and B.H. Smaill, *Biaxial testing of membrane biomaterials: testing equipment and procedures.* J Biomech Eng, 1991. **113**(3): p. 295-300.

205. Nielsen, P.M., et al., *Mathematical model of geometry and fibrous structure of the heart.* Am J Physiol, 1991. **260**(4 Pt 2): p. H1365-78.

206. Noda, T., et al., *Curvilinearity of LV end-systolic pressure-volume and dP/dtmax-end-diastolic volume relations.* Am J Physiol, 1993. **265**(3 Pt 2): p. H910-7.

207. Norton, G.R., et al., *Myocardial Stiffness Is Attributed to Alterations in Cross-Linked Collagen Rather Than Total Collagen or Phenotypes in Spontaneously Hypertensive Rats.* Circulation, 1997. **96**(6): p. 1991-1998.

208. Novak, V.P., F.C. Yin, and J.D. Humphrey, *Regional mechanical properties of passive myocardium.* J Biomech, 1994. **27**(4): p. 403-12.

209. O'Callaghan, C.J. and B. Williams, *Mechanical strain-induced extracellular matrix production by human vascular smooth muscle cells: role of TGF-beta(1).* Hypertension, 2000. **36**(3): p. 319-24.

210. Ohara, K., *Current surgical strategy for post-infarction left ventricular aneurysm--from linear aneurysmecomy to Dor's operation.* Ann Thorac Cardiovasc Surg, 2000. **6**(5): p. 289-94.

211. Okamoto, R.J., et al., *Epicardial suction: a new approach to mechanical testing of the passive ventricular wall.* J Biomech Eng, 2000. **122**(5): p. 479-87.

212. Okies, J.E., et al., *Early and late results of resection of ventricular aneurysm.* J Thorac Cardiovasc Surg, 1978. **75**(2): p. 255-60.

213. Okoshi, M.P., et al., *Comparative mechanical study of isolated papillary muscle from Wistar-Kyoto and Wistar rats.* Jpn Heart J, 1994. **35**(3): p. 333-43.

214. Olsen, C.O., et al., *Diastolic anisotropic properties of the left ventricle in the conscious dog.* Circ Res, 1991. **69**(3): p. 765-78.

215. Omens, J.H., D.A. MacKenna, and A.D. McCulloch, *Measurement of strain and analysis of stress in resting rat left ventricular myocardium.* J Biomech, 1993. **26**(6): p. 665-76.

216. Omens, J.H., K.D. May, and A.D. McCulloch, *Transmural distribution of three-dimensional strain in the isolated arrested canine left ventricle.* Am J Physiol, 1991. **261**(3 Pt 2): p. H918-28.

217. Omens, J.H., D.E. Milkes, and J.W. Covell, *Effects of pressure overload on the passive mechanics of the rat left ventricle.* Ann Biomed Eng, 1995. **23**(2): p. 152-63.

218. Omens, J.H., T.R. Miller, and J.W. Covell, *Relationship between passive tissue strain and collagen uncoiling during healing of infarcted myocardium.* Cardiovasc Res, 1997. **33**(2): p. 351-8.

219. Oomman, A., et al., *Dor's endoaneurysmorrhaphy in severe heart failure due to giant cell myocarditis.* Ann Thorac Surg, 2001. **71**(6): p. 2036-8.

220. Opie, L.H., *Mechanism.* 2001.

221. Pagel, P.S., et al., *Left ventricular diastolic function in the normal and diseased heart. Perspectives for the anesthesiologist (1).* Anesthesiology, 1993. **79**(4): p. 836-54.

222. Pagel, P.S., et al., *Left ventricular diastolic function in the normal and diseased heart. Perspectives for the anesthesiologist (2).* Anesthesiology, 1993. **79**(5): p. 1104-20.

223. Palmer, R.E., A.J. Brady, and K.P. Roos, *Mechanical measurements from isolated cardiac myocytes using a pipette attachment system.* Am J Physiol, 1996. **270**(2 Pt 1): p. C697-704.

224. Pao, Y.C. and E.L. Ritman, *Comparative characterization of the infarcted and reperfused ventricular wall muscles by finite element analysis and a myocardial muscle-blood composite model.* Comput Biomed Res, 1998. **31**(1): p. 18-31.

225. Parmley, W.W., et al., *In vitro length-tension relations of human ventricular aneurysms. Relation of stiffness to mechanical disadvantage.* Am J Cardiol, 1973. **32**(7): p. 889-94.

226. Pasque, M.K., *Mathematic modeling and cardiac surgery.* J Thorac Cardiovasc Surg, 2002. **123**(4): p. 617-20.

227. Pfeffer, J.M., et al., *Progressive ventricular remodeling in rat with myocardial infarction.* Am J Physiol, 1991. **260**(5 Pt 2): p. H1406-14.

228. Pfeffer, M.A. and E. Braunwald, *Ventricular remodeling after myocardial infarction. Experimental observations and clinical implications.* Circulation, 1990. **81**(4): p. 1161-72.

229. Pinto, J.G. and A. Boe, *A method to characterize the passive elasticity in contracting muscle bundles.* J Biomech Eng, 1991. **113**(1): p. 72-8.

230. Pinto, J.G. and Y.C. Fung, *Mechanical properties of the stimulated papillary muscle in quick-release experiments.* J Biomech, 1973. **6**(6): p. 617-30.

231. Pinto, J.G. and Y.C. Fung, *Mechanical properties of the heart muscle in the passive state.* J Biomech, 1973. **6**(6): p. 597-616.

232. Pinto, J.G., et al., *A device for testing mechanical properties of biological materials--the "Biodyne".* J Appl Physiol, 1975. **39**(5): p. 863-7.

233. Pollack, P.S., et al., *Mechanical properties of adult feline ventricular myocytes in culture.* Am J Physiol, 1991. **260**(1 Pt 2): p. H234-41.

234. Poulsen, S.H., *Clinical aspects of left ventricular diastolic function assessed by Doppler echocardiography following acute myocardial infarction.* Dan Med Bull, 2001. **48**(4): p. 199-210.

235. Prates, P.R., et al., *Surgical repair of ventricular aneurysms. Early results with Cooley's technique.* Tex Heart Inst J, 1993. **20**(1): p. 19-22.

236. Prohaska, J.R. and L.J. Heller, *Mechanical properties of the copper-deficient rat heart.* J Nutr, 1982. **112**(11): p. 2142-50.

237. Przyklenk, K., et al., *Effect of myocyte necrosis on strength, strain, and stiffness of isolated myocardial strips.* Am Heart J, 1987. **114**(6): p. 1349-59.

238. Quarterman, R.L., et al., *A finite element model of left ventricular cellular transplantation in dilated cardiomyopathy.* Asaio J, 2002. **48**(5): p. 508-13.

239. Radhakrishnan, S., D.N. Ghista, and G. Jayaraman, *Mechanics of left ventricular aneurysm.* J Biomed Eng, 1986. **8**(1): p. 9-23.

240. Rahko, P.S., *Comparative efficacy of three indexes of left ventricular performance derived from pressure-volume loops in heart failure induced by tachypacing.* J Am Coll Cardiol, 1994. **23**(1): p. 209-18.

241. Raman, J.S., G. Sakaguchi, and B.F. Buxton, *Outcome of geometric endoventricular repair in impaired left ventricular function.* Ann Thorac Surg, 2000. **70**(3): p. 1127-9.

242. Ratcliffe, M.B., et al., *The effect of ventricular volume reduction surgery in the dilated, poorly contractile left ventricle: a simple finite element analysis.* J Thorac Cardiovasc Surg, 1998. **116**(4): p. 566-77.

243. Ratcliffe, M.B., et al., *Ventricular volume, chamber stiffness, and function after anteroapical aneurysm plication in the sheep.* J Thorac Cardiovasc Surg, 2000. **119**(1): p. 115-24.

244. Ratcliffe, M.B., et al., *Radio frequency heating of chronic ovine infarct leads to sustained infarct area and ventricular volume reduction.* J Thorac Cardiovasc Surg, 2000. **119**(6): p. 1194-204.

245. Redaelli, G., et al., *Effects of constitutive overexpression of insulin-like growth factor-1 on the mechanical characteristics and molecular properties of ventricular myocytes.* Circ Res, 1998. **82**(5): p. 594-603.

246. Reddy, J.N., *An introduction to the finite element method.* 2nd ed. McGraw-Hill series in mechanical engineering. 1993, New York: McGraw-Hill. xix, 684.

247. Reif, T.H. and M.D. Silver, *Role of stress concentration in the pathogenesis of cardiac rupture following acute myocardial infarction.* Can J Cardiol, 1995. **11**(9): p. 757-62.

248. Robinson, T.F., L. Cohen-Gould, and S.M. Factor, *Skeletal framework of mammalian heart muscle. Arrangement of inter- and pericellular connective tissue structures.* Lab Invest, 1983. **49**(4): p. 482-98.

249. Robinson, T.F., et al., *Structure and function of connective tissue in cardiac muscle: collagen types I and III in endomysial struts and pericellular fibers.* Scanning Microsc, 1988. **2**(2): p. 1005-15.

250. Robinson, T.F., et al., *Extracellular structures in heart muscle.* Adv Myocardiol, 1985. **5**: p. 243-55.

251. Robinson, T.F., et al., *Morphology, composition, and function of struts between cardiac myocytes of rat and hamster.* Cell Tissue Res, 1987. **249**(2): p. 247-55.

252. Robinson, T.F., S.M. Factor, and E.H. Sonnenblick, *The heart as a suction pump.* Sci Am, 1986. **254**(6): p. 84-91.

253. Robinson, T.F., et al., *Coiled perimysial fibers of papillary muscle in rat heart: morphology, distribution, and changes in configuration.* Circ Res, 1988. **63**(3): p. 577-92.

254. Rodriguez, E.K., et al., *Effect of residual stress on transmural sarcomere length distributions in rat left ventricle.* Am J Physiol, 1993. **264**(4 Pt 2): p. H1048-56.

255. Sacks, M.S. and C.J. Chuong, *A constitutive relation for passive right-ventricular free wall myocardium.* J Biomech, 1993. **26**(11): p. 1341-5.

256. Sacks, M.S. and C.J. Chuong, *Biaxial mechanical properties of passive right ventricular free wall myocardium.* J Biomech Eng, 1993. **115**(2): p. 202-5.

257. Sagawa, K., ,Maughan, W., Suga, H., Sunagawa, K. Cardiac Contraction and the Pressure-Volume Relationship. 1988, New York: Oxford University Press. 232-298.

258. Sakamoto, T., *Apical hypertrophic cardiomyopathy (apical hypertrophy): an overview.* J Cardiol, 2001. **37 Suppl 1**: p. 161-78.

259. Salati, M., et al., *Functional results of left ventricular reconstruction.* Ann Thorac Surg, 1993. **56**(2): p. 316-22.

260. Salati, M., et al., *Left ventricular geometry after endoventriculoplasty.* Eur J Cardiothorac Surg, 1993. **7**(11): p. 574-8; discussion 579.

261. Savage, E.B., et al., *Repair of left ventricular aneurysm. Changes in ventricular mechanics, hemodynamics, and oxygen consumption.* J Thorac Cardiovasc Surg, 1992. **104**(3): p. 752-62.

262. Schertel, E.R., *Assessment of left-ventricular function.* Thorac Cardiovasc Surg, 1998. **46 Suppl 2**: p. 248-54.

263. Schmeling, T.J., et al., *Changes in passive but not active mechanical properties predict recovery of function of stunned myocardium.* Ann Biomed Eng, 1999. **27**(2): p. 131-40.

264. Sebbag, L., et al., *Protection of ischemic myocardium in dogs using intracoronary 2,3-butanedione monoxime (BDM).* J Mol Cell Cardiol, 2003. **35**(2): p. 165-76.

265. Shacklock, A., *Biaxial Testing of Cardiac Tissue*. 1987, University of Auckland, New Zealand: Auckland.

266. Shapira, O.M., et al., *Repair of left ventricular aneurysm: long-term results of linear repair versus endoaneurysmorrhaphy.* Ann Thorac Surg, 1997. **63**(3): p. 701-5.

267. Shaw, R.C., et al., *Left ventricular aneurysm resection: indications and long-term follow-up.* Ann Thorac Surg, 1978. **25**(4): p. 336-9.

268. Shen, W.F., et al., *Left ventricular aneurysm and prognosis in patients with first acute transmural anterior myocardial infarction and isolated left anterior descending artery disease.* Eur Heart J, 1992. **13**(1): p. 39-44.

269. Shlyachover, V.E. and O.K. Zenin, *Mechanical characteristics of the globally ischaemic heart.* Cardiovasc Res, 1993. **27**(5): p. 807-10.

270. Shroff, S.G., D.R. Saner, and R. Lal, *Dynamic micromechanical properties of cultured rat atrial myocytes measured by atomic force microscopy.* Am J Physiol, 1995. **269**(1 Pt 1): p. C286-92.

271. Sinatra, R., et al., *Left ventricular aneurysmectomy; comparison between two techniques; early and late results.* Eur J Cardiothorac Surg, 1997. **12**(2): p. 291-7.

272. Smaill, B.H., et al., *The effect of synthetic patch repair of coarctation on regional deformation of the aortic wall.* J Thorac Cardiovasc Surg, 2000. **120**(6): p. 1053-63.

273. Sodums, M.T., et al., *Evaluation of left ventricular contractile performance utilizing end-systolic pressure-volume relationships in conscious dogs.* Circ Res, 1984. **54**(6): p. 731-9.

274. Solomon, S.D., et al., *Assessment of regional left ventricular wall stress after myocardial infarction by echocardiography-based structural analysis.* J Am Soc Echocardiogr, 1998. **11**(10): p. 938-47.

275. Song, G., et al., *Altered mechanical properties and intracellular calcium signaling in cardiomyocytes from annexin 6 null-mutant mice.* Faseb J, 2002. **16**(6): p. 622-4.

276. Sonnenblick, E.H., *Force-velocity relations in mammalian heart muscle.* Am J Physiol, 1962. **202**: p. 931-939.

277. St John Sutton, M., et al., *Cardiovascular death and left ventricular remodeling two years after myocardial infarction: baseline predictors and impact of long-term use of captopril: information from the Survival and Ventricular Enlargement (SAVE) trial.* Circulation, 1997. **96**(10): p. 3294-9.

278. St John Sutton, M., et al., *Quantitative two-dimensional echocardiographic measurements are major predictors of adverse cardiovascular events after acute myocardial infarction. The protective effects of captopril.* Circulation, 1994. **89**(1): p. 68-75.

279. Streeter, D.D., Jr. and W.T. Hanna, *Engineering mechanics for successive states in canine left ventricular myocardium. I. Cavity and wall geometry.* Circ Res, 1973. **33**(6): p. 639-55.

280. Streeter, D.D., Jr. and W.T. Hanna, *Engineering mechanics for successive states in canine left ventricular myocardium. II. Fiber angle and sarcomere length.* Circ Res, 1973. **33**(6): p. 656-64.

281. Streeter, D.D., Jr., et al., *Fiber orientation in the canine left ventricle during diastole and systole.* Circ Res, 1969. **24**(3): p. 339-47.

282. Strobeck, J.E. and E.H. Sonnenblick, *Myocardial and ventricular function. Part II: Intact heart.* Herz, 1981. **6**(5): p. 275-87.

283. Strumpf, R.K., J.D. Humphrey, and F.C. Yin, *Biaxial mechanical properties of passive and tetanized canine diaphragm.* Am J Physiol, 1993. **265**(2 Pt 2): p. H469-75.

284. Stuyvers, B.D., M. Miura, and H.E. ter Keurs, *Diastolic viscoelastic properties of rat cardiac muscle; involvement of Ca2+.* Adv Exp Med Biol, 1997. **430**: p. 13-28.

285. Sudhir, K., et al., *Mechanical strain stimulates a mitogenic response in coronary vascular smooth muscle cells via release of basic fibroblast growth factor.* Am J Hypertens, 2001. **14**(11 Pt 1): p. 1128-34.

286. Surakiatchanukul, S., *Repair of the left ventricular aneurysm: twenty-two years of experience with long-term results.* Ann Thorac Cardiovasc Surg, 1999. **5**(6): p. 396-401.

287. Tasche, C., E. Meyhofer, and B. Brenner, *A force transducer for measuring mechanical properties of single cardiac myocytes.* Am J Physiol, 1999. **277**(6 Pt 2): p. H2400-8.

288. Tavakoli, R., et al., *Repair of postinfarction dyskinetic LV aneurysm with either linear or patch technique.* Eur J Cardiothorac Surg, 2002. **22**(1): p. 129-34.

289. Thomas, C.H., et al., *Engineering gene expression and protein synthesis by modulation of nuclear shape.* Proc Natl Acad Sci U S A, 2002. **99**(4): p. 1972-7.

290. Tikiz, H., et al., *Left ventricular aneurysm formation after anterior myocardial infarction: clinical and angiographic determinants in 809 patients.* Int J Cardiol, 2002. **82**(1): p. 7-14; discussion 14-6.

291. Tischler, M.D. and J. Niggel, *Exercise echocardiography in combined mild mitral valve stenosis and regurgitation.* Echocardiography, 1993. **10**(5): p. 453-7.

292. Toda, G., et al., *Left ventricular aneurysm without coronary artery disease, incidence and clinical features: clinical analysis of 11 cases.* Intern Med, 2000. **39**(7): p. 531-6.

293. Toombs, C.F., et al., *Nonlinearity of indexes of left ventricular performance: effects on estimation of slope and diameter axis intercepts.* Am J Physiol, 1991. **260**(6 Pt 2): p. H1802-9.

294. Vayo, H.W., *The theory of the left ventricular aneurysm.* Bull Math Biophys, 1966. **28**(3): p. 363-70.

295. Wakatsuki, T. and E.L. Elson, *Reciprocal interactions between cells and extracellular matrix during remodeling of tissue constructs.* Biophys Chem, 2003. **100**(1-3): p. 593-605.

296. Wakatsuki, T., R.B. Wysolmerski, and E.L. Elson, *Mechanics of cell spreading: role of myosin II.* J Cell Sci, 2003. **116**(Pt 8): p. 1617-25.

297. Wallace, A., H.W. Lam, and D.T. Mangano, *Linearity, load dependence, hysteresis, and clinical associations of systolic and diastolic indices of left ventricular function in man. Multicenter Study of Perioperative Ischemia (McSPI) Research Group.* J Card Surg, 1995. **10**(4 Suppl): p. 460-7.

298. Wang, J.H., et al., *Leukotrienes and tyrosine phosphorylation mediate stretching-induced actin cytoskeletal remodeling in endothelial cells.* Cell Motil Cytoskeleton, 2000. **46**(2): p. 137-45.

299. Wang, J.H., et al., *Specificity of endothelial cell reorientation in response to cyclic mechanical stretching.* J Biomech, 2001. **34**(12): p. 1563-72.

300. Watanabe, T., et al., *Computer simulation of ventricular wall motion using the finite element method.* Radiat Med, 1988. **6**(4): p. 165-70.

301. Weber, K.T., *Cardiac interstitium in health and disease: the fibrillar collagen network.* J Am Coll Cardiol, 1989. **13**(7): p. 1637-52.

302. Weber, K.T., Y. Sun, and E. Guarda, *Structural remodeling in hypertensive heart disease and the role of hormones.* Hypertension, 1994. **23**(6 Pt 2): p. 869-77.

303. Weber, K.T., et al., *Collagen network of the myocardium: function, structural remodeling and regulatory mechanisms.* J Mol Cell Cardiol, 1994. **26**(3): p. 279-92.

304. Weis, S.M., et al., *Myocardial Mechanics and Collagen Structure in the Osteogenesis Imperfecta Murine (oim).* Circ Res, 2000. **87**(8): p. 663-669.

305. Weitzman, I., et al., *Phialophora parasitica, an emerging pathogen.* Sabouraudia, 1984. **22**(4): p. 331-9.

306. White, H.D., et al., *Left ventricular end-systolic volume as the major determinant of survival after recovery from myocardial infarction.* Circulation, 1987. **76**(1): p. 44-51.

307. White, H.D., et al., *Effect of intravenous streptokinase on left ventricular function and early survival after acute myocardial infarction.* N Engl J Med, 1987. **317**(14): p. 850-5.

308. Whittaker, P., D.R. Boughner, and R.A. Kloner, *Role of collagen in acute myocardial infarct expansion.* Circulation, 1991. **84**(5): p. 2123-34.

309. Whittaker, P., et al., *Stunned myocardium and myocardial collagen damage: differential effects of single and repeated occlusions.* Am Heart J, 1991. **121**(2 Pt 1): p. 434-41.

310. Wigle, E.D., *Novel insights into the clinical manifestations and treatment of hypertrophic cardiomyopathy.* Curr Opin Cardiol, 1995. **10**(3): p. 299-305.

311. Wigle, E.D., et al., *Hypertrophic cardiomyopathy. The importance of the site and the extent of hypertrophy. A review.* Prog Cardiovasc Dis, 1985. **28**(1): p. 1-83.

312. Wu, Y., et al., *Changes in titin isoform expression in pacing-induced cardiac failure give rise to increased passive muscle stiffness.* Circulation, 2002. **106**(11): p. 1384-9.

313. Yamaguchi, A., et al., *Left ventricular volume predicts postoperative course in patients with ischemic cardiomyopathy.* Ann Thorac Surg, 1998. **65**(2): p. 434-8.

314. Yettram, A.L. and M.C. Beecham, *An analytical method for the determination of along-fibre to cross-fibre elastic modulus ratio in ventricular myocardium--a feasibility study.* Med Eng Phys, 1998. **20**(2): p. 103-8.

315. Yin, F.C., *Ventricular wall stress.* Circ Res, 1981. **49**(4): p. 829-42.

316. Yin, F.C., P.H. Chew, and S.L. Zeger, *An approach to quantification of biaxial tissue stress-strain data.* J Biomech, 1986. **19**(1): p. 27-37.

317. Yin, F.C., et al., *Quantification of the mechanical properties of noncontracting canine myocardium under simultaneous biaxial loading.* J Biomech, 1987. **20**(6): p. 577-89.

318. Yin, F.C., et al., *A video-dimension analyzer.* IEEE Trans Biomed Eng, 1972. **19**(5): p. 376-81.

319. Zile, M.R., et al., *Constitutive properties of adult mammalian cardiac muscle cells.* Circulation, 1998. **98**(6): p. 567-79.

Chapter 9

Appendix

Explanation of Terms:

cardiovascular disease - category of disease that includes rheumatic fever/rheumatic heart disease; hypertensive diseases; ischemic (coronary) hear disease; pulmonary heart disease and diseases of the pulmonary circulation; other forms of heart disease; cerebrovascular disease (stroke); atherosclerosis; other diseases of arteries, arterioles and capillaries; diseases of veins, lymphatics and lymph nodes, not classified elsewhere; and other and unspecified disorders of the circulatory system [1].

Cauchy Stress - force in deformed configuration per unit of deformed area [2]

continuum - an isomorphism of three dimensional Euclidean space such that between any two material particles there is another material particle [3].

coronary heart disease - category of cardiovascular disease that includes acute myocardial infarction; other acute ischemic (coronary) heart disease; angina pectoris; atherosclerotic cardiovascular disease; and all other forms of chronic ischemic heart disease [1].

curvilinear coordinates - coordinate system in which a point in three-dimensional space can be located by the intersection of three unique and non-coincident curvilinear surfaces [4].

global matrix - refers to a matrix in the finite element method that contains information (i.e. stiffness) for all nodes in the finite element mesh.

heterogeneous - a material whose properties vary from point to point or depend upon location [5].

incompressible - a material whose volume is conserved under deformation.

interpolation - the process of estimating a solution between nodes by using an assumed mathematical relation.

isotropic material - material that exhibits symmetry in all rotations about all possible axes and reflections in any plane [6].

Kronecker Delta (δ_{ij}) - has the value of 1 when i=j, and 0 when i≠j [3].

large deformation - describes analyses in which the infinitesimal strain tensor is not appropriate to be used,

nodes - connect adjacent elements at discrete points on their common boundaries. Nodes are usually the vertices of the elements but can exist along the element boundry line or be within the element.

non-linear - describes a process that cannot be accurately be described by a simple linear relationship

refinement - the process of breaking a finite element mesh into smaller elements.

scalars - physical quantities that are completely represented by giving their magnitude.

Second Piola-Kirchhoff Stress - force mapped to undeformed configuration per undeformed area [2].

small deformation - analyses in which it is appropriate to use the infinitesimal strain tensor.

strain - measure of deformation that a material is experiencing.

stress - force acting upon a material divided by the cross-sectional area it is acting upon [3].

tensors - physical quantity represented by a matrix whose value is insensitive to coordinate system changes [2].

time dependent - describes a physical quantity whose value varies with time.

vectors - physical quantities that are completely represented by their magnitude and direction.

References:

1. *2003 Heart and Stroke Statistical Update*. 2003, American Heart Association: Dallas, TX.
2. Fung, Y.C., Tong, P., *Classical and Computational Solid Mechanics*. 2001, Singapore: World Scientific Publishing Co. 930.
3. Fung, Y.C., *Biomechanics : mechanical properties of living tissues*. 2nd ed. 1993, New York: Springer-Verlag. xviii, 568.
4. Narasimhan, M.N.L., *Principles of Continuum Mechanics*. 1992, New York: Wiley-Interscience. 567.
5. Daniel. I.M., I., O., *Engineering Mechanics of Composite Materials*. 1 ed. 1994, Oxford: Oxford University Press. 395.
6. Spencer, A.J.M., *Continuum Mechanics*. 1994, New York: Longman Scientific and Technical. 183.

6258R

UC San Francisco LIBRARY

UNIVERSITY OF CALIFORNIA · UNIVERSITY OF CALIFORNIA

For reference

Not to be taken
from the room.

7230470

3 1378 00723 0470